Investigation of the neural correlates of ongoing pain states using quantitative perfusion arterial spin labelling

Andrew R. Segerdahl

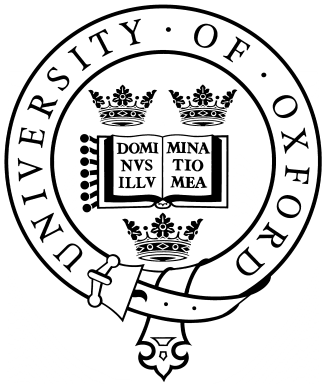

Wolfson College

Michaelmas Term 2011

Investigation of the neural correlates of ongoing pain states using quantitative perfusion arterial spin labelling

Andrew R. Segerdahl

Michaelmas Term 2011, Wolfson College

A thesis submitted in partial fulfillment of the requirements for the degree of Doctor of Philosophy in the University of Oxford

Abstract

At present, there are few clinically effective pain therapies available to treat chronic pain. One reason is due to a lack of understanding about how pain emerges in the brain. Excitingly, an emerging body of work suggests that the perfusion imaging technique, arterial spin labelling (ASL), is particularly well-suited to investigate this issue. The primary aim of this thesis is to develop and optimise a quantitative perfusion imaging approach to investigate the neural correlates of both experimental and pathological tonic pain.
In Chapter 2, we explore different methods of inducing ongoing pain in healthy subjects. Results from this study show that mechanically induced pain is well suited for use in ASL FMRI experiments. In Chapter 3, we compare currently available ASL FMRI approaches for investigating tonic states, using a range of sensory paradigms. Results from these experiments support the use of an optimised version of Continuous ASL (CASL) FMRI to obtain whole-brain perfusion. Additionally, we discuss our decision to proceed with the newly acquired pseudo-continuous ASL (pCASL); a novel ASL technique that benefits from maximal signal-to-noise (SNR) across a whole-brain volume. In Chapter 4 we implement the pCASL FMRI approach to image the neural correlates of ongoing experimental pain. Results from the investigation of parametrically modulated ongoing mechanical pain show robust pain-related activation of key pain related regions that are monotonically active with an increase in stimulus intensity. Additionally, data from this experiment shows the presence of complex perfusion dynamics relative to pain worthy of further study. In Chapter 5, we optimised the pCASL sequence to obtain absolute perfusion changes across the whole-brain volume, using multi-inversion times, so that we could investigate the perfusion dynamics observed in Chapter 4. Results show that absolute perfusion changes during tonic pain are considerably less than for regions recruited during a non-pain task. Additionally, dynamic perfusion changes show complex stimulus responses across all active regions regardless of stimulus type. We conclude that while the technique is well suited to quantify absolute perfusion, the mechanisms underlying the dynamic changes in CBF (neuronal signal, neurovascular coupling) need further study. Finally, in Chapter 6, we implement the absolute perfusion approach developed in Chaper 5 to interrogate the neural correlates of the genetic pain disease, Erythromelalgia, and pleasurable relief. The results of this study show pain-related activation (and relief-induced reduction) of key pain-related regions. We conclude from these results that the ASL technique developed over the course of this thesis can be used to study a range of pain pathologies.

Taken together, the results of this thesis document the development of a powerful perfusion imaging technique capable of quantifying absolute perfusion changes across a whole-brain volume. The data presented here from investigations of both experimental and

pathological pain states supports the use of this technique in future tonic pain studies, as well as other neuroscience applications. We are confident that implementation of this imaging approach will provide integral insight into the mechanisms of ongoing pain states; and further the development of novel efficacious pain treatment options.

This thesis contain approximately 40,000 words.

TABLE OF CONTENTS

I. Acknowledgements

I am writing this last final, very essential part of my thesis somewhere between Oxford and London. Peering from the window I can see the expanse of Oxfordshire landscape lit brilliantly by a sliver of moon. Oh how many times I've stared out at this view. Its the perfect mise en scène really... to think about pain.

There are so many people I owe my deepest thanks.

To Professor Irene Tracey for being a superb supervisor, a valued mentor, and a wonderful friend. You have given me a sense of myself and my potential as a scientist unlike anyone I have ever worked for. I am honored to have been one of your students and I am excited to continue working with you in the future. Many, many thanks to you Irene.

To Dr. Jingyi Xie for being everything one could ever want in a collaborator; for being an excellent teacher, an unphasable optimist in the face of broken scanners, blank brains and buggy scripts; for being a wonderful friend; for showing me the way.

To Dr. Rebeccah Slater for continuing to be my guiding light from the day I started in Mariah's lab at UCL to now. Thank you for being the best *ad hoc* supervisor a student could wish for; and more importantly, for being a great friend. When I think of the type of scientist I hope to one day become, I think of you!

To Dr. Katja Wiech for always having time for me; for being my toughest critic; for being my greatest supporter; for being an excellent role-model and a wonderful friend. Thank you for graciousness and for the totally organic, cruelty-free snacks!

To Dr. Katie Warnaby for graciously taking me under her wing at the FMRIB Centre; for patiently teaching me the basics of functional imaging; for letting me be a part of her research; for being a brilliant colleague; for being a wonderful friend.

To Dr. David Bennett for being a brilliant *ad hoc* second supervisor; for being a superb collaborator and an excellent role model. Thank you for giving my work some context. I promise we will get that study published.

To Dr. Eugene Duff for not killing me for asking the most banal questions; for challenging me every step of the way to make my science better, stronger, more relevant; for reminding me that all is not lost when in fact all in fact has been lost; for being an ace friend.

To Dr. Tamar Makin for being everything one could want in a friend; for being everything one should dread in a reviewer; for being an endless supply of wisdom; for the endless chat and the non-stop silliness. What can I say, you're the best.

To Dr. Yazhuo Kong; Dr. Tom Okell; Dr. Michael Chappell; Dr. Emily Johns; Kathryn Paterson; and Dr. Juan Ramirez for being brilliant, insightful, and reliable collaborators. People would kill to have you on their team and I would kill to keep you.

To the PI's of the LPC. In particular, to Tony, Mac, Andrew, Kenji and Mariah for your guidance and expert training.

To all the members of the Pain Group at FMRIB, especially Dr. Jon Brooks, Dr. Steve Gwilym, Dr. Roisin Ni Mhurcheartaigh, Dr. Vishvarani Wanigasekera, and Dr. Katherine Fairhurst for being the best, most hilarious, lab ever.

To Apple and my dearest friend, caffeine...without you I am nothing.

To Sue and Marilyn for always sorting us out...without you FMRIB is nothing.

And last but certainly not least, I would like to thank my wonderful family and friends that have been there for me every step of the way. I can't wait to discuss each chapter with you!

I feel particularly thankful to have had the opportunity to not only work with so many brilliant people but also, to be able to call them my friends. For this, I am truly lucky.

II. Publications arising from this thesis

Segerdahl A.R., Xie J., Paterson K., Ramirez J.D., Tracey I., Bennett D.L.H. (2011). Imaging the neural correlates of neuropathic pain and pleasurable relief associated with inherited erythromelalgia in a single subject with quantitative arterial spin labelling. Pain, *In Review.*

Segerdahl A.R., Xie J. Duff E., Kong Y. Minett, M., Okell T. Tracey I. (2011). Imaging the neural correlates of a parametrically modulated tonic mechanical pain state using arterial spin labelling. Pain, *In preparation.*

Segerdahl A.R., Xie J., Chappell M., Jezzard P., Tracey I. (2011) Imaging absolute CBF changes across a whole-brain volume during tonic pain in healthy subjects. *In preparation.*

Segerdahl A.R., Xie J. Duff E., Kong Y. Minett, M., Okell T. Tracey I. (2011). Imaging the neural correlates of ongoing, parametrically modulated, mechanical pain in healthy human subjects using arterial spin labelling. Society for Neurosicence Abstract Presentation; SFN 2011, Washington D.C.

Xie J., Segerdahl A.R., Tracey I., Jezzard P. (2011) Simultaneous functional and quantitative ASL: an optimal tool for imaging ongoing pain states. ISMRM Abstract Presentation; 19th Annual Meeting, Montreal.

Xie J., Segerdahl A.R., Li L., Brooks J., Andersson J., Tracey I., Jezzard P. (2010) A true whole brain arterial spin labelling perfusion fMRI Technique. HBM Abstract Presentation; 16th Annual Meeting, Barcelona.

III. Declaration

I declare that the work presented in this thesis is my own and has not been submitted for any other degree in this or any other university or institute of learning.

IV. List of abbreviations

3D	3-dimensional
ACC	Anterior cingulate cortex
ANOVA	Analysis of variance
ASL	Arterial spin labelling
BET	Brain extraction tool
BOLD	Blood oxygen level dependent
CASL	Continuous arterial spin labelling
CNS	Central nervous system
DLPFC	Dorsal lateral prefrontal cortex
DMPFC	Dorsal medial prefrontal cortex
EEG	Electroencephalography
EPI	Echo planar imaging
EV	Explanatory variable
FEAT	FMRIB expert analysis tool
fig	Figure
FIRST	FMRIB's integrated registration and segmentation tool
FLIRT	FMRIB's linear image registration tool
FNIRT	FMRIB's nonlinear image registration tool
FMRI	Functional magnetic resonance imaging
FMRIB	Functional magnetic resonance imaging of the brain
FOV	Field of view
FSL	FMRIB software library
GLM	General linear model
GRASE	Gradient and spin echo
L	Left
MCFLIRT	Motion correction FMRIB's linear image registration tool
MELODIC	Multivariate exploratory optimized decomposition into independent components
MNI 152	Montreal Neurological Institute 152 average brain
MRI	Magnetic resonance imaging
Multi	Multiple
N Acc	Nucleus accumbens
NRS	Numerical rating scale
OFC	Orbital frontal cortex
PAG	Periaqueductal grey
PASL	Pulsed arterial spin labelling
pCASL	Pseudo-continuous arterial spin labelling
PE	Parameter estimate
PET	Postitron emission tomography
PCC	Posterior cingulate cortex

PFC	Prefrontal cortex
PPI	Psychophysiological interaction
R	Right
rACC	Rostral anterior cingulate cortex
RF	Radio-frequency
ROI	Region of interest
SI	Primary somatosensory cortex
SII	Secondary somatosensory cortex
SMA	Supplementary motor area
SNR	Signal-to-noise ratio
TE	Echo-time
TI	Inversion time
TR	Repetition time
VAS	Visual analogue scale
VTA	Ventral tegmental area
zstat	z statistic

Chapter 1

Introduction

1.1 Pain: a lifesaver, a disease, an epidemic

The sensation and experience of pain is, in an acute setting, an essential, evolutionarily well-conserved ‘alarm bell’ to warn of imminent danger. The primary reason we experience pain is to signal the possibility of tissue damage. Consequently, pain triggers both a spinally mediated reflex-withdraw response to remove oneself from the noxious insult in addition to imprinting a strong cognitive signal so that we remember and therefore learn from the experience to prevent it from happening again.

However, when acute pain becomes chronic, its evolutionary utility is lost. What remains is a disease of the central nervous system that puts the sufferer in a constant state of misery. If left unabated, the pain will gradually destroy both the mind and body. Present estimates project that approximately 20% of the adult population in the western world suffer from chronic pain, which is defined as pain that persists longer than 3 months (1,2). In the United States alone, it is estimated that 116 million adults- more than that total affected by heart disease, cancer and diabetes combined; are chronic pain sufferers (3). This is linked to significant financial burden on society due to lost productivity in the work place and continual referral to the health care system (1,4). For example, the most recent consensus report from the Institute of Medicine projects that pain costs the US up to $635 billion each year due to these factors. Currently, no pain therapies are able to cure chronic pain. For example, treatment success with presently available chronic pain drugs is low as it has been shown that the best options provide a maximum of only 30% relief, on average (5). To add, the most

potent painkillers prescribed, opioid-based drugs like OxyContin and Vicodin, are also some of the most heavily abused drugs on the market. Recent reports document how overdoses from prescription painkillers are now a leading cause of accidental death in the US (6).

The reasons for the lack of safe, clinically effective drugs are many. The common theme throughout this discussion is that conventional measures of pain (e.g. intensity or degree of physical impairment) fail to reflect both the complexity of pain as a multisensory experience. The pain a person experiences is an interpretation of nociceptive input from the peripheral nervous system filtered through a complex set of higher cognitive factors that include one's emotions, memories, personality traits, and cognitive state. Additionally, factors such as a person's hormones, genetics, and neurophysiology (e.g. neurochemical and structural phenotypes) will also have an effect on how a person constructs a particular sensation of pain. In short, pain is a subjective experience. Unsurprisingly, this complexity can't be fully modeled in an animal. At present, the common approach to study this is based on verbal reporting. Which is to say that our experimental process to date relies on reducing this complexity to a linear, numerical scale where a patient is meant to condense a complex, often semi-conflicting 'experience' into a single word or number. It can be argued that there is a substantial disconnect between what the sufferers of chronic pain are experiencing and the behaviour pain scientists are studying.

Human pain research needs to implement investigative approaches that incorporate a multifaceted approach to quantify the complex set of cognitive and

psychosocial variables through which nociceptive signals are filtered through to yield the sensation of pain. Without this insight, development of novel, reliable treatment options will remain elusive.

The advent of pain neuroimaging has provided a massively powerful tool to this end. Not only can functional imaging be used to procure a much-needed objective measure of the sensory aspects of pain but also it can be used to reliably investigate the emotional, cognitive and contextual aspects of the pain experience. Implicitly, pain imaging experiments test the hypothesis posited first by Jensen et al. (2003) and echoed recently by Backonja & Woolf (2010) that states pain mechanisms are reflected and therefore recognizable by the specific pattern of pain-related symptoms and signs they elicit (7,8). Here, much has been done in the way of investigating the neurophysiology of acute pain with blood oxygen level dependent (BOLD) FMRI (9). The key finding from these studies is there no single 'pain centre' in the brain; but rather that acute pain recruits a large widely distributed network of brain regions (10). Specifically, it is well known from BOLD pain studies that various key cortical regions, well known to play integral roles across various non-pain related functional tasks, are recruited during acute pain experiences and even show modulation in the presence of pain relieving drugs. This core network is constituent of regions such as primary somatosensory cortex I (SI), secondary somatosensory cortex (SII), insula cortex, anterior cingulate cortex (ACC), prefrontal cortex (PFC), and the thalamus (11,12). However, regions such as the amygdala, hippocampus, basal ganglia, and sub-regions of the parietal and temporal areas have been shown to play a role in pain processing (13).

Given that a person's pain is a subjective experience influenced by many factors, it is not surprisingly that there are numerous cortical regions recruited during the experience. Each of these regions has a well-defined cortical role that is not necessarily pain-specific. Rather, it is the dynamic interplay between these regions in which the overall experience of pain is able to emerge – as a complex entity constituent of multiple sensory, cognitive, and psychological variables. So, it is conceivable that while core cortical regions are likely to be observed during pain, it is also highly likely that various other regions may be present depending on the experience. Recently, this concept has evolved to suggest that individuals, especially those suffering from chronic pain, have a specific cerebral signature for their pain (14). It is not unrealistic to imagine the future of pain medicine will include tailoring treatment to each person's unique experience. Before it is possible to develop bespoke pain treatments for individuals, it is first of paramount concern to understand how pain arises from nociception; and further, how the pain that is experienced can evolve into a disease of the CNS.

1.2 From nociception to pain

Pain arises from nociception; the neural coding and processing of noxious stimuli. Nociceptors, which were first described by Sherrington (1906), are the basic neural units that process painful stimuli and exist in the peripheral nervous system (15). As mentioned previously, pain is the conscious perception of sensory information transmitted by nociceptors layered with a complex set of cognitive factors that give the sensation a highly personalized weight. This summated sensation is what we call pain. The process through which pain

emerges from the conscious perception of nociceptive input occurs in the brain. Nociceptors are responsible for translating information about the noxious insult (e.g. stimulus type, magnitude, duration, location) from the periphery to the brain.

1.2.1 Nociceptors

Nociceptor structure and function is a complex and continually evolving field of research. There is a great deal we still do not know about how noxious information is transmitted to the brain, and further how this trajectory changes in the context of chronic pain. In general though, there are some fundamental concepts about nociceptor structure and function that are widely accepted. Specifically, there are two main subtypes of nociceptors, defined primarily by their axonal structure, and relatedly, how they transmit action potentials to the CNS.

Much of our understanding about somatosensation in the periphery originates from extensive single and multi-unit recordings done in various animal models. The results from these studies helped to articulate a working understanding of how to categorize first-order neurons in the periphery based on responsiveness to various modalities. In general, first-order afferents can be placed into three groups: mechanosensitive, thermosensitive and nociceptive. These neurons can be further categorized based on their size and conduction velocity. For example, the myelinated, relatively large axonal diameter Aβ fibres conduct at 50 m/s (16,17). In contrast, the smaller myelinated Aδ fibres conduct at approximately 20 m/s and are known to code sharp, prickling sensations (16). The thinest and

slowest conducting fibres, also known as C-fibres transmit action potentials at conduction velocities < 2m/s (Kandel et al. 2000).

An elegant microneurographic study exploring the stimulus-response features of these afferent fibres was completed by Vallbo et al. (1979) in which electrical stimuli were delivered to glabrous skin of the hand in healthy human subjects. Microneurographic recordings of stimulus response profiles of specific single-units subtypes were recorded in response to increasing stimulus intensity. Here, at threshold for perception, the electrical stimuli elicited activation of Aα units to yield a sensation of light tapping or fluttering. When the stimulus intensity was increased 5-10 times the threshold of perception, Aδ units were recruited. With single impulses, subjects reported the sensation of sharp pricks. When the stimulus intensity was repeated at a frequency of 50Hz, the subjects reported intense pain. A subsequent increase in the stimulus intensity applied by 15-20 times threshold recruits C-fibre units. Here, single impulses excite the perception of acute sharp pain followed by an aching “after pain”. With repeated stimulation at 5Hz, subjects reported a sever burning pain sensation. Additionally, with repeated stimulation both the C-fibre responsiveness and the subject’s perception of pain abated thereby suggesting a key feature of C-fibre physiology is its relatively quick exhaustion with continued stimulation (16).

This study is helpful in explaining how different fibre types are recruited at different stimulus intensities. However, while electrical stimuli are an excellent method of parsing out the stimulus-response profiles of afferent subtypes, this

method does not help explain the way in which different fibre types are recruited by different stimuli.

Aβ fibres respond to mechanical stimuli applied to the skin. However, the specific stimulus-response function of these fibres depends on the specific subclass of Aβ fibre being recruited. In general, there are four Aβ subclasses which can be differentiated based on their receptive field size and adaptation to sustained stimulation. These subtypes include: rapidly adapting (RA), Pacini fibres (PC), slowly adapting type I (SAI), slowly adapting type II (SAII) (18,19,20,21,22). Single-unit recordings in primates studied the relationship between stimulus intensity and extent of afferent activity in SA units. The key finding from these studies was that the relationship between SA activity and stimulus intensity could be described by power functions thereby suggesting that there is a linear relationship between SA unit activity and the magnitude of mechanical stimulus applied (23,24,25). These findings were then confirmed in humans by Gybels & van Hees (1972) who showed that there was a linear relationship between the recorded neural response and the subjects' perception of the stimulus intensity applied (26).

In order to understand the stimulus-response profile of Aδ and C-fibres investigators had to remove the Aβ component by using a compression-block preparation. Here, before any recordings are made, a constant mechanical stimulus is applied to the subjects arm (i.e. nerve compression) to exhaust the Aβ fibre component. For example, groundbreaking microneurographic work by Torebjork & Hallin (1970) used this technique to record the first single unit

recordings of C-fibres in humans. This initial study successfully characterized the receptive field population, conduction velocity and latency changes with repeat stimulation of C-fibres in addition to helping differentiate C-fibre responses from the more ubiquitous sympathetic fibre responses (27). The results from this study showed that there are a range of distinct C-fibre subtypes innervating the periphery which exhibit a range of conduction velocities (1.8-0.4m/s); respond to intense mechanical, thermal and chemical stimuli and even showed the presence of low-threshold C-mechanoreceptors that respond to both touch and cooling (27). Subsequent investigations showed how specific C-fibre type are involved in coding intense needle pricks and pinching (16); cooling stimuli below 20[degrees] C (28); warming fails to elicit a response (29,30); heating (> 45°C) recruits a strong response (29,30,31). Additionally, various studies showed how C-fibre responsiveness changed post-injury such that the fibres became hypersensitive to both mechanical and thermal stimuli (32,33). Investigators were also able to show how chemical irritants such as histamines, acetic acid, and potassium chloride were sufficient to induce a strong C-fibre response (29, 34, 35).

A key component of these initial investigations was to articulate the stimulus-response functions of specific C-fibre subtypes to changes in stimulus intensity. In general, due to the thin, unmyelinated nature of C-fibres, the basic stimulus response is characterized by an initial burst of activity that tapers quickly with prolonged stimulation. Generally, C-fibre discharge rate increases with stimulus intensity; whereby the most robust response is triggered by stimulus intensity that threaten to damage the skin (16). Occasionally, units may continue to

discharge after the stimulus has ceased (16). In the case of C-fibres that respond to chemical irritants, it was observed that even after the stimulus has ceased the C-fibre response may be maintained for minutes with bursts of activity interspersed with quiescent intervals (29; 35). Additionally, it was observed that while acute noxious stimuli elicit C-fibre responses in which the burst activity is approximately 40-115 spike/s; when the stimulus is maintained the frequency drops off precipitously to only a few spikes/s (16). Additionally, repeated stimuli often results in depleted after-discharge and/or 'fatigue' (27, 29, 30, 35).

1.2.2 Trajectory of pain stimulus: from the periphery to the brain

Sensation requires the integration of information gathered from several subcortical and cortical sources. This information ascends to the cortex through several distinct, hierarchically organized pathways. The spinal cord is a key site of integration of sensory information gathered from the periphery into the central nervous system. For example, nociceptive input can trigger reflex-withdrawal response as it synapses to second-order neurons responsible for transmitting the information to the cortex. Likewise, descending tracts from the cortex synapse onto the dorsal horn and are capable of either increasing (pronociception) or decreasing (antinociception) the nociceptive input.

Anatomically, the spinally cord consists of a core region of gray matter that is enveloped by a layer of white matter; the overall structure of which resembles a pair of wings constituent of the dorsal (posterior) and ventral (anterior) horns. Specifically, the dorsal horn gray matter is constituent of axons of sensory nuclei

whereas the ventral horn gray matter is made up of motor nuclei. Additionally, an array of interneurons are present within the gray matter of the ventral and dorsal horns to integrate the multiple sources of communication between nociceptors, descending circuits and motor neurons. The white matter surrounding the gray matter can be divided into dorsal, lateral and ventral columns: each of which defines a specific variety of axon bundles responsible for relaying sensory input up to the cortex (i.e. ascending tracts) and from the cortex down to the spinal cord (i.e. descending tracts). Specifically, the dorsal column contains ascending axons that are responsible for transmitting sensory information to the brainstem. The lateral and ventral columns constitute parallel pathways made up of both ascending and descending axons from the brainstem and cortex which are responsible for relaying sensory information to the cortex whilst simultaneously controlling muscle movement and posture (17).

The dorsal root ganglia (DRG) defines the bundle of sensory neurons that simultaneously innervate the skin, muscle and joints of the periphery and the spinal cord. The DRG sits within the vertebral column adjacent to the spinal cord and consists of both peripheral and central processes: the former innervates the skin; the later innervates the dorsal horn. At the level of the dorsal horn, the DRG branches into both local and ascending branches to allow for simultaneous activation of local reflex circuitry and higher brain centers. Most importantly, the DRG axons are somatotopically organized such that information about stimulus location on the body is maintained as it ascends to higher cortical structures (17, 36).

In general, different types of sensation (touch, pain, body position) are processed through related but unique cortical pathways. However, primary afferent fibres are the first relay point for sensory input to enter the body and become integrated into the central nervous system. Here, the first synapse between primary afferent and the CNS occurs at the ipsilateral dorsal column. Traditionally, tract tracing studies were used to map out dorsal horn connectivity. Here, using immunohistochemistry, researchers began to articulate the complexity of how primary nociceptor afferents innervate specific laminae of the dorsal horn.

For example, nociceptors that express peptides such as substance P, calcitonin gene-related peptide (CGRP) and somatostatin (e.g. termed 'peptidergic' neurons) were noted to project mainly to lamina I and II (outer). In contrast, non-peptidergic expressing nociceptors that are IB4 positive cells (i.e. 'non-peptidergic') are said to innervate lamina II (inner) (37,38,39,40). To add, laminae layer I (LI) is typically innervated by large, long axons that project directly to higher cortical regions; while LII neurons are typically short and project locally (41). Here, LI and II are constituent of mostly nociceptors (e.g. 75% of overall neural population); whilst LV are mostly wide-dynamic range (WDR) neurons that code both innocuous and noxious stimuli (42) (see figure 1).

While these tracing studies provided integral insight towards understanding the complexity of dorsal horn innervation, they are limited by various technical limitations. Recent advances in the development of transgenic animal models have made it possible to more precisely observe the specific anatomy of the dorsal horn without the need for injected dyes or radiotracers. For example, recent work suggests that nociceptive information is transmitted to the CNS by

both convergent and divergent pathways. Specifically, Braz and Basbaum (2009) used a transgenic mouse model with Cre-recombinase dependent expression of a transneuronal tracer to differentiate the extent to which myelinated and unmyelinated afferents engage different spinal circuits (43). Results from this study show that spinal neurons in lamina I are postsynaptic to both classes of nociceptors (i.e. both myelinated (i.e. small Aδ fibres) and peptidergic, unmyelinated afferents). Additionally, these researchers observed that nociceptors have distinct (i.e. divergent) connections in other laminae. Lamina II consists of the following mapping: LII_{outer} receives unmyelinated peptidergic inputs; LII_{inner} receives unmyelinated fibers in the IB4+ zone and myelinated fibres in the PKCγ+ zone. Deeper laminae (e.g. III-V) are innervated directly by myelinated fibres but are mostly indirectly innervated (i.e. route of innervation is polysynaptic) from unmelinated fibres.

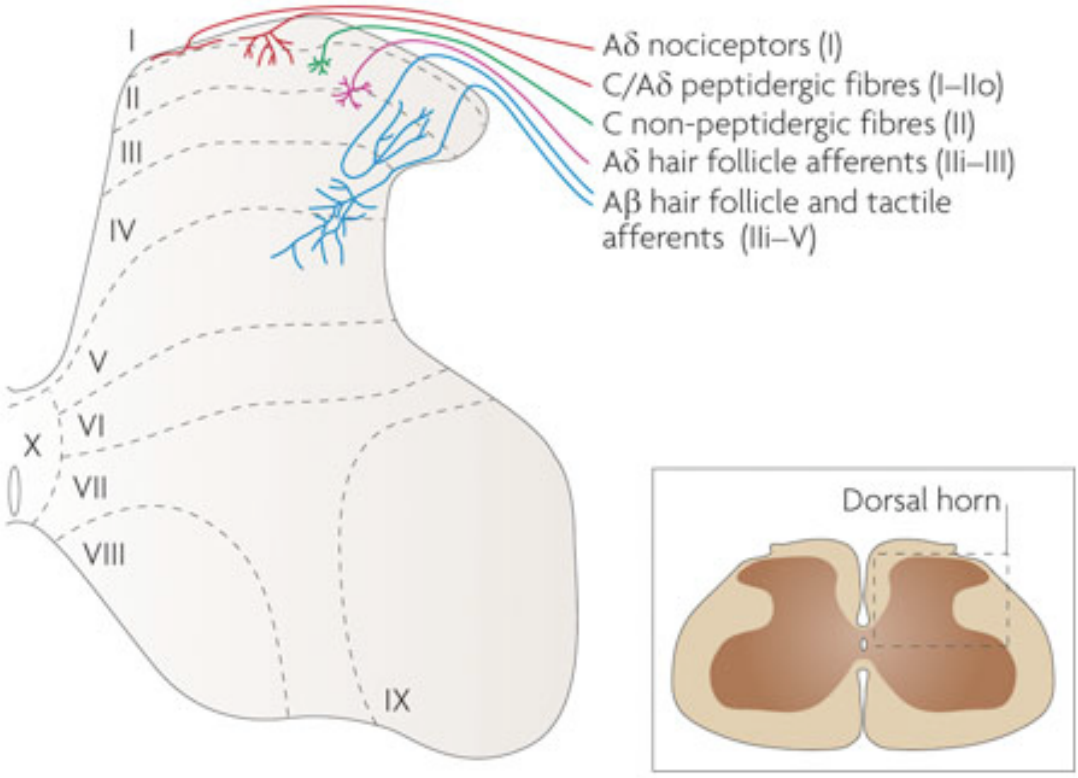

Figure 1: Schematic of a rat dorsal horn. Primary afferents innervate specific lamina of the dorsal horn in a specific and well organized way defined both by each fibre's morphology and function. For example, Aβ tactile and hair afferents terminate in lamina III-V, with some fibres innervating lamina IIi. Aβ hair follicle afferents innervate both lamina II and III whereas Aδ nociceptors innervate lamina I. Peptidergic primary afferents (i.e. A[delta] and C fibres) arborize in lamina I and IIo, while non-peptidergic C fibres terminate within the central part of laina II. This schematic was adapted from Todd, A.J. 2010 (44).

1.2.3 Spinal pain processing: from the dorsal horn to the cortex

From the dorsal horn, a second order neuron then transmits this sensory information (including: somatotopy, intensity, modality) to the forebrain by way of the brainstem and the thalamus via distinct pathways that include the spino-thalamic (STT), the spinoreticular (spinoparabrachial) and the spinomesencephalic tracts (44,45). Specifically, sensory input from the lower body projects along the gracile funiculus and terminates in the gracile nucleus; while input from the upper body runs in the cuneate funiculus and terminates in the cuneate nucleus. Neurons in the gracile and cuneate nuclei are constituent of axons that cross to the opposite side of the brain and ascend to the thalamus where they terminate in the ventral posterior nucleus (17).

The thalamus defines the dorsal portion of the diencephalon and is commonly referred to as the gatekeeper for information entering the cerebral cortex. While this description belies the multitude of functions the thalamus performs, it appropriately highlights its role as a main relay site to the somatosensory cortex. Additionally, various thalamic sub-nuclei project to frontal cortices, amygdala, hypothalamus, basal ganglia, and the midbrain thereby implicating it in the integration of sensory information with a range of cognitive tasks such as memory, emotion, and cognition.

To note, our understanding of spinal processing of nociceptive information is still limited. For example, it is not yet well known how the spinal cord is able to maintain a wealth of information about the noxious input (i.e. somatotopy, intensity, modality, laterality) as it ascends to the cortex.

More recent investigations employing the use of transgenic Cre-recombinase mouse models have begun to delineate the specific pathways through which nociceptive input ascends to the brain. Recent work by Braz JM et al. (2005) suggests that there are distinct and separable ascending tracts through which nociceptive input ascends to the brain depending on whether the primary afferent nociceptor is peptidergic. Here, by selectively targeting Nav1.8+ nociceptors (i.e. non-peptidergic) this group was able to map the projection path from the deep lamina of the dorsal horn to both limbic centres and the globus pallidus (43). This path was distinct from peptidergic expressing nociceptors which primarily project to the thalamus and the brainstem.

Presently, there are only a few studies presently able to untangle the complexity of multiple synaptic circuits involved in transporting nociceptive information from the periphery to the cortex. Considerable work is still needed to fully understand exactly how nociception arrives in the brain and further, how this pathway is likely to change in the context of different pain pathologies.

1.2.4. Brain: where pain emerges from nociception

As discussed previously, because pain is a complex, multifactoral experience, multiple cortical regions are recruited in the generation of a given pain state. The type of pain experienced is largely a factor of the specific, individualized aspects of the person in pain. As such, it is useful to think of cortical activation during pain not as triggering a well-defined entity of regions necessarily, but rather that key cortical regions likely act as a kind of substrate that is modulated by different brain regions depending on the type of pain being experienced (11). It is the

dynamic interaction between cortical and subcortical regions that the overall pain state emerges and is defined by the sufferer.

Additionally, it is helpful to note that because pain is a complex, subjective experience it is difficult to quantify in a reliable and reproducible manner. Before the advent of neuroimaging, researchers were fundamentally limited by nature of trying to reduce this complex experience into a single word or phrase. Neuroimaging allows us to look at the experience of pain by observing what parts of the brain are active during pain. The key here is to view these activations not as surrogate markers of pain per se but rather to see these activations as defining a network of regions from which the experience of pain emerges.

Historically, the notion that pain is generated by the brain was not commonly accepted as no one was able to show any relationship between cortical lesions and pain; nor were investigators able to elicit pain by electrically stimulating the superficial cortex (46,47). However, with the advent of more invasive radiolabel-based perfusion imaging techniques, researchers began to understand that multiple cortical regions were significantly more active during experimentally induced pain compared to rest. Lassen, N.A. et al. (1978) injected the radioisotope ^{133}Xe to show that experimentally induced heat pain triggered increased perfusion in frontal cortices (48). Subsequent PET and SPECT imaging studies further elucidated these initial findings by showing that experimentally induced heat pain was able to excite multiple cortical regions compared to a the absence of pain (50,51,52). To date, numerous PET and BOLD FMRI pain experiments have repeatedly shown various parts of the brain to be involved in pain processing. An early review of the pain imaging literature

by Apkarian, A et al. (2005) described these key regions to include the: primary and secondary somatosensory cortices (SI and SII: 53,54,55,56,57); anterior cingulate and insula (58,59,60); prefrontal cortex (PFC: 54,61); thalamus (52).

A more recent review of the pain neuroimaging literature further articulated these regions to include: sensorimotor cortex at the central sulcus (S1/M1); parieto-insular region near the lateral operculum (SII); anterior insula; anterior cingulate (ACC); prefrontal cortices; periaqueductal gray (PAG); hypothalamus; amygdala; hippocampus; and cerebellum (63,64). While the specific neurophysiological function of each of these regions is not wholly pain specific, considerable work has begun to articulate how each of these regions is likely to be involved in processing pain. For example, the posterior insula is often discussed as playing a key role in the sensory-discriminative aspects of pain processing as it receives afferent input from the dorsal horn of the spinal cord and has been shown to encode a somatotopic map of the body (65,66). In contrast, the anterior insula is known to have connections to key descending control-related brainstem structures such as the RVM and has been shown to play a key role in mediating the affective dimensions of pain (67,68). In addition, structures such as a the amygdala are well known from rodent pain investigations to play a role in facilitating pain hypersensitivity during injury (69,70). In humans the relationship of amygdala activation and pain perception is less clear. However, a few studies have shown that anxiety-related increases in pain perception are related to increased activation in the amygdala (69).

While these regions are consistently reported to be involved in pain, there are a few key caveats to consider: i) each of these regions have distinct cortical roles independent of pain processing; ii) one does not necessarily see all of these

regions in every pain neuroimaging study; iii) often, other cortical regions are recruited depending on the type of pain experiment. For example, regions such as the nucleus cuneformis (NCF), the inferior frontal gyrus, putamen, and nucleus accumbens are also often linked to aspects of pain processing. Overall, the key conclusion from a discussion of these regions is that there is no single cortical region devoted solely to pain. Which is to say, there is no P1 for pain as is the case for vision (primary visual cortex; V1) or motor (primary motor cortex; M1) (36). There is however regions such as the thalamus and the dorsal posterior insula that are often observed to receive direct input from the dorsal horn via the STT and therefore may act as gateway relay regions from which nociceptive afferent input is directed to a range of receptive cortical regions to process the pain (72,73,74).

1.2.5. Cortical regions of interest underlying pain processing

Recently, there has been a move within pain imaging experiments to articulate how the functional interaction and synchronicity between regions underlies key aspects of the pain experience. For example, from BOLD FMRI studies, there are a few well known 'pain networks' that are worth discussing to illustrate this concept.

Perhaps the most well known example of this is the descending pain modulatory circuit; an anatomically well-defined network of regions which can directly modulate spinal nociceptive processing to either increase (pronociception) or decrease (antinociception) the pain experienced (75,76,77,78,79). Here, the interaction of multiple regions including: the frontal lobe, ACC, insula, amygdala,

hypothalamus, periaqueductal grey (PAG), rostral ventral medulla (RVM), and nucleus cuneiformis (NCF) is able to modulate the pain.

Working in concert with other regions, it is possible for higher brain regions to harness the descending control circuitry to either increase or decrease pain depending on the experimental paradigm. Numerous imaging studies have interrogated the relationship between cognitive state and pain processing to highlight numerous functional interactions between nuclei of the prefrontal cortex and various other brain regions. For example, in the context of distraction, it has been shown how cingulo-frontal regions exert top-down control over the posterior thalamus and the PAG to reduce pain during a distracting cognitive task (80,81,82). Relatedly, studies of reappraisal wherein subjects are guided to reinterpret the meaningfulness of the pain experienced show that the pain experienced can be modulated to be less noxious. For example, Wiech, K. et al. (2006) showed that activity within the venterolateral PFC mediates the analgesic efficacy related to an increased belief that pain can be controlled (82). A similar study by Wager, T. et al. (2008) showed that activation within the dorsolateral PFC mediates the ability for a subject to regulate one's negative emotions to control their pain experience via modulation of both the nucleus accumbens and the amygdala (83).

It is also possible that regions, upon receiving nociceptive input, amplify its valence to induce a heightened overall pain experience. For example, various studies have shown that heightened anxiety enhances pain perception through parahippocampal-mediated mechanisms (85,86). Similarly, it was shown that in people suffering from fibromyalgia, those with higher castrophizing personality traits had significantly increased activity in brain regions well known to modulate

the anticipation of (e.g. medial frontal cortex, cerebellum), attention to (dorsal ACC, dorsolateral prefrontal cortex), and emotional aspects (amygdala) of pain (88).

Perhaps most interestingly, it has also been shown how these functional relationships between active regions changes in the context of chronic pain. For example, there is consistent evidence for increased activation in both the anterior insula and PFC across multiple chronic pain conditions (12, 89,90,91,92). Additionally, disruptions in the descending pain modulatory circuit (including regions such as: PAG, RVM, NCF, parabrachial nucleus (PB), and the dorsal reticular nucleus) is also consistently reported across central sensitized pain states (91,92); a key feature likely mediating the transition from acute to chronic pain post-injury.

To note however, there is considerable controversy about the meaningfulness of these activations. For example, a number of studies have shown that even in the absence of a painful stimulus, subjects are able to activate pain-related structures just by watching someone receive a painful stimulus (94,95,96); or by inducing a nocebo effect (84). More critical evidence of BOLD FMRI studies of pain have challenged the meaningfulness of these pain-related statistical maps, often reported as the “pain matrix”, by showing them to be similar active in non-pain related sensory tasks (97). The key conclusion from this study being that some BOLD FMRI investigations of acute pain states are potentially imaging mechanisms of salience-detection in general as opposed to anything specific to pain-processing alone.

1.2.6. Dynamic flow of information

While numerous pain imaging studies exist and often report lists of regions that show statistically significant associations with different pain stimuli, little is known about the dynamic flow of information between regions. This is mostly due to the technical limitations of FMRI: that it has high spatial but poor temporal resolution. In order to study how different pain-relevant regions function in relation to one another, multimodal experimental approaches are needed. This often entails either more invasive electrophysiology or complex dynamic modeling approaches. In general, from the handful of imaging studies focused on this, there appears to be an emerging conceptual framework to suggest that the brain processes nociceptive inputs in parallel, across multiple receptive regions simultaneously (i.e. not in a linear, sequential region-by-region approach) (98). Additionally, electrophysiological investigations have shown that the emergence of perception occurs at a much later time-point relative to the very early nociceptive-specific potentials that reach the brain. This suggests that perhaps conscious detection of painful stimuli arises after a complex integration of initial early synaptic events occurring across multiple regions (99,100).

At present, we are not capable of employing FMRI alone to interrogate how the pain-relevant regions integrate nociceptive information with higher cortical processes to generate the overall experience of pain. Arguably, the field of pain imaging is still at a point where we do not yet know which regions discussed above are active during a tonic pain state; and further, the extent to which each region remains active over time. The goal of this thesis is to develop the perfusion imaging technique arterial spin labelling (ASL) to image the brain during tonic pain. It is our hope that the work of this thesis will provide a basic

methodological and conceptual framework to begin to understand how the brain remains active during various ongoing pain states.

1.3 Cerebral blood flow

Cerebral perfusion ensures brain tissue is maintained by a constant delivery of nutrients and oxygen. The major direction of blood flow into the brain is up through the neck towards the centre of the brain where it extends both to the frontal and parietal-occipital lobes simultaneously.

Fundamentally, the basic technical workings of ASL exploit the cerebral vasculature to non-invasively image how perfusion changes across different parts of the brain. Specifically, ASL tags blood at the level of the Common Cartoid and Vertebral arteries: the main sources of arterial blood delivery to the brain. So, as the fresh arterial blood is ascending to the brain, ASL manipulates the magnetic properties of the blood to effectively ‘tag’ it. Once tagged, the arterial blood is then transported across the cortex by way of the anterior, middle and posterior cerebral arteries. The capillary beds form the essential juncture between the arterial supply and grey matter to allow delivery of essential nutrients to neurons. It is here that the ‘tagged‘ signal is transfered to the nearby tissue; and consequently, this is as close to the actual site of neural activation as one can get when using this technique. It is in this way that ASL measures perfusion as a correlate of neural activation.

1.3.1. Neural activity, metabolic demand, and changes in CBF

The human brain, though only a fraction of the total body weight, consumes 20% of global metabolic energy output at rest (102,103). In general, neural activity is highly energy demanding and these costs are primarily associated with maintaining the necessary ionic stoichiometry across the cell membrane (104,105). For example, researchers have measured the relationship between membrane conductance, neurotransmitter release and amount of ATP consumed to generate a signal. Conclusion from these studies shows that energy usage is dominated by action potential propagation along axons and the related postsynaptic current propagation (106).

If every neural signaling event uses energy and neurons are constantly active, a basic question to pose then is how are neurons able to sustain activation given their very high metabolic costs? Briefly, the capacity for a neuron to fire is reliant on adequate supply of oxygen and nutrients. The maintenance and availability of these staples are orchestrated by a complex and not entirely well known relationship between neurons, astrocytes, surrounding vasculature and an array of chemical intermediaries. Historically, researchers such as Mosso (1880) and Roy & Sherington (1890) hypothesized the concept that an increase in neural activity paralleled a related change in CBF (107,108). Further, they posited that these events were linked by 'vasoactive agents' released into the extracellular space. Until recently, this concept has dominated our basic understanding of the relationship between neural activity and changes in CBF: active neurons generate a metabolic signal (e.g. change in oxygen, glucose, etc) to trigger an increase in CBF. This signal could be anything from a lack of O_2 or glucose to an

increase in CO_2. However, experimental manipulation of any of these candidate 'signals' does not lead to a predictable change in CBF.

Recently however, new insight into the link between neural activity, oxygen consumption and changes in CBF posit that this relationship is far more complex than originally thought. As discussed recently by Atwell, D. et al. (2010), it is more likely that neural demand for blood is mediated by a 'feed-forward mechanism' in which neurons and astrocytes are able to signal directly to both blood vessels; leading to a cascade of glutamate-mediated release of vasoactive agents on surrounding vasculature (109).

Much of the current theories about this process can be divided into mechanisms associated with neural versus astrocyte control of vasculature changes. Neural communication to vessels entails synaptic release of glutamate such that there is an increased conductance of Ca^{2+} into the cell, leading to activation of nitric-oxide (NO) synthase, and subsequent NO release to trigger vasodilation (109).

More recently however, the role of astrocytes in this process has become more pronounced. Morphologically, astrocytes form a physical link between neurons and the surrounding vasculature, as they are well documented to have end-feet that bridge both synapses and blood vessels (110). In this way, it is possible that astrocytes are ideally positioned to link neurons to the surrounding vasculature. However, the mechanism through which this is done remains unclear. One main theory is that astrocytes are able to initiate vasodilation by releasing K^+ from their end-feet. Here, a release of K^+ leads to hyperpolarization of smooth muscle resulting in vasodilation. For example, it was shown that glutamate released from neurons is able to cause a release of K^+ astrocytes by way of activation of

Ca-mediated K^+ channels on the endfeet (109,110). Additionally, it was observed that astrocytes are able to control CBF via archadonic acid metabolites. Here, glutamate released from neurons acts on metabotropic glutamate receptors (mGlu-R) on astrocytes leading to an increase in Ca^{2+}_{in}. Subsequently, phospholipase A_2 is activated leading to the production of arachidonic acid (and, consequently, related metabolites such as prostaglandins and epoxyeicosatrienoic acid (EET)), which are capable of triggering vasodilation (111,112,113,114,115).

1.4 Imaging brain function

It is reasonable to conclude from the work presented above that absolute energy consumed does not directly regulate CBF as a change in CBF is related to an array of synchronized changes specific to both neurons and glia. Multiple players are involved with complex interactions that are yet to be fully described. For example, the functional dynamics of how endothelial cells, pericytes, smooth muscle cells, extracellular ions, metabolic factors, and neurotransmitters interact and change to regulate CBF is complex and non-linear. In contrast however, traditional FMRI employs a basic understanding of the relationship between local neural activity and CBF changes; namely that an imaging blob reflects energy use by active neurons specific to an experimental task. Here, it is not possible to quantify exact changes in neural activity as would be possible with intra- and/or extracellular electrophysiological recordings. Instead, FMRI analysis employs a 'transfer function' to describe the relation between local neural activity based on a well-characterized change in specific imaging parameters. It is perhaps more

realistic to state that FMRI visualizes neurovascular signaling related to neural activation (116).

1.4.1. fMRI: imaging metabolic features relative to neural activity

Types of FMRI tools can be categorized based on the metabolic variable it is weighted to image. In the case of BOLD FMRI, images are constructed based on magnetic signal disturbances caused by fluctuations in oxygenated:deoxygenated haemoglobin (Hb) content in venous blood, proximal to the site of neural activity (117,118). Because oxygenated-Hb is diamagnetic (all electrons are paired), it does not have a magnetic moment and is therefore incapable of disrupting a magnetic field (i.e. induces very little signal change). In contrast, deoxygenated-Hb is paramagnetic (has unpaired electrons) and therefore is capable of disrupting a magnetic field (causes signal loss). When neurons become active, the related demand for oxygen is met with an abundant increase in oxygenated-Hb. Because not all oxygen that is delivered is used, there is an over-abundance of oxygenated-Hb in venous tissue. This causes a large increase in magnetic signal. As discussed previously, the signal(s) that generate(s) this changes in Hb, and therefore links neural activity to changes in the magnetic signal is a complex composite of factors that change with respect to neural activity. These factors include activity-dependent changes in CBF, CBV, and $CMRO_2$.

ASL FMRI however utilizes changes in CBF alone to monitor changes in neural activity. Here, the statistical image that is observed relates to the amount of magnetically tagged arterial blood that flowed to various ‘active’ brain regions.

Meaningful signal in ASL FMRI relates specifically to the difference between images acquired when arterial blood is tagged (and therefore visible) versus 'control' images in which no tag is applied and only the background tissue signal is acquired.

1.4.2. Acquisition of meaningful signal: what do the fMRI images reflect?

In general, MRI uses a strong magnetic field to create images of biological tissue, and in the case of functional MRI, images of physiological events taking place therein. Regardless of the type of FMRI approach, imaging utilizes a well-synchronized combination of magnetic gradients and radio-frequency pulses of energy to manipulate the atomic energy states of electron spins within hydrogen atoms. In the case of BOLD, these H-spins are suspended within both oxy- and deoxygenated Hb localized in venous supply; whereas ASL is weighted to arterial (oxygenated) blood in arterial supply. In both, the ability to translate excitation-relaxation profiles of individual H^+- spins underlies the capacity for FMRI to decipher tissue –specific, spatially encoded information about brain activity.

When placed into a magnetic field such as what is commonly used in a 3T scanner, the spins will precess around an axis that is parallel with the direction of the magnetic field. Here, the spins are in the lowest (and therefore, most stable) energy state and are said to have longitudinal magnetization. If energy is applied to the system however (in the radio frequency range), the spins are excited to a high energy state in which longitudinal magnetization is converted to transverse magnetization; thereby resulting in the spin precessing around an axis that is perpendicular to the direction of the magnetic field. This high-energy

state is unstable and results in the spin relaxing back into the low energy state in which the spin precesses about the longitudinal axis. For the spin to relax, it must emit energy (also in the range of RF) which, when recorded by the receive coils in the scanner, provides the information necessary to construct MR images.

Fundamentally, the goal of FMRI image acquisition is to optimize the reception of signal as it decays such that the difference between the rate of longitudinal recovery and transverse decay is maximal for various tissue types.

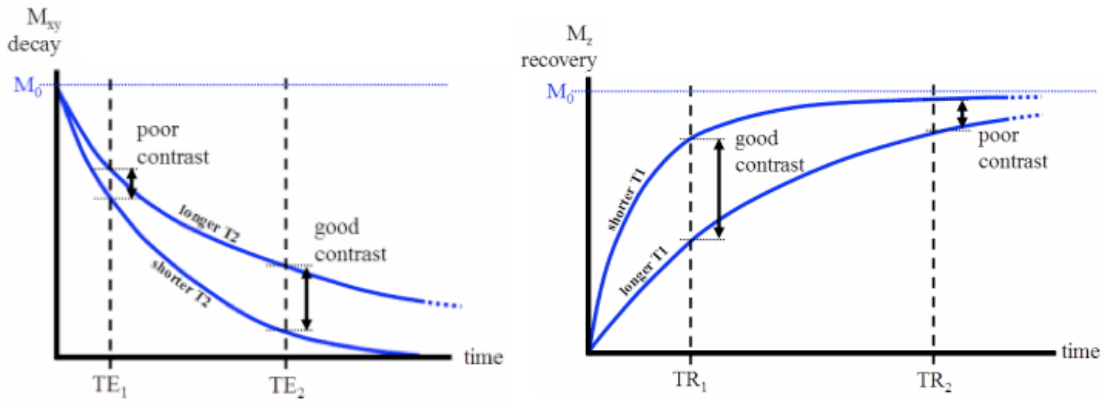

Figure 2: Schematic of both T2 decay (a) and T1 recovery (b) showing optimal TR and TE values to employ for optimisation of tissue contrast. In general, the use of very long TR and very short TE will result in minimal signal resolution and very poor tissue contrast. Instead, the ideal setting is to employ TE values that are not so small that the excited spins have not yet begun to experience transverse decay (i.e. they are still in an excited state), and TR values that are not so big that the spins have been fully recovered (i.e. experienced full longitudinal recovery). Overall, the schematic shows how selection of TE and TR values such that there is sufficient T1 recovery with minimal T2 decay will result in optimal MR signal with good tissue contrast.

The key factor however is to be able to resolve spatially specific information about spin precession. To do this, gradients are used to vary the effect of the magnetic field on the spins in a spatially specific manner. As such, the presence

of the gradients causes the spins at different locations to preccess at different rates. Reception of the different precession frequencies can then be translated into spatial information about where in the brain different spins were active, and to what extent.

The magnetic field is always in the direction of the longitudinal axis but the gradients manipulate the strength of the field at a given spatial location such that when an RF pulse is applied, excited spins gradually relax back into phase with the magnet at different rates; a feature that is recorded with the receive coils. Consequently, the spatial locations of spins can be determined based on their emission spectra.

While BOLD and ASL FMRI pulse-sequences follow different protocols to selectively image aspects of neurovascular changes relative to neural activity, both acquire this spatially-selective signal information through a process called echo-planar imaging (EPI). Here, the whole brain volume is divided into a stack of 2-D slices. Signals (or 'echos' as they are commonly referred to) are then acquired by very rapidly switching between the X- and Y- gradients to transverse a stepwise path across each slice. The sequence does this fast enough such that it is possible to acquire all lines of k-space, across all slices within each image repetition time (TR). In short, EPI allows one to acquire data from whole brain volume every TR.

The key to each technique is to coordinate the acquisition of functional images to the time at which the metabolic signal of interest is reaching a peak maximum relative to the onset of the stimulus. For BOLD FMRI, one is focused on looking what is called the hemodynamic response function (HRF): the MR signal

generated by the fluctuation in deoxy- to oxy-genated Hb proximal to the site of neural activation. In general, the peak of the HRF takes about 4-6 seconds to be reached from the time of the stimulus onset; and will take an additional 20-30s to return back to baseline. In general, BOLD FMRI experiments continually acquire images to characterize the full HRF shape relative to a given stimulus paradigm. Analysis of BOLD data then entails modeling the time of stimulus onset with the related peak HRF response to generate meaningful statistical maps of activation.

For ASL, the key is to image arterial blood as it arrives at a given part of the cortex. Different parts of the cortex will receive fresh arterial blood at different times; a factor that ASL sequences must account for in the timing of the image acquisition. This is commonly accounted for in single-slice ASL studies by optimizing the post-labelling delay (PLD) time to account for the time it will take arterial signal to reach a peak maximum within the part of the cortex the imaging slice is positioned. However, most ASL sequences today acquire whole brain datasets and do not account for differences in arterial delivery (and exit) times. Instead a commonly employed PLD equal to 1.0 sec is used; an approximation based on the rate of T1 decay of arterial blood from the moment of tagging (119,120).

1.5 Conclusion

At present, much of our understanding of the brain in pain is based largely on acute pain studies employing BOLD FMRI. Much of this is due to the fact that as

an imaging framework, BOLD FMRI is relatively easy to employ on a standard FMRI scanner. Subsequently, the method of studying pain in the brain has relied on stimulus paradigms that are well suited to this specific imaging technique. Which is to say, our primary focus in the BOLD pain imaging setting is to observe the brain during acute (i.e. short) pain stimuli as this is within the temporal domain the imaging technique is best suited to. While the various acute pain FMRI studies discussed previously are immensely insightful towards guiding our understanding of the complexity of pain, it is still not known how these regions and the dynamic interaction between them relates to chronic pain states. Additionally, it must be stated that BOLD FMRI is ill-suited to investigate fundamental components of the chronic pain experience; namely that the pain is *ongoing* and often *spontaneous*; characteristics that evade BOLD's imaging capacities. Excitingly, an emerging body of work suggests that the neuroimaging technique Arterial Spin Labelling (ASL) is optimally suited to investigate these aspects of the pain experience.

1.6 Synopsis of the thesis

When we began this project, ASL FMRI was largely a tool in development by our MR Physics department at the FMRIB Centre. The practical utilization of it was therefore limited to answering scientific questions far removed from the world of pain neuroscience. The goal of this work is to describe the process of taking a predominately 'physics group' tool and developing it for use in a pain imaging context. The work presented in this thesis largely exhibits the evolution of that development process such that by the final experimental chapters (Chapter 5 &

6) we are able to image the brain in pain in a robust and reliable way. We are confident that future experiments employing the ASL technique we've developed here will provide integral insight into the mechanisms underlying the perception and experience of pain in man.

1.6.1. Research aims

The primary aim of this thesis is to develop, optimize and implement the noninvasive perfusion imaging technique ASL to interrogate the neural correlates of ongoing pain. The primary model we have chosen for this is healthy human subjects. Because we are interested in studying pain, our observations will be limited to the brain. Chiefly, we are interested to interrogate how key regions well known from BOLD pain studies are recruited and behave in the context of pain states that are tonic and therefore more analogous to chronic pain conditions.

We organized our approach to this task into three related experimental tasks: A) the development and validation of a safe, reliable ongoing experimental pain paradigm for use in healthy human subjects; B) the optimization of a whole-brain ASL experimental paradigm to image different types of ongoing pain experiences; C) the application of our ongoing pain imaging approach into both healthy and clinical populations. The experimental approach, hypotheses, results and discussion for tasks A and B are highlighted in chapters 2 and 3, respectively. The execution of experimental task C is interrogated in chapters 4-6. In Chapter 4, we describe the first implementation of an optimized whole brain pCASL approach to image the neural correlates of parametrically modulated pain in healthy subjects. Chapter 5 expands on this approach by

implementing an optimized version of the pCASL sequence to obtain absolute quantification of CBF changes across the whole brain during tonic pain in healthy human subjects. In Chapter 6 we show how it is possible to employ this optimized pCASL approach to image ongoing pain and relief associated with the inherited pain pathology Erythromelalgia in a single subject.

1.6.2 Outline of research questions

The thesis is organized into the following projects, each corresponding to a specific research question:

i) Is it possible to obtain a safe, robust, and well-maintained ongoing tonic pain in healthy subjects? In chapter 2 we designed and tested two different pain paradigms to induce specific ongoing pain experiences within subjects. The outcome of these psychophysics experiments were then used to inform the development of different ongoing pain ASL FMRI studies to be done in subsequent chapters.

ii) What is the optimal ASL FMRI approach to be used for imaging ongoing pain states? In chapter 3 we discuss the fundamental aspects ASL FMRI investigations need to account for when studying ongoing pain states. We then tested different ASL parameter settings including pulse sequence parameters, acquisition approaches and ways to obtain whole brain data sets. The outcomes from these studies were then implemented in subsequent imaging studies outlined in chapters 4-6.

iii) What are the neural correlates of a tonic, parametrically modulated mechanical pain experience? The aim of chapter 4 was to employ our safe and robust ongoing pain psychophysics paradigm outlined in chapter 2 in an ASL FMRI experimental paradigm developed in chapter 3. We used an initial version of our ASL FMRI approach to interrogate the neural correlates of ongoing pain induced by graded stimulus intensities applied to subject's hands.

iv) Is it possible to obtain both relative and absolute changes in CBF from pain-relevant regions during an ongoing pain experience? The aim of chapter 5 was to employ an optimized version of the ASL FMRI approach employed in the previous study to obtain absolute changes in CBF during an ongoing pain experience from multiple cortical slices.

v) What are the neural correlates of a genetically inherited neuropathic pain and relief? In chapter 6 we employed our fully optimized multi-TI ASL FMRI approach to image the ongoing pain associated with the genetic pain condition Erythromelalgia in a single subject. The aims of this study were: a) to show the technique could be used to look at clinical pain states on a single-subject basis; b) to observe the absolute changes in CBF during phases of pain versus relief across different regions of interest that span the whole cortex.

1.7 References

1. Breivik, H. et al. (2006). Survey of chronic pain in Europe: Prevalence, impact on daily life, and treatment. Eur J Pain 10:287-333.

2. Finnerup NB, Otto M, McQuay HJ., Jensen TS, Sindrup SH. (2005). Algorithm for neuropathic pain treatment: an evidence based proposal. Pain 118(3): 289-305.

3. Institute of Medicine; Consensus Report (June 29, 2011). “Relieving Pain in America: A Blueprint for Transforming Prevention, Care, Education and Research”

4. Stewart WF, Ricci JA, Chee E, Morganstein D, Lipton R. (2003). Lost productive time and cost due to common pain conditions in the US workforce. JAMA 290(18):2443-54.

5. Haanpaa, M. et al. (2009). Assessment of Neuropathic pain in primary care. American J of Medicine. 112(10):S13-21.

6. Cicero TJ, Inciadri JA, Munoz A. (2005). Trends in abuse of Oxycontin and other opioid analgesics in the United States: 2002-2004. J Pain 6(10):662-72.

7. Jensen, TS et al. (2003) Translation of symptoms and signs into mechanisms in neuropathic pain. Pain 102:1-8

8. Backonja, M. & Woolf CJ. (2010). Future directions in neuropathic pain therapy: closing the translational loop. Oncologist 10(15) Suppl2:24-9

9. Tracey, I. & Bushnell, C. (2009). How neuroimaging studies have challenged us to rethink: Is chronic pain a disease? J Pain 10(11):1113-1120.

10. Tracey, I. & Manyth, P. (2007) The cerebral signature for pain perception and its modulation. Neuron 55(3):377-91.

11. Apkarian AV, Buschnell MC, Treede RD, Zubieta JK. (2005). Human brain mechanisms of pain perception and regulation in health and disease. Eur J Pain 9(4):463-84.

13. Tracey, I. (2008) Imaging Pain. Br J Anaesthesia. 101(1):32-9.

14. Baliki MN, Chialvo DR, Geha PY, Levy RM, Harden RN, Parrish TB, Apkarian AV. (2006) Chronic pain and the emotional brain: specific brain activity associated with spontaneous fluctuations of intensity of chronic back pain. J Neuroscience 26(47):12165-73.

15. Sherrington CS (1906). The integrative action of the nervous system. Scribner, New York

16. Vallbo, A.B., Hagbarth, K. E., Torebjork, H.E., Wallin, B.G.(1979) Somatosensory, Proprioceptive, and sympathetic activity in human peripheral nerves. Psychological Reviews 59(4):919-957

17. Martin, J.H. & Jessell, T.M. (2000) “Anatomy of the somatic sensory system” In: Principles of Neural Science, Third Edition, edited by E.R. Kandel, J.H. Schwartz, T.M. Jessell. London: Prentice-Hall International Inc., p353-366.

18. Johansson R.S. Skin mechanoreceptors in the human hand: receptive field characteristics. In: *Sensory Functions of the Skin in Primates,* edited by Y. Zotterman. Oxford: Pergamon, 1976, p. 159-170

19. Johansson R.S. (1978) Tactile sensibility in the human hand: receptive field characteristics of mechanoreceptive units in the glabrous skin. J Physiol. 281: 101-123.

20. Knibestol, M. (1973) Stimulus-response functions of rapidly adapting mechanoreceptors in the human glabrous skin area. J Physiol. 232:427-452.

21. Knibestol M. (1975) Stimulus-response functions of slowly adapting mechanoreceptors in the human glabrous skin area. J Physiol. 245: 63-80.

22. Knibestol M. & Vallbo, A.B. (1970) Single unit analysis of mechanoreceptor activity from the human glabrous skin. Acta Physiol. Scand. 80: 178-195.

23. Mountcastle, V.B., Talbot, W.H., Kornhuber, H.H. The neural transformation of mechanical stimuli delivered to the monkey’s hand. In: *Ciba Found. Symp. Touch, Heat, and Pain*, edited by V.S. de Reuck & J. Knight. London: Churchill, 1966, p.325-345

24. Werner, G. & Mountcastle, V.B. (1965) Neural activity in mechanoreceptive cutaneous afferents: stimulus-response relations, Weber functions and information transmission. J Neurophysiol. 28:359-397.

25. Werner, G. & Mountcastle, V.B. (1968) Quantitative relations between mechanical stimuli to the skin and the neural responses evoked by them. In: *The skin senses*, edited by D.R. Kenshalo. Spingfield, IL: Thomas, 1968, p. 112-137

26. Gybels, J. & van Hees, J. (1972) Unit activity from mechanoreceptors in human peripheral nerve during intensity discrimination of touch. In: *Neurophysiology studied in Man,* edited by G.G. Somjen. Amsterdam: Excerpta Med. Int Congr. Ser. No. 253, 1972, p. 198-206

27. Torebjork, H.E. & Hallin, R.G. (1970) C-fibre units recorded from human sensory nerve fascicles in situ. Acta. Soc. Med. Ups. 75:81-84

28. Torebjork, H.E. & Hallin, R.G. (1974) Identification of afferent C units in intact human skin nerves. Brain Res. 67:387-403.

29. Torebjork, H.E. & Hallin, R.G. (1976) Skin receptors supplied by unmyelinated nerve fibres in man. In: *Sensory Function of the Skin in Primates,* edited by Y. Zotterman. Oxford: Pergamon, 1976, p. 475-487.
30. van Hees, J. Human C fibre input during painful and nonpainful skin stimulation with radiant heat. In: *Advances in Pain Research and Therapy,* edited by J.J. Bonica and D. Albe-Fessard. New York: Raven, 1976, vol. 1, p. 35-40.

31. Torebjork, H.E. & Hallin, R.G. (1977) Sensitization of polymodal nociceptors with C fibres in man. Proc. Int. Union Physiol. Sci. 13:758.

32. Torebjork, H.E. & Hallin, R.G. (1978) Recordings of impulses in unmyelinated nerve fibres in man: afferent C fibre activity. Acta. Anaesthesiol. Scand. Suppl. 70:124-129.

33. Sundolf, G. & Wallin, B.G. (1978) Human muscle nerve sympathetic activity at rest. Relationship to blood pressure and age. J Physiol. 278:621-637.

34. van Hees, J. & Gybels, J.M. (1972) Pain related to single afferent C-fibres from human skin. Brian Res. 48:397-400.

35. Hallin, R.G. & Torebjork, H.E. (1970) C-fibre components in electrically evoked compound potentials recorded from human median nerve fascicles. Acta Soc. Med. Ups. 75:77-80.

36. Julius, D. & McCleskey, E.W. Cellular and molecular properties of primary afferent neurons. In: Wall & Melzack's Textbook of Pain, Fifth Edition, edited by S.B. McMahon & M. Koltzenburg. Elsevier Limited, 2006, p. 35-48.

37. Hunt SP & Rossi J (1985). Peptide- and non-peptide-containing unmyelinated primary afferent: the parallel processing of nociceptive information. Philos Trans R Soc Lond B308:283-89.

38. Silverman JD & Kruger L (1988). Lectin and Neuropeptide Labelling of Separate Populations of Dorsal Root Ganglion Neurons and Associated "nociceptor" thin axons in Rat Testis and Cornea Whole-Mount Preparations. Somatosensory & Motor Research 5(3):259-67.

39. Woodbury JC, Ritter AM, Koerber HR. (2000). On the problem of lamination in the superficial dorsal horn of mammals: A reappraisal of the substantia gelatinosa in postnatal life. J of Comparative Neurology 417:88-102.

40. Todd, A. (2002) Anatomy of primary afferents and projection neurones in the rat spinal dorsal horn with particular emphasis on substance P and the neurokinin 1 receptor. Experimental Phsyiology 87:245-49

41. Sorkin LS, Xiao WH, Wagner R, Myers RR. (1997) Tumor necrosis factor-alpha induces extopic activity in nociceptive primary afferent fibres. Neuroscience 81(1):255-262.

42. Dostrovsky JO & Craig AD (2006). Ascending projection systems. In: Wall and Melzack's textbook of pain (McMahon SB, Koltzenburg M, ed), Ed 5, pp 187-203. Philadelphia: Elsevier Churchill Livingstone.

43. Braz JM & Basbaum AI. (2009). Triggering genetically-expressed transneuronal tracers by peripheral axotomy reveals convergent and segregated sensory neuron-spinal cord connectivity. Neuroscience 163(4): 1220-32.

44. Todd, AJ. (2010) Neuronal circuitry for pain processing in the dorsal horn. Nat Rev Neuroscience 11(12):806-26.

45. Dostrovsky JO & Craig AD (2006). Ascending projection systems. In: Wall and Melzack's textbook of pain (McMahon SB, Koltzenburg M, ed), Ed 5, pp 187-203. Philadelphia: Elsevier Churchill Livingstone.

46. Head, H. & Holmes, G. (1911) Sensory disturbances from cerebral lesions. Brian Res. 34:102-254.

47. Penfield, W. & Boldrey, E. (1937) Somatic motor and sensory representation in the cerebral cortex of man as studied by electrical stimulation. Brain 60:389-443.

48. Lassen, N.A., Larsen, B., Orgogozo, J.M. (1978) Cortical localizations seen by the dynamic gamma-camera: a new approach in neuropsychology. Encephale 4(3):233-49.

49. Talbot JD, Marrett S, Evans AC, Meyer E, Bushnell MC, Duncan GH. (1991) Multiple representations of pain in human cerebral cortex. Science 251(4999):1355-1358.

50. Jones AKP, Friston KJ, Brown D, Qi L, Frackowiak RSJ. (1991). Cortical and subcortical localization of response to pain in man using positron emission tomography. Roc Roy Soc B 244:39-44.

51. Apkarian, A.V., Stea, R.A., Manglos, S.H., Szeverenyi, N.M., King, R.B., Thomas, F.D. (1992) Persistent pain inhibits contralateral somatosensory cortical activity in humans. Neuroscience Letters 140(2):141-7.

52. Apkarian AV, Bushnell MC, Treede RD, Zubieta JK. (2005). Human brain mechanisms of pain perception and regulation in health and disease. Eur J Pain. 9(4):463-84.

53. Coghill RC, Sang CN, Maisog JMA, Iadarola J. (1999). Pain intensity processing within the human brain: A bilateral, distributed mechanism. J Neurophysiol 82(4):1934-43.

54. Peyron R, Laurent B, Garcia-Larrea L. (2000). Functional imaging of brain responses to pain: A review and meta-analysis (2000). Neurophysiol Clin. 30(5):263-88.

55. Bushnell, M.C., Duncan, G.H., Hofbauer, R.K. Ha, B., Chen, J.I., Carrier, B. Pain perception: is there a role for primary somatosensory cortex? Proc Natl Acad Sci USA 96:548-54.

56. Chen, J.I., Ha, B., Bushnell, M.C., Pike, B., Duncan, G.H. (2002) Differentiating noxious- and innocuous-related activation of human somatosensory cortices using temporal analysis of fMRI. J Neurophysiol. 88:464-74.

57. Rainville, P. Duncan, G.H., Price, D.D., Carrier B., Bushnell, M.C. (1997) Pain affect encoded in human anterior cingulate but not somatosensory cortex. Science 277:968-71.

58. Tolle, T.R., Kauffmann, T., Siessmeier, T., Lautenbacher, S., Berthele, A., Munz, F.(1999) Region-specific encoding of sensory and affective components of pain in the human brain: a positron emission tomography correlation analysis. Ann Neurol. 45:40-7.

59. Fulbright, R.K., Troche, C.J., Skudlarski, P., Gore, J.C., Wexler, B.E. (2001) Functional MR imaging of regional brain activation associated with the affective experience of pain. AJR AM J Roentgenol 177:1205-10.

60. Strigo, I.A., Duncan, G.H., Boivin, M., Bushnell, M.C. (2003) Differentiation of visceral and cutaneous pain in the human brain. J Neurophysiol. 89:3294-303.

61. Apkarian AV, Bushnell MC, Treede RD, Zubieta JK. (2005). Human brain mechanisms of pain perception and regulation in health and disease. Eur J Pain. 9(4):463-84.

62. Tracey, I. & Manyth, P.W. (2007) The cerebral signature for pain perception and its modulation. Neuron 55:377-391.

63. Lee, M.C. & Tracey, I. (2010). Unraveling the mystery of pain, suffering and relief with brain imaging. Curr Pain Headache Rep 14:124-131.

64. Craig, A.D. (2003) Pain mechanisms: labeled lines versus convergences in central processing. Annu Rev Neuroscience 26:1-30.

65. Brooks, J.C., Zambreanu, L., Godinez, A., et al. (2005) Somatotopic organisation of the human insula to painful heat studied with high resolution functional imaging. Neuroimage 27:201-209.

66. Fields, H.L., Basbaum, A.I., Heinricher, M.M. Central nervous system mechanisms of pain modulation. In Wall & Melzack's Textbook of Pain.

Edited by S.M. McMahon, M. Kolzenburg. Philadelphia: Elsevier, 2006:125-142.

67. Kong, J., White, N.S., Kwong, K.K. (2006) Using fMRI to dissociate sensory encoding from cognitive evaluation of heat pain intensity. Human Brain Mapp 27:715-721.

68. Neugebauer, V., Li, W., Bird, G.C., Han, J.S. (2004) The amygdala and persistent pain. Neuroscientist 10:221-234.

69. Gracely RH, Geisser ME, Giesecke T, Grant MA, Petzke F, Williams DA, Clauw DJ. (2004) Pain catastrophizing and neural responses to pain among persons with fibromyalgia. Brain 127(Pt 4):835-43.

70. Kim, M.J., Loucks, R.A., Palmer, A.L., Brown, A.C., Solomon, K.M., Marchante, A.N., Whalen, P.J. (2011). The structural and functional connectivity of the amygdala: from normal emotion to pathological anxiety. Behav. Brain Res. 223(2):403-10.

71. Brooks J & Tracey I. (2005) From nociception to pain perception: imaging the spinal and supraspinal pathways. J Anat. 207(1):19-33.

72. Henderson lA, Gandevia SC, Macefield VG. (2007) Somatotopic organization of the processing of muscle and cutaneous pain in the left and right insula cortex: a single fMRI study. Pain 128(1-2):20-30.

73. Bjornsdotter M, Loken L, Olausson H, Valbo A, Wessberg J. (2009) Somatotopic organization of gentle touch processing in the posterior insular cortex. J Neuroscience 29(29):9314-20.

74. Basbaum AI & Fields HL (1984). Endogenous pain control systems: brainstem spinal pathways and endorphin circuitry. Annu Rev Neuroscience 7:309-38.

75. Porreca F, Ossipov MH, Gebhart GF. (2002) Chronic pain and medullary descending facilitation. Trends Neuroscience 25(6):319-25.

76. Ren K & Dubner R. (2002). Descending modulation in persistent pain: an update. Pain 100(1-2):1-6.

77. Hoffman GA, Harrington A, Fields HL (2005) Pain and placebo: what we have learned. Perspect Biol Med. 48(2):248-65.

78. Hagbarth KE & Kerr DIB. (1954) Central influences on spinal afferent conduction. J Neurophysiology 17:295-307.

79. Tracey, I., Plaghaus, A., Gati, J.S. et al. (2002) Imaging attentional modulation of pain in the periaqueductal gray in humans. J Neuroscience 22:2748-2752.

80. Bantick, S.J., Wise, R.G., Ploghaus, A. et al. (2002) Imaging how attention modulates pain in humans using functional MRI. Brain 125:310-319.

81. Valet, M., Sprenger, T. Boecker, H. et al. (2004) Distraction modulates connectivity of the cingulo-frontal cortex and the midbrain during pain: an fMRI analysis. Pain 109:399-408.

82. Wiech, K., Kalisch, R., Weiskopf, N. et al. (2006) Anterolateral prefrontal cortex mediates the analgesic effect of expected and perceived control over pain. J Neuroscience 26:11501-11509.

83. Wager, T.D., Davidson, M.L., Hughes, B.L. et al. (2008) Prefrontal-subcortical pathways mediating successful emotion regulation. Neuron 59:1037-1050.

84. Schiller D, Levy I, LeDoux JE, Phelps EA. (2008) From fear to safety and back: reversal of fear in the human brain. J Neuroscience 5(28):11517-25.

85. Ploghaus A, Narain C, Beckmann CF, Clare S, Bantick S, Wise R, Mathews PM, Rawlins NP, Tracey I. (2001) exacerbation of pain by anxiety is associated with activity in a hippocampal network. J Neuroscience 21(24): 9896-9903.

86. Gracely RH, Geisser ME, Giesecke T, Grant MA, Petzke F, Williams DA, Clauw DJ. (2004) Pain catastrophizing and neural responses to pain among persons with fibromyalgia. Brain 127(Pt 4):835-43.

87. Apkarian AV, Thomas PS, Krauss BR, Szeverenyi NM. (2001) Imaging the pain of low back pain: functional magnetic resonance imaging in combination with monitoring subjective pain perception allows the study of clinical pain states. 299(1-2):57-60.

88. Lorenz J & Garcia-Larrea L. (2003) Contribution of attentional and cognitive factors to laser evoked potentials. Neurophysiol Clin. 33(6):293-301.

89. Faymonville ME, Roediger L, Del Fiore G, Delgueldre C, Phillips C, Lamy M, Luxen A, Maquet P, Laureys S. (2003). Increased cerebral functional connectivity underlying the antinociceptive effects of hypnosis. Brain Res Cogn Brain Res 17(2):255-62.

90. Witting N, KUpers RC, Svensson P, Jensen TS. (2006) A PET activation study of brush-evoked allodynia in patients with nerve injury pain. Pain 120(1-2):145-154.

91. Zambreanu L, Wise RG, Brooks JCW, Iannetti GD, Tracey I. (2005) A role for the brainstem in central sensitisation in humans. Evidence from functional magnetic resonance imaging. Pain 114: 397-407.

92. Wanigasekera V, Lee MCH, Rogers R, Hu P, Tracey I. (2011). Neural correlates of an injury-free model of central sensitization induced by opioid withdrawal in humans. Journal of Neuroscience, 31(8):5412-10.

93. Singer, T., Seymour, B., O'Doherty, J. et al. (2004) Empathy for pain involves the affective but not sensory components of pain. Science 303:1157-1162.

94. Loggia, M.L., Mogil, J.S., Bushnell, M.C., (2008) Empathy hurts: compassion for another increases both sensory and affective components of pain perception. Pain 136:168-176.

95. Danziger, N., Faillenot, I., Peyron, R. (2009) Can we share a pain we never felt? Neural correlates of empathy in patients with congenital insensitivity to pain. Neuron 61:203-212.

96. Kong, J., Gollub, R.L., Polich, G.,et al. (2008) A functional magnetic resonance imaging study on the neural mechanisms of hyperalgesic nocebo effect. J Neuroscience 28:13354-13362.

97. Legrain, V., Iannetti, G.D., PLaghki, L., Mouraux, A. (2011) The pain matrix reloaded: a salience detection system for the body. Prog. Neurobiology 93(1): 111-24.

98. Frot m, Mauguiere F, Magnin M, Garcia-Larrea L. (2008). Parallel processing of nociceptive A-delta inputs in SII and midcingulate cortex in humans. J Neuroscience 28(4):944-52.

99. Lee MC, Zambreanu L, Menon DK, Tracey I. (2009) Identifying brain activity specifically related to the maintenance and perceptual consequence of central sensitization in humans. J Neuroscience 28:11642-11649.

100. Schurger A, Pereira F, Treisman A, Cohen JD. (2010) Reproducibility distinguishes conscious from unconscious neural representations. Science 327(5961):97-9.

101.

102.Mangia S, Simpson IA, Vannucci SJ, Carruthers A. (2009) The i*n vivo* neuron-to-astrocyte lactate shuttle in human brain: evidence from modelling of measured lactate levels during visual stimulation. J Neurochem. 109(s1): 55-62

103.Sokoloff L. (1960) Chapter 10. Local cerebral energy metabolism: Its relationship to local functional activity and blood flow. In: Ciba Foundation Symposium 56- Cerebral vascular smooth muscle and its control (Organizer, KE & O'Connor M) Ciba Foundation.

104.Sibson NR, Shen J, Mason GF, Rothman DL, Behar KL, Shulman RG. (1998). Functional energy metabolism: *In vivo* ^{13}C-NMR spectroscopy

evidence for coupling of cerebral glucose consumption and glutamatergic neuronal activity. Dev Neuroscience 20:321-330.

105. Rothman DL, Sibson NR, Hyder F, Shen J, Behar KL, Shulman RG. (1999) *In vivo* nuclear magnetic resonance spectroscopy studies of the relationship between the glutamate-glutamine neurotransmitter cycle and functional neuroenergetics. Phil Trans R. Soc. Lond. B 354:1165-1177.

106.Laughlin SB. (2001). Energy as a constraint on the coding and processing of sensory information. Curr Opin Neurobiol. 11(4):475-80.

107. Mosso A (1880) Sulla circolazione del cervello dell'uomo. Att R Accad Lincei 5, 237-358.

108.Roy & Sherington (1890). On the regulation of the blood-supply of the brain. J Physiology 11(1-2):85-108

109.Attwell D, Buchan AM, Charpak S, Lauritzen M, Macvicar BA, Newman EA. (2010). Glial and neuronal control of brain blood flow. Nature 468(7321): 232-43.

110.Filosa, JA & Blanco M. (2007) Neurovascular coupling in the mammalian brain. Exp Physiol. 92(4):641-6.

111.Zonta M, Sebellin A, Gobbo S, Fellin T, Pozzan T, Carmignoto G. (2003) Glutamate-mediated cytosolic calcium oscillations regulate a pulsatile prostaglandin release from cultured rat astrocytes. J Phyisol. 553(Pt2): 407-14.

112.Metea MR. & Newman EA. (2006) Glial cells dilate and constrict blood vessels: a mechanism of neurovascular coupling. J Neuroscience 26(11): 2862-70.

113.Gordon GRJ., Mulligan SJ, MacVicar B. (2007) Astrocyte control of the cerebrovasculature. Glia 55:1214-1221.

114.Peng X, Carhuapoma JR, Bhardwaj A, Alkayed NJ, Falck JR, Harder DR, Traystman RJ, Koehler RC. (2002). Supression of cortical functional hyperemia to vibrissal stimulation in the rat by epoxygenase inhibitors. Am J Physiol Heart Circ Physiol. 283(5):H2029-37.

115.Peng X, Zhang C, Alkayed NJ, Harder DR, Koehler RC. (2004) Dependency of cortical functional hyperemia to forepaw stimulation on epoxygenase and nitric oxide synthase activities in rats. J Cereb Blood Flow Metab. 24(5): 509-17.

116.Logothetis NK, Pauls N, Augath M, Trinath T, Oeltermann A. (2008). Neurophysiological investigation of the basis of the fMRI signal. Nature, 412:150-

117.Ogawa S, Lee TM, Kay AR, Tank DW. (1990) Brain magnetic resonance imaging with contrast dependent on blood oxygenation. Proc Natl Acad Sci USA 87(24):9868-72

118. Ogawa S, Lee TM, Barrere B. (1993) The sensitivity of magnetic resonance imaging signals of a rat brain to changes in the cerebral venous oxygenation. Magn Reson Med. 29(2):205-10.

119.Buxton RB, Frank LR, Wong EC, Siewert B, Warach S, Edelman RR. (1998) A general kinetic model for quantitative perfusion imaging with arterial spin labelling. MRM 40:383-396

120.Ye FQ, Pekar JJ, Jezzard P, Duyn J, Frank JA, McLaughlin AC. (1996) Perfusion imaging of the human brain at 1.5 T using a single-shot EPI spin tagging approach. MRM 36: 219-224

Chapter 2

Development of tonic pain paradigms for use in a perfusion neuroimaging context

2.1 Introduction

One of the primary goals of pain imaging research in humans is to develop experimental settings that mirror the clinical experience. The development and implementation of clinically relevant paradigms that approximate the sensory, emotional, cognitive and even pharmacological context is of paramount interest. The first step towards accomplishing this is to ensure the sensory component of the experiments incorporates stimuli that are tonic in nature.

Various ongoing pain models exist and can be grouped into categories based on the modalities: thermal, mechanical, electrical, chemical, and ischemic stimuli. Each technique activates a specific nociceptive pathway (or set of pathways) to elicit a particular pain perception. For example, ongoing thermal pain is primarily accomplished with the use of a contact thermode to generate the perception of noxious heat (1,2,3) or cold (4). Ongoing mechanical pain is primarily accomplished with the use of constant force applied to the skin either with the use of pressure algometers (5) or with calibrated vonFrey hairs (6,7). Electrodes applied or implanted into the skin are used to elicit electrical-induced pain (8). Chemical modalities are most commonly used to elicit an ongoing, often spontaneous and/or oscillating burning pain. Commonly used agents include: capsaicin (9,10); bradykinin (11,14); mustard oil (12); substance P (13); serotonin (14); and hypertonic saline (15,16). Ischemic pain is commonly investigated with the use of a pneumatic tourniquet inflated around the leg or arm after exsanguination of the extremity by gravity (17).

While the objective of the above approaches is to induce tonic pain, the nature of

the sensory experience and the neurophysiological changes underlying it differ greatly. So too does the reliability and robustness of each method. The ideal ongoing pain model should include a steady-state experience (both sensory and psychological) that is robust, reproducible, and safe. With this in mind, many of the above paradigms are not ideal for use in these initial tonic pain imaging experiments. Specifically, models that do not induce steady-state experiences (i.e. models with high incidence of habituation, temporal and/or spatial summation) such as pressure, contact heat with a high temperature thermode, ischemic blocks, or cold-water submersion are not ideal for use with perfusion FMRI at present. This is simply because we do not yet know: i) what the neural correlates of ongoing pain are; and ii) what the best ASL approach is to image them. Consequently, it is of paramount interest to ensure that the pain experience itself is robust, reliable and uniform in nature.

One solution to this problem is to exploit the capacity for select populations of nociceptors to provide a sustained afferent input to the CNS when a continued stimulus is applied to the skin. For example, models that include inducible thermal (e.g. capsaicin, UV burn, mustard oil) and/or mechanical (sustained pin-prick stimulation) hypersensitivity provide a highly controllable means of experimentally inducing sustained levels of tonic pain in a dose-dependent manner. Additionally, because of the inherently low stimulus frequency of these paradigms (i.e. long blocks of sustained painful stimuli), they are potentially well suited to be employed in an ASL imaging experiment.

We posit that another essential factor guiding the development of tonic pain

imaging paradigms is the ability to translate this work in humans back into animal models. The ultimate goal of this being that more invasive animal work analogous to human imaging experiments will allow us to not only uncover *what* the neural correlates are during tonic pain, but also *how* these regions (dys)function across different pain pathologies. With this in mind, many pain modalities do not have realistic translational potential between human and animal models. To this end, we have configured two sets of psychophysical paradigms employing either an ongoing heat or mechanical modality. The reason for exploring both modalities is twofold: 1) the nature of the nociceptive neurophysiology of each modality is well established in animals but the related neural correlates of each pain state has been minimally explored; 2) each modality has specific experimental utility that can be exploited for the purpose of further optimising ASL sequences for use in clinically relevant pain imaging contexts (e.g. parametric pain designs) simultaneous to being 'back' translated for the improvement of animal pain models.

2.2 Heat Pain

When painful heat is applied to the skin, this nociceptive information is projected to the spinal cord by way of unmyelinated C-fibres and finely myelinated Aδ fibres. Briefly, the C-fibres are slow conducting and are thought to convey poorly localised information about the magnitude of pain, often lingering beyond the actual stimulus duration itself. In contrast, the fast conducting Aδ component is thought to convey the more sensory-discriminative aspects of the stimulus (18,19,20,21,22,23). To note, continuous heat stimuli are likely to evoke continued activity from C-fibres, compared to the faster adapting Aδ fibre

component. Additionally, the work of McMullin & Lumb (2001) and Lumb, BM (2001) have shown the rate at which the skin is heated also affects the population of nociceptors recruited to convey the presence of the noxious input: slow heating rates (2.5°C s^{-1}) activate capsaicin sensitive heat nociceptors; faster heating rates (7.5°C s^{-1}) activate capsaicin-insensitive heat nociceptors (24,25).

In total, there is considerable evidence to suggest that different nociceptor fibre types are processed differently in the CNS and are likely to play different roles in the emergence and maintenance of pain (26). For example, each fibre type plays different roles in the mechanisms underlying central sensitisation; projects to different nuclei of the brainstem and therefore are potentially able to play differing roles in the maintenance of chronic pain. While there is considerable experimental evidence to separate the behaviour of each fibre type in animals (see: 27,28), this approach is still too invasive for common use in healthy human volunteers.

As such, our approach to employing tonic heat pain in human subjects is to excite a heterogeneous peripheral nociceptor response to engage a strong, well maintained sensation of heat pain. This approach has been used extensively in previous imaging experiments (PET: 29,30). For example, Lautenbacher S. et al. (1995) defined the use of a pulsating contact heat thermode to create the sensation of 5-minutes of ‘continuous’ painful heat. Specifically, a contact heat thermode (PATH Tester, surface area = 1.6cm x 3.6cm) was attached to a male subject’s volar forearm. The stimulus itself consisted of a continuous pulsating heat sensation created by employing a ‘saw-toothed’ heat energy profile (defined

as a heat-cool ramp of 2°C s^{-1}, oscillating at a maximum of 1°C above each subject's pain threshold (31). While this model is capable of inducing a well - maintained state of continuous pain for periods in the minute timescale, there are a few limitations to its use in a pain imaging context. Firstly, it is not possible to modulate the pain intensity of the sensation beyond 'just painful' in a reliable way. The primary use of the model necessitates a block design of what is effectively 'low' tonic pain. Secondly, the 'saw-tooth' shape of the energy profile used to elicit the continuous heat 'spikes' give the sensation of a very rapid, rhythmic oscillation between two different heat sensations (e.g. the peak versus the trough of the 'saw-tooth'). Recent work by Derbyshire *et al.* (2008, 2009) described how this type of sensory profile can potentially result in an overall reduced pain experience (32). This is due to the phenomena of 'offset analgesia' which occurs when an increased noxious heat is followed by a less noxious heat thereby resulting in an overall reduced pain experience (33). Additionally, it was shown that during the phases of pain offset (i.e. the troughs), increased activation in the periaqueductal gray (PAG) and the rostral ventral medulla (RVM), regions well known to mediate descending inhibitory control of pain, was observed thereby providing strong evidence that this type of pain paradigm induces an oscillating, non-uniform pain experience (33). In conclusion, by employing such a tonic pain approach, the functional dynamics of the brain regions recruited are complex and potentially outside the current capacities of our ASL approach. Therefore, the aim of our initial experiments is to image a uniform experience of ongoing pain before moving on to future experiments targeting more complex pain experiences.

A simple approach to this end is to apply a suprathreshold heat stimulus to the skin for an extended period of time. Previous attempts to induce ongoing heat pain avoided this approach as it was likely to : i) damage skin; and/or ii) induce habituation. While there is some data to suggest it is possible to apply a very painful, sustained heat to human subjects' thighs for up to 7-minutes without damage to the skin or reduced pain ratings (34), our group had difficulty replicating the paradigm safely. Consequently, we employed a slightly modified version of this basic heat paradigm by inducing a state of capsaicin-induced thermal hypersensitivity to the skin before application of the thermode.

2.2.1. 1% Capsaicin heat pain paradigm

Capsaicin is the active ingredient in chili peppers and can be used experimentally to induce heat pain in subjects. For example, application of capsaicin cream topically activates TRPV1 receptors on peripheral nociceptors to signal the presence of a noxious chemical irritant that feels hot (35,36,37). With continued activation, inflammatory mediators (e.g. substance P) and cytokines are recruited to induce a prolonged inflammatory reaction at the site. Additionally, this alters the neurophysiological characteristics of the local TRPV1+ nociceptors such that the threshold for activation is lowered (38). This peripheral sensation is reflected perceptually by the presence of thermal allodynia. Now, previously innocuous thermal stimuli are perceived as painful. Experimentally, this sensitized site can be very easily modulated by the presence of a warming thermode. Here, even though the level of heat applied is low, it is perceived as noxious. This phenomenon can be employed to elicit prolonged pain states where risk of skin damage is minimal.

The goal of this experiment was to test the validity of applying a sub-threshold heat stimulus onto capsaicin-treated allodynic skin, to yield a well-maintained state of ongoing heat pain. We employed the highest dose of capsaicin available for use in human subjects without the need for a prescription (1% w/w capsaicin cream). We predicted that the use of this 'high' dose of capsaicin would induce a more potent primary hyperalgesia response in subjects to yield consistent, robust heat hypersensitivity over the duration of the experiment. Additionally, by employing a block design, with shorter block lengths, we predicted that it would be possible to reduce exhaustion of the peripheral nociceptive responsiveness such that perceived pain ratings do not habituate over time.

2.2.1.1. Method

1.0 % capsaicin cream (Pharmasol, UK) was applied to a 1 x 1 inch square on each subject's (n=18 total; 8 responders, 7 non-responders, 3 drop-outs; right handed; age: 18-40yrs) volar forearm. The capsaicin cream was left on the subject's arm until the time at which the subject rated the sensation of the cream as 'just painful' (NRS = 1 out of 10). At this time, the capsaicin cream was removed from the subject's arm. A contact thermode (MEDOC, Israel) was placed over the site of the capsaicin treated skin. Subjects were thresholded using a modified ascending staircase method until the subject was able to give reliable pain ratings for a strong (NRS >5) pain sensation. Once a stimulus temperature was established to elicit a strong pain, a block design stimulation paradigm consisting of five cycles of 2-minute ON (heat applied), OFF (no heat) blocks was performed. Subjects were asked to rate verbally the pain intensity

and unpleasantness every 30-seconds using the NRS (1-10). Please see Figure 1 for a detailed description of the paradigm used.

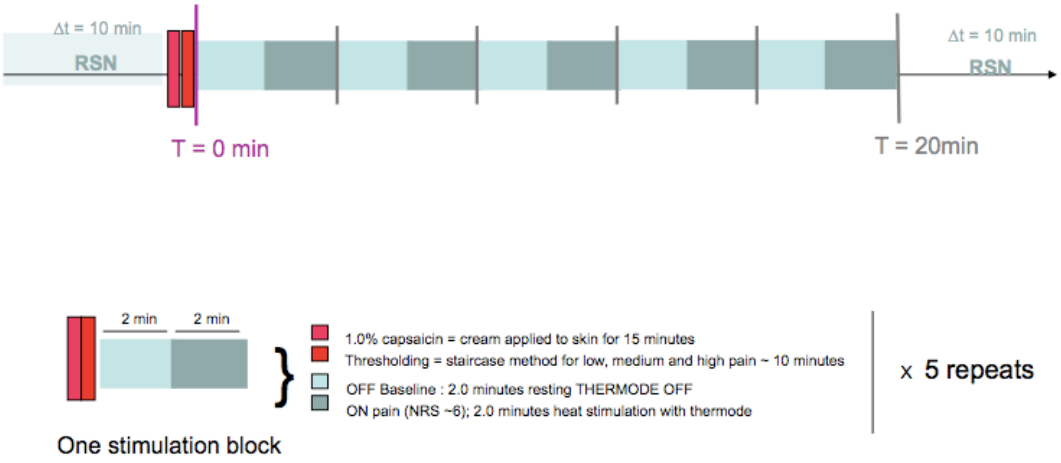

Figure 1. Graphic representation of the 1% capsaicin-heat paradigm. For clarity, each colored block represents a phase of the paradigm. Pink: 1.0% capsaicin cream was applied to a 1x1 inch square on the subjects volar forearm where it remained until the subject reported the pain intensity = 1; at which time the cream was removed and replaced with a contact thermode (Red). Subjects were thresholded as described previously to elicit a robust, reliable sensation of high pain (NRS>5 out of 10). Once a stimulus temperature was established, a block-design stimulation paradigm consisting of five cycles of 2-minute OFF (no heat; blue) versus ON (heat applied; gray) blocks were observed. Subjects were asked to rate verbally the stimulus intensity and unpleasantness every 30-seconds using the NRS (0-10).

2.2.1.2. Results

Figure 2 shows the mean duration of time needed for subjects to report the presence of a heat pain associated with the capsaicin cream treatment. The mean time for perception of capsaicin-induced thermal pain (NRS=1) was 10.28 minutes (n=18; s.d. = 4.06 min) (Figure 2). The mean temperature applied to elicit a strong heat pain in subjects was 38.7°C (s.d.=1.35). Heat applied to capsaicin-treated skin was able to elicit a robust and reliable increase in pain perception in subjects for the duration of the 2-minute ON blocks. Pain reports were observed to drop off to non-painful (NRS<1) levels during the OFF blocks where no heat was present (Figure 3a). Reported pain scores were maintained at similarly high levels (mean NRS = 5.3, s.d. 0.47) for the duration of the 2-minute ON blocks. There was no significant difference in perceived pain reports for any of the ON blocks (Figure 3a,b)

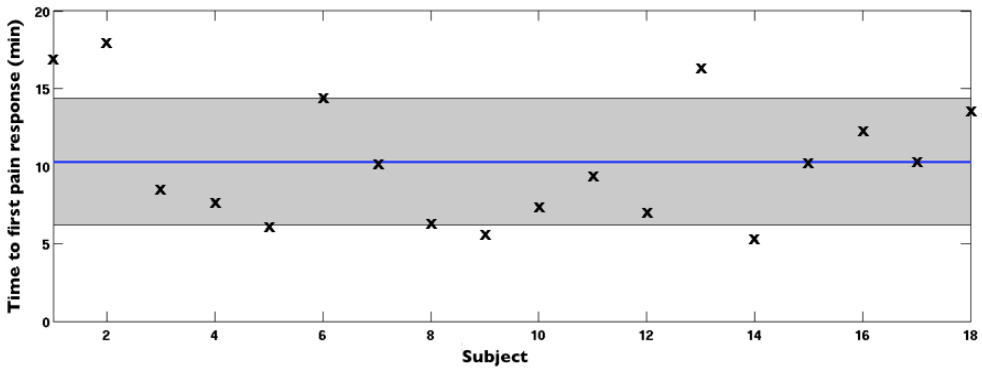

Figure 2: Scatter plot of 1.0% capsaicin response time. The time for each subject (x) to report the sensation of 'just painful' (i.e. NRS = 1 out of 10) from the time (t=0) of capsaicin application to each subject's volar forearm. The group mean response time to report heat pain associated with the dose of capsaicin applied was 10.1 minutes (blue line). The standard deviation of time to report pain is defined by the gray shading(+/- 4.06 min).

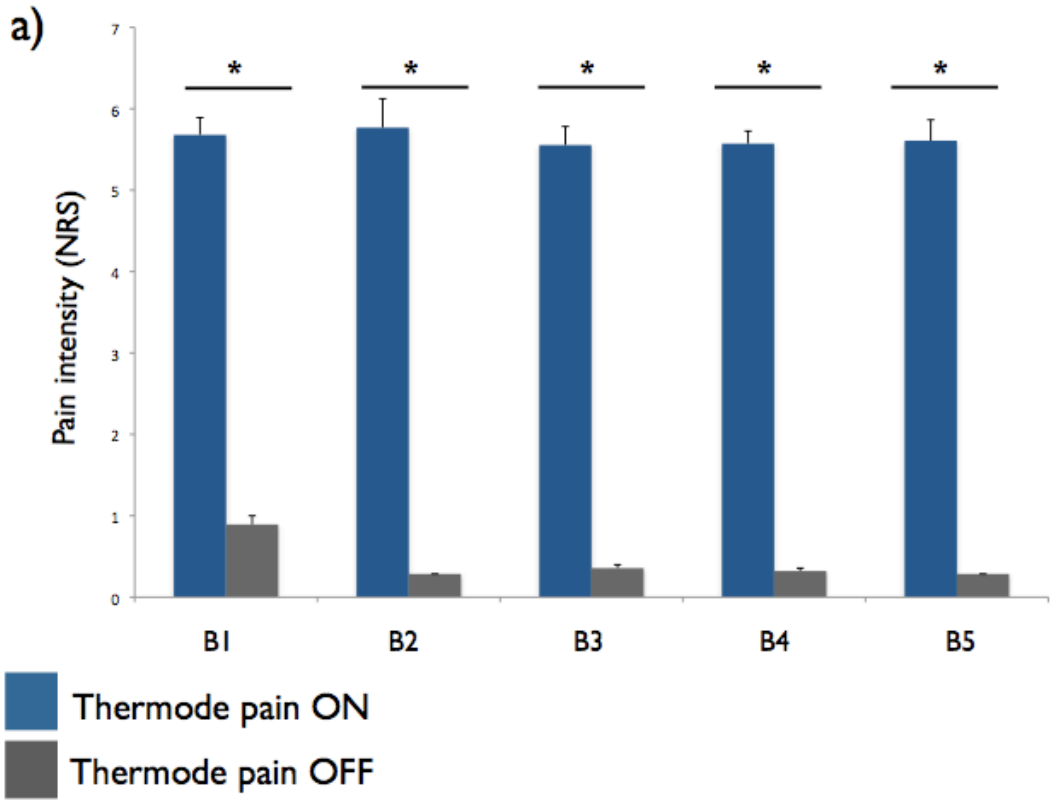

Figure 3: Psychophysical data for capsaicin responders (n=8). Group mean pain intensity ratings as a function of heat stimulus applied to the site of capsaicin exposure: a) Pain intensity was significantly different during the ON blocks (blue) compared to OFF blocks (gray) across the entire paradigm (one-way ANOVA; * $p<0.001$). There was no significant difference in pain intensity ratings between blocks. Error bars represent standard error of the mean (SEM).

b)

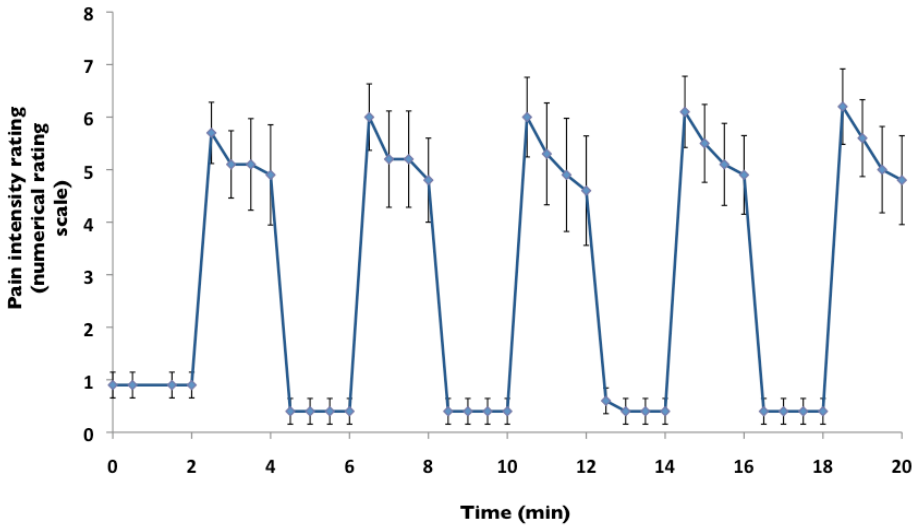

Figure 3: Psychophysical data for capsaicin responders (n=8). Group mean pain intensity ratings as a function of heat stimulus applied to the site of capsaicin exposure: b) Pain intensity ratings over time reveal a characteristic response curve for each ON vs OFF block revealing that the response to the onset of the pain stimulus peaks at the beginning and gradually begins to drop by the end of the ON block. While this shift is expected it does support the use of this design for block lengths no longer than those used here to avoid significant habituation over a block length. Error bars represent standard error of the mean (SEM).

2.2.1.3. Discussion

Application of the 1.0% capsaicin cream was sufficient to induce a primary hyperalgesia response in subjects relatively quickly. The related heat hypersensitivity experienced from the capsaicin treatment was successfully employed to elicit a strong heat pain sensation with a mild warming stimulus. Because of the higher dose of capsaicin used combined with the relatively short

(for a tonic pain paradigm) duration of each stimulus block, less total energy was necessitated to elicit this perception in subjects. The benefit of this is that there is less overall chance of damaging skin tissue (34,39). Similarly, for all typical capsaicin responders, there was no significant change in perceived pain ratings between ON blocks. Additionally, the pain did not appear to habituate over the course of the paradigm. Note however, that a number of subjects (n=7) did not respond in a consistent manner. Specifically, these 'atypical' subjects either did not experience pain from capsaicin application within 30 minutes of application or habituated to the heat pain such that mid-way through the paradigm, the subject was no longer hypersensitive. With this in mind, while capsaicin is a very useful tool to induce ongoing pain states, there are a number of caveats that may explain these findings. For one, topical application does not ensure an exact dose has been reliably applied to active receptors within the skin. Additionally, differences in skin temperature, skin permeability, and ambient temperature can all have an effect on how responsive a subject is to capsaicin (40,41).

In order to ensure that the afferent nociceptive input is well maintained over the course of the pain experiment, future experiments will employ a criterion for 'responders.' Here, subjects will have to have a clear pain response within 20-minutes of application that is well maintained for a minimum of 30-minutes post-application of the cream.

In total, this paradigm appears to safely induce extensive heat hypersensitivity that can be manipulated safely and reliably to elicit a strong, stable pain perception during the ON blocks of the paradigm within typical capsaicin

responders. We are confident that this can be successfully translated into an ASL imaging experiment in which cerebral perfusion changes are observed during the ON vs OFF blocks.

2.2.2. Parametric modulation of capsaicin-induced heat pain

A fundamental limitation to block-design experiments is that they can only provide insight as to whether a particular brain region is recruited in an ON versus an OFF phase of the paradigm (main effect of stimulus). No information about how that region modulates (or, is modulated by) the sensory experience can be obtained. In general, block designs suffer from the assumption of pure insertion whereby a single cognitive process (i.e. the ON block) can be inserted into experimental setting without affecting the other ongoing cognitive processes. Cognitive processing is likely to be more complex than this and so it is important to acknowledge that interpretation of differences in FMRI data here is potentially a simplification of what is actually occurring (42).

Experimentally, the next step towards understanding and validating the role of specific brain regions involved in the ongoing pain experience would be to employ a parametric design in which there is a graded change in stimulus intensity. As in the case of a block paradigm, this is still a one-factor design but the goal is to test the presence of a parametric (linear or non-linear) change in the CBF response. This information can be used to infer if the graded change in the stimulus intensity results in a similar modulation of the brain response. To this end, we wanted to test the possibility of employing this capsaicin-thermode

paradigm to induce parametric increases in tonic heat pain without injury or habituation. In order to ensure it would be possible to produce the perception of well separated sensations of low, moderate and strong pain, a lower dose of capsaicin cream was used to induce thermal hypersensitivity. Here, a 0.075% cream was employed instead of the 1.0% cream.

The goal of this experiment was to test the possibility of employing capsaicin to yield a state of thermal hypersensitivity that can be parametrically modulated with the use of a contact heat thermode. The direct measures we were interested in observing were: 1) the possibility of obtaining three separable levels of perceived heat pain (experiment 1); and 2) the stability of subjects' ratings over time and across repeated runs (experiment 2).

2.2.2.1. METHOD

0.075% capsaicin cream (Pharmasol, UK) was applied to a 1 x 1 inch square on each of the subject's (n=8; 5 female; right handed; age: 18 to 45 yrs) volar forearm. The capsaicin cream was left on the subject's arm until the time at which the subject rated the sensation of the cream as 'just painful' (NRS = 1 out of 10). At this time, the capsaicin cream was removed from the subject's arm. A contact thermode (home-made device) was placed over the site of the capsaicin treated skin. Subjects were thresholded using a modified ascending staircase method until the subject was able to give reliable pain ratings for low (NRS < 3), moderate (3<NRS <5), and strong (NRS >5) pain.

Experiment 1

The goal of experiment 1 was to see if it was possible to parametrically modulate the capsaicin-induced thermal hypersensitivity to obtain separable levels of reported thermal pain. Here, once the thermal hypersensitivity was established, the order of each stimulus block was pseudo-randomised and the length of each stimulus block was elongated to 5-minutes. The reason we lengthened the stimulus block was to enhance the 'tonic' nature of the pain in addition to potentially enhancing the SNR of an ASL signal if the paradigm were used in an FMRI setting. Each stimulation block was separated by a 2-minute rest block (no stimulus input).

Experiment 2

In order to test if the hypersensitivity induced by the initial capsaicin pre-treatment would be sufficient for a longer stimulus paradigm, a group of five subjects were asked to partake in an extended version of the first paradigm. Simply, these subjects received two repeat runs of the stimulus paradigm in series (i.e. only the 2-minute rest block separating run 1 and 2). The order of all stimuli was pseudo-randomized across subjects.

In both experiments, subjects were asked to rate verbally the heat pain intensity and unpleasantness every 30-seconds using the NRS (0-10). See Figure 4 for a detailed description of the paradigm used to elicit different levels of ongoing heat pain.

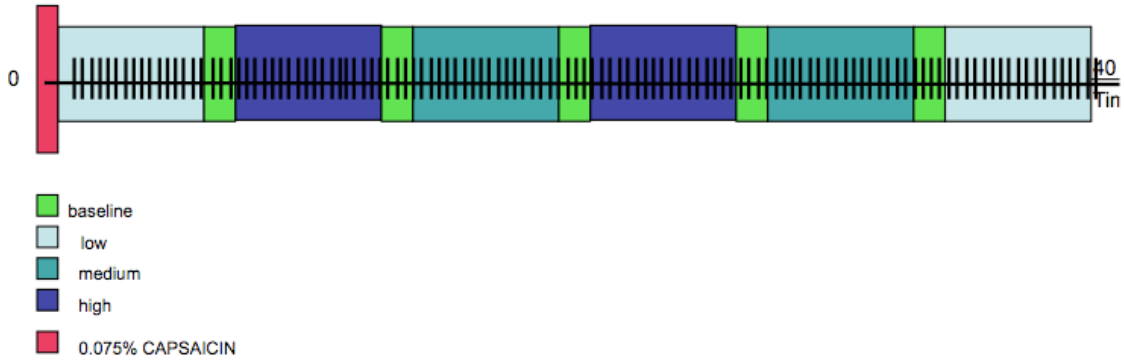

Figure 4: Graphic representation of the capsaicin-heat paradigm incorporating both runs of the experiment. For clarity, each colored block represents a phase of the paradigm: 1) 0.075% capsaicin cream was applied to a 1x1 inch square on the subject's volar forearm where it remained until the subject reported the pain intensity = 1; at which time the cream was removed and replaced with contact thermode (pink). Once the subject was thresholded and reliable pain ratings for low, medium and high pain were elicited with specific stimulus temperatures, longer blocks (5 minutes each) of heat stimuli were applied to the skin (low pain = light blue; medium pain = green; high pain = purple). Each stimulus block was separated by a 2-minute rest block (no stimulus input; light green). Subjects were asked to rate verbally the heat pain intensity and unpleasantness every 30-seconds using the NRS (0-10). In experiment 1, subjects only participated in a single run of the experiment (i.e. only 3 stimulus blocks applied). In experiment 2, subjects participated in two runs of the experiment (i.e. all 6 stimulus blocks applied as seen above).

2.2.2.2. RESULTS

Figure 5a shows the mean pain intensity and unpleasantness ratings for the three stimulus conditions used in experiment 1 (low, moderate and strong heat pain). There was a significant increase in pain intensity (one-way ANOVA, $p<0.05$) and unpleasantness (one-way ANOVA, $p<0.05$) within increasing stimulus intensity. The temperature levels used to elicit each heat pain level

were significantly different for each condition (low pain = 35°C; medium pain = 36.7°C; high pain =38°C; one-way ANOVA, $F(3,12)=58.130$; $p<0.001$).

To observe whether subjects' pain perception habituated with repeat runs of the experiment, we tested for the effect of experimental session on pain ratings within the five subjects that completed back-to-back runs of the experiment (experiment 2). Figure 5b shows there was a significant effect of session on reported pain intensity scores for each stimulus condition as observed by the drop in pain intensity ratings from run 1 to 2 [$n=5$; $F(1,4)=115.184$; $p<0.001$].

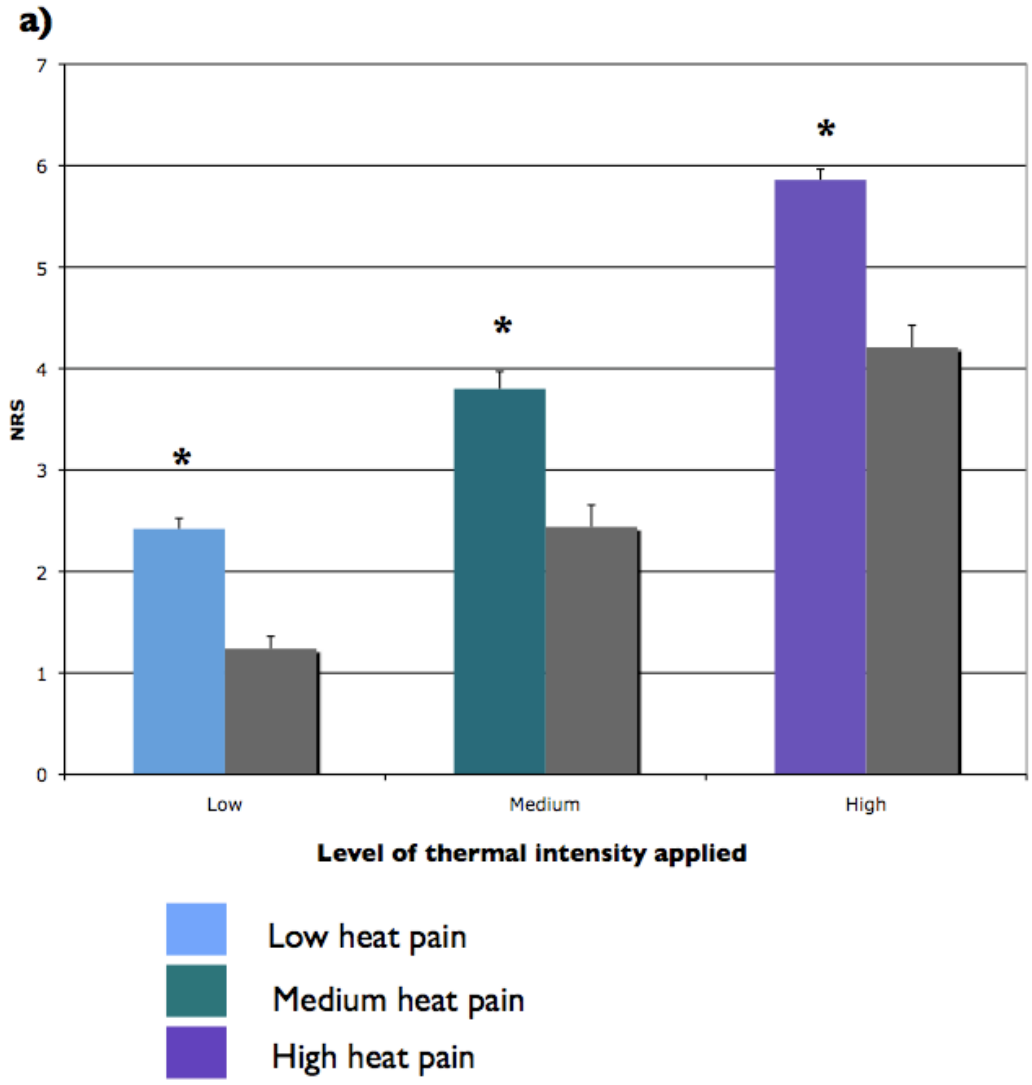

Figure 5a: Psychophysical data for capsaicin responders (n=8). Group mean pain intensity (colors) and unpleasantness (gray) ratings as a function of stimulus intensity applied to the site of capsaicin application. Pain intensity and unpleasantness significantly increased with stimulus intensity (Experiment 1, n=8; one-way ANOVA * $p<0.001$). Error bars represent the standard error of the mean (SEM).

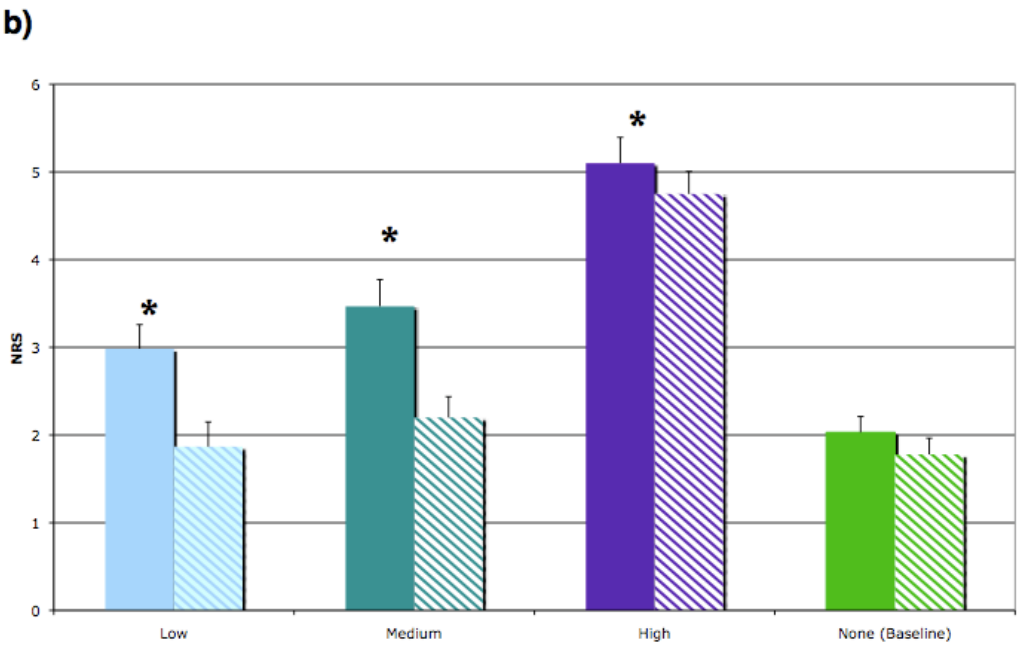

Figure 5b: Psychophysical data for capsaicin responders that participated in two runs of the experiment (n=5). Group mean pain intensity (colors) ratings as a function of stimulus intensity applied to the site of capsaicin application. To test for the presence of habituation of pain responsiveness over time, pain intensity ratings were compared between run 1 (solid colors) and a repeat run (hatched colors) immediately following the completion of run 1. A significant effect of session was observed (Experiment 2, n=5; ANOVA, *$p<0.001$). Error bars represent the standard error of the mean (SEM).

2.2.2.3. DISCUSSION

Application of a 0.075% capsaicin cream was sufficient to induce a primary heat hyperalgesia response that was reliable enough to be parametrically modulated with the use of a contact heat thermode. We show that three levels of heat pain could be elicited in subjects with this capsaicin preparation. Additionally, we show that each level of pain was maintained for the five-minute stimulus block. Ability to reliably induce constant perception of differing levels of heat pain is a primary goal for translating this design into an ASL imaging experiment. Interestingly however, a clear habituation occurs over time as reported pain scores decrease with repeat runs of the experiment. Previous work in humans employing a capsaicin cream has shown similar habituating effects over time (43,44,45,46). These data suggest two potential weaknesses in the design: 1) the dose of capsaicin used is insufficient to yield a maintained heat hypersensitivity for experiments longer than 30-minutes; 2) the rest blocks are perhaps too short to prevent habituation. Additionally, due to the long exposure times to contact heat, subjects that necessitated stimulus temperatures >43 °C were at risk of blistering (34,39).

While it is clear from the results of the capsaicin-thermode experiments that it is possible to use the model to induce a strong pain sensation, there are significant caveats to consider before employing it within an FMRI study. Issues relating to the large number of non-responders, potential for habituation and safety concerns of employing stimulus blocks longer than 2 minutes limit the utility of the capsaicin-thermode model.

2.3 MECHANICAL PAIN

Mechanical stimulation is another commonly investigated modality used to elicit pain states by applying a single sustained stimulus to the skin. Similar to the capsaicin model above, pain is induced via a well-defined peripheral nociceptive pathway. However, the specific underlying pathophysiology of the ongoing sensation is different for capsaicin and therefore is likely to generate a different type of ongoing pain state. For example, capsaicin induces a complex array of peripheral and central changes that include recruitment of fast-adapting unmyelinated fibres, release of inflammatory cytokines and excitatory neurotransmitters. Additionally, activation of TRPV1 is also affected by temperature (body and ambient) (47). Perceptually, this has the effect of inducing an oscillating, non-uniform pain sensation. In contrast, ongoing mechanical stimulation was previously documented in rats (48,49) and humans (49) to excite a well-maintained response from a class of myelinated high-threshold, slowly-adapting A-fibres that perceptually is less susceptible to spontaneous fluctuations in pain intensity and unpleasantness.

It is well documented that the underlying peripheral source of ongoing mechanical pain is reliant on complex and distinct response profiles from both A and C fibre types. Previous experiments in rats (48), cats (49) and monkeys (50) have demonstrated that during tonic mechanical stimulation, the A- and C- fibre responses differed greatly. Specifically, the C-fibre response peaked at pain threshold and adapted quickly at higher stimulus intensities. In contrast, A-fibres showed both rapid and slowly adapting characteristics, the later continuing to fire over the course of the tonic stimulus. From human studies however, it is clear

that over time, even as these slow-adapting fibres begin to adapt, the reported pain scores remain high and even increase. While the underlying physiology of this effect is still unclear, a number of related factors are likely to be involved in coding the sensation of ongoing mechanical pain. For example, tonic stimuli are likely to induce the release of inflammatory mediators (e.g. prostaglandins, bradykinins) able to recruit otherwise silent nociceptor subtypes (51). Additionally, from investigations of rat dorsal horn neurons during tonic mechanical stimuli, it was shown that primary nociceptor adaptation coincided with increased activity of WDR neurons; lending support to the idea that the maintenance of ongoing pain is also related to central changes at the level of the spinal cord (52). As with investigations of heat pain, differentiating the peripheral source of the tonic mechanical pain is beyond the scope of the current investigation. The current aim is to exploit these complex nociceptor dynamics to trigger a prolonged state of pain that is safe and reproducible. With this in mind, we tested the utility of this model employed by Andrews & Greenspan (1999) to obtain robust, well-maintained parametric increases in ongoing pain perception in healthy subjects.

2.3.1. Parametric modulation of mechanical pain

The goal of this experiment was to observe whether brain regions recruited during an ongoing pain experience are parametrically modulated by graded stimulus intensities. To do this, MR-compatible pin-prick devices calibrated to deliver a range of stimulus forces when applied to the skin were used. The direct measures of this study include quantification of the subjective report of stimulus intensity, unpleasantness and duration.

2.3.1.1. METHOD

Experiments were performed on 18 healthy subjects (10 female; right handed; age: 18-40yrs). Subjects were asked if they were suffering from pain or were on any medications. No subject reported being in any background pain. No one was on medication likely to interfere with the pain responsiveness. All subjects gave informed consent and the Oxfordshire Clinical Ethics Committee approved this study.

Stimuli

Mechanical probes (MRC, Germany) calibrated to give a constant force (64mN, 256mN and 512mN) were applied to the skin separating the thumb and first finger for a period of 5 minutes. A homemade plastic handle was used to comfortably expose the stimulus site over the duration of the experiment.

Psychophysics

Subjects were told they would receive a series of stimulations that would last for a few minutes but were not told the exact duration of the stimulus block. Mechanical stimuli were applied to the hand by placing the probe into a stabilizing apparatus that securely held the probe at a constant force on the stimulus site for the duration of the 5-minute stimulus block. The stimulus order was pseudo-randomised across subjects to control for confounding effects of stimulus order, sensitisation and habituation. A 10-minute rest block (no stimulus present) was observed after each stimulus block. Here, subjects were asked to maintain the position of their hand but in the absence of a stimulus probe. During

the stimulation, subjects were asked to keep their eyes closed and to focus on the stimulation being received. Subjects rated the stimulus intensity and unpleasantness verbally using an 11-point numerical rating scale (NRS; 0= no pain; 10= worst pain imaginable) every 30 seconds. Please see Figure 6 for a detailed description of the paradigm used.

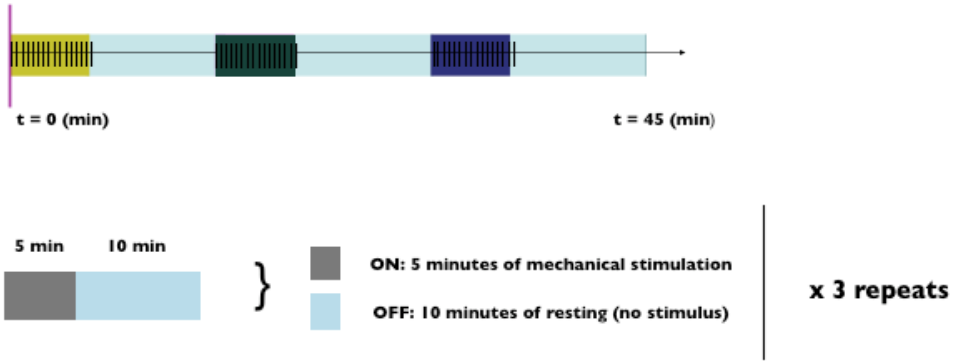

Figure 6: Graphic representation of the mechanical pin-prick paradigm. For clarity, each colored block represents a phase of the paradigm: Mechanical stimuli were applied to the stimulation site by placing the force-calibrated probe into a home-made apparatus that securely held the probe at a constant force at the exact stimulus site over the course of the 5-minute block. The magnitude of forces used were: 64mN, 256mN, and 512mN to elicit the perception of low pain, medium pain, and strong pain, respectively.

Stimuli were pseudo-randomised to control for confounding effects of stimulus order, sensitisation and habituation. Between each stimulus block (colour), a 10-minute rest block was observed in which the subject's hand remained positioned on the handle with the absence of any mechanical stimuli (light blue). We doubled the size of the rest blocks to ensure the peripheral neurophysiology was unaltered by inflammation, sensitisation or habituation that is likely to occur if

stimuli are applied too closely together in time. During stimulation, subjects were asked to remain still with their eyes closed and to focus on the stimulation being received. Subjects were asked to rate verbally the stimulus intensity and unpleasantness using the NRS (0-10) every 30-seconds. Ratings were only acquired during the ON blocks.

2.3.1.2. RESULTS

Figure 7a,b shows the mean pain intensity ratings for the three stimuli conditions used in this study (low, moderate and strong pain). The mean pain intensity pain rating for each condition was (low = 0.89, S.E. = 0.032; moderate = 2.71, S.E. = 0.11; strong = 4.91. S.E. = 0.16, respectively. The mean pain unpleasantness rating for each condition was (low = 0.75, S.E. = 0.026; moderate = 2.78, SE = 0.075; strong = 5.12, SE = 0.178), respectively. There was a significant increase in pain intensity (one-way ANOVA; $p<0.001$) and unpleasantness (one-way ANOVA; $p<0.001$) across the three conditions (Figure 7a). The pain intensity and unpleasantness ratings habituated slightly during the high pain condition when comparing the first and last ratings (Figure 7b; Student t test, $p<0.05$). The reported pain perception did not significantly habituate over the course of the stimulus block for the medium or low pain intensity conditions.

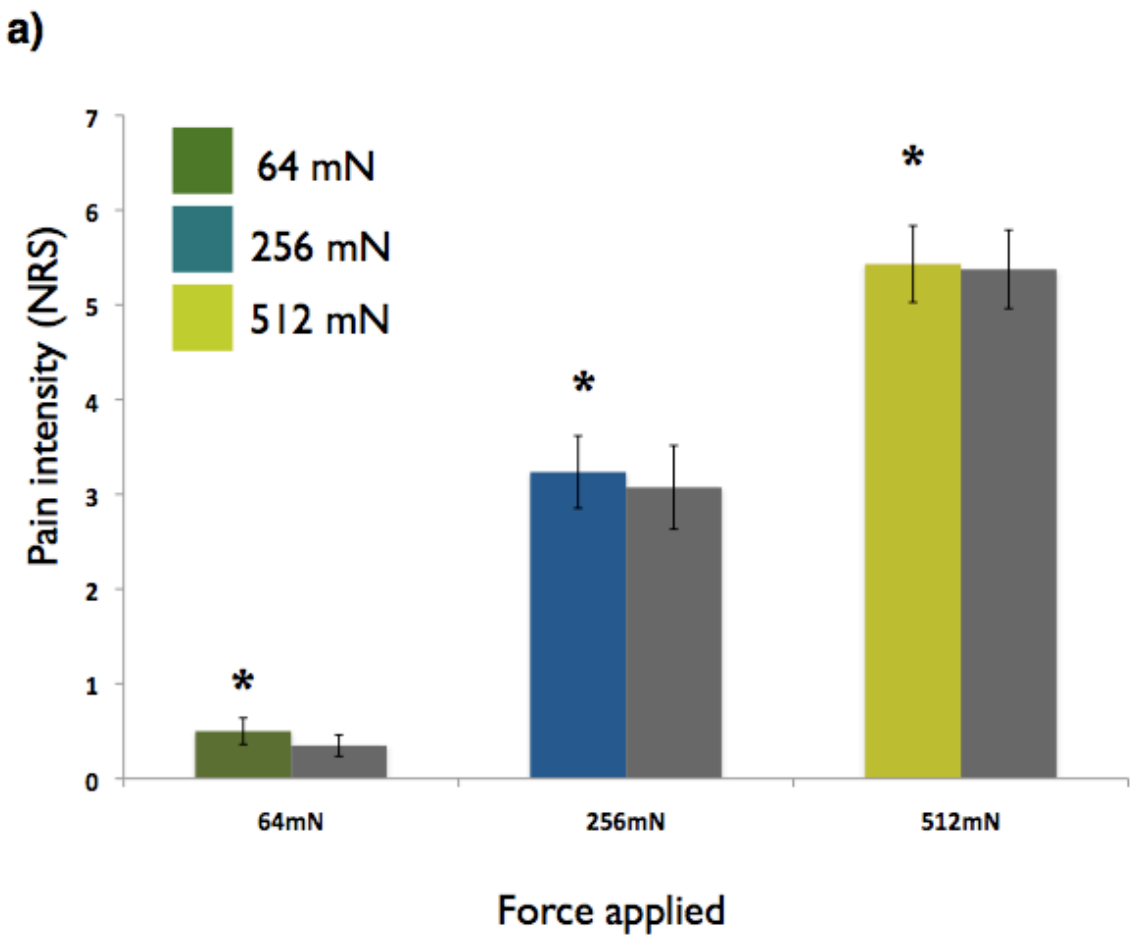

Figure 7: Psychophysical data. Group mean pain intensity and unpleasantness ratings as a function of stimulus intensity applied to subjects' hands. a) Pain intensity (blue) and unpleasantness (gray) significantly increased with stimulus intensity (n=18; * one-way ANOVA, $p<0.001$). Error bars represent the standard error of the mean (SEM).

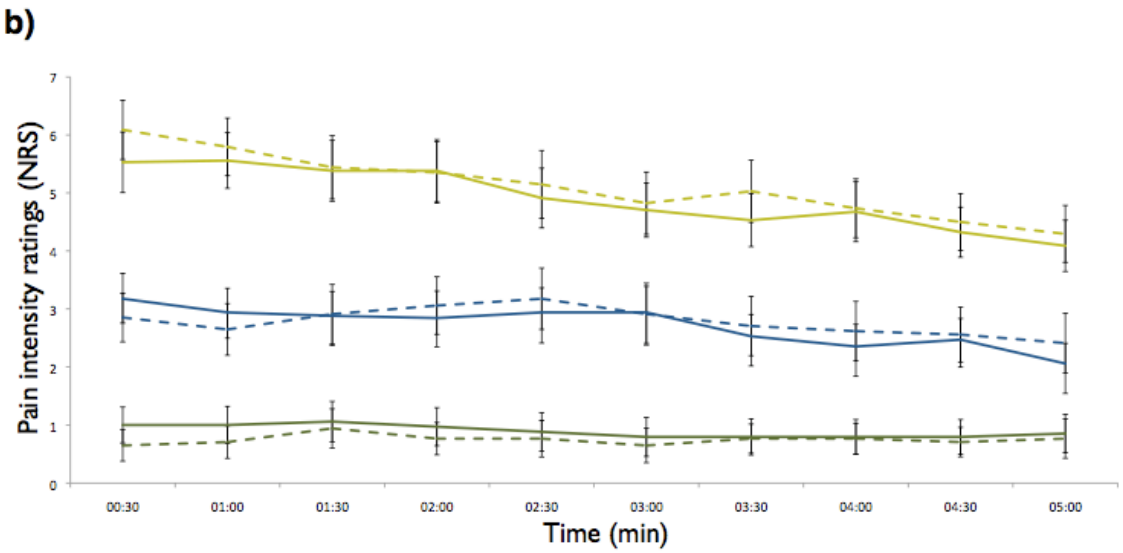

Figure 7: Psychophysical data. Group mean pain intensity and unpleasantness ratings as a function of stimulus intensity applied to subjects' hands. b) Pain intensity (solid lines) and unpleasantness (dotted lines) over the time-course of the stimulus block for each level of force applied (64mN = green; 256mN = blue; 512mN = yellow). There was a significant difference in reported pain perception (intensity and unpleasantness) when comparing the first and last pain ratings during the high pain condition only (Student t test, $p<0.05$). Error bars represent the standard error of the mean (SEM).

2.3.1.3. DISCUSSION

Application of mechanical stimuli to subjects' hands elicited pain reports that reflected the graded change in stimulus intensity. These pain reports were well maintained over the course of the 5-minute stimulus blocks. Importantly, the group average pain reports show no indication of habituation or sensitisation to the medium and low pain experiences and only slight (ΔNRS < 1) habituation during the high pain condition when comparing the first and last pain ratings. We are confident therefore that these data provide strong evidence to support the use of the paradigm to elicit steady-state blocks of ongoing pain at levels that are easily separable.

Previous work by Andrew, D. & Greenspan, JD (1999) compared human psychophysics with rat nociceptor activity to look at peripheral coding of tonic mechanical cutaneous pain. Using a similar paradigm to ours, the study showed that the prolonged pain reports in humans coincided with maintained responses in rats from both slow and fast adapting C and A fibres, particularly a class of A-fibre nociceptors that have a high threshold and are slowly adapting (39). These results confirm that the ongoing pain precept is, in part, related to a well-maintained afferent input from the periphery that does not habituate over the experiment.

Because these data show clearly separable levels of pain that are well-maintained over the stimulus blocks; with no subject drop-out or reported skin damage; we chose to utilise this paradigm in an ASL FMRI experiment to investigate the neural correlates related to this type of ongoing pain experience.

2.4 Conclusion

Our initial tonic pain psychophysical pilot studies show that it is indeed possible to induce tonic pain in a safe, robust and reliable way by using pain modalities that are well characterised and are employed ubiquitously within animal pain research. The key objectives for these pain models are to induce a steady-state pain experience that is easily manipulated within a controlled experimental setting. The reason for this is simply that we do not yet know what the neural correlates of tonic pain are. It is therefore of paramount concern that the pain experience used within an imaging context be a uniform, non-fluctuating one. We predicted that this would be possible by employing pain modalities that are well known to engage select populations of nociceptors to engage sustained

afferent input to the CNS.

Our heat pain pilots show that it is possible to obtain tonic heat pain safely by employing capsaicin to induce a state of thermal hypersensitivity before applying a temperature controlled thermode. The 1% capsaicin block design data reveal that it is possible to get robust, well maintained pain responses from subjects that are capsaicin-responsive. The 0.075% capsaicin experiment employed graded increases in thermal pain to obtain well-maintained pain responses over the 5-minute stimulus blocks. However, the model suffered from: i) a high incidence of habituation when the session was repeated; and ii) a potential for skin damage (i.e. higher stimulus temperatures for longer exposure times more likely to induce blistering). Additionally, from both capsaicin pilots, there was an interesting 'non-responder' population that made subject recruitment difficult. Here, subjects were characterised as 'non-responders' if s/he either did not feel heat pain at any point after the onset of capsaicin application or if the subject reported a very strong habituation of the thermal-hypersensitivity shortly after the initial heat pain sensation was first reported. In addition, topical application of capsaicin is likely to be associated with considerable variability in the dose concentration actually reaching the target receptor population. This may also explain the large number of 'non responders' observed. Future studies employing capsaicin cream will have to account for these potential setbacks.

Overall, it is clear that the use of capsaicin-thermode induced heat pain is perhaps best suited for a block design paradigm. However, the results from the mechanical pain pilot support its use in parametric studies of ongoing pain. We

employed a stimulus force-locked design in which subjects reported robust, well differentiated pain responsiveness to three force probes applied to the subjects' hands. Importantly, the psychophysics data show that the response profiles were well maintained over the course of the 5-minute stimulus blocks as no significant habituation to the pain stimuli were observed. There were no incidence of injury and no subjects failed to find the stimuli 'painful' (i.e. all subjects were 'responders'). These data provide promising support for the implementation of the mechanical pain paradigm in our initial investigations with ASL. We posit that this mechanical pain model is well-suited for an initial exploration of the neural correlates of ongoing pain where we do not yet know what/how the brain responds to ongoing pain. Here, it will be possible to rely on this modality to obtain a constant pain state such that it will be possible to optimise the imaging approach for more complex ongoing pain phenotypes where the CBF dynamics are likely to reflect the complexity and non-uniformity of the pain state itself.

Additionally, these data also provide exciting insight into future investigations employing more invasive electrophysiological techniques. For example, it would be possible with the current models to employ microneurography and FMRI to observe the exact peripheral sources of different ongoing pain states. Coincidently, it would be advisable to translate this work back into an animal model. For example, by employing the tonic mechanical pain model in a rat model, it would be possible to obtain intracortical recordings from brain regions highlighted from the human imaging work. Here, it would then be possible to begin to look not just at key pain regions involved but also at the effective

connectivity between them; and relatedly, how this can be altered with specific pharmacological and/or genetic manipulation.

We are confident that the results from these initial psychophysics studies of capsaicin and mechanical induced tonic pain states will inform future imaging studies of the neural correlates of various ongoing pain states and pathologies.

2.5 References

1. Lauchtenbacher, S. *et al. (*1995). Tonic pain evoked by pulsating heat: temporal summation mechanisms and perceptual qualities. Somatosensory and Motor Res. 12(1):59-70

2. Sprenger, T *et al. (*2006). Opioidergic activation in the medial pain system after heat pain. Pain 122:63-67

3. Kupers, R. *et al.* (2009). Painful tonic heat stimulation induces GABA accumulation in the prefrontal cortex in man. Pain 142:89-93

4. Fowler, CJ *et al.* (1988). The conduction velocities of peripheral nerve fibres conveying sensations of warming and cooling. J Neurol Neurosug Psychiatry 51:1164-70

5. Brennum J. et al. (1989). Measurement of human pressure-pain threshold on fingers and toes. Pain 38(2):211-7

6. Adriaensen *et al.* (1984). Response properties of thin myelinated (A-delta) fibers in human skin nerves. J Neurophysiology 49:111-22

7. Andrew, D. & Greenspan, JD (1999). Mechanical and heat sensitization of cutaneous nociceptors after peripheral inflammation in the rat. J Neurophysiology 82:2649-2656

8. Laursen, RJ *et al.* (1997). Quantification of local and referred pain in humans induced by intramuscular electrical stimulation. Eur J Pain 1(2):105-13

9. Lee, MC et al. (2008). Identifying brain activity specifically related to the maintenance and perceptual consequences of central sensitization in humans. J Neuroscience 28(45):11642-9

10. Zambreanu, L. et al. (2005). A role for the brainstem in central sensitization in humans. Evidence from functional magnetic resonance imaging. Pain 114(3): 397-407

11. Jensen, K *et al.* (1990). Pain, tenderness, wheal and flair induced by substance P, brdaykinin, and 5-hydroxytryptamine in humans. Peptides 11(6):1133-8

12. Jordt, SE. et al. (2004). Mustard oils and cannabinoids excite sensory nerve fibres through the TRP channel ANKTM1. Nature 427(6971):260-5

13. Jensen, K *et al.* (1991). Pain, tenderness, wheal and flair induced by substance P, brdaykinin, and 5-hydroxytryptamine in humans. Cephalagia 11(4):175-82

14. Babenko, V. *et al.* (1999). Experimental human muscle pain and muscular

hperalgesia induced by combinations of serotonin and bradykinin. Pain 82(1):1-8

15. Graven-Nielsen, T. *et al.* (1997). In vivo model of muscle pain: quantificaiton of intramuscular chemical, electrical, and pressure changes associated with saline-induced muscle pain in humans. Pain 69(1-2):137-43

16. Stohler, CS *et al.* (1999). Spatial and temporal summation of sensory and affective dimensions of deep somatic pain. Pain 79(2-3):165-73

17. Estebe, JP et al. (2002). Pilot study of the effect of tourniquet use on sufentanil pharmacokinetics. J Clin Anesth. 14(8):578-83

18. Schmelz, M. et al. (2000). Encoding of burning pain from capsaicin-treated human skin in two catergories of unmylinated nerve fibres. Brain: 123, 560-571

19. Clark, D., Hughes, J. & Gasser, H.S. (1935). Afferent function in the group of nerve fibers of slowest conduction velocity. American Journal of Physiology 114, 69-76

20. Landau, W. & Bishop, G. H. (1953). Pain from dermal, periosteal, and fascial endings and from inflammation. Archives of Neurological Psychiatry 69, 490-504

21. Collins, W.F., Nulsen, F.E., & Randt, C.T. (1960). Relation of peripheral nerve fiber size and sensation in man. Archives of Neurology 425, 323-344

22. Schady, W. J. L., Torebjork, H. E. & Ochoa, J. L. (1983). Peripheral projection of nerve fibers in the human median nerve. Brain Research 277, 249-261

23. Torebjrok, H. E. & Ochoa, J. L. (1990). A new method to identify nociceptor units innervating glabrous skin of the human hand. Experimental Brain Research 81, 509-514

24. McMullan, S. & Lumb, B. M. (2001). Differential midbrain control of responsiveness to C- and Aδ- nociceptor activation. Journal of Physiology. 533.P, 72P

25. Lumb B.M. (2002). Inescapable and escapable pain is represented in distinct hypothalamic-midbrain circuits: specific roles for Aδ- and C- nociceptors. Experimental Physiology. 87(2), 281-6

26. Price, D.D. (1996). Selective activation of A-delta and C nociceptive afferents by different parameters of nociceptive heat stimulation: a tool for analysis of central mechanism. Pain. 68(1), 1-3

27. Yeomans, D.C. , Pirec, V. & Proudfit, H.K. (1996). Nociceptive responses to high and low rates of noxious cutaneous heating are mediated by different nociceptors in the rat: electrophysiological evidence. Pain. 68, 133-140

28. McMullan, S. & Lumb, B.M.. (2004). A reliable method for preferential activation of C- or A- fiber heat noiceptors. J Neuroscience Methods. 138(1-2): 133-9

29. Sprenger, T. et al. (2006). Opiodergic activation in the medial pain system after heat pain. Pain. 122(1-2):63-7

30. Huber, M. T. (2006). EEG responses to tonic heat pain. Exp Brain Res. 173(1):14-24

31. Lauthenbacher S., Roscher S., Strian F. (1995). Tonic pain evoked by pulsating heat: temporal summation mechanisms and perceptual qualities. Somatosens Mot Res. 12(1): 59-70

32. Derbyshire S.W. & Osborn, J. (2008). Enhancement of offset analgesia during sequential testing. Eur J Pain. 12(8):980-9

33. Derbyshire, S.W. & Osborn, J. (2009). Offset analgesia is mediated by activation in the region of the periaqueductal grey and rostral ventromedial medulla. Neuroimag. 47(3):1002-6

34. Naert, N.L. , Kehlet H., & Kupers, R. (2008). Characterization of a novel model of tonic heat pain stimulation in healthy volunteers. Pain. 138(1): 163-71

35. Caterina, MJ et al. (2000). Impaired nociception and pain sensation in mice lacking the capsaicin receptor. Science: 288:306-313

35. Tai, C. et al. (2008). TRPA1: The Central Molecule for Chemical Sensing in Pain Pathway? J. Neuroscience: 28(5):1019-1021

36. Latremoliere, A. & Woolf, CJ (2009). Central sensitization: a generator of pain hypersensitivity by central neural plasticity. J Pain: 9:895-926

37. Stone, L. & Dallenbach, KM.(1934) Adaptation to the pain of radiant heat. The American J of Psychology: 46(2):229-242

38. Drummond, PD. (2001) The effect of sympathetic activity on thermal hyperalgesia in capsaicin-treated skin during body cooling and warming. Eur J Pain 5(1):59-67

39. Andrew, D. & Greenspan, JD (1999) Mechanical and heat sensitization of cutaneous nociceptors after peripheral inflammation in the rat. J Neurophysiology 82(5):2649-56

40. Cevero, R. & Handwerker, HO (1998) Prolonged noxious mechanical stimulation of the rats tail: responses and encoding properties of dorsal horn neurones. J Physiology 404:419-436

41. Logothetis, N.K. (2008). What we can do and what we cannot do with fMRI. Nature. 453(7197):1729-34

(28,29,30,31)

42. Greene, L. & Hardy, JD (1961). Adaptation of thermal pain in the skin. J of Applied Physiology 17: 693-696

43. Bingel, U. et al. (2007). Habituation to painful stimulation involves the antinociceptive system. Pain 131:21-30

44. Rennefeld, C. et al. (2010). Habituation to pain: Further support for a central component. Pain 148:503-508

45. Moritz & Henriques (1946). Studies of thermal injury. The importance of time and surface temperature in cause of cutaneous burn.

46. Patapoutian, A., Peier, A.M., Story, G.M., Viswanath, V. (2003) ThermoTRP channels and beyond: mechanisms of temperature sensation. Nat Rev Neuroscience 4(7):529-39.

47. Woolf, CJ & King, AE (1987) Physiology and morphology of mulitreceptive neurons with C-afferent fiber inputs in the deep dorsal horn of the rat lumbar spinal cord. J Neurophysiology 58(3):460-477

48. Andrew, D. & Greenspan, JD (1999) Peripheral coding of tonic mechanical cutaneous pain: comparison of nociceptor activity in rat and human psychophysics. J Neurophysiology 82(5):2641-8

49. Garell et al. (1996). Mechanical response properties of nociceptors innervating feline hairy skin. J Neurophysiology 75:1177-1189

50. Slugg et al. (1994). Response of cutaneous A- and C- fiber nociceptors in the monkey to controlled-force stimuli. Journal of Neurophysiology 83(4)2179-2191

51. Woolf, C.J. & Salter, M.W. (2000). Neuronal plasticity: Increasing the gain in pain. Science 288(5472):1756-68.

52. Cervero, F. (1987). Fine afferent nerve fibers and pain, ed. Schmidt, R.F., Schaible H.G. & Vahle-Hinz, C. pp323-331. VCH Verlagsgesellschaft, Berlin.

Chapter 3

Development of a whole brain ASL approach for use in fMRI investigations of tonic pain states

3.1 Introduction

Arterial spin labeling (ASL) is a quantitative perfusion imaging technique that measures changes in neural activity based on related fluctuations in local cerebral blood flow (CBF). Unlike positron emission tomography (PET), which uses an injected radioactive tracer to image changes in CBF, ASL non-invasively tags blood by manipulating its inherent magnetic properties. Because ASL does not necessitate the use of unstable radioactive compounds to be injected and can therefore be used repeatedly within a subject without any contraindications, it offers promising experimental and clinical utility.

Measuring perfusion with MRI has become a widely used clinical tool. Often, perfusion images are generated with the use of injected tracers. Unfortunately, this technique is invasive, potentially hazardous, and limited in its experimental usefulness due to the volatile and expensive nature of the tracers. In contrast, ASL magnetically labels protons suspended in water within arterial blood to generate an endogenous tracer. ASL is completely non-invasive and significantly less limited in its experimental utility therefore.

The fundamental principle of measuring CBF with ASL is based on the pioneering work of Kety and Schmidt (1948) (1). Here, Nitrous Oxide (N_2O) was used as a freely diffusible tracer that, once inhaled, could be monitored over time to quantify the magnitude of perfusion. Once subjects inhaled the N_2O, the concentration of tracer in arterial and venous blood samples was monitored. What Kety and Schmidt observed was that the average time it takes for the N_2O to flow across the tissue is proportional to the rate of blood flow and the volume of blood flowing.

This concept is the foundational principle of ASL imaging where instead of using a freely diffusible tracer, magnetically labeled water is used as an intravascular tracer to measure the volume of blood flowing over time (2,3). Regardless of the type of ASL sequence used, perfusion images are generated by tagging arterial blood with an RF pulse, allowing the tagged blood to flow to a region of interest and then capturing an image to observe how much tagged flow innervated that region.

When we began this work, there were two main types of ASL available: Continuous ASL (CASL) and Pulsed ASL (PASL) but no clear indication which technique was best suited to image the brain in pain and neither gave whole brain data - severely limiting their utility for pain studies. Fundamentally, the key difference between the two is based on the duration of the radio-frequency (RF) pulse applied to tag arterial blood and how to reduce the confounding effects of magnetization transfer introduced by RF tagging (see Diagram 1).

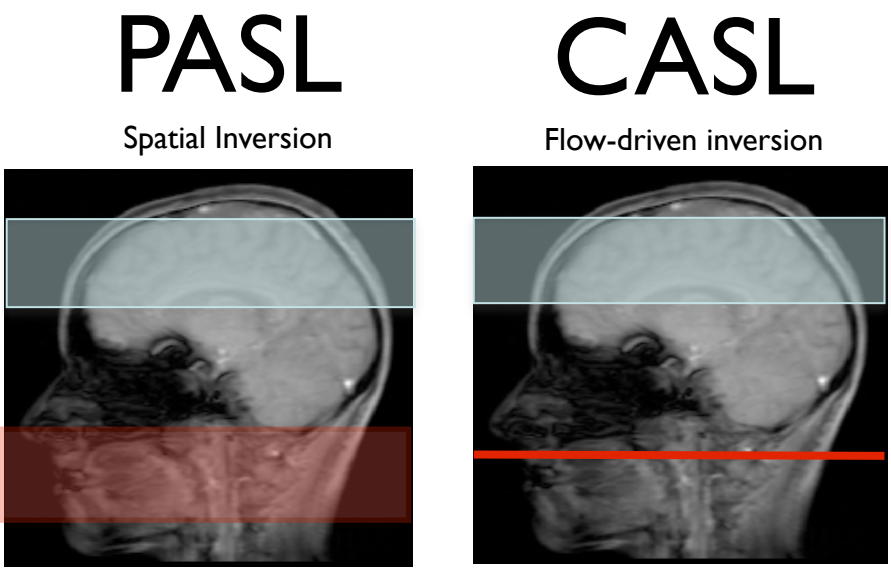

Diagram 1: Graphic representation of the differences between pulsed (PASL) and continuous (CASL) arterial spin labeling methods. For clarity, the sagittal slice shows approximately where anatomically the labeling (red) versus imaging (blue) planes are defined for the each technique. In general, there are two main types of ASL: Continuous ASL (CASL) and Pulsed ASL (PASL). The key difference between the two is based on the duration of the radio-frequency (RF) pulse applied to tag arterial blood and how to reduce the confounding effects of magnetization transfer introduced by RF tagging. CASL was the first ASL technique to be developed and is based on the application of a single, continuous RF pulse alongside slice-selective gradients that adiabatically invert arterial magnetization to 'tag' blood flowing into the brain (4). To nullify the confounding effects of MT, a 'control' image is taken in which the RF pulse is applied in the absence of the slice-selective gradients so blood is not tagged. For a review of the various technical permutations of this method please see Golay, X. et al. (2004) (2). PASL employs a significantly reduced RF pulse to tag blood and therefore is arguably easier to implement. The two main types of PASL are known as Flow-sensitive Alternating Inversion Recovery (FAIR) and Echo-planar Imaging with Signal Targeting by Alternating Radio-Frequency Pulses (EPISTAR) (5,6,7). At FMRIB, the EPISTAR PASL technique is used. Specifically, the tag image is generated by applying an inversion pulse sequence to a slab proximal to the image volume of interest. As blood flows through the slab, it is tagged and then flows into the volume of interest, which is imaged. In the control image, the slab is shifted the same distance distally from the volume of interest to control for MT effects (3).

Briefly, while PASL labels arterial blood by inverting all blood within a defined volume using a very short (~10ms) radio-frequency pulse, CASL defines a labeling plane (defined by the arterial flow, long (~2s) RF pulse and the gradient orientations) through which arterial spins are inverted ('tagged') through adiabatic inversion. In general, it was thought that while CASL benefited from optimal spatial SNR, PASL could image a larger volume of cortex, and more quickly than CASL.

To note, neither of these techniques were capable of acquiring a whole brain volume of activation; a key goal for our initial imaging investigations of ongoing pain. However, at that time, our MR Physics collaborators were developing a single-shot 3D GRASE acquisition approach that would enable us to acquire a whole brain volume whilst employing the PASL labeling approach. However, few people had experience applying the technique to image activation related to a basic functional task. Consequently, the goal of this chapter is to describe the process through which we endeavored to articulate which ASL approach was best suited to be image perfusion changes related to a basic functional task; and relatedly, how we developed this approach for use in a tonic pain imaging context.

3.2 Investigation of standard FMRI sequences: a comparison of ASL & BOLD

BOLD FMRI is a widely used, successful tool to image changes in brain function. BOLD signal reflects dynamic changes in regional magnetic susceptibility that arises from physiological changes (i.e. fluctuations in CBF, CBV, $CMRO_2$)

coincident with neural activity. These changes trigger a fluctuation in the concentration of venous deoxygenated haemoglobin, which, due to its paramagnetic nature, results in a disturbance in the local magnetic field. Because of the timing of these changes relative to the onset of neural activation, BOLD FMRI is ideally suited to acute, phasic stimulus paradigms.

Historically, pain imaging has relied almost entirely on Blood Oxygen Level Dependent (BOLD) FMRI to observe changes in brain activation related to pain. Numerous studies employing this technique have elucidated a complex array of sub/cortical regions involved in pain processing and consequently have helped articulate the complex, multidimensional nature of different pain experiences (for review: 9).

As a technique however, BOLD is susceptible to low frequency signal drift inherent to the MR environment. Specifically, low-frequency stimulus paradigms (i.e. paradigms with long stimulus blocks) are associated with drift (i.e. noise) that is very high powered (10). Consequently, in the analysis of BOLD data acquired with a high prevalence of low-frequency drift, the overall SNR of the images generated is low. So, even though neurons are very much active relative to the paradigm, it is just not possible to observe it with BOLD. Consequently, experimental designs that incorporate low stimulus frequencies (e.g. stimulus blocks longer than a minute), are poorly resolved with BOLD FMRI (7). The availability of clinically relevant experimental pain imaging studies therefore is sparse.

ASL FMRI, while less widely used, offers an exciting alternative to BOLD as it observes brain function by directly measuring changes in CBF. A fundamental

principle of ASL is that it generates perfusion contrast by employing a pair-wise subtraction of adjacent (i.e. tag minus control) images. This effectively eliminates the low frequency drift present within the spectrum, thereby allowing the technique to be used to image paradigm designs otherwise outside the capacities of BOLD FMRI. To add, because ASL directly measures CBF, it is argued to have less inter-subject variability during task activation compared to BOLD (11). While these potential benefits of employing ASL are clear, it is not well known which type of ASL sequence is best to employ within this experimental context.

There are fundamental weaknesses with ASL imaging that need to be considered before it is implemented in a pain imaging study. For one, ASL suffers from low signal to noise (SNR) compared to BOLD. This is due to many reasons: firstly, a change in BOLD reflects a composite of physiological changes that include task-related increases in cerebral blood flow (CBF), volume (CBV) and metabolic rate ($CMRO_2$). In comparison, ASL measures CBF alone. While task-related changes in CBF can be large, there is a fundamentally low fraction of arterial blood to brain tissue in the human brain (e.g. 1-2%)(12). Consequently, ASL inherently has a low SNR. Because the ASL signal is approximately 1% of background signal to begin with, the added presence of physiological noise (cardiac, motion, respiration etc.) can significantly undermine meaningful signal changes.

Experimentally, ways to overcome these fundamental limitations to ASL can be generally broken down into two main categories: 1) maximize meaningful perfusion signal; 2) reduce confounding noise artifacts.

Reduction of noise includes a range of methods such as: eliminating subject motion, modeling physiological parameters that confound CBF signal, background suppression techniques (e.g. train of inversion pulses during the post-label delay), optimization of TI's, and/or single-shot 3D-acquisition of k-space (13). These factors apply to all ASL experiments regardless of the type of ASL sequence employed. In contrast however, to maximize ASL SNR, fundamental aspects of the ASL sequence itself must be considered. The key means of increasing ASL SNR is to optimize the amount of perfusion signal available to be imaged. As the name suggests, continuous ASL (CASL) should, in theory, produce the largest amount of signal (Wong, et al. 1998) (14). However, multi-slice CASL approaches often result in less total SNR due to problems with artifacts in the control images and inefficient signal labeling over longer scan acquisitions (Alsop & Detre, 1998) (15). In contrast, pulsed ASL (PASL) only labels a net volume of blood defined within an imaging slab. Although there is less total blood labeled, the labeling phase is considerably shorter and therefore is said to have improved temporal SNR. In practice, the PASL technique has been more widely applied due to its relative ease of implementation and low signal absorption rate (SAR) even though it suffers from a much lower sensitivity compared to CASL. These factors can be explained by the fact that PASL inverts a defined 'slab' of spins using a single very short RF pulse; a highly efficient means of 'tagging' blood. In contrast, CASL uses a continuous RF pulse to invert arterial spins that are flowing (i.e. have a velocity) perpendicular to the labeling plane. Here, it is possible for irregular flow velocities (e.g. spins with imperfectly aligned directions of flow relative to the direction of the RF pulse) to result in considerable loss of labeling efficiency (Detre JA &

Aslop DC, 1999)(16). For a summary of the potential benefits and risks of each MR technique please see the table (Table 1) included below.

Parameter	Benefit	Risks
BOLD	> good temporal and spatial SNR > well-suited to paradigms with high task frequency	> undermined by low-frequency drift in MR spectrum > poorly suited to paradigms with low task-frequency
CASL	> maximum arterial label applied yields improved SNR > ability to obtain absolute quantification	> Continuous tag regime = SAR limitations i) no full brain acquisition ii) no simultaneous use of body/head coils
PASL	> pulsed tag regime yields faster (i.e. lower TR) sequence > pulsed tag regime = lower SAR limits i) acquire larger brain volume	> Pulsed regime excites less overall 'tag' per TR i) lower spatial SNR > Possibility for absolute quantification limited i) no true estimation of bolus width
3D-GRASE	> full 3D kspace acqusition per TR i) acqusition of whole brain volume	> deleterious warp artefact in z-direction i) induces non-physiological artefact into data that can't be easily ameliorated

Table 1: A summary of the key benefits and risks associated with each MR technique and acquisition parameter discussed in this chapter. BOLD, CASL and PASL are specific FMRI technqiues. 3D GRASE is a specific acquisiton approach used in concert with PASL. Both BOLD and CASL employ a standard echo-planar imaging (EPI) acquisition method. For clarity, BOLD stands for Blood Oxygen Level Dependent FMRI; CASL stands for Continuous Arterial Spin Labelling; PASL stands for Pulsed Arterial Spin Labelling; 3D-GRASE stands for 3 dimensional gradient and spin-echo

To add, it is also desirable to optimize perfusion signal within the shortest amount of time (i.e. acquire arterial signal before relaxation within a given TR). In general, temporal and spatial SNR are inversely related. For example, technical manipulations that maximize the amount of signal available often have longer TR values. Ideally, imaging experiments aim to acquire a maximum amount of signal (i.e. before relaxation to B_0) in an optimum period of time. In the case of ASL, the time between labeling and acquisition has to allow the arterial signal to perfuse the brain. Relatedly, the time at which an image volume is acquired must ensure that the presence of perfusion signal does not: i) relax back to to B_0 , or ii) leave the region of interest- factors likely to be a problem with longer TRs.

While the theoretical gains of working with ASL are evident, it is still not well known which technique is best suited for our imaging centre to do pain experiments. Additionally, it is not well known how a given ASL approach should be optimized to capture brain activation relative to ongoing pain states. To investigate these ambiguities, we devised two different pilot experiments to help inform the development of an ASL sequence optimized for future use in pain imaging studies. The aim of these experiments are to: 1) decide which ASL approach resolves the best SNR (spatial and temporal) relative to BOLD; and 2) adapt that ASL approach to a pain-imaging experiment where a whole brain acquisition of long stimulus blocks is needed.

3.2.1. Study 1: Comparison of PASL, CASL and BOLD

In study 1, we proposed to test the feasibility of employing an ASL acquisition approach by comparing it to our standard BOLD FMRI paradigm. We employed a basic primary sensory block design paradigm to stimulate key sensory regions associated with a combined visual/motor task. This type of paradigm is well known to trigger robust, well-maintained increases in both CBF (17) and BOLD (18) and can therefore be used as a reliable indicator of brain function to parse how each ASL approach compares to BOLD. The direct measures we wanted to compare across techniques included: 1) extent and location; 2) volume; 3) temporal and spatial SNR of activation within both the visual and motor cortices.

3.2.1.1. METHODS

Briefly, healthy subjects (n=10; 3 female; right handed; age: 27-45yrs) were asked to perform simultaneous visual (8Hz flashing checkerboard) and motor (finger-tapping) tasks whilst being scanned in the Siemens 3T TIM Trio system (see Figure 3). Subjects were asked to perform the task whilst being scanned with a different imaging sequence (BOLD, CASL, or PASL). Both the BOLD and CASL approaches were acquired with a standard EPI approach. The PASL data was acquired with a 3D-GRASE approach. Because of significant signal-artifact commonly observed with 3D-GRASE approaches, we employed the use of a novel analysis method to attempt to reduce the noise (Chapell, M. unpublished). We included the artifact-laden data (labeled GRASE) and the denoised data (labeled: GRASE deblur) in the figures below for discussion purposes. Additionally, we compared different variations of the CASL sequence. These

differences between the CASL sequences relate to alterations in each sequence's TR, label duration and post-label delay. Table 2 outlines the exact differences in imaging parameters used.

	BOLD	CASL1	CASL2	CASL3	GRASE
TR (ms)	3000	3050	3640	3450	6000
TE (ms)	30	11	11	11	11
Vox (mm3)	3x3x3	4x4x5	4x4x5	4x4x5	4x4x5
Label Duration	n.a.	1600	2000	2000	1000
Post-Label Delay	n.a.	1000	1200	1000	1600

Table 2: Comparison of PASL, CASL and BOLD sequence parameters for use in a block-design paradigm looking at a combined visual/motor task. Generally, the key means of increasing ASL SNR is to optimize the amount of perfusion signal available to be imaged. As the name suggests, Continuous ASL (CASL) produces the largest amount of available ASL signal (14). However, multi-slice CASL approaches often result in less total SNR due to problems with artifacts in the control image (15). In comparison, Pulsed ASL (PASL) only labels a net volume of blood defined within an imaging slab. Although there is less total blood labelled, the labeling phase is considerably shorter and therefore is said to have improved temporal SNR.

Data were analyzed using the FMRIB software library (FSL). Perfusion images were generated using FSLtools, motion corrected and spatially smoothed (FWHM = 8mm) (Mixed Effects, cluster corrected, $z>2.3$, $p<0.05$). Anatomical masks were generated for the visual and motor cortices using the Harvard-Oxford Atlas of Cortical Structures in FSLview. All masks were binarized and spatially thresholded to ensure accurate anatomical alignment to the MNI standard space brain. Key outcome measures included group mean: i) zstats; ii) location of peak active voxels within each ROI; iii) both spatial and temporal signal-to-noise (SNR) within each ROI. The calculation of SNR was observed by

dividing the mean signal by the standard deviation of the signal within each ROI. Spatial SNR employed the thresholded zstat image whilst temporal SNR calculations were completed on the overall timeseries image for each subject.

3.2.1.2. RESULTS

Figures 1,2,&3 show the extent of activation, localisation and SNR resolved with each ASL technique compared to BOLD. i) *Extent of activation.* A comparison of the peak (a; p. 94)) and group mean (b; p. 95) zstat active within the visual (figure 1) and motor (figure 2) cortices shows that BOLD is consistently more robustly active than any of the ASL approaches (one-way ANOVA, $p<0.01$). There is no significant difference between any of the ASL techniques as all are similarly active relative to one another. ii) *Localisation.* Figure 1c (p. 96) shows how well localised the statistical maps are during the task for each technique. Our outcome measures for this included the volume of the activation cluster (visual cortex: figure 1c, p96; motor cortex: figure 2c, p100) and displacement of the peak zstat relative to BOLD (visual cortex: figure 3a, p102; motor cortex: figure 3b &c, p.103-4). Our results confirm the prediction that the peak activation was more localised (i.e. smaller activation volume, less displaced peak zstats within each anatomical region) for the ASL techniques compared to BOLD (one-way ANOVA, $p<0.01$). This was true for all ASL sequence parameters as there was no significant difference for volume of activation or peak zstat displacement when comparing the ASL approaches. To note, activation was not well resolved within the motor cortex across the all the ASL approaches due to limited slice coverage (see: CASL 3 and GRASE, figure 2,3). iii) *SNR.* Comparison of group

mean signal-to-noise ratio (SNR) for all ASL approaches (visual cortex: figure 1d, p97; motor cortex: figure 2d, p101) shows that CASL1 (TR= 3050ms) revealed improved spatial and temporal SNR relative to the other perfusion sequence parameters used (one-way ANOVA, $p<0.01$).

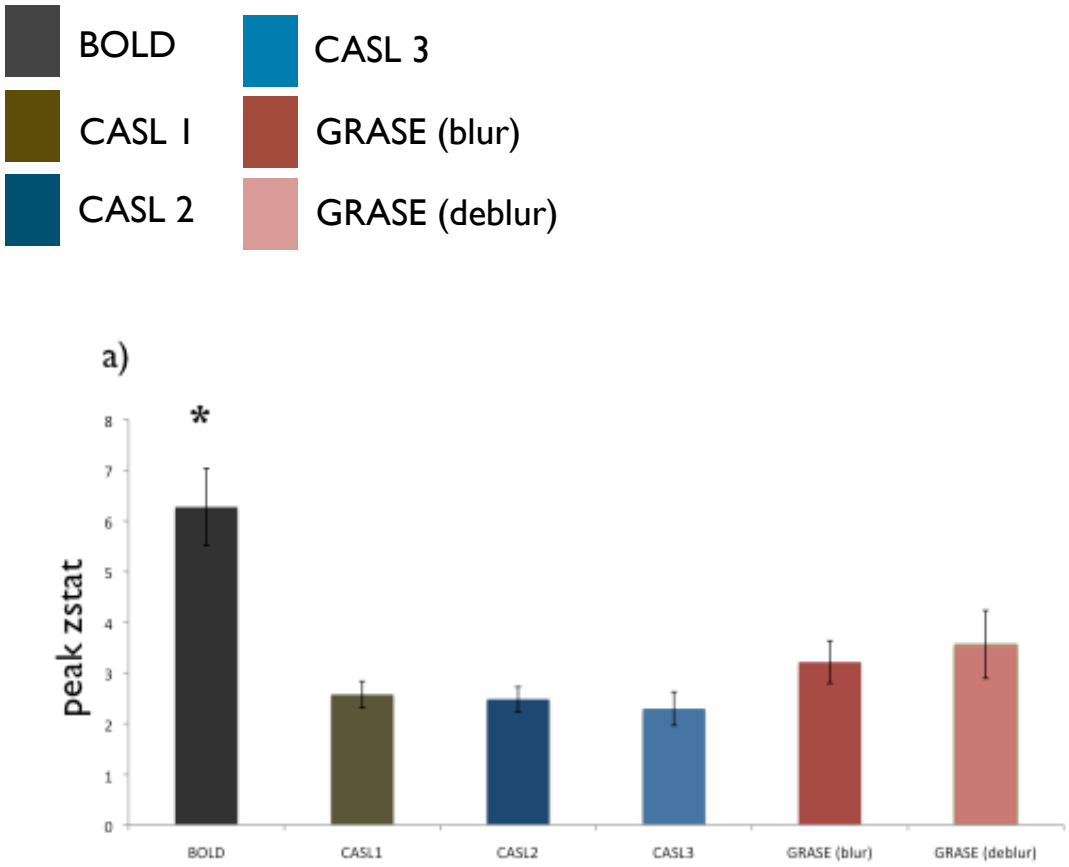

Figure 1a: Visual cortex activation. Comparison of brain perfusion data to BOLD acquired during a combined visual/motor task. **a)** Peak zstat values within anatomical mask as observed at the group level in FEAT. Analysis of all data was completed using FEAT (Mixed Effects: $z>2.3$, $p<0.05$); (* one-way ANOVA, $p<0.01$). Error bars represent the standard error of the mean (SEM). For an explanation of the differences between CASL 1-3 please see table 1. GRASE (blur) refers to perfusion data at the group level without any de-blurring post-processing steps. GRASE (deblur) refers to the post-processed perfusion data in which a de-blur filter was applied (Michael Chappel; ASL analysis tools development; unpublished).

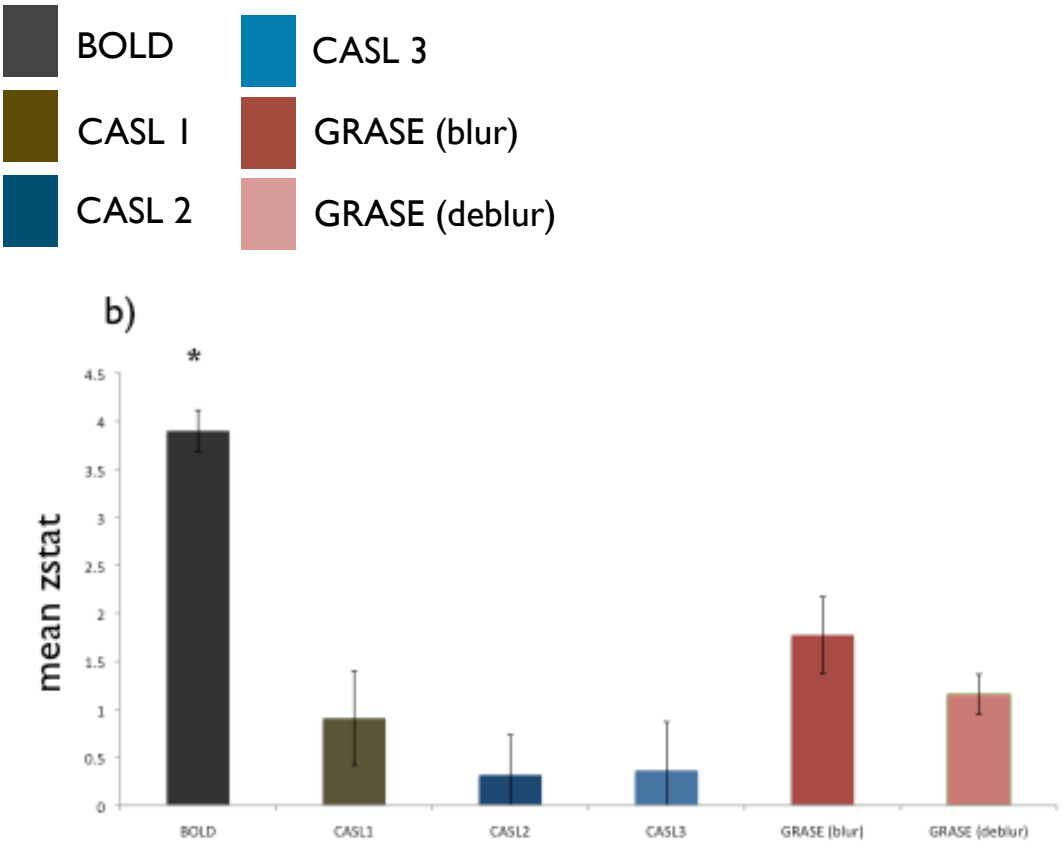

Figure 1b: Visual cortex activation. Comparison of brain perfusion data to BOLD acquired during a combined visual/motor task. **b)** Group mean zstat values within the anatomical mask for each MR sequence observed. Analysis of all data was completed using FEAT (Mixed Effects: $z>2.3$, $p<0.05$); (* one-way ANOVA, $p<0.01$). Error bars represent the standard error of the mean (SEM). For an explanation of the differences between CASL 1-3 please see table 1. GRASE (blur) refers to perfusion data at the group level without any de-blurring post-processing steps. GRASE (deblur) refers to the post-processed perfusion data in which a de-blur filter was applied (Michael Chappel; ASL analysis tools development; unpublished).

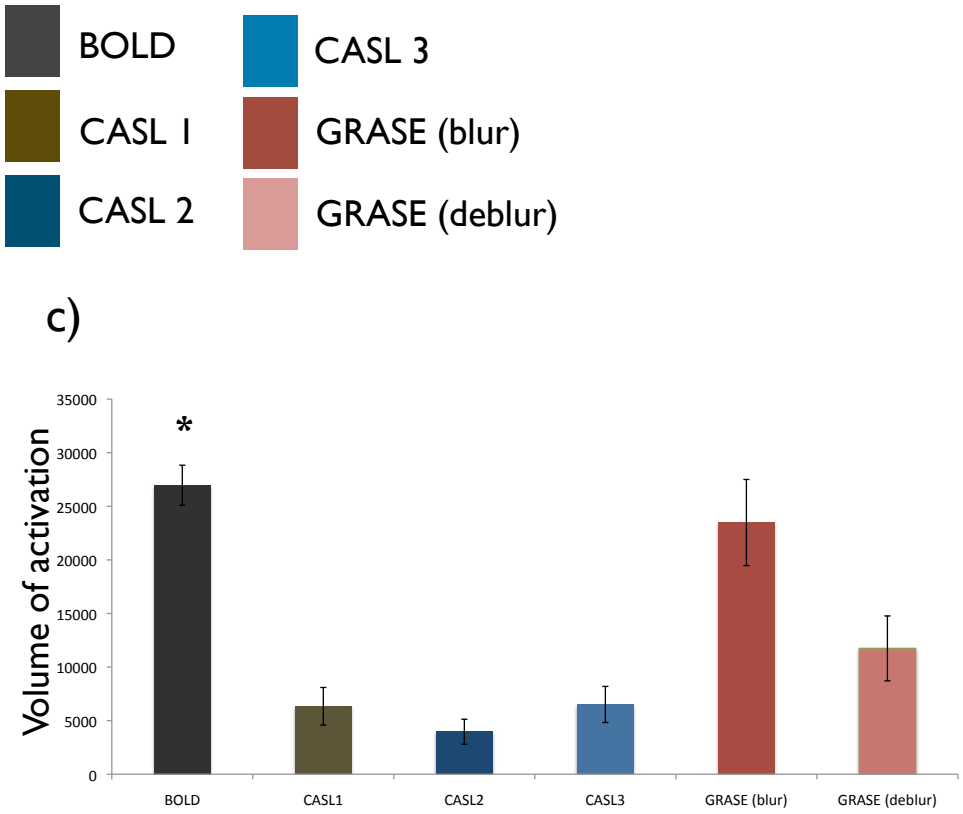

Figure 1c: Visual cortex activation. Comparison of brain perfusion data to BOLD acquired during a combined visual/motor task. **c)** Group mean volume of activation voxels within the anatomical mask for each MR sequence observed. Analysis of all data was completed using FEAT (Mixed Effects: $z>2.3$, $p<0.05$); (* one-way ANOVA, $p<0.01$). Error bars represent the standard error of the mean (SEM). For an explanation of the differences between CASL 1-3 please see table 1. GRASE (blur) refers to perfusion data at the group level without any de-blurring post-processing steps. GRASE (deblur) refers to the post-processed perfusion data in which a de-blur filter was applied (Michael Chappel; ASL analysis tools development; unpublished).

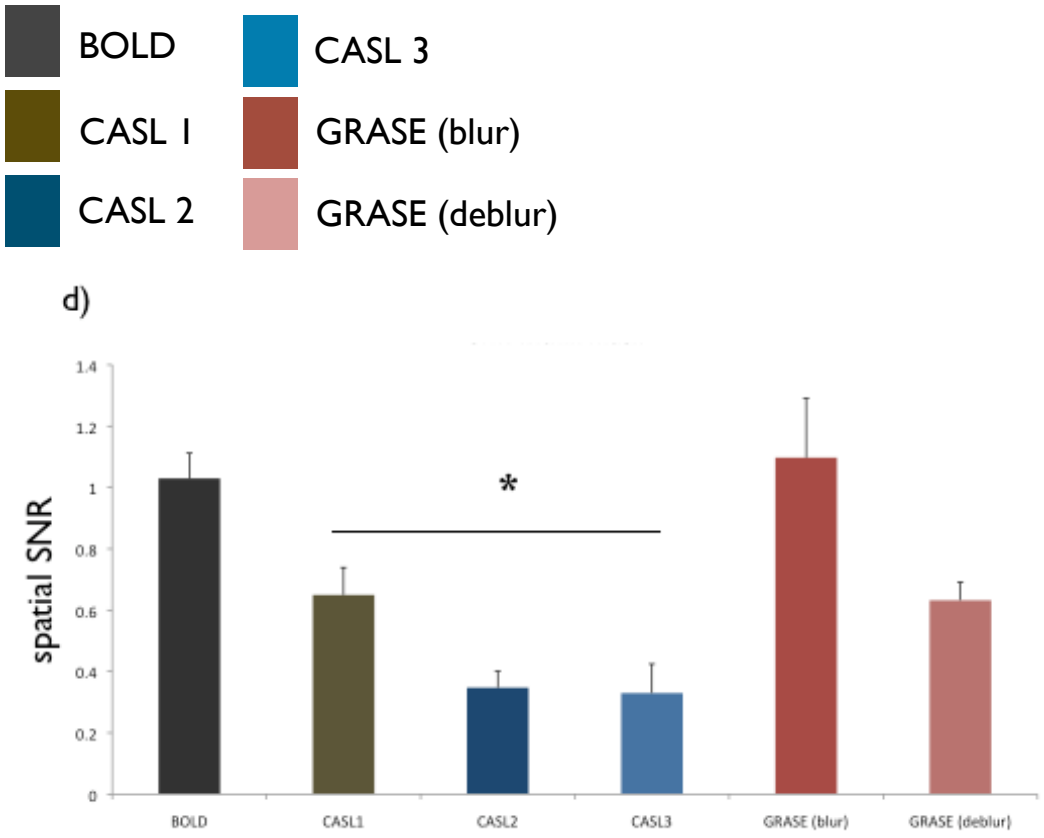

Figure 1d: Visual cortex activation. Comparison of brain perfusion data to BOLD acquired during a combined visual/motor task. **d)** Comparison of the spatial SNR (mean signal/ standard deviation of signal) within the anatomical mask for each MR sequence observed. Analysis of all data was completed using FEAT (Mixed Effects: $z>2.3$, $p<0.05$); (* one-way ANOVA, $p<0.01$). Error bars represent the standard error of the mean (SEM). For an explanation of the differences between CASL 1-3 please see table 1. GRASE (blur) refers to perfusion data at the group level without any de-blurring post-processing steps. GRASE (deblur) refers to the post-processed perfusion data in which a de-blur filter was applied (Michael Chappel; ASL analysis tools development; unpublished).

a)

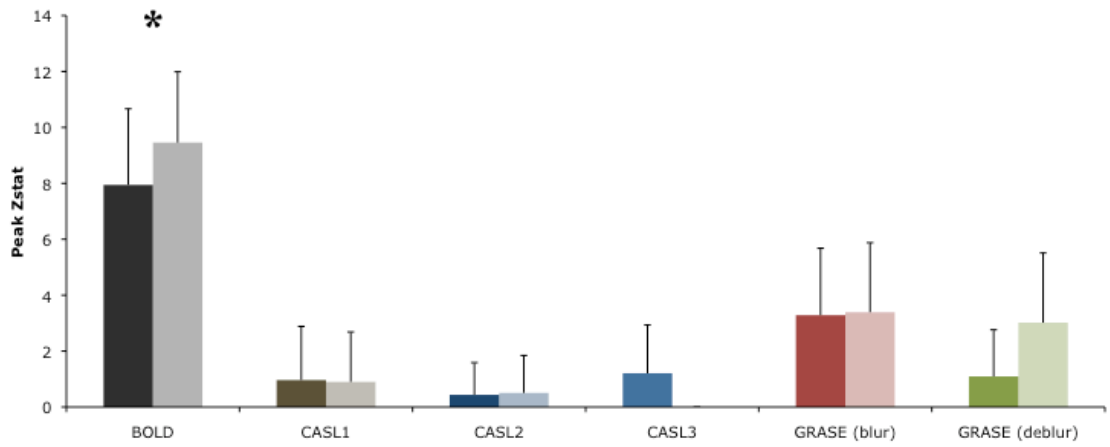

Figure 2a: Motor cortex activation. Comparison of brain perfusion data to BOLD acquired during a combined visual/motor task. Left hemisphere (solid); Right hemisphere (shaded): **a)** Peak zstat values within anatomical mask as observed at the group level in FEAT. Analysis of all data was completed using FEAT (Mixed Effects: $z>2.3$, $p<0.05$); (* one-way ANOVA, $p<0.01$). Error bars represent the standard error of the mean (SEM). For an explanation of the differences between CASL 1-3 please see figure 7. GRASE (blur) refers to perfusion data at the group level without any de-blurring post-processing steps. GRASE (deblur) refers to the post-processed perfusion data in which a de-blur filter was applied (Michael Chappel; ASL analysis tools development; unpublished).

b)

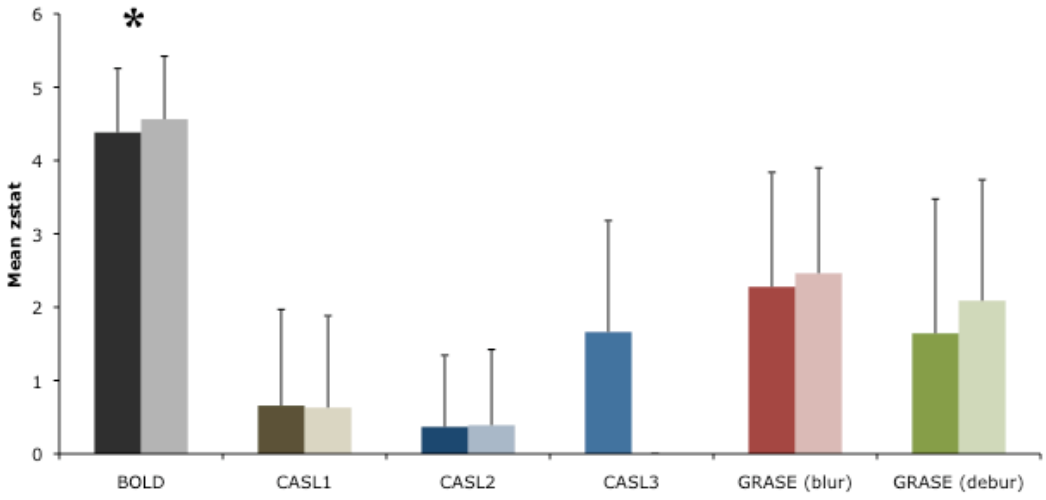

Figure 2b: Motor cortex activation. Comparison of brain perfusion data to BOLD acquired during a combined visual/motor task. Left hemisphere (solid); Right hemisphere (shaded): **b)** Group mean zstat values within the anatomical mask for each MR sequence observed. Analysis of all data was completed using FEAT (Mixed Effects: $z>2.3$, $p<0.05$); (* one-way ANOVA, $p<0.01$). Error bars represent the standard error of the mean (SEM). For an explanation of the differences between CASL 1-3 please see figure 7. GRASE (blur) refers to perfusion data at the group level without any de-blurring post-processing steps. GRASE (deblur) refers to the post-processed perfusion data in which a de-blur filter was applied (Michael Chappel; ASL analysis tools development; unpublished).

c)

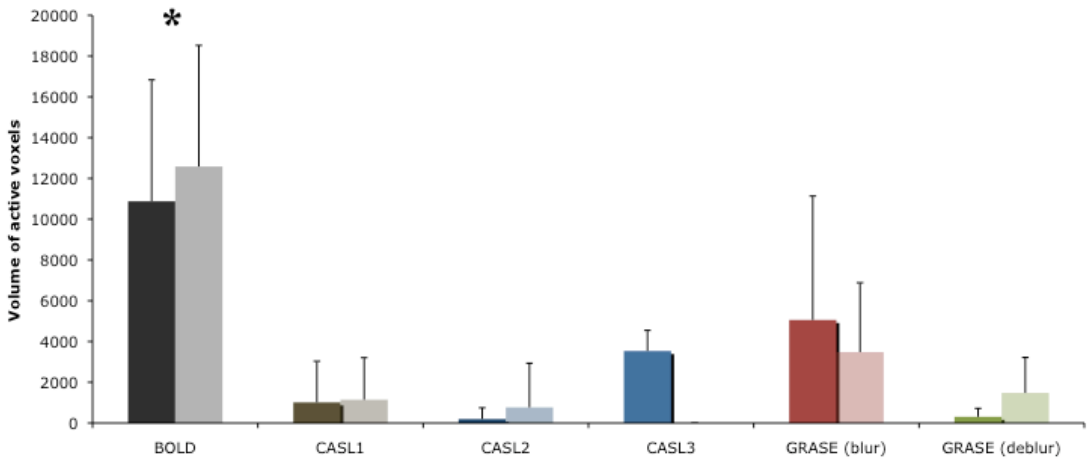

Figure 2c: Motor cortex activation. Comparison of brain perfusion data to BOLD acquired during a combined visual/motor task. Left hemisphere (solid); Right hemisphere (shaded): **c)** Group mean number volume of activation within the anatomical mask for each MR sequence observed. Analysis of all data was completed using FEAT (Mixed Effects: $z>2.3$, $p<0.05$); (* one-way ANOVA, $p<0.01$). Error bars represent the standard error of the mean (SEM). For an explanation of the differences between CASL 1-3 please see figure 7. GRASE (blur) refers to perfusion data at the group level without any de-blurring post-processing steps. GRASE (deblur) refers to the post-processed perfusion data in which a de-blur filter was applied (Michael Chappel; ASL analysis tools development; unpublished).

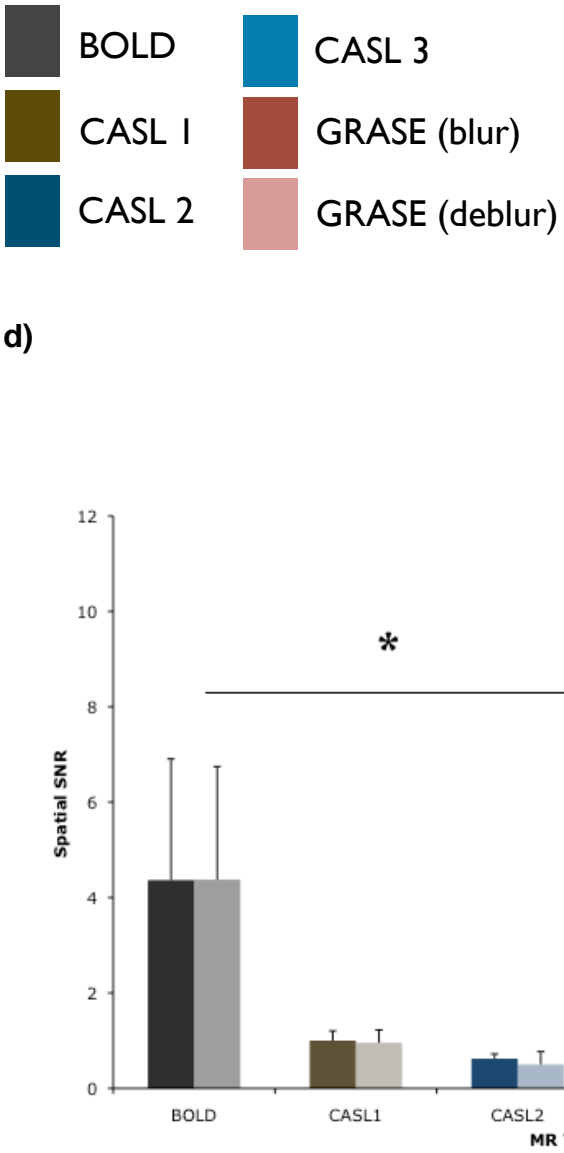

Figure 2d: Comparison of brain perfusion data to BOLD acquired during a combined visual/motor task. Left hemisphere (solid); Right hemisphere (shaded): **d)** Group mean signal-to-noise(SNR) of activation within the anatomical mask for each MR sequence observed (SNR = mean activation / standard deviation of activation). Analysis of all data was completed using FEAT (Mixed Effects: $z>2.3$, $p<0.05$); (* one-way ANOVA, $p<0.01$). Error bars represent the standard error of the mean (SEM). For an explanation of the differences between CASL 1-3 please see figure 7. GRASE (blur) refers to perfusion data at the group level without any de-blurring post-processing steps. GRASE (deblur) refers to the post-processed perfusion data in which a de-blur filter was applied (Michael Chappel; ASL analysis tools development; unpublished).

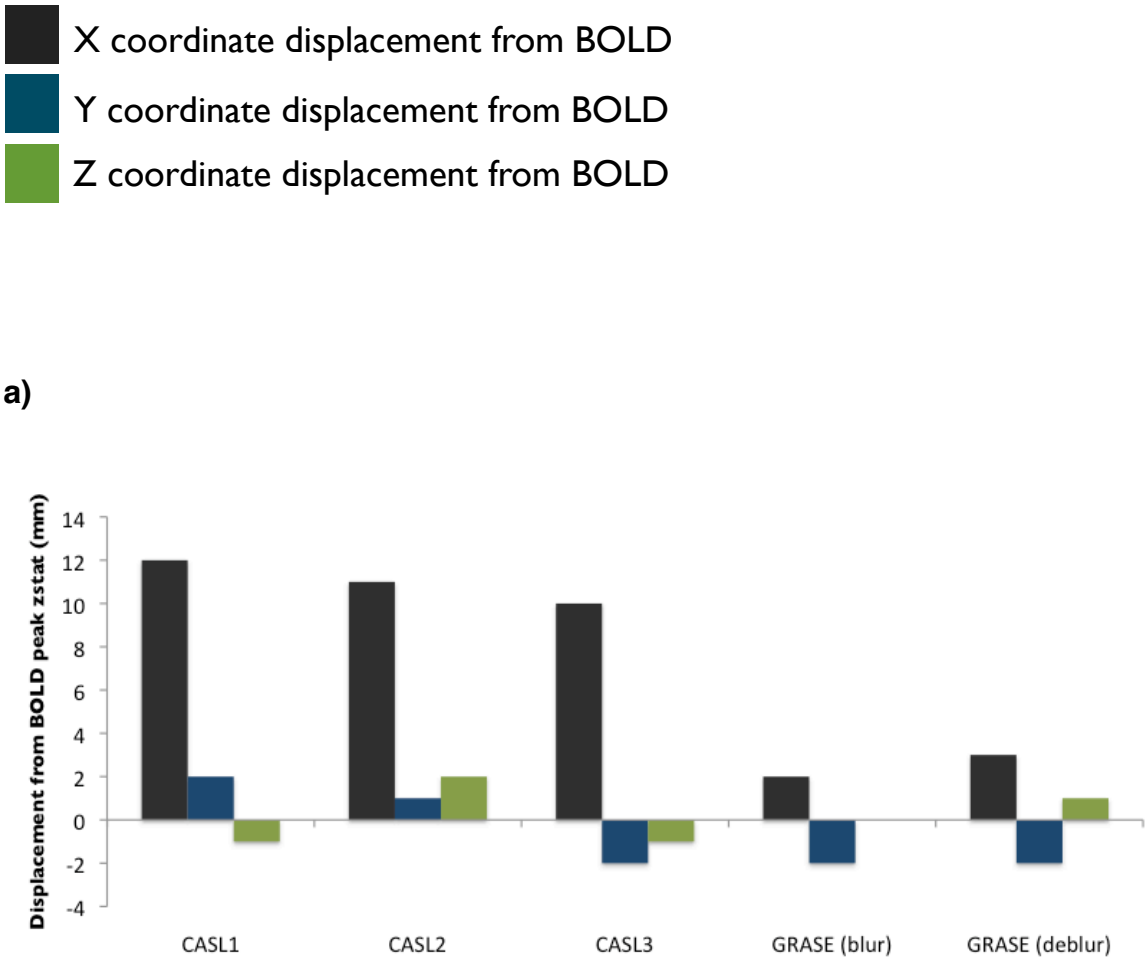

Figure 3a: Comparison of peak voxel displacement within the visual cortex. Figures represent absolute values as calculated by the displacement of the location (x: gray; y: blue; z: green) of the peak active voxel observed with each perfusion technique discussed previously compared to the peak voxel observed with BOLD. Analysis of all data was completed using FEAT (Mixed Effects: $z>2.3$, $p<0.05$). Error bars are not present because each bar is reflective of group mean data for each technique. For an explanation of the differences between CASL 1-3 please see table 1. GRASE (blur) refers to perfusion data at the group level without any de-blurring post-processing steps. GRASE (deblur) refers to the post-processed perfusion data in which a de-blur filter was applied (Michael Chappel; ASL analysis tools development; unpublished).

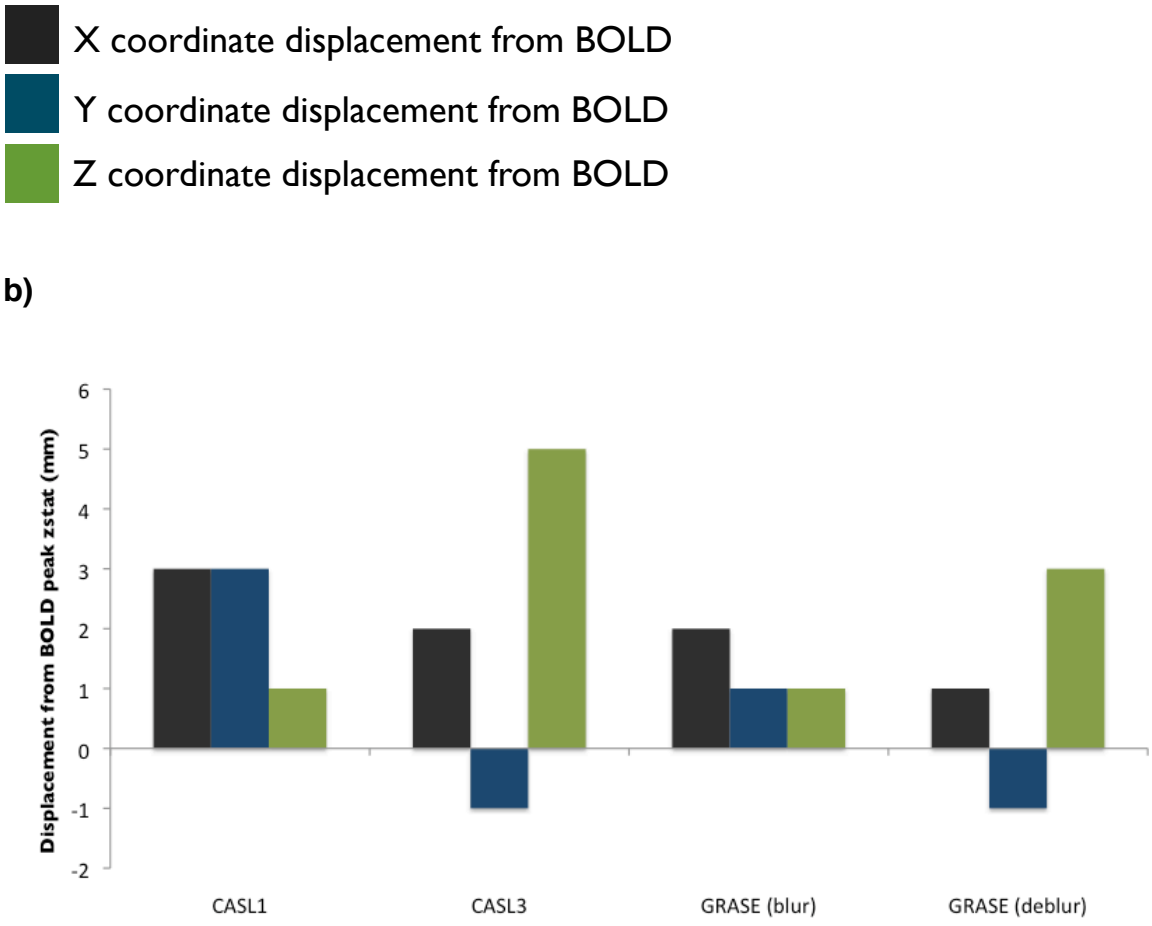

Figure 3b: Comparison of peak voxel displacement within the left motor cortex. Figures represent absolute values as calculated by the displacement of the location (x: gray; y: blue; z: green) of the peak active voxel observed with each perfusion technique discussed previously compared to the peak voxel observed with BOLD. CASL 2 is not included in figures b & c because no significant activations were resolved at the group level here. Analysis of all data was completed using FEAT (Mixed Effects: $z>2.3$, $p<0.05$). Error bars are not present because each bar is reflective of group mean data for each technique. For an explanation of the differences between CASL 1-3 please see table 1. GRASE (blur) refers to perfusion data at the group level without any de-blurring post-processing steps. GRASE (deblur) refers to the post-processed perfusion data in which a de-blur filter was applied (Michael Chappel; ASL analysis tools development; unpublished).

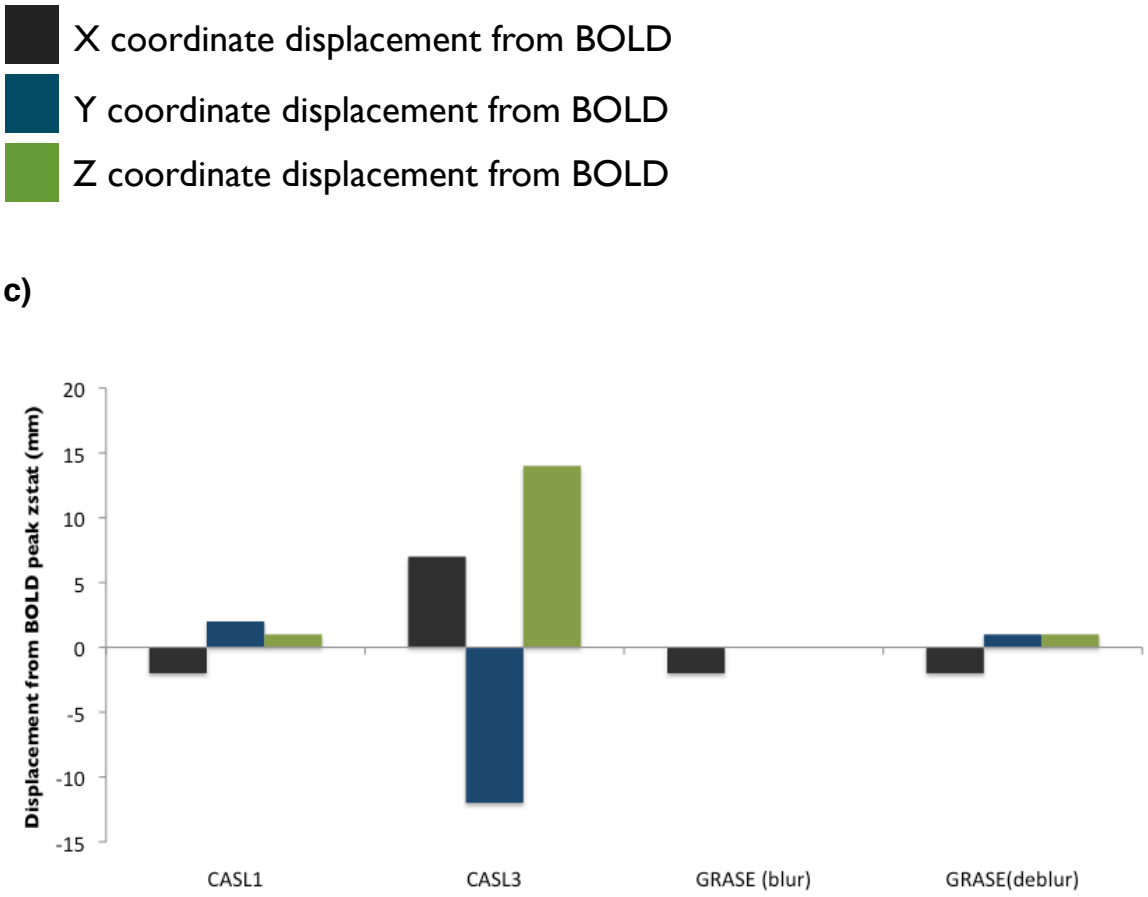

Figure 3c: Comparison of peak voxel displacement within the right motor cortex. Figures represent absolute values as calculated by the displacement of the location (x: gray; y: blue; z: green) of the peak active voxel observed with each perfusion technique discussed previously compared to the peak voxel observed with BOLD. CASL 2 is not included in figures b & c because no significant activations were resolved at the group level here. Analysis of all data was completed using FEAT (Mixed Effects: $z>2.3$, $p<0.05$). Error bars are not present because each bar is reflective of group mean data for each technique. For an explanation of the differences between CASL 1-3 please see table 1. GRASE (blur) refers to perfusion data at the group level without any de-blurring post-processing steps. GRASE (deblur) refers to the post-processed perfusion data in which a de-blur filter was applied (Michael Chappel; ASL analysis tools development; unpublished).

3.2.1.3. Discussion

BOLD was consistently more robustly active as evidenced by the higher zstat values, larger volume of activation and larger overall temporal and spatial SNR compared to the ASL techniques examined. These results are expected given the short task-frequency of the paradigm that biases the results towards BOLD data. An appropriate next step would be to compare these results to a paradigm in which the task was more tonic in nature (i.e. beyond a minute). Previous work by Wang et al. (2003) compared BOLD to a standard CASL approach to show that as the task block increased in time, the ASL signal gradually outpaces BOLD in terms of statistical significance (7). This is due primarily to low-frequency drift that undermines BOLD but not ASL with longer task blocks. Here then, it would be possible to see which ASL approach is best suited for task paradigms in a tonic setting.

Interestingly, the perfusion signal was more localized compared to BOLD. While it is not possible to observe exactly where the perfusion signals originate within the tissue, it is accepted that ASL measures arterial signal. As such, peak activations can be expected to originate from capillary beds contiguous to the site of activation (19). We expect that for a given primary sensory region like the visual cortex, this type of stimulus would activate a well-defined population of neurons similar to what is observed. In contrast, however, BOLD signal reflects magnetic changes on the venous side of the capillary bed. Venous perfusion is far less well defined spatially as the venules are dilated and are therefore less specifically aligned with neurons directly. Additionally, the BOLD signal change also reflects changes in $CMRO_2$, CBV and additional factors like the presence of astrocytes. As such, it is not surprising that the location of peak voxels within the

visual cortex is less well localized compared to the ASL signals. To note however, not all ASL sequence parameters were able to successfully image the motor cortices reliably (see CASL2 results, figure 3). This is primarily due to a lack of consistent slice coverage. Future work is needed to better optimize the relationship between the position of the labeling plane relative to location of the anatomical region being imaged. For example, employing a time of flight (TOF) scan could possibly aid in the process of defining the optimal labeling plane based on each subject's vascular anatomy relative to the size of that subject's brain. Ensuring that the position of where the label is applied relative to the slice stack orientation is consistent over long scan sessions will likely protect against poor CBF contrast across subjects.

From a comparison of the ASL approaches to one another, for all outcome measures, GRASE appears to be the strongest candidate for implementation in future studies. Note however, the substantial difference between GRASE 'blur' and 'deblur'. Here, due to complexities of the 3D-single shot acquisition protocol used, a very large, non-physiologically relevant artifact was observed in the CBF time courses (referred to as : 'blur')(see example in Figure 4).

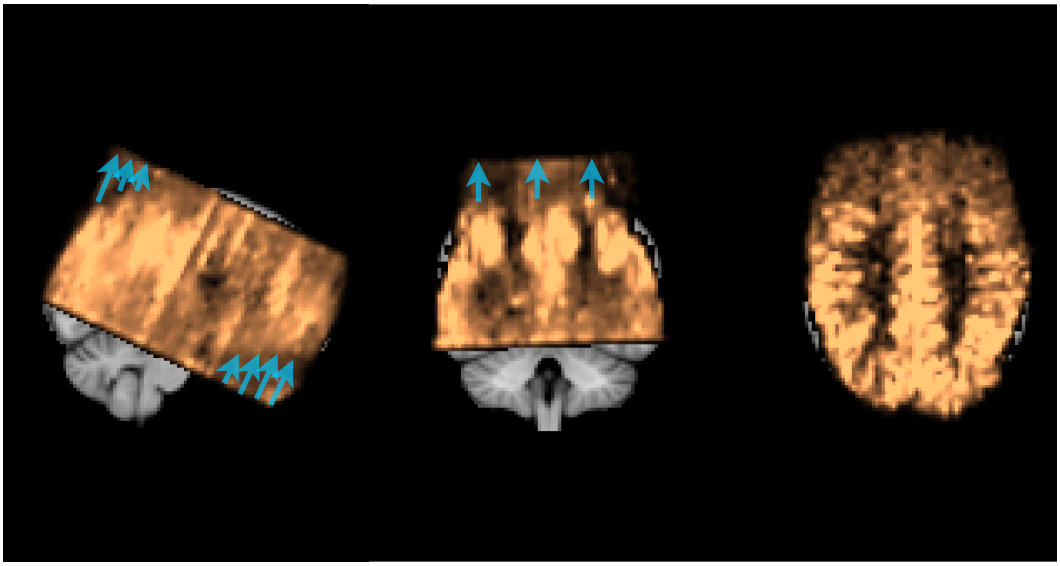

Figure 4: An example 3D slice view from the PASL-GRASE acquisition in a single subject. For clarity, the perfusion map (orange) was acquired with a 3D GRASE sequence paradigm overlaid onto the MNI standard template brain. The overlaid blue arrows signify the extent and location of artifact in the z-direction. In general, this z-direction warping artificially bolsters the magnitude of the perfusion signal. While the sagittal and coronal orientations clearly display the artifact, the axial view belies these errors.

This blur causes very robust 'false positives' as seen in the figures (e.g. GRASE blur) as the value of the zstats (peak and mean) and volume of activation are likely driven by this non-physiological artifact. At present, there is no accepted method of 'de-bluring' the artifact. We attempted to do so by employing a novel analysis tool that diminishes the artifact by employing a non-standard Bayesian statistical-modeling approach that attempts to 'model out' the blur. This analysis approach is currently under development by Dr. Michael Chappel (Analysis Group, FMRIB Centre) and is not currently in a state for common use. Further, as the error lies at the point of acquisition, there will be limitations regarding success in completely removing this spatial blurring of signal. Therefore, given that the 3D-GRASE acquisition approach induces very strong artifacts into the

data and there is no established way of removing them, we concluded to cease work with PASL-3D GRASE for any future studies. Consequently, we were left to develop the CASL-EPI technique for use in future pain imaging experiments.

Comparison of the CASL approaches lends support towards employing a sequence similar to CASL 1 as it was capable of resolving the most robust effects compared to the other non-GRASE techniques. However, further development is needed to optimize the sequence for use in a tonic pain experiment. For one, it is essential that future experiments employ a tonic stimulus paradigm (i.e. stimulus blocks longer than 1-minute) to more accurately assess different aspects of the ASL sequence. Additionally, it is essential that the sequence acquire a whole brain dataset so that it is possible to observe perfusion changes across all pain-relevant regions (i.e. both subcortical and cortical regions).

To accomplish these tasks, we designed a follow-up experiment aimed to develop the CASL-EPI framework so that it is optimised for a pain imaging context. In this experiment, we repeated a version of the above study but with longer stimulus blocks whilst obtaining a whole brain volume of perfusion changes.

3.2.2. Study 2: Optimization of CASL for a pain imaging context

Previously, ASL experiments have relied on imaging specific parts of the cortex alone (i.e. motor and/or visual cortex) and have not needed to observe cerebral perfusion across sub-cortical (including the brain stem) and cortical structures simultaneously. Currently, it is not known what the neural correlates of an

ongoing pain experience are. Further, it is not known if/how the regions shown to be recruited during acute, phasic pain (previously termed: 'the pain matrix') are functionally relevant for ongoing pain states. Because of this, initial ASL investigations of pain must obtain signal from the whole brain simultaneously as these pain-relevant regions are spread across a disparate spatial region (9). Currently, there is not a true whole-brain CASL-EPI approach readily available. Subsequently, a key aim of this study was to test the utility of a novel CASL acquisition and analysis protocol that obtains both subcortical and cortical slices in an alternating fashion (i.e. TR_1 = acquisition of 10 subcortical slices; TR_2 = acquisition of 10 cortical slices; etc.) to effectively obtain a whole brain dataset. In this way, it would be possible to observe CBF changes over time within both subcortical and cortical regions without the need for problematic 3D acquisition approaches similar to the PASL-GRASE data from Study 1.

As discussed previously, BOLD FMRI is not well suited to image paradigms with low task-frequency (i.e. long block lengths) task designs (7). Subsequently, the paradigms used to observe the effect of pain on the brain are not, by their outset, clinically relevant as they do not capture key facets of the experience of chronic pain. In order for pain imaging experiments to model more closely what is experienced clinically by patients, it is essential for these early ASL pain experiments to develop an imaging approach that is capable of looking at brain activation changes over time periods that are tonic (i.e. on the minute timescale) in nature. As a first step towards this end, we have proposed the following study with the aim of: 1) optimizing the CASL sequence to obtain a true whole brain perfusion dataset; 2) utilizing the optimized sequence within an experimental paradigm that is tonic in nature.

3.2.2.1. METHODS

Healthy subjects (n=9; 2 female; right handed; age: 20-38yrs) were asked to perform simultaneous visual (8Hz flashing checkerboard) and motor (finger-tapping) tasks whilst being scanned in the Siemens 3T TIM Trio system using a single channel head coil.

A whole brain was acquired by dividing the volume into two contiguous stacks of ten slices each (6mm slice thickness). Acquisition of each slice stack alternated between stack 1 and 2 over time. To add, 'tag' images for both stacks were acquired first, followed by 'controls'. For both 'tag' and 'control' acquisitions, stack 1 was acquired before stack 2 (Figure 4).

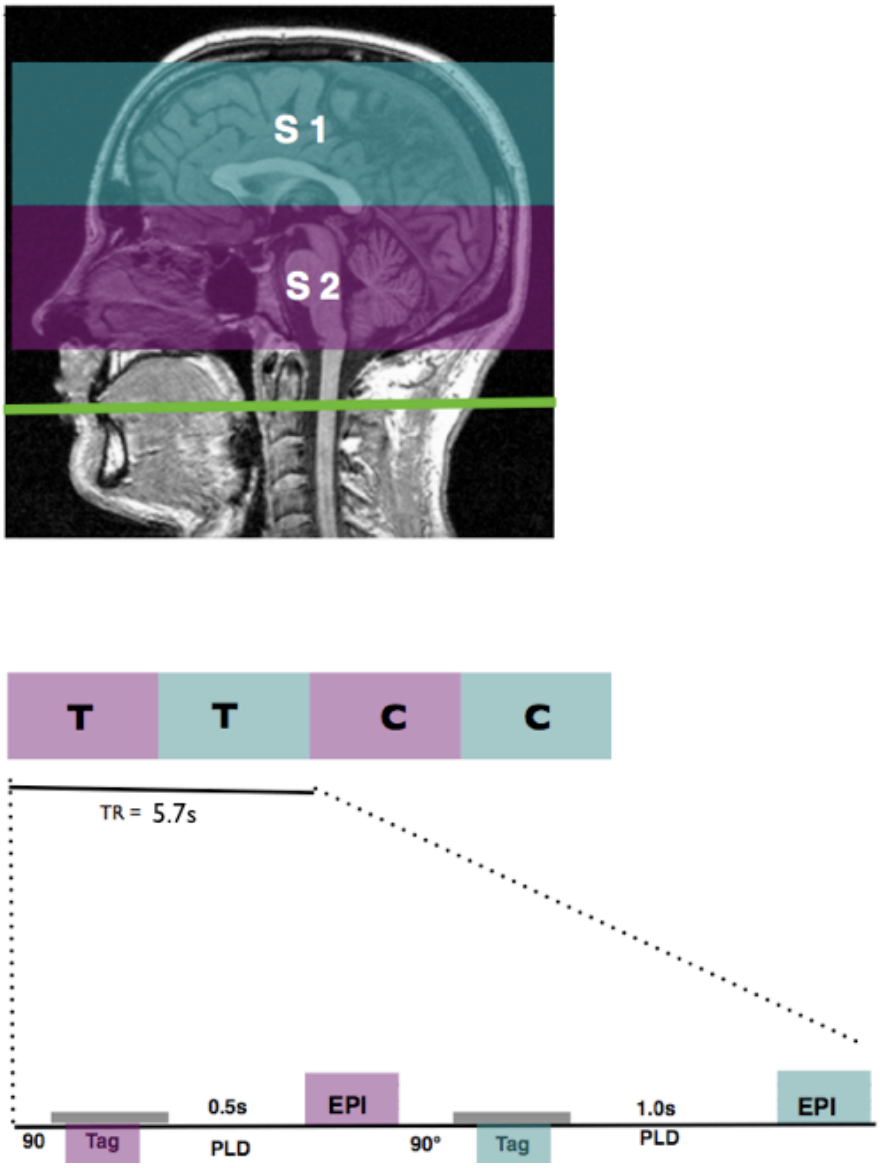

Figure 4: Graphic representation depicting the data acquisition of the interleaved CASL-EPI approach to image a whole brain volume. A whole brain was acquired by dividing the volume into two contiguous stacks of ten slices (6mm slice thickness). The labeling plane (green line) was placed 10 cm inferior to the centre of the 20 slices. Arterial blood was tagged continuously for 1.6s. Signals within each stack were acquired separately and in an alternating manner. To account for different TI decay times across the slices, a different post-label delay was used for each stack: Stack one (S1) post-label delay (PLD) was 0.5s; stack two (S2) was 1.0s. The ASL parameters used were: CASL sequence with gradient-echo EPI (TE = 11ms, 6/8 k-space); 20 axial slices (4 x 4 x 6 mm voxels, 1.2 mm inter-slice gap); labeling offset was 10 cm inferior to centre of the 20 slices. Acquisition was in an ascending order and required ~5.7s for a whole brain volume.

The labeling plane was placed 10 cm inferior to the centre of the 20 slices. Arterial blood was tagged continuously for 1.6s. The post labeling delay of stack 1 was 0.5s; for stack 2 it was 1.0s. The ASL parameters used included: CASL sequence with gradient-echo EPI (TE = 11 ms, 6/8 k-space); 20 axial slices (4x4x4mm voxels, 1.2 mm inter-slice gap); labeling offset was 10 cm inferior to the centre of all 20 slices. Acquisition was in an ascending order and required ~5.7 sec for each whole brain volume. A single-channel head coil was used.

All time series were concatenated offline and analyzed using the FMRIB software library (FSL). Perfusion images were generated using FSL tools, motion corrected and spatially smoothed (FWHM = 8mm). Anatomical masks for the motor and visual cortices were generated using the Harvard-Oxford Atlas of Cortical Structures in FSLview. All masks were binarized and spatially thresholded to ensure accurate anatomical alignment to the MNI standard space brain.

Previous studies show that residual BOLD effects can contaminate the CBF hemodynamic estimation and decrease the sensitivity of the perfusion contrast (20). To avoid this potential source of noise, we employed the following experimental approaches to further optimize the ASL signal acquired: 1) implementation of a short echo-time (TE); 2) delay the acquisition of task-relevant signal by five seconds after commencement of the stimulus paradigm to avoid acquisition of hemodynamic transients; 3) implement long stimulus/rest blocks.

We employed this optimized ASL sequence within a paradigm consisting of 5 cycles of 2 minute ON (8 Hz flashing checkerboard, combined with a finger tapping task) and 2 minute OFF (baseline; subjects were asked to remain awake with their eyes closed) blocks.

The direct tests employed were: 1) acquisition of reliable perfusion signal across the 20 slices; 2) observation of robust task dependent (On > Off contrast) perfusion signal in the motor and visual cortices at the group level; 3) calculation of percent perfusion signal change during the task within the relevant ROIs.

3.2.2.2. Results

Figure 5 shows the perfusion changes resolved from the interleaved CASL approach during the visual/motor task compared to rest. Figure 5a is a representative perfusion map from a subject scanned (randomly selected from the group) showing the definition of the labelling plane and alignment of two acquisition ‘slice stacks’ establishing maximal brian coverage with good CBF contrast from the brainstem to the top of the cortex. Figure 5b shows the group mean CBF maps for the contrast task ON> task OFF. Coloured regions represent voxels with suprathreshold t-statistics generated from the group-level FEAT analysis. Significant activations were observed in the expected visual and motor cortices (Mixed effects. n=9, $z>2.3$; $p<0.05$). Figure 5c shows the group mean perfusion time courses extracted from the visual (blue) and motor (red) cortices over the course of the entire paradigm. Time courses show robust changes in signal activation that were well maintained during ON compared to

OFF phases. The average increase in CBF observed with this approach was 42.5% for motor activation and 39.9% for visual activation.

a)

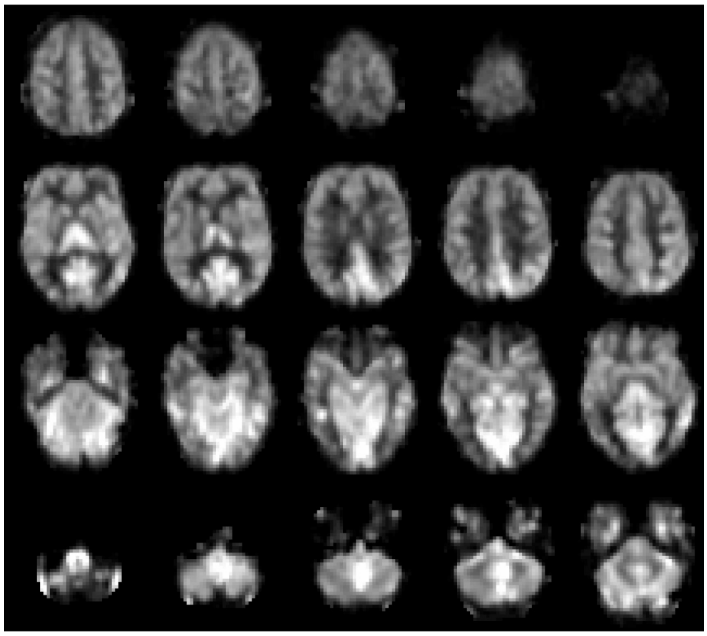

Figure 5a: Brain perfusion data from the interleaved CASL sequence during a combined visual/motor task. **a)** A representative subject's CBF scan after spatial smoothing (FWHM = 8mm) averaged over time for the entire stimulus paradigm. Good CBF contrast mapping was achieved throughout the whole brain including the cerebellum and brain stem using the interleaved acquisition method.

b)

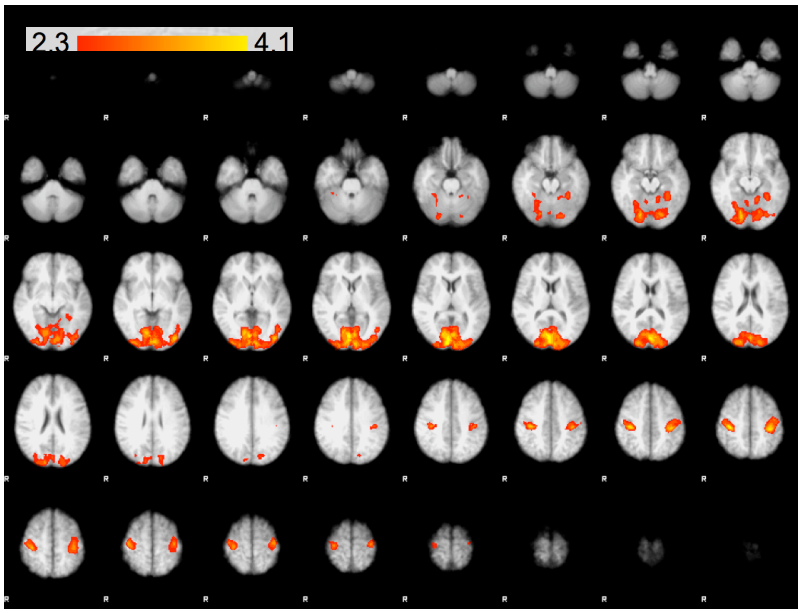

Figure 5b: Brain perfusion data from the interleaved CASL sequence during a combined visual/motor task. **b)** Group zstat maps (n=9) of perfusion activation superimposed on the MNI152 standard template brain. Robust activations localised to the visual and motor cortices were observed even though each ROI resides in a different slice stack.

c)

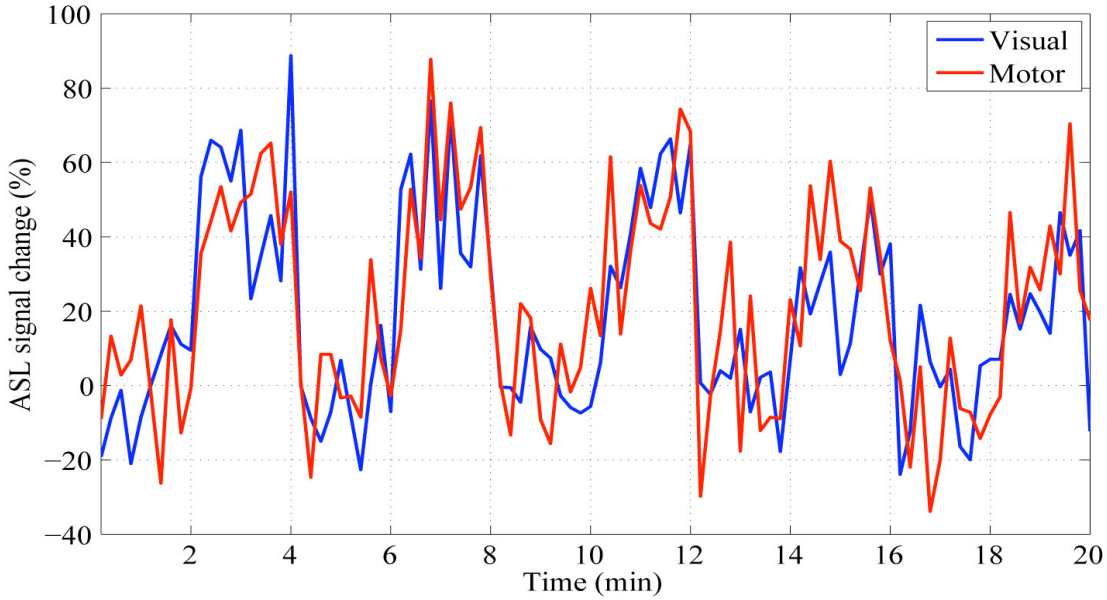

Figure 5c: Brain perfusion data from the interleaved CASL sequence during a combined visual/motor task. **c)** Group average time course of relative CBF signal changes in visual (blue) and motor (red) cortices over the course of the stimulus paradigm.

3.2.2.3. DISCUSSION

The results of this study show that the implementation of a novel whole brain CASL-EPI technique is possible. The single-subject perfusion maps suggest reliable whole brain coverage from the brain stem, encapsulating the cerebellum and extending over the cortex. Group level analysis of task-related changes in perfusion show the technique to be robust as functionally relevant signals were anatomically well defined within the motor and visual cortices. This was regardless of the two-stack design that necessitated offline concatenation. Additionally, percent signal change observed here coincides well with previously published data employing non-whole brain ASL methods (21). One potential

limitation of this technique is that it suffers from poor temporal resolution compared to conventional BOLD and ASL methods. For example, this interleaved CASL sequence has an effective TR = 5.7seconds compared to the commonly employed BOLD TR=3.0 seconds. This may be less of a concern for functional studies employing very low frequency task designs.

3.3 Conclusion

From the results of the ASL development experiments presented we articulated an ASL approach to proceed with future tonic pain imaging experiments. The results from Study 1 show that all ASL approaches are significantly less capable of resolving meaningful neural activity compared to BOLD for acute paradigm designs; and, it is therefore essential for all future developmental work to be based on tonic (i.e. stimulus blocks >2min) paradigms for the ASL parameters to be appropriately assessed. In addition, we concluded that the 3D-GRASE acquisition approach was associated with deleterious artifacts; removal of which proved to evade current image analysis approaches. Consequently, because the 3D-GRASE approach is still far too undeveloped to reliably image a whole brain volume of meaningful functional data, we decided to cease use of GRASE for future ASL pain investigations.

Results of Study 2 show that it is indeed possible to optimize the standard CASL sequence to obtain a whole brain perfusion dataset. The results of this study show, for the first time, acquisition of meaningful CBF signal changes in expected anatomical regions for a tonic visual/motor stimulus paradigm using a CASL sequence that alternates acquisition between slice stacks for sub/cortical

regions. The key drawback of this approach however is the relatively poor temporal SNR related to the time it takes to acquire both 'tag' and 'control' images for both slice stacks.

Coincident with the results of these studies, advances in ASL sequence development were made that ameliorated the inherent weaknesses of CASL and PASL and therefore, offer a very strong alternative means of acquiring perfusion signals across a whole brain. Specifically, our MR Physics Group at the FMRIB gained access to a relatively new ASL sequence called pseudo-CASL (pCASL). Specifically, pCASL can be thought of as benefiting from the strengths of PASL (temporal SNR and label efficiency) and CASL (spatial SNR) in one sequence (22,23). The defining features of pCASL are: 1) its use of short trains of RF pulses to achieve labeling of inflowing spins; 2) ability to employ both head (transmit) and body (receive) coils simultaneously; and 3) low specific absorption rate (SAR) constraints. All of these features allow the sequence to achieve highly efficient arterial signal labeling (i.e. maximal signal-to-noise (SNR) of raw images) that is less susceptible to flow velocity and vasculature abnormalities. Additionally, because of the ability to use both the head and body coils, the sequence expedites the efficiency of spin inversion (i.e. it maximizes the amount of labeling applied) for multi-slice acquisitions while controlling for magnetization transfer effects (i.e. without increasing the presence of background noise likely to reduce the overall meaningfulness of the perfusion signal) (12, 22,24). In practice, application of a pCASL sequence will allow for a whole brain acquisition with a TR <4.0s with a labelling efficiency of up to 90% (23,24,25).

Very recent studies comparing pCASL to more standard ASL approaches (e.g. CASL and PASL) show major benefits in employing this optimized approach due

to its increased SNR and reproducibility. Specifically, Chen, Y. et al (2011) compared PASL, CASL and pCASL on 12 healthy subjects to show that pCASL resulted in the highest temporal and spatial SNR relative to the other techniques during a simple resting state scan. Additionally, they showed that pCASL benefitted from the highest within and between subjects reproducibility (across 1hr, 1day, and 1 week scan sessions) (26).

A related study by Gevers, S. et al. (2011) investigated the intra- and multicenter reproducibility of the mainsteram ASL methods (e.g. pCASL, CASL, single TI-PASL, and multi-TI PASL) for measuring cerebral perfusion by scanning the same subjects multiple times across multiple scan centers. The results of this study showed that pCASL had the least data dispersion and best reproducibility for both intra- and multi-center data (27). Insightfully, the authors conclude that the strengths of pCASL relate to the use of background suppression during 'control' image acquisition and utilization of well defined labeling schemes. Specifically, pCASL employs a background suppression technique that effectively crushes all arterial signal within tissue during the 'control' image collection. This means that the presence of any residual arterial tag will be nullified and therefore will not produce artifacts the overall perfusion image. Additionally, background suppression is capable of minimizing physiological noise within a region and can therefore help boost SNR. Interestingly, the pCASL sequence employs a time-of-flight (TOF) scan to optimize the orientation of the labeling plane on an individual subject basis. Additionally, because the pCASL approach is able to acquire a full whole brain dataset with a TR <4 sec, less assumptions are made about arterial arrival time as is the case with other ASL approaches. Taken together, by reducing variability across subjects in labeling efficiency and optimal slice

acquisition timing, pCASL benefits from being more reproducible and therefore, more reliable (27). With these benefits in mind, we posit that the use of a whole brain pCASL sequence will be optimally suited for our initial ongoing pain imaging experiments and therefore decided to employ this method for the next set of pain experiments despite efforts made optimising and testing these earlier versions of ASL sequences.

3.4 References

1. Kety SS & Schmidt CF (1948). The nitrous oxide method for the quantitative determination of cerebral blood flow in main; theory, procedure and normal values. J Clin Invest 27:476-483

2. Golay, X. et al. (2004) Perfusion imaging using arterial spin labelling. Top Magn Reson Imaging 15:10-27

3. Golay, X. et al. (2007) Arterial spin lableing: a one-stop-shop for measurement of brain perfusion in the clinical settings. Proceedings of the 29th Annual International Conference of the IEEE EMBS, Cite Internationale, Lyon, France. Aug 23-24, 2007pp4320-4323

4. Kwong, KK et al. (1995) MR perfusion studies with T1-weighted echo-planar imaging. Magn Reson Med 34:878-87

5. Kim, SG (1995) Quanitification of relative cerebral blood flow change by flow-sensitive alternating inversion recovery (FAIR) technique: application to functional mapping. Magn Reson Med 34:293-301

6. Edelman, RR et al. (1994) Qualitative mapping of cerebral blood flow and functional localization with echo-planar MR imaging and signal targeting with alternating radio-frequency. Radiology 192:513-20

7. Wang, J. et al. (2003) Arterial spin labelling perfusion fMRI with very low task frequency. Magn Reson Med 49(5):796-802

8. Williams, DS et al. (1992) Magnetic resonance imaging of perfusion using spin inversion of arterial water. Proc Natl Acad Sci USA 89:212-

9. Tracey, I. & Bushnell, M.C. (2009). How neuroimaging studies have challenged us to rethink: is chronic pain a disease? J Pain 10(11):1113-20

10. Zarahn E., Aquirre G., D'Esposito M. (1997). A trial-based experimental design for fMRI. Neuroimage 6(2):122-38

11. Aguirre, GK et al. (2002). Experimental design and the relative sensitivity of BOLD and perfusion fMRI. Neuoimage 15(3): 488-500

12. Ito, H., Kanno, I., Fukuda, H. (2005). Human cerebral circulation: positiron emission tomography studies. Ann Nuccl Med. 19(2):65-74.

13. Fernandez-Seara, M.A et al. (2008) Minimizing acquisition time of arterial spin labelling at 3T. Magn Reson Med 59(6):1467-71

14. Wong, E.C., Buxton R.B., Frank L.R. (1998). A theoretical and experimental comparison of continuous and pulsed arterial spin labeling techniques for quantitative perfusion imaging. Magn Reson Med. 40(3): 383-96

15. Aslop, D.C. & Detre J.A. (1998). Multisection cerebral blood flow MR imaging with continuous arterial spin labeling. Radiology 208(2):410-6

16. Detre J.A. & Aslop, D.C. (1999). Perfusion magnetic resonance imaging with continuous arterial spin labeling: methods and clinical applications in the central nervous system. Eur J. Radiol. 30(2):115-24

17. Ye FQ, Yang Y, Duyn J, Mattay VS, Frank JA, Weinberger DR, McLaughlin AC. (1999). Quantitation of regional cerebral blood flow increases during motor activation: A multislice, steady-state, arterial spin tagging study. Magn Reson Med. 42(2)404-7

18. Hoge et al. 1999. Stimulus-dependent BOLD and perfusion dynamics in human V1. Neuroimage 9(1999),pp.573-585

19. Wong, E.C., Buxton, R.B., Frank, L.R. (1997). Implementation of quantitative perfusion imaging techniques for functional brain mapping using pulsed arterial spin labeling. NMR in Biomed. 10:237-249.

20. Lu, H., Donahue M.J., van Zijil P.C. (2006). Detrimental effects of BOLD signal in arterial spin labeling fMRI at high field strength. Magn Reson Med 56(3):546-52

21. Olson, I.R. et al. (2006) Using perfusion fMRI to measure continuous changes in neural activity with learning. Brain Cogn 60(3):262-71

22. Garcia, DM et al. (2005) Pseudo-continuous flow driven adiabatic inversion for arterial spin labelling. In: Proceedings of ISMRM 2005, Miami FL. p.37

23. Wu, WC. et al. (2007) A theoretical and experimental investigation of the tagging efficiency of pseudocontinuous arterial spin labelling. Magn Reson Med 58:1020-1027

24. Fernandez-Seara, M. et al. (2008) Imaging mesial temporal lobe activation during scene encoding: comparison of fMRI using BOLD and Arterial Spin Labeling. Human Brain Mapping 28:1391-1400

25. Wu, WC. et al. (2007) A theoretical and experimental investigation of the tagging efficiency of pseudocontinuous arterial spin labelling. Magn Reson Med 58:1020-1027

26. Chen, Y., Wang, D.J.J., Detre, J.A. (2011). Test-Retest Reliability of Arterial Spin Labeling With Common Labeling Strategies. J Magnetic Resonance Imaging 33:940-9

27. Gevers, S. *et al.* (2011). Robustness and Reproducibility of Flow Territories Defined by Planning-Free Vessel_Encoded Pseudocontinuous Arterial Spin-Labeling. AJNR AM J Neuroradiol. [Epub ahead of print]

Chapter 4

Imaging the neural correlates of ongoing pain in healthy volunteers using a whole brain arterial spin labelling technique (pCASL)

4.1 Introduction

From the results of our experiments outlined in the previous chapter, we concluded that we would no longer pursue experimental work with the PASL 3D-GRASE approach due to the various technical limitations it presented. Additionally, we successfully optimised a CASL-EPI approach to obtain a whole brain volume of activation by interleaving the slice-stack between sub-cortical and cortical slices; the key set-back of which was the relatively sluggish temporal SNR of the approach. Simultaneous to the completion of the interleaved-CASL study, we obtained access to a pCASL sequence which offered an array of attractive benefits: the ease of application on a 3T scanner (e.g. no need for specialised coils or software); reduced SAR limitations on a 3T scanner; the ability to employ both the body (transmit) and head (receive) coils to normalise magnetisation across every image acquisition and bolster SNR; and the possibility for more accurate absolute quantification of CBF. Each of these strengths were likely to be unmatched by any of the other perfusion methods discussed thus far. Consequently, we decided to implement the pCASL approach in two initial tonic pain experiments to observe the efficacy of the technique to resolve meaningful perfusion changes during pain.

4.1.1. Previous studies of ASL FMRI investigations of ongoing pain

To date, ASL pain imaging studies are few. The relative paucity of studies is likely due to nontrivial factors related to the difficulty of employing a safe, well-maintained, ongoing pain state in healthy subjects that is truly tonic and does not habituate. The investigations of Owen et al (2008, 2010) provide strong initial

evidence for the utility for ASL pain imaging (18,19). Their 2010 study showed how to successfully induce a robust, well-maintained deep muscle pain to generate significant increases in CBF in regions well known to be involved in pain processing (e.g. anterior insula bilaterally, anterior mid-cingulate, bilateral thalamus, and contralateral posterior insula). However, they used an unpaired group design in which the control group found the saline condition somewhat painful (19). We posit that new improvements in the experimental design of imaging a tonic pain experience are necessary. Generally, these improvements are centred on: 1) the type of pain used; 2) the paradigm within which the pain is applied; 3) and the ASL imaging approach used to observe the brain in pain.

i) Ongoing pain modalities

The stimulus used to elicit ongoing pain must also be robust, reproducible and clinically relevant (i.e. approximating the sensory, emotional and/ or cognitive pain experience). The approach of Owen et al (2010) was to use injection of hypertonic saline into deep muscle tissue (19). A more recent study by Howard, M.A. et al. (2011) employed a molar-extraction model to image ongoing 'post-surgical' pain with ASL (20). While the approach of both studies is to induce a robust, tonic pain (i.e. hypertonic saline injection as a model of deep muscle pain; molar extraction as a model of post-surgical, neuropathic pain) both necessitate the use of invasive procedures with little cross-species translational research potential. So, while each technique successfully induces tonic pain, it is not clear what the nociceptive source of this pain is (i.e. purely nociceptive, inflammatory, and/or ischemic) and to what extent this approach could be

employed in an animal model to drive more mechanism driven, future work. As a start, we propose the use of non-invasive modalities (thermal or mechanical stimuli) that target slowly adapting nociceptor populations capable of exciting prolonged activation of the CNS during long stimulus blocks.

ii) Ongoing pain paradigms

The specific design of the experimental paradigm will determine the extent of information able to be acquired about how the brain responds to the pain stimulus applied. For example, the experimental paradigms employed by both Owens *et al.* (2008, 2010) and Howard M.A. (2011) can only provide insight as to whether a particular brain region is recruited in ON phases versus an OFF phases of the paradigm. Little information about how that region modulates (or, is modulated by) the sensory experience was reported due to the on/off block design of the experiment. Parametric designs offer a sensible alternative to this end by investigating if a graded change in the stimulus intensity results in a similar modulation of the brain response in specific regions. Additionally, this approach offers the ability to observe potentially different stimulus response profiles in key regions over the length of the long stimulus blocks and across each pain condition.

iii) Optimising ASL for imaging ongoing pain

Because there is a fundamentally low fraction of arterial blood to brain tissue in the human brain (e.g. 1-2%), ASL suffers from inherently low signal-to-noise ratio

(SNR). Currently, of all the different ASL imaging approaches, it is not yet know which is the best suited to image the brain in pain. From BOLD pain imaging, we know that multiple sub/cortical regions are likely to be involved in processing aspects of the pain experience (21). It is therefore essential to image perfusion changes across the whole brain (e.g. brainstem to cortex). Exciting advances in pulse-sequence programming have made it possible to acquire a true whole brain perfusion dataset (e.g. >24 contiguous slices extending from the brainstem) with robust, reproducible SNR (22). The current study will be the first to implement this new ASL approach in an experimental pain imaging context.

To do this, we adapted two different experimental ongoing pain paradigms to elicit specific types of tonic pain states in healthy human subjects. The first paradigm employs the use of topically applied capsaicin cream to excite an ongoing heat pain. The second experiment uses a mechanical stimulation paradigm developed in Chapter 2 that was shown previously in rats (23,24,25) and humans (25) to excite a strong pain response originating from a class of myelinated, high-threshold, slowly adapting A-fibre nociceptors.

We tested the utility of each model to obtain robust, well-maintained ongoing pain perception in healthy human subjects whilst observing the extent of CBF changes across a whole brain volume.

4.2 Experiment 1: Imaging capsaicin-related ongoing heat pain

In experiment 1, we employed a capsaicin pain paradigm to excite a strong ongoing heat pain sensation in healthy subjects. The key aim of the study was to

test the ability of the pCASL approach to image a robust, well-maintained pain experience over a ten-minute stimulus block.

4.2.1. Methods

Experiments were performed on 12 healthy subjects (8 female, mean age = 30). Subjects were asked to partake in a single FMRI experiment carried out on a Siemens 3T Trio scanner. Subjects were asked if they were suffering from pain or were on any medications. No subject reported being in any background pain. No one was on medication likely to interfere with the pain responsiveness. All subjects gave informed consent and the Oxfordshire Ethics Committee approved this study.

Stimuli

Subjects were asked to lie in a scanner with their eyes closed during two scan sessions. During session 1, no stimulus was present (baseline scan). During session 2, 5 ml's of a 1.0% capsaicin cream was applied topically to a 3 x 1 inch section of the midline of the lower abdomen. A piece of cling-film was used to maintain the site of the capsaicin treatment and to prevent the cream from spreading outside the designated stimulus site.

Psychophysics

Subjects were asked to verbally report the extent of the pain intensity experienced during session 2 only. Subjects were asked to rate the pain using the numerical rating scale (0= no pain; 10 = worst pain imaginable). All ratings

were reported verbally before the scan sequence began. Ratings were taken every minute until the subject reached a pain intensity level of NRS = 5 out of 10, at which time the scan commenced. No ratings were taken during the 10-minute pain scan. A final verbal pain rating was taken after the scan finished.

MR Parameters

All subjects were scanned with a pseudo-continuous ASL sequence (22) using a gradient-echo EPI readout (TR=3.75s, TE=13ms, 6/8 k-space). Twenty-six axial slices in ascending order (3x3x4.5mm voxels, 0.5mm inter-slice gap) were prescribed for each subject, and provided whole brain coverage (including brainstem and cerebellum). The labelling offset was defined 10 cm inferior to the centre of the 26 slices. A 90° pre-saturation pulse was applied before the labelling pulses. Labelling duration was 1.4s and a single post-label delay time of 1.0s was used. All subjects were scanned using a Siemens 3T Verio system fitted with a 32-channel head coil.

Analysis

ASL data were analysed using the FMRIB Software Library (FSL) (26). At the first level, the following pre-processing steps were carried out: brain extraction with Brain Extraction Tool (BET) (27), motion correction with MCFLIRT (28) and spatial smoothing with a Gaussian kernel of full-width-half-maximum = 8mm. Intensity normalisation was carried out with a single scaling factor and high-pass temporal filtering performed with a Gaussian-weighted least squares straight line

fit and high-pass cut off filter of 600s. Standard linear registration of subjects' functional datasets to a standard MNI152 T1-weighted brain were used.

Statistical analysis was performed with the use of FMRIB's Expert Analysis Tool (FEAT) (27). At the first level, individual subject's perfusion time series were generated by fitting a model of the relevant 'tag' and 'control' images to the raw four-dimensional datasets. Each voxel was fit to the perfusion model to yield a resultant parameter estimate (PE) image that was proportional to localised blood flow. To determine the percent signal change in CBF relative to the pain stimuli, a model of capsaicin pain (CAPSAICIN) versus baseline (REST) was convolved to each subject's perfusion time series using a fixed effects group level analysis. Cluster-based thresholding was used to find clusters of CBF changes showing effects with a significance level of $p<0.05$, using a z-score cut-off of 2.0 to generate clusters.

4.2.2. Results

Psychophysics:

Pain intensity ratings

Figure 1 shows the mean pain intensity ratings for the capsaicin cream treatment. The mean pain intensity rating was (7.04, sem = 0.32). There was a significant increase in pain intensity when comparing the capsaicin to baseline (*Student t-test, $p<0.01$).

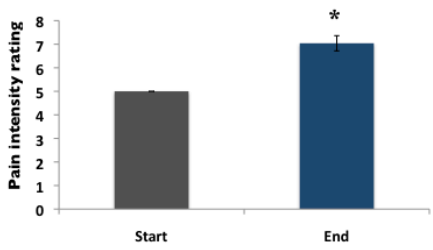

Figure 1: Pyschophysical data from the capsaicin-pain scan. Group mean pain intensity ratings as a function of time are shown. The pain scan commenced when subjects rated the capsaicin-associated pain as 5 out of 10 (start). A second pain rating was taken after the 10-minute scan (End). There was a significant difference in pain intensity ratings from start to end (n=12, * Student t-test, $p<0.01$). Error bars represent the standard error of the mean (SEM).

Perfusion imaging data:

The only significant changes in CBF during the capsaicin-related pain (CAPSAICIN) versus baseline (REST) were visible using a Fixed Effects analysis. Active regions represent voxels with suprathreshold t-statistics generated from the group level Fixed Effects FEAT analysis. Active regions include: dorsal lateral prefrontal cortex, anterior and posterior cingulate cortex, precentral gyrus and the postcentral gyrus (Figure 2).

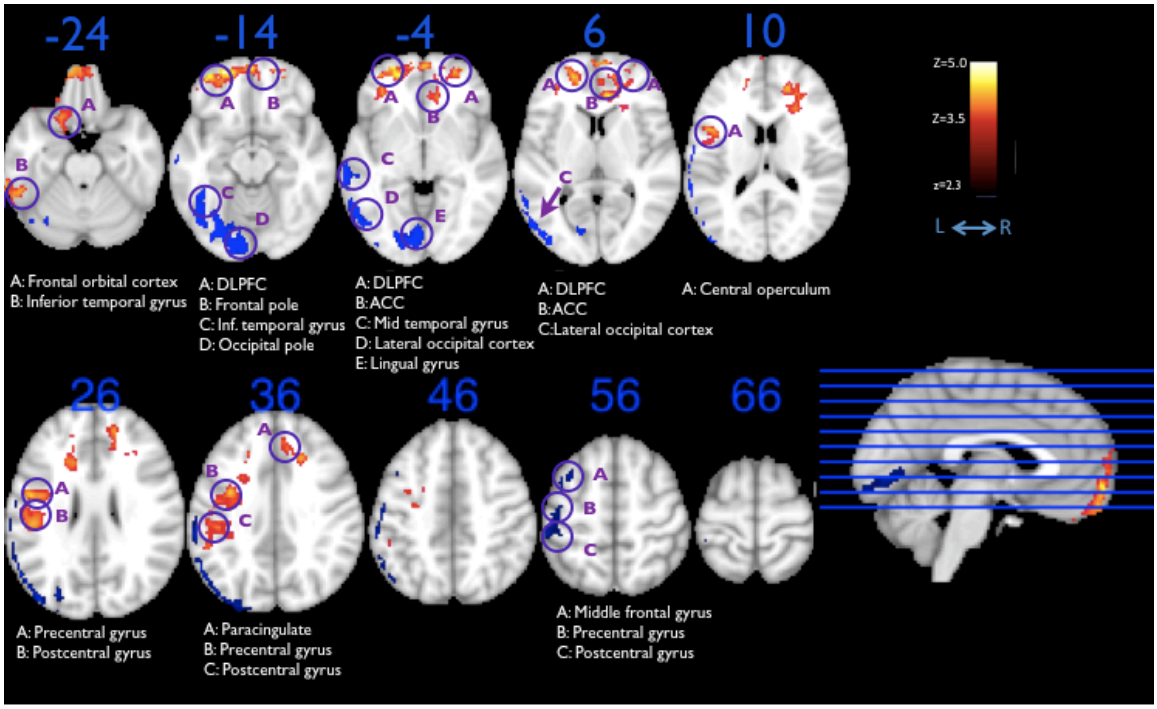

Figure 2: Brain perfusion data showing the contrast of pain (CAPSAICIN) versus baseline (REST). Group zstat maps (n=12) of perfusion activation (red) and deactivation (blue) superimposed on the MNI152 standard template brain (Fixed Effect, $z>2.0$, $p<0.05$, cluster corrected). The sagittal slice shows the column of activation across the whole brain. Axial slices (-24 to 66) correspond to the plane indicated in the sagittal slice.

4.2.3. Discussion

The aim of this investigation was to test the utility of the pCASL approach to image a very strong ongoing heat-pain sensation in a simple OFF/ON experimental design. The psychophysical data shows that the capsaicin cream excites a strong, well maintained heat pain sensation for the duration of the pain scan. However, it was not possible to resolve significant CBF changes in twelve subjects using a Mixed Effects analysis. Only a Fixed Effects analysis showed promising CBF changes during pain in key pain regions. These regions include: dorsal lateral prefrontal cortex, anterior and posterior cingulate cortex, and SI. Noticeably however, significant activations were absent in regions well known

from both BOLD and ASL investigations of experimental pain such as: thalamus, insula, SII, hippocampus and the amygdala.

We posit that the reason for this is due to limitations both in the ASL approach and experimental paradigm employed. While this data provides an exciting first look at the whole brain in pain during a novel capsaicin-pain model; it is clear that the imaging technique and the analysis approach used need to be further optimised. Fundamentally, this dataset is undermined by inherently low SNR. There are a number of ways to bolster this. An obvious way to bolster this is to increase the group size from twelve to as many as eighteen subjects. A second way to bolster SNR is to increase the voxel size. The present investigation employed a standard voxel size of 3x3x4.5 mm. However, it would be sensible to increase the size of the voxel slightly (e.g. 4x4x5.5 mm) to effectively triple the SNR. In addition, as per the advice of our MR Physics collaborators, we employed parallel imaging; a technical feature that may sacrifice spatial SNR to gain temporal resolution. It would be sensible here to exclude this variable (i.e. discontinue the use of parallel imaging) to ensure we are able to maximise the spatial resolution for these initial pain studies.

Additionally, it could be argued that changes need to be made to the pain paradigm used. The psychophysics data clearly show the capsaicin cream effectively induces a strong pain sensation for the duration of the scan, thereby nullifying the argument that a lack of effect observed within the imaging data is due to a lack of pain responsiveness. However, the psychophysics data also show that the pain intensity significantly increases over the duration of the pain

scan. Effectively, this means that pain experienced by individuals is changing in a non-uniform way over the duration of the stimulus block. However, our analysis approach is to model the pain state as a block within which we try to fit the CBF changes relative to the baseline condition. In reality, the stimulus response profile of CBF changes relative to a gradually increasing pain experience is likely to be more complex. Future ASL analyses must try to account for this complexity to accurately resolve how brain function is changing over the long stimulus blocks. We attempted to model this effect by testing the correlation between pain ratings and CBF over time but we were unable to resolve any significant effect.

It could be argued that while the capsaicin model is practically very simple to use, it induces a complex pain state that is slightly beyond our current imaging capacities with ASL at the present time. Instead, it might be useful to employ an equally robust modality that does not sensitise or habituate over the pain block as is the case with the mechanical pain model (25).

A key aim of Experiment 2 is to improve upon the weaknesses of the first experiment to better resolve meaningful brain activation during tonic pain. For example, a larger experimental group size will be recruited; a mechanical pain model well known to elicit a constant pain sensation will be used; and novel ASL analysis methods will be employed.

4.3 Experiment 2: Imaging parametrically modulated mechanical pain

In experiment 2, we employed a mechanical stimulation paradigm to excite graded increases in ongoing pain perception in healthy subjects. Key aims of the current study are to: i) test the utility of a true whole brain ASL sequence to image ongoing pain associated with a pain model previously well characterised in animal models of tonic mechanical pain; and ii) observe whether brain regions recruited during an ongoing pain experience are parametrically modulated by graded stimulus intensities.

To do this, we employed the psychophysical paradigm discussed in Chapter 2 and show previously in rats (23,24,25) and humans (25) to excite a strong pain response originating from a class of myelinated, high-threshold, slowly adapting A-fibre nociceptors. We tested the utility of this model to obtain robust, well-maintained parametric increases in ongoing pain perception in healthy subjects. Key aims of the current study are to: i) test the utility of a true whole brain ASL sequence to image ongoing pain associated with a pain model previously well characterised in animal models of tonic mechanical pain; and ii) observe whether brain regions recruited during an ongoing pain experience are parametrically modulated by graded stimulus intensities.

4.3.1. Methods

Experiments were performed on 18 healthy subjects (10 female; right handed; age: 18-40yrs). Subjects were asked to partake in two sessions: session 1 consisted of a psychophysics protocol completed outside the scanner; session 2

(one week later) consisted of the same psychophysics protocol carried out within a Siemens 3T Trio scanner. No one was on medication likely to interfere with the pain responsiveness. All subjects gave informed consent and the Oxfordshire Clinical Ethics Committee approved this study.

Stimuli

Mechanical probes (MRC, Germany) calibrated to give a constant force (64mN, 256mN and 512mN) were applied to the skin separating the thumb and first finger for a period of 5 minutes. A homemade plastic handle was used to comfortably expose the stimulus site over the duration of the experiment.

Psychophysics

For both sessions, subjects were told they would receive a series of stimulations that would last for a few minutes but were not told the exact duration of the stimulus block. Mechanical stimuli were applied to the hand by placing the probe into a stabilising apparatus that securely held the probe at a constant force on the stimulus site for the duration of the 5-minute stimulus block. The stimulus order was pseudo-randomised across subjects to control for confounding effects of stimulus order, sensitisation and habituation. A 10-minute rest block (no stimulus present) was observed after each stimulus block. Here, subjects were asked to maintain the position of their hand but in the absence of a stimulus probe. During the stimulus, subjects were asked to keep their eyes closed and to focus on the stimulation being received. Subjects rated the stimulus intensity and unpleasantness verbally using an 11-point numerical rating scale (NRS; 0= no

pain; 10= worst pain imaginable) every 30 seconds. During the FMRI session, verbal ratings were taken 30-seconds after the stimulus onset but before the 5-minute ASL scan was acquired. A second verbal rating was taken immediately after the last imaging volume was acquired. Verbal pain scores were then averaged to generate an overall pain rating for each stimulus block scanned. This was done to protect the pain imaging from potential cognitive confounds associated with rating.

FMRI Pain Protocol

Once the subject was placed in the scanner, a ten-minute resting baseline scan was acquired. Immediately after, mechanical stimuli were delivered as discussed previously. Ratings were reported verbally after the first 30-seconds of stimuli and then after the 5-minute scan. The 30-second 'rating phases' that flanked the five minute 'pain scan' were not scanned as discussed above. Ten-minute rest blocks following each pain block were also scanned to determine whether the CBF returns to baseline. Pain intensity and unpleasantness scores were taken at the end of each rest block to monitor any residual pain effects. Subjects were asked to remain still with their eyes closed throughout the entire scan session. See schematic 1 for an illustration of the paradigm used.

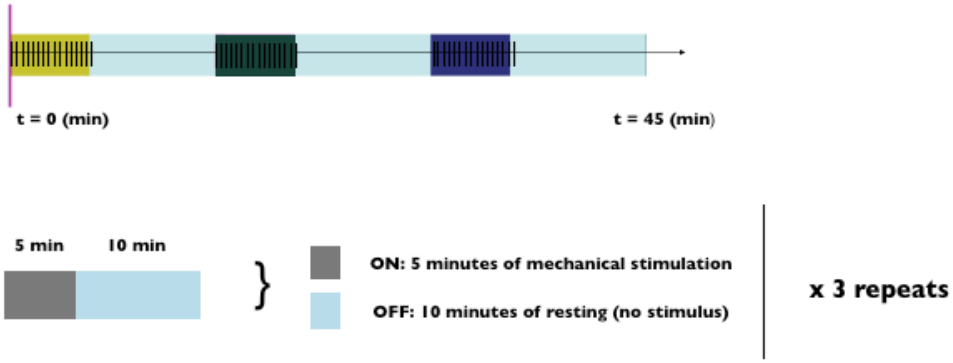

Schematic 1: Graphic representation of the psychophysical paradigm. For clarity, each coloured block represents the presence of a pain stimulus applied to the subjects' hands for a period of 5 minutes (yellow: high pain; blue: medium pain; green: low pain). The light blue block represents the OFF condition (duration =10 minutes) in which no pain stimulus was present. Each pain condition was imaged once per subject. Verbal pain intensity and unpleasantness ratings were acquired after 30-seconds of the commencement of the pain stimulus but before the onset of the scan. An additional pain intensity and unpleasantness rating was taken immediately following the end of the 5 minute pain scan.

MR Parameters

All subjects were scanned with a pseudo-continuous ASL sequence (22) using a gradient-echo EPI readout (TR=3.75s, TE=13ms, 6/8 k-space). Twenty-six axial slices in ascending order (3 x 3 x 4.5 mm voxels, 0.5 mm inter-slice gap) were prescribed for each subject, providing whole brain coverage (including brainstem and cerebellum). The labelling offset was defined 10 cm inferior to the centre of the 26 slices. A 90° pre-saturation pulse was applied before the labelling pulses. Labelling duration was 1.4s and a single post-label delay time of 1.0s was used. All subjects were scanned using a Siemens 3T verio system fitted with a 32-channel head coil.

Analysis

ASL data were analysed using the FMRIB Software Library (FSL) (26). At the first level, the following pre-processing steps were carried out: brain extraction with Brain Extraction Tool (BET) (27), motion correction with MCFLIRT (28) and spatial smoothing with a Gaussian kernel of full-width-half-maximum = 5mm. Intensity normalisation was carried out with a single scaling factor and high-pass temporal filtering performed with a Gaussian-weighted least squares straight line fit and high-pass cut off filter of 320s. Data were denoised of non-physiological artefacts through visual inspection of independent component maps generated using MELODIC (29). Registration of subject's functional datasets was completed in three stages: 1) a single-slice EPI image from one subject was used as an initial structural image to register all subjects' main high-resolution structural images into a standard orientation. Subsequently, subjects' functional datasets were co-registered onto their high-resolution structural images and finally to a standard MNI152 T1-weighted brain using a nonlinear transformation (FNIRT, FSL).

Statistical analysis was performed with the use of FMRIB's Expert Analysis Tool (FEAT) (27). At the first level, individual subject's perfusion time series were generated by fitting a model of the relevant 'tag' and 'control' images to the denoised four-dimensional datasets. Each voxel was fit to the perfusion model

to yield a resultant parameter estimate (PE) image that was proportional to localised blood flow. To determine the percent signal change in CBF relative to the pain stimuli, a model of low, medium and high pain was convolved to each subject's perfusion time series using a fixed effects second level analysis. At the top level, a mixed effects analysis incorporating both within and across subjects variance was used to obtain group mean activation maps for the main effect of each stimulus condition on changes in CBF across the whole brain. Cluster-based thresholding was used to find clusters of CBF changes showing effects with a significance level of $p<0.05$, using a z-score cut-off of 2.3 to generate clusters.

CBF Changes: parametric increase in CBF with stimulus intensity

To examine the group mean cerebral responses relative to a graded change in stimulus intensity, we employed a tripled t-test to monitor changes in CBF across the three levels of pain applied. We employed this approach in order to adequately explore all possible relationships between a change in stimulus intensity and CBF across the whole-brain. A tripled t-test is a natural extension of a t-test but includes contrasts of main conditions of interest: i) high pain > medium pain; ii) high pain > low pain; iii) medium pain > low pain. To show there is a graded change with stimulus intensity, we first generated a statistical map showing where there was a significantly greater response in the high condition compared to the low condition (high pain> low pain). To identify those regions showing a consistent graded response across the three levels of pain applied, we masked this map with the contrast of medium pain> low pain. The results from this analysis will reveal only those regions that show a significant monotonic

increase in CBF relative to an increase in stimulus intensity across all levels of pain applied. We applied this approach to ensure that our analysis did not make any assumptions about the relationship between a graded increases in stimulus intensity and changes in CBF.

Region of interest (ROI) investigation of CBF time courses

Because the response profiles are not well know for any brain region during prolonged pain, we aimed to investigate the effect of each stimulus intensity over time within regions well known from previous experiments to be recruited during the pain experience. To do this, group mean time courses were extracted from relevant ROIs at each stimulus condition. This approach made it possible to visualise dynamic changes in CBF over time for each stimulus condition. The following ROIs were selected based on *a priori* information regarding brain activation during ongoing pain: amygdala, thalamus, insula, cingulate, SI and SII (19,20).

Anatomical masks were defined with the use of the Harvard-Oxford Atlas in FSL. Individual subject's time courses for each ROI were averaged to obtain group mean CBF time courses for each stimulus condition. Because each stimulus and related pre-stimulus baseline periods were acquired in separate scans, data from each stimulus condition were normalised to the preceding pre-stimulus baseline condition. Normalised time courses were then temporally smoothed using a 'moving average' low pass filter that corresponds to a temporal width of 35 seconds to better visualise the overall temporal trends for each ROI.

4.3.2. Results

Psychophysics:

Pain intensity ratings: Session 1 (outside the scanner)

Figure 3a,b shows the mean pain intensity ratings for the three stimuli conditions used in this study (low, moderate and strong pain) as reported previously in Chapter 2 (Figure 7b, p.73). The mean pain intensity pain rating for each condition was (low = 0.89, S.E. = 0.032; moderate = 2.71, S.E. = 0.11; strong = 4.91. S.E. = 0.16, respectively. The mean pain unpleasantness rating for each condition was (low = 0.75, S.E. = 0.026; moderate = 2.78, SE = 0.075; strong = 5.12, SE = 0.178), respectively. There was a significant increase in pain intensity (one-way ANOVA; $p<0.001$) and unpleasantness (one-way ANOVA; $p<0.001$) across the three conditions. A significant difference was observed between the first and last pain ratings (both intensity and unpleasantness) for the high pain condition (Student T-Test, $p<0.05$). There was no significant change in pain ratings over the medium and low stimulus intensity blocks.

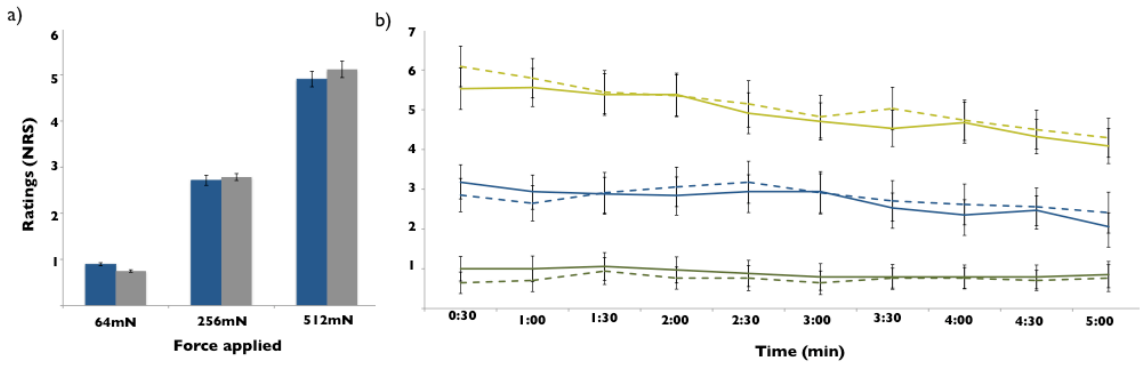

Figure 3: Psychophysical data from outside the scanner (as reported previously in Chapter 2, p72-73). Group mean intensity and unpleasantness ratings as a function of stimulus intensity applied to subjects' hands. **a)** Pain intensity (blue) and unpleasantness (grey) significantly increased with stimulus intensity (n=18; * one-way ANOVA, $p<0.001$). **b)** Pain intensity (solid lines) and unpleasantness (dotted lines) over the time course of the stimulus blocks for each level of force applied (64mN = green; 256mN = blue; 512mN = yellow). The pain intensity and unpleasantness ratings habituated slightly during the high pain condition when comparing the first to the last rating (Student t-test, $p<0.05$). Pain perception did not significantly habituate over the course of the stimulus blocks for intensity or unpleasantness ratings for the medium or low pain conditions. Error bars represent the standard error of the mean (SEM).

Pain intensity ratings: Session 2 (inside the scanner)

Figure 4 shows the mean pain intensity ratings for the three stimuli conditions used in this study (low, moderate and strong pain). The mean pain intensity rating for each condition was: low = 0.53, S.E. = 0.15; moderate = 3.23, SE = 0.38; strong = 5.42, SE = 0.43, respectively. The mean pain unpleasantness rating for each condition was: low= 0.36, SE = 0.12; medium = 3.07, SE = 0.44; strong = 5.40, SE = 0.44.

There was a significant difference in reported pain scores (intensity and unpleasantness) between the high (512mN), medium (256mN) and lower (64mN) forces (n=18; one-way ANOVA, $p<0.001$)(Figure 2). These differences were well maintained over the ON blocks as there was no significant habituation or sensitization of pain reports for a given stimulus intensity over time (Student t-test, $p>0.05$).

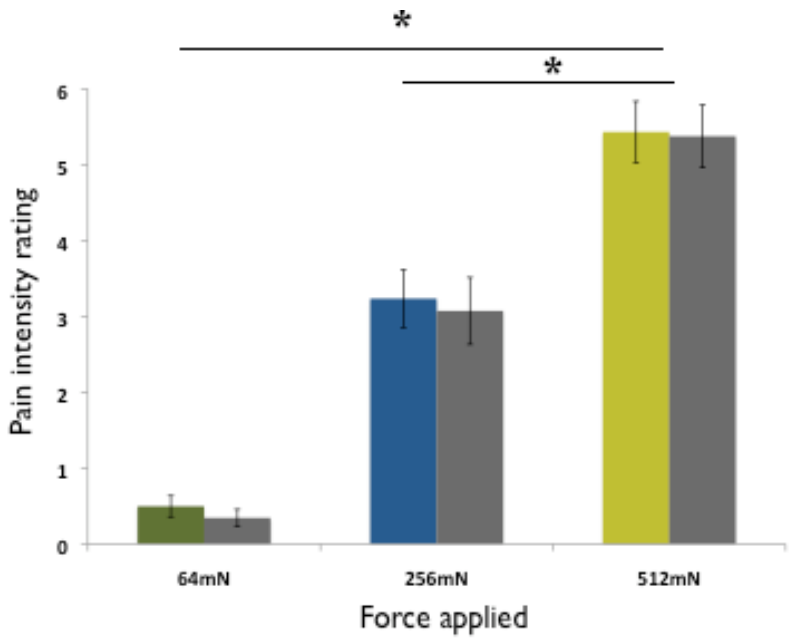

Figure 4: Psychophysical data from inside the scanner. Group mean intensity and unpleasantness ratings as a function of stimulus intensity applied to subjects' hands. Pain intensity (blue) and unpleasantness (gray) significantly increased with stimulus intensity (n=18; * one-way ANOVA, $p<0.001$). Pain perception did not significantly habituate over the course of the stimulus blocks for intensity or unpleasantness ratings. Error bars represent the standard error of the mean (SEM).

Perfusion imaging data:

Significant changes in CBF across the high pain condition versus the respective pre-pain baseline are listed in Table 1. Regions listed represent voxels with suprathreshold t-statistics generated from the group-level FEAT analysis. Significant increases in CBF occurred in many regions shown previously to be involved in processing acute (30,31) and phasic (ASL: 18,19,20; PET: 4,5,34,35,36,37,38) pain. These include: frontal gyrus, cingulate cotex (posterior and anterior), thalamus, anterior insula, caudate, and the prefrontal cortex. All coordinates are given in MNI space.

ROI	**Laterality**	**(MNI)**	**(TAL)**	**zstat**
DLPFC	Left	(57,92,39)	(-24,58,6)	3.12
Frontal_opperculum	Left	(62,78,39)	(-34,30,6)	3.11
Anterior_Insula	Left	(61,70,39)	(-32,14,6)	2.65
DMPFC	Left	(57,91,43)	(-24,56,14)	2.61
DLPFC	Left	(62,82,43)	(-34,38,14)	2.57
Inferior_frontal_gyrus	Left	(67,74,43)	(-44,22,14)	2.3
Central_operculum	Left	(65,63,43)	(-40,0,14)	2.53
ACC	Right	(38,80,43)	(14,34,14)	2.58
Caudate	Left	(52,67,43)	(-14,8,14)	2.41
Thalamus	Left	(51,55,43)	(-12,-16,14)	2.62
DLPFC	Left	(59,85,48)	(-28,44,24)	2.31
Middle_frontal_gyrus	Left	(65,80,48)	(-40,34,24)	2.64
ACC	Right	(39,75,48)	(12,24,24)	2.87
PCC	Left	(47,40,48)	(-4,-46,24)	2.33
PCC	Right	(44,41,48)	(2,-44,24)	2.4
DMPFC	Left	(51,86,53)	(-12,46,34)	3.12
Paracingulate	Left	(50,79,53)	(-10,32,34)	3.28
Paracingulate	Right	(41,84,53)	(8,42,34)	2.5
Middle_frontal_gyrus	Left	(64,75,53)	(-38,24,34)	3.3
ACC	Left	(49,68,53)	(-8,10,34)	2.58
DMPFC	Right	(42,79,58)	(6,32,44)	2.85
Middle_frontal_gyrus	Left	(60,75,58)	(-30,24,44)	3.3
Paracingulate	Right	(42,71,58)	(6,16,44)	2.74
Paracingulate	Left	(49,69,58)	(-8,12,44)	3.17
SMA	Left	(51,63,58)	(-12,0,44)	3.28
Precentral gyrus	Left	(66,58,58)	(-42,-10,44)	2.78
PCC	Left	(48,51,58)	(-6,-24,44)	3.23
DMPFC	Left	(49,76,63)	(-8,26,54)	3.85
DMPFC	Right	(41,73,63)	(8,20,54)	2.62
Middle_frontal_gyrus	Right	(31,66,63)	(28,6,54)	2.6
Middle_frontal_gyrus	Left	(59,66,63)	(-28,6,54)	3.39
Superior_frontal_gyrus	Left	(56,71,63)	(-22,16,54)	3.77
Precentral gyrus	Left	(62,56,63)	(-34,-14,54)	2.99

Superior_frontal_gyrus	Left	(56,64,68)	(-22,2,64)	3.57
Precentral gyrus	Left	(58,56,68)	(-26,-14,64)	2.93
Precentral_gyrus	Right	(42,49,68)	(6,-28,64)	2.5

Table 1: Brain responses to High pain versus the pre-pain baseline (High pain > pre-high pain). Note: DLPFC, dorsal lateral prefrontal cortex; DMPFC, dorsal medial prefrontal cortex; ACC, anterior cingulate cortex; PCC, posterior cingulate cortex; SMA, supplementary motor area.

Parametric changes in CBF with stimulus intensity:

Regions showing a significant monotonic increase in activation with a graded change in stimulus intensity are shown in Figure 5. Coloured regions represent voxels with suprathreshold t-statistics generated from the group-level FEAT analysis. Significant changes in CBF representative of a monotonic increase in activation with a graded increase in stimulus intensity occurred in many regions shown previously to be involved in processing acute and phasic pain. These regions include: bilateral anterior and posterior cingulate cortex, central operculum, parietal operculum, precentral gyrus, postcentral gyrus; and contralateral amygdala, putamen, posterior insular cortex, thalamus.

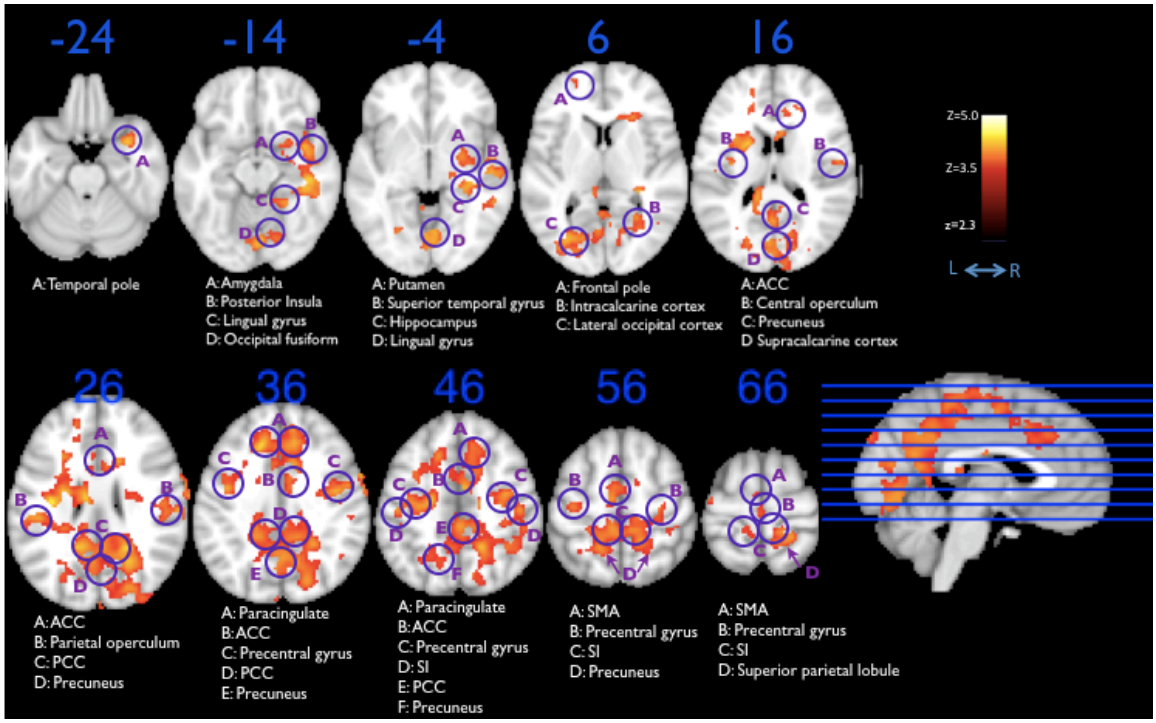

Figure 5: a) Brain perfusion data showing monotonic increase in perfusion with increasing stimulus intensity. Group zstat maps (n=18) of perfusion activation superimposed on the MNI152 standard template brain (Mixed Effects, $z>2.3$, $p<0.01$; cluster corrected). The sagittal slice shows the column of activation across the whole brain. Axial slices (-24 to 66) correspond to the plane indicated in the sagittal slice.

ROI time courses

Figure 6a shows the dynamic changes in CBF over each stimulus condition for key pain-relevant anatomical masks listed above. To note, these timecourses are not reflective of the functional maps defined in Figure 5c. Group mean changes in CBF over the 5-minute stimulus blocks were normalised to each pain condition's preceding resting baseline condition (no pain present). Interestingly, only the bilateral posterior cingulate and contralateral amygdala show a stepwise increase in perfusion changes with increases in stimulus intensity. The more common trend across regions is that there is a less clear difference in perfusion between 'low pain' and 'moderate pain' compared to the very large increases in CBF during 'high pain'. For example, the thalamus shows that CBF changes are similar for both the low and medium pain conditions but significantly greater during the high pain condition.

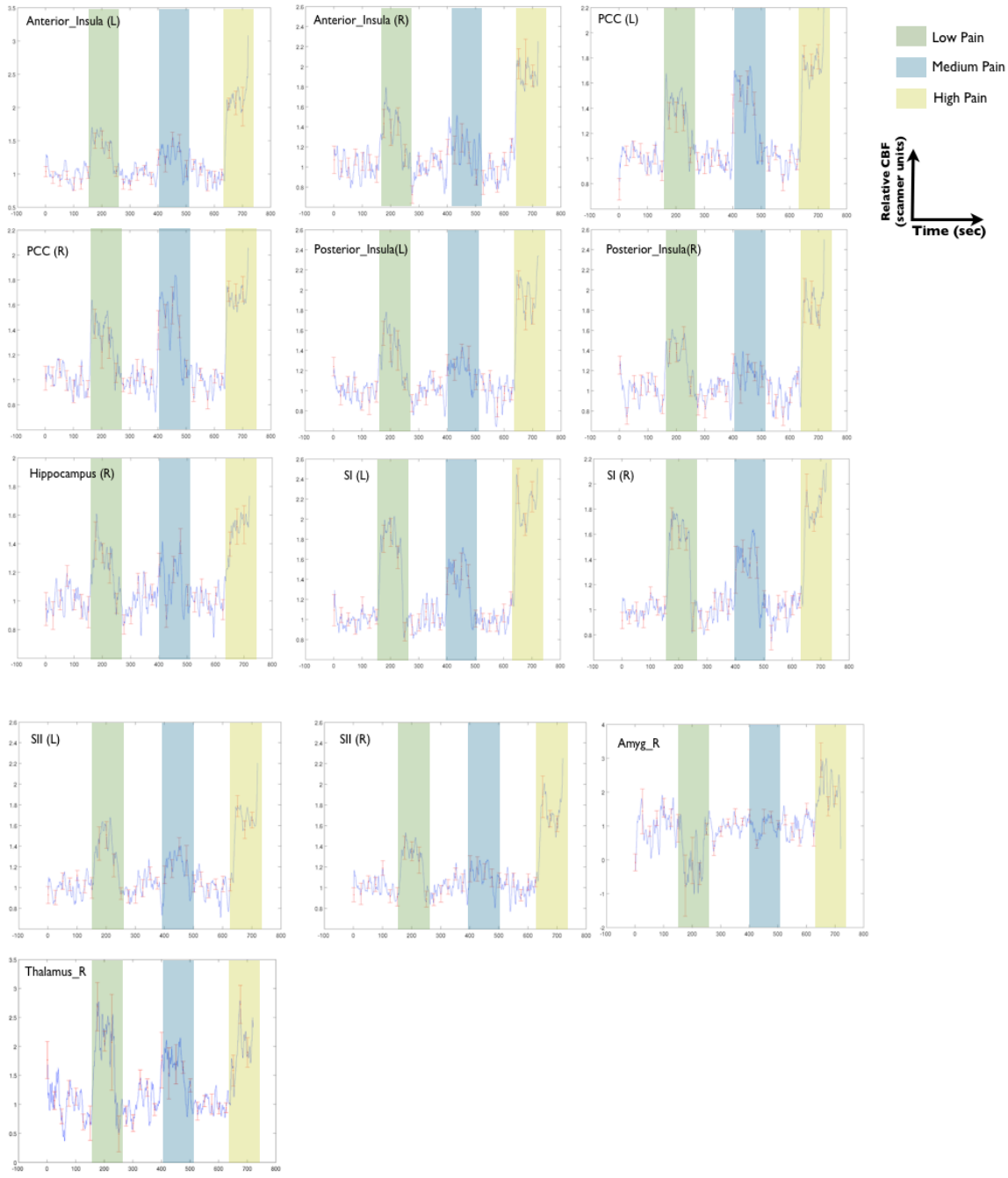

Figure 6a: Group mean time courses extracted from key ROIs defined by anatomical masks for pain-relevant regions. Non-shaded regions define the pre-pain REST blocks where no stimulus is present versus shaded regions showing activation relative to a given stimulus force (green= low pain; blue = medium pain; yellow = high pain). The following ROIs are list in the order they are displayed above: anterior insular cortex, posterior cingulate cortex, posterior insular cortex, hippocampus, SI,SII, amygdala, and thalamus. Error bars represent the standard error of the mean (SEM).

To confirm these time course observations, group mean parameter estimates were extracted from each ROI for each stimulus condition (Figure 6b). While all regions show significantly increased perfusion versus baseline for each pain condition (compared to baseline), there is a less clear relationship between low and medium pain over the duration of the stimulus block compared to the very robust increase in CBF observed during the high pain condition.

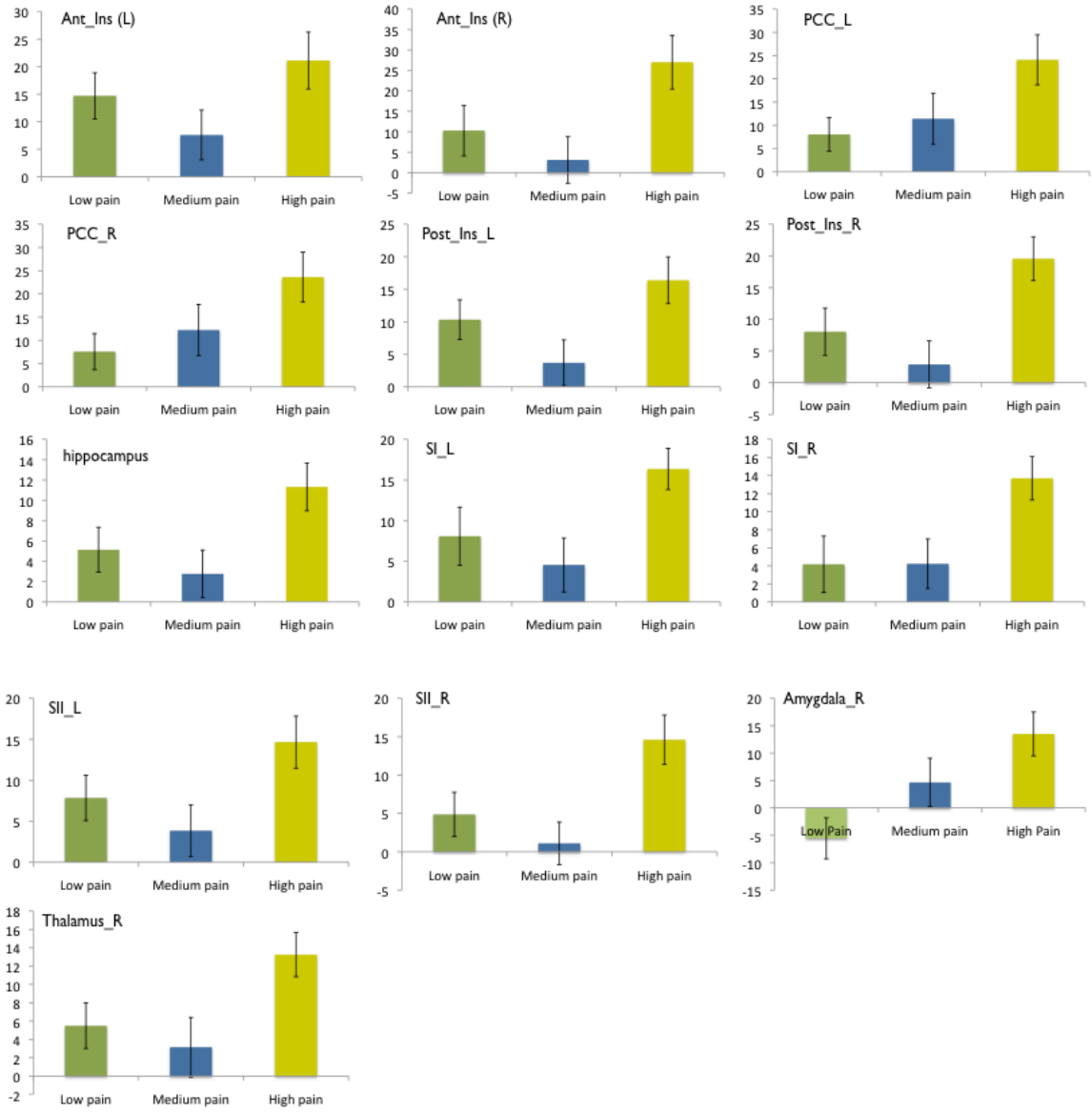

Figure 6b: Group mean parameter estimates extracted from the *a priori* defined ROIs defined by anatomical masks of pain relevant regions are plotted for each stimulus force ((green= low pain; blue= medium pain; yellow = high pain). The following ROIs are list in the order they are displayed above: anterior insular cortex, posterior cingulate cortex, posterior insular cortex, hippocampus, SI,SII, amygdala, and thalamus. Error bars represent the standard error of the mean (SEM).

4.3.3. Discussion

The aim of this investigation was to image the neural correlates of ongoing, parametrically modulated pain using ASL in healthy human subjects. Our data confirm that it is indeed possible to image perfusion changes relative to a tonic pain stimulus that is parametrically modulated. This is the first investigation of parametrically modulated pain to be imaged using a whole-brain ASL imaging approach.

We used a stimulus force-locked design in which subjects reported robust, well differentiated pain responsiveness to three force probes applied to the subjects' hands. Importantly, the psychophysical data show that the stimulus responses were well maintained over the course of the 5-minute stimulus blocks as no significant habituation to the pain stimuli were observed. Additionally, our imaging data show that as the pain intensity increases, so to does the number of regions that become active. These data align well with previous parametric pain investigations completed using PET imaging (10,37,38).

Investigation of the dynamic changes in stimulus response profiles of key ROIs over each pain condition reveals that only a few of the regions show a clear step-wise increase in CBF with increasing stimulus force. More evident was the similarity in extent of CBF changes during the 'low' and 'medium' conditions whilst the 'high' pain condition always showed a clear, robust increase in CBF compared to the other pain conditions. Interestingly, the psychophysical data

shows a clearly separable pain experience as reported by the subjects for each stimulus type. It is possible that regions recruited during pain are functioning with a less clear stimulus response profile in the context of this experimental pain paradigm. It is also possible that while the overall pain experienced during each condition is clearly unique, differences in the functional and related metabolic demand of key regions underlying less painful sensations might not be discernible with the current approach.

What is clear however is that during the 'high' pain condition, large increases in CBF are observable for each of the ROIs; potentially because of the strongly aversive nature of the stimulus and the related signalling of tissue damage that experience is likely to trigger within the subjects. It is possible that for this paradigm, the 'low' and 'medium' conditions while differently painful were similarly 'innocuous' in their capacity to trigger an unabated sense of 'danger' to the body. Anecdotally, some subjects mentioned that the high pain was always 'very painful' and 'difficult to get used to' while no one mentioned as such for the other conditions.

Numerous parametric studies of acute (BOLD: 35,36) and phasic (PET: 10,37,38) pain have highlighted the relationship between stimulus intensity, pain rating and changes in neural activity in key brain regions such as: cerebellum, putamen, thalamus, insula, anterior cingulate, SI, SII, prefrontal and inferior parietal cortices. Generally, these studies show that as the stimulus intensity increases, so to do the number of brain regions that become active. A key

outcome of the current study was to understand how different pain-relevant regions are able to track changes in stimulus intensity. Here, our data show regions such as the thalamus, posterior insular cortex and SI, which are known to receive direct afferent input from the dorsal horn, show monotonic responsiveness with an increase in stimulus intensity. In this way, an increase in stimulus intensity applied to the periphery will excite a greater afferent drive into the CNS: a feature which these regions appear to be tracking even over the course of the 5-minute stimulus blocks. More interestingly, a number of regions commonly thought to code more affective dimensions of the pain experience; namely, the amygdala, the anterior cingulate cortex, the putamen also show a similar monotonic response profile with an increase in stimulus intensity. It is possible that these data highlight how the key sensory-discriminative structures (e.g. SI, thalamus, posterior insular cortex) track the incoming afferent barrage from the dorsal horn to monitor the sensory-discriminative properties of the noxious stimulus over the long block. Relatedly, these more affective regions appear to track changes in the afferent nociceptive input; possibly to integrate key aspects of one's emotional and cognitive state to generate an overall experience that is differentially painful across each stimulus intensity. While these data are not sufficient to unravel the interaction between active regions over time, this is the first demonstration that regions thought to encode both sensory and affective dimension of pain show a monotonic responsiveness to a change in stimulus intensity as well as sustained responses to tonic inputs.

The present investigation sought to expand on this and the setbacks of previous ASL pain experiments by employing a pain paradigm that could be easily shut off

(i.e. presence of a true pain-free condition) whilst also being able to be parametrically modulated with increasing stimulus intensities within each subject in a single FMRI session. The data show each stimulus force recruited a number of regions showing significant increases in CBF across both sub-cortical and cortical regions. For example, regions such as the amygdala, insula, thalamus, putamen, SI, SII, ACC and the frontal cortex have been shown previously in PET, ASL and BOLD imaging studies to play integral roles in pain processing. We interpret this alignment across studies as strong supporting evidence for the use of this pain imaging approach for future work on mechanisms of tonic pain processing.

The extent to which changes in CBF are maintained over the course of the long stimulus blocks is another key interest of this work. For example, Owen et al. (2010) report very large percent reductions in CBF over the course of the long stimulus blocks (e.g. 70% reduction in thalamic activity after 15-minutes of infusion) (19). In the present study, while the overall trend of each stimulus block is a net increase in CBF with pain, large dips in CBF are visible in the time course. The underlying source of this potential habituation is not known. It is possible that the relationship between neural activation, CBF demand, and arterial signal over long stimulus blocks is likely to be complex and potentially non-uniform across sub-cortical and cortical structures. For example, it is possible that not all pain-relevant regions necessitate a constant and prolonged CBF demand over long pain stimuli, as has been shown previously in animal models of visual adaptation (39,40). To add, the present study and those of Owen et al. (2008, 2010) use a single inversion time (TI) to report relative changes in CBF (18,19). Neither study is reporting absolute CBF time course

data; information that is integral to fully characterise exactly how arterial signal changes over time across different parts of the brain. Consequently, it is still unclear to what extent shifts in temporal CBF dynamics reflect relevant functional neuronal events.

Excitingly, new developments in pulse-sequence programming have made it possible to image absolute changes in CBF across the whole brain by employing a multi-TI pCASL approach (41). Obtaining absolute perfusion changes is essential to understand if the complex CBF dynamics observed in the present study are in fact related to meaningful neuronal and/or neurovascular events, or are just an artifact of the technique. Absolute quantification of CBF allows also for true longitudinal experiments to be performed where tracking changes in CBF over time as the pain condition changes is desired. An essential next step to this end will be to employ this optimised approach in a tonic pain experiment.

4.4 Conclusion

In summary, our results show that it is possible to image ongoing pain in healthy subjects using a modality that can be parametrically modulated. Subjects report each stimulus as inducing a robust, well maintained pain. Additionally, the imaging data shows a number of regions well known from BOLD and PET literature to be involved in pain processing. But future work is needed to both confirm these results and also to better understand the complex relationship between CBF demand and tonic pain across various regions of the brain. We argue that future tonic pain ASL investigations must include: i) a clear baseline condition; ii) a pain state that is well maintained for a duration that is longer than

a minute to be considered ‘tonic’; iii) a clear separation between the stimulus response and the rating condition to avoid any cognitive load artefact inherent to rating while experiencing an experimental condition; iv) a within-groups comparison between control and experimental conditions; and v) an acquisition protocol that encapsulates time series information from the whole brain (e.g. brainstem to cortex).

4.5 Appendix: Table of activations

Cluster	zstat	MNI	Laterality	ROI
4	4.65	(46 30 29)	L	Cerebellum
4	4.38	(54 36 21)	L	Cerebellum
4	4.09	(33 39 17)	R	Cerebellum
4	4.06	(49 31 27)	L	Cerebellum
4	3.95	(51 32 22)	L	Cerebellum
4	3.84	(41 36 31)	R	Cerebellum
4	3.77	(32 53 22)	R	Parahippocampal gyrus
4	3.71	(55 38 28)	L	Temporal occipital fusiform
4	3.7	(34 58 39)	R	Putamen
4	3.59	(32 37 20)	R	Cerebellum
4	3.51	(32 27 23)	R	Cerebellum
4	3.42	(51 31 33)	L	Lingual gyrus
4	3.34	(50 34 31)	L	Lingual gyrus
4	3.33	(53 56 22)	L	Parahippocampal gyrus
4	3.33	(64 38 23)	L	Temporal occipital fusiform
4	3.26	(47 30 37)	L	Lingual gyrus
4	3.18	(37 71 25)	R	Frontal orbital cortex
4	3.17	(54 21 28)	L	Occipital fusiform gyrus
3	3.9	(60 66 38)	L	Putamen
3	3.69	(62 70 41)	L	Anterior insula/frontal operculum
3	3.49	(72 41 41)	L	Supramarginal gyrus
3	3.39	(61 53 44)	L	Posterior insula
3	3.3	(51 44 38)	L	Hippocampus
3	3.27	(64 54 46)	L	Central operculum
3	3.25	(63 54 48)	L	Central operculum
3	3.23	(68 60 55)	L	Precentral gyrus
3	3.21	(70 40 43)	L	Supramarginal gyrus
3	3.16	(57 59 49)	L	White Mater
3	3.04	(52 63 35)	L	Pallidum
3	3.02	(51 61 36)	L	Pallidum
3	3.01	(63 51 38)	L	Posterior insula
3	2.97	(71 45 35)	L	Middle temporal gyrus
3	2.96	(69 51 53)	L	Postcentral gyrus
3	2.95	(69 51 51)	L	Postcentral gyrus
3	2.94	(65 58 62)	L	Precentral gyrus
3	2.94	(66 56 62)	L	Precentral gyrus
3	2.89	(68 58 59)	L	Precentral gyrus
3	2.88	(54 49 40)	L	Thalamus
3	2.87	(75 45 48)	L	Parietal operculum
3	2.85	(58 63 68)	L	Superior frontal gyrus
3	2.85	(52 47 42)	L	Thalamus
3	2.84	(49 55 36)	L	Thalamus

2	4.75	(24 51 35)	R	White Mater
2	4.4	(17 49 34)	R	Middle temporal gyrus
2	4.33	(15 49 42)	R	White Mater
2	4.27	(20 52 43)	R	Parietal operculum
2	4.21	(16 53 45)	R	Parietal operculum
2	3.95	(21 45 45)	R	Planum temporale
2	3.91	(20 53 39)	R	Heschl's gyrus
2	3.83	(21 43 42)	R	Supramarginal gyrus
2	3.77	(34 45 35)	R	Hippocampus
2	3.76	(20 49 45)	R	Parietal operculum
2	3.68	(17 52 37)	R	Superior temporal gyrus
2	3.58	(16 63 40)	R	Central operculum
2	3.32	(17 53 26)	R	Middle temporal gyrus
2	3.09	(16 39 44)	R	Angular gyrus
2	3.01	(31 51 31)	R	Hippocampus
2	2.99	(19 57 24)	R	Middle temporal gyrus
2	2.96	(27 46 44)	R	Planum temporale
2	2.93	(14 38 27)	R	Inferior temporal gyrus
2	2.88	(10 50 28)	R	Middle temporal gyrus
2	2.86	(17 47 27)	R	Inferior temporal gyrus
2	2.84	(14 44 26)	R	Inferior temporal gyrus
2	2.83	(22 36 39)	R	Middle temporal gyrus
2	2.83	(11 57 41)	R	Central operculum
1	3.64	(37 58 51)	R	White Mater
1	3.51	(39 55 56)	R	PCC
1	3.24	(41 54 49)	R	PCC
1	3.11	(47 58 57)	R	Mid-anterior cingulate
1	3.09	(44 60 59)	R	Mid-anterior cingulate
1	3.07	(48 52 50)	R	PCC
1	2.98	(42 57 61)	R	SMA
1	2.96	(35 56 62)	R	White Mater
1	2.95	(44 50 57)	R	PCC
1	2.92	(43 57 59)	R	Midcingulate
1	2.83	(47 33 54)	L	Precuneus
1	2.82	(43 42 51)	R	PCC
1	2.76	(34 51 62)	R	White Mater
1	2.76	(29 53 59)	R	Precentral gyrus
1	2.76	(41 44 60)	R	Precuneus
1	2.75	(51 38 48)	L	White Mater
1	2.71	(49 50 69)	L	Precentral gyrus
1	2.66	(48 29 53)	L	Precuneus
1	2.57	(49 58 61)	L	SMA

Table A: Parametric modulation of ongoing mechanical pain. Brain response to the triple-t-test showing regions that display significant monotonic increases in perfusion with a change in stimulus intensity. Note: PFC, prefrontal cortex; ACC, anterior cingulate cortex; PCC, posterior cingulate cortex; SMA, supplementary motor area.

4.6 References

1. Breivik H, Collett B, Ventafridda V, Cohen R, Gallacher D. (2006). Survey of chronic pain in Europe: prevalence, impact on daily life, and treatment. Eur J Pain 10(4):287-333

2. Thunberg J, Lyskov E, Korotov A, Ljubisavljevik M, Pakhomov S, Katayeva G, Radovanovic S, Medvedev S, Johansson H. (2005). Brain processing of tonic muscle pain induced by infusion of hypertonic saline. Eur J Pain. 9(2): 185-94

3. Wang J, Aquirre GK, Kimberg DY, Detre JA. (2003). Arterial spin labelling perfusion fMRI with very low task frequency. Magn Reson Med 49(5):796-802

4. Talbot JD, Marrett S, Evans AC, Meyer E, Bushnell MC, Duncan GH. (1991) Multiple representations of pain in human cerebral cortex. Science 251(4999): 1355-1358.

5. Jones AKP, Friston KJ, Brown D, Qi L, Frackowiak RSJ. (1991). Cortical and subcortical localization of response to pain in man using positron emission tomography. Roc Roy Soc B 244:39-44.

6. Casey KL, Minoshima S, Morrow TJ, Koeppe RA (1996). Comparison of human cerebral activation pattern during cutaneous wamth, heat pain and deep cold pain. J Neurophsyiol 76(1):571-81.

7. Coghill RC, Talbot JD, Evans AC, Meyer E, Gjedde A, Bushnell MC, Duncan GH (1994). Distributed processing of pain and vibration by the human brain. J Neuroscience 14(7):4095-4108

8. Derbyshire SWG, Jones AKP (1998). Cerebral responses to a continual tonic pain stimulus measured using positron emission tomography. Pain 76: 127-135.

9. Iadarola MJ, Max MB, Berman KF, Byas-Smith MG, Coghill RC, Gracely RH, Bennett GJ. (1995). Unilateral decrease in thalamic activity observed with positron emission tomography in patients with chronic neuropathic pain. Pain 63(1):55-64.

10. Tolle TR, Kaufmann T, Siessmeier T, Lautenbacher S, Berthele A, Munz F, Zieglgansberger W, Willoch F, Schwaiger M, Conrad B, Bartenstein P. (1999). Region-specific encoding of sensory and affective components of pain in the human brain: a positron emission tomography correlation analysis. Ann Neurol. 45(1):40-7.

11. Aquirre GK, Detre JA, Zarahn E, Aslop DC. (2002). Experimental design and the relative sensitivity of BOLD and perfusion fMRI. Neuroimage 15(3): 488-500.

12.Wang J, Aquirre GK, Kimberg DY, Detre JA. (2003). Arterial spin labelling perfusion fMRI with very low task frequency. Magn Reson Med 49(5):796-802

13.Detre, J.A., Leigh, J.S., Williams, D.S., Koretsky, A.P. (1992) Perfusion imaging. Magn. Reson. Med. 23(1):37-45

14.Kim, SG (1995) Quanitification of relative cerebral blood flow change by flow-sensitive alternating inversion recovery (FAIR) technique: application to functional mapping. Magn Reson Med 34:293-301

15. Kim J, Whyte, J., Wang, J., Rao, H., Tang, K.Z., Detre, J.A. (2006) Continuous ASL perfusion fMRI investigation of higher cognition: quantification of tonic CBF changes during sustained attention and working memory tasks. Neuroimage 31(1):376-85.

16.Olson, I.R. et al. (2006) Using perfusion fMRI to measure continuous changes in neural activity with learning. Brain Cogn 60(3):262-71

17.Garraux, G., Hallett, M. & Talagala, S.L. (2005) CASL fMRI of subcortico-cortical perfusion changes during memory-guided finger sequences. Neuroimage. 25:122-32.

18.Owen DG, Bureau Y, Thomas AW, Prato FS, St Lawrence KS. (2008). Quantification of pain-induced changes in cerebral blood flow by perfusion MRI. Pain 136(1):85-96.

19.Owen DG, Clarke CF, Ganapathy S, Prato FS, St Lawrence KS. (2010). Using perfusion MRI to measure the dynamic changes in neural activation associated with tonic muscular pain. Pain 148(3):375-86.

20. Howard, M.A., Krause, K., Khwaja, N., Massat, N., Zelaya, F., Schumann, G., Huggins, J.P., Vennart, W., Williams, S.C.R., Renton, T.F. (2011) Beyond patient reported pain: Perfusion magnetic resonance imaging demonstrates reproducible cerebral representation of ongoing post-surgical pain. PLoS One 6(2):1-10.

21.Tracey I & Manyth PW. (2007). The cerebral signature for pain perception and its modulation. Neuron 55(3):377-91.

22.Dai W, Garcia D, de Bazelaire C, Aslop DC. (2008). Continuous flow-driven inversion for arterial spin labelling using pulsed radio frequency and gradient fields. Magn Reson Med. 60(6):1488-97.

23.Cervero F, Handwerker HO, Laird JM. (1988). Prolonged noxious mechanical stimulation of the rat's tail: responses and encoding properties of dorsal horn neurones. J Physiol. 404:419-36.

24.Woolf C. J. & King A. E. (1987) Physiology and morphology of multireceptive neurons with C-afferent fiber inputs in the deep dorsal horn of the rat lumbar spinal cord. J Neurophysiology 58(3):460-79.

25.Andrew, D. & Greenspan, J.D. (1999). Peripheral coding of tonic mechanical cutaneous pain: comparison of nociceptor activity in rat and human psychophysics. J Neurophysiol. 82(5):2641-8.

26. Smith SM, Jenkinson M, Woolrich MW, Beckmann CF, Behrens TE, Johansen-Berg H, Bannister PR, De Luca M, Drobnjak I, FLitney DE, Niazy RK, Saunders J, Vickers J, Zhang Y, De Stefano N, Brady JM, Matthews PM. (2004). Advances in functional and structural MRI image analysis and implementation as FSL. Neuroimage 23(Supp1):S208-19.

27.Smith SM. (2002). Fast robust automated brain extraction. Human Brain Mapp. 17(3):143-55.

28.Jenkinson M, Bannister P, Brady M, Smith S. (2002). Improved optimization for the robust and accurate linear registration and motion correction of brain images. Neuroimage 17(2):825-41

29. Kelly RE Jr, Alexopoulos GS, Wang Z, Gunning FM, Murphy CF, Morimoto SS, Kanellopoulos D, Jia Z, Lim KO, Hoptman MJ. (2010). Visual inspection of independent components: defining a procedure for artifact removal from fMRI data. J Neuroscience Methods. 189(2):233-45.

30. Apkarian AV, Bushnell MC, Treede RD, Zubieta JK. (2005). Human brain mechanisms of pain perception and regulation in health and disease. Eur J Pain. 9(4):463-84.

31.Peyron R, Laurent B, Garcia-Larrea L. (2000). Functional imaging of brain responses to pain: A review and meta-analysis (2000). Neurophysiol Clin. 30(5):263-88.

32.Apkarian AV. (1995). Functional imaging of pain: new insights regarding the role of the cerebral cortex in human pain perception. Semin Neurosci. 7:279-293.

33.Svensson P, Graven-Nielsen T, Matre D, Arendt-Nielsen L. (1998). Experimental muscle pain does not cause long-lasting increases in resting electromyographic activity. Muscle & Nerve 21(11):1382-1389

34. Iadarola MJ, Max MB, Berman KF, Byas-Smith MG, Coghill RC, Gracely RH, Bennett GJ. (1995). Unilateral decrease in thalamic activity observed with positron emission tomography in patients with chronic neuropathic pain. Pain 63(1):55-64.

35.Buchel C, Bornhovd K, Quante M, Glauche V, Bromm B, Weiller C. (2002). Dissociable neural responses related to pain intensity, stimulus intensity, and

stimulus awareness within the anterior cingulate cortex: a parametric single-trial laser functional magnetic resonance imaging study. J Neuroscience 22(3): 970-6.

36.Bornhovd K, Quante M, Glauche V, Bromm B, Weiller C, Buchel C. (2002). Painful stimuli evoke different stimulus-response functions in the amygdala, prefrontal, insula, and somatosensory cortex: a single-trial fMRI study. Brain 125(Pt 6):1326-36.

37.Coghill RC, Sang CN, Maisog JMA, Iadarola J. (1999). Pain intensity processing within the human brain: A bilateral, distributed mechanism. J Neurophysiol 82(4):1934-43.

38.Derbyshire SWG, Jones AKP (1998). Cerebral responses to a continual tonic pain stimulus measured using positron emission tomography. Pain 76: 127-135.

39.Kim T, Kim SG. (2011). Temporal dynamics and spatial specificity of arterial and venous blood volume changes during visual stimulation: implication for BOLD quantification. J Cereb Blood Flow Metab. 31(5):1211-22.

40.Goense JB & Logothetis NK. (2008). Neurophysiology of the BOLD fMRI signal in awake monkeys. Curr Biol. 18(9):631-40.

41. Xie, J. Segerdahl, A,R., Tracey, I., Jezzard P. Simultaneous functional and quantitative ASL: an optimal tool for imaging ongoing pain states. ISMRM Abstract, 2011. Montreal Congress.

Chapter 5

Simultaneous acquisition of relative and absolute CBF changes across a whole-brain volume during tonic pain in healthy subjects

5.1 Introduction

As discussed in the previous chapter, pseudo-continuous arterial spin labelling (pCASL) is an optimised ASL approach that offers a strong alternative means of acquiring perfusion signals from across a whole brain without the inherent weaknesses of earlier ASL approaches (3,4). The results of Chapter 4 support the continued use of pCASL within a pain imaging context given its capacity to robustly resolve meaningful activation across a whole-brain volume during a tonic experimental pain experience.

However, while the results from the previous chapter are promising and suggest that pCASL is an optimal technique to image the brain during long blocks of continuous pain, work is still needed to strengthen the technique such that it is possible to quantify absolute perfusion changes related to tonic pain. By obtaining absolute perfusion it is possible to optimize both the temporal and spatial SNR (5), to bolster the reproducibility of the data observed (6); and explore more sophisticated analyses such as dynamic causal modeling (DCM) or psychophysiological interaction (PPI) analyses to interrogate how tonic-pain relevant regions are interacting to generate the experience of pain. At present, no ASL pain investigation has fully described the absolute perfusion profile of active brain regions during pain. The goal of this chapter is to optimize the pCASL sequence such it is possible to obtain absolute perfusion changes during an ongoing experimental pain state in healthy subjects.

5.1.2. Optimizing pCASL to measure absolute CBF

A key source of error in perfusion imaging is variability in the time between when arterial blood is tagged and when the signal is acquired. Fundamentally, all ASL experiments aim to acquire the maximal arterial signal within active cortical regions. To do this, one must ensure that the timing of the acquisition allows for the arterial signal to actually arrive within a region, while at the same time ensuring minimal delay such that the signal itself has not been depleted by T1 decay. When collecting whole brain datasets this becomes even more of any issue as arrival times will vary as the distance from the labelling plane increases with more superior-lying cortical structures.

In general, most ASL protocols employ a standard post-label delay (PLD) time of 1000ms. This value was derived from early ASL experiments looking at the shift in T1 decay of water in blood when it moves into tissue across the capillary bed. Here, Ye FQ et al. (1996) showed that this transition typically occurs at 1s after the application of the tag (7, 8). In general, ASL experiments assume there to be a complete exchange of water between blood and tissue so employing a PLD = 1.0s ensures that one is observing an approximately maximum amount of cerebral signal before it is undermined by substantial T1-decay of blood (8,9,10).

However, this value does not take into account that the arrival time of arterial signal varies spatially across the cortex. For example, subcortical regions which rest very close to the labelling plane will be perfused with a maximum arterial

signal at earlier time points relative to cortical structures which take more time to perfuse. Early studies by Buxton, R.B. et al. (1998) modelled these effects by showing that as the arrival time of tag to a region varies, so to does the amount of CBF signal observed: the earlier the arrival time, the earlier time point at which a maximum arterial signal is observed in that region (9).

Recent advances in pulse-sequence programming make it possible to account for these effects by employing multiple inversion times to fully sample the perfusion signal changes occurring over time across the whole brain. This approach makes it possible to resolve the maximal perfusion signal across disparate brain regions regardless of differences in the arrival time of tagged arterial blood. Additionally, because multiple TI's are sampled, it is also possible to generate absolute values of CBF changes occurring at baseline and during an experimental task without the need for multiple repeat scans (11).

As such, the standard pCASL approach is undermined by two key weaknesses: i) utilization of a single TI introduces systematic error to the data because assumptions must be made about when the maximal arterial signal exists in a region; ii) implementation of multiple TI's within the present approach restricts imaging of absolute perfusion to a single slice thereby making full characterization of absolute CBF across a whole brain very time consuming.

The present investigation introduces a novel pCASL approach that makes it possible to ameliorate these weaknesses. Specifically, we introduce a multi-TI

pCASL method that obtains full quantification across the whole brain in a single scan. Here, a TI schedule optimized with a range of post-labelling delay (PLD) times for both subcortical and cortical regions is integrated into the pCASL sequence. Novel analysis methods are also discussed that ensures accurate modeling of perfusion changes without significant loss in temporal resolution. We show how this novel pCASL approach can be used to fully quantify CBF such that pure perfusion contrast can be used to investigate changes in brain states across different experimental paradigms.

We investigated the utility of this approach to obtain meaningful CBF changes (both relative and absolute) across a whole brain by employing two different experimental paradigms targeting different sensory systems that span the whole brain. The first paradigm was a standard combined visual/motor task aimed to engage the primary motor and visual cortices. The second paradigm utilized a tonic mechanical pain stimulus to activate key sub/cortical structures known to underlie pain processing.

The aims of this study are to: i) demonstrate the utility of this model for imaging absolute CBF changes relative to different sensory experiences likely to engage various subcortical and cortical structures; ii) investigate what the dynamic changes in CBF are over time for the different regions recruited for each task; iii) compare the CBF dynamics between different active regions to infer how changes in CBF over time may differ between regions based on the nature of the stimulus applied.

5.2 Methods

Experiments were performed on 12 healthy subjects (2 female; right handed; age: 18-40yrs). Subjects were asked to partake in two experiments: i) a combined motor-visual task (no pain stimuli present); ii) a tonic mechanical pain paradigm, whilst being scanned in a Siemens 3T Verio scanner. No one was on medication likely to interfere with the pain responsiveness. All subjects gave informed consent and the Oxfordshire Clinical Ethics Committee approved this study. To note, two subjects did not participate in the visual/motor paradigm because of time constraints related to a technical error.

Experimental paradigm

For both sessions, subjects participated in a block design paradigm that consisted of four repeat blocks of either stimulus ON or stimulus OFF. Each block was 2 minutes long. The difference between the experiments however was the type of stimulus used during the ON blocks.

Stimuli

I) Combined visual/motor experiment.

Subjects were asked to perform simultaneous visual (8Hz flashing checkerboard) and motor (finger-tapping) tasks whilst being scanned. The paradigm consisted of 4 cycles of 2 minute ON (8Hz flashing checkerboard; combined with a finger

tapping task) and 2 minute OFF (baseline; subjects were asked to remain awake with their eyes closed) blocks.

II) Pain experiment.

Mechanical probes (MRC, Germany) calibrated to give a constant force (512mN) were applied to the skin separating the thumb and first finger for a period of 2 minutes (ON block). Mechanical stimuli were applied to the hand by placing the probe into a stabilising apparatus that securely held the device at a constant force on the stimulus site for the duration of the stimulus block. During the stimulus, subjects were asked to keep their eyes closed and to focus on the stimulation being received. To note, a 30-sec stimulus-rating phase preceded the 2-min scan block to allow for an accurate verbal pain rating to be acquired. A second verbal rating was taken immediately after the last imaging volume was acquired. Verbal pain scores were then averaged to generate an overall pain rating for each stimulus block scanned. This was done to protect the pain imaging from potential cognitive confounds associated with rating continuously throughout the FMRI acquisition.

A 2-minute rest block (no stimulus present) was observed after each stimulus block. Here, subjects were asked to maintain the position of their hand but in the absence of a stimulus probe. To note, commencement of each REST block was reliant on the subject reporting no pain after the probe was removed.

MR Parameters

All subjects were scanned with a pseudo-continuous ASL sequence (12) using gradient-echo EPI readout (TR=3.75s, TE=13ms, 6/8 k-space). Twenty-six axial slices in ascending order (3 x 3 x 4.5 mm voxels, 0.5 mm inter-slice gap) were prescribed for each subject, providing whole brain coverage (including brainstem and cerebellum). The labelling plane was chosen optimally for each subject based on a time-of-flight scan of the neck, located ~8-10 cm inferior to the centre of the 26 slices. A 90° pre-saturation pulse was applied before the labelling pulses. The labelling duration was 1.4s and five different post labelling delay (PLD) times were adopted. The five PLD values, [0.64s, 0.792s, 0.896s, 1s, 1.152s], were generated according to Optimal Sampling Schedule theory (13). PLD times were pseudo-randomised per TR. The same order was applied to every Subject. 16 PLD values were applied per each two-minute stimulus block. Volunteers were scanned using a Siemens 3T Verio system fitted with a 32-channel head coil.

Data analysis

I. Absolute quantification of CBF values

Parameters of interest (CBF and arrival time, Δt) were fitted from every five contiguous TI data points (a sliding 5-point time window) using BASIL, a novel ASL data analysis tool using Bayesian inference (14). Both the equilibrium magnetization of blood at 3T and the sensitivity profile of the 32-channel head coil were calibrated. The absolute CBF time series were then used as inputs in

the first level GLM analysis in FEAT. The GLM models we adopted are described in detail in below.

II. FEAT analysis

Absolute CBF time courses at different functional states were temporally concatenated off-line and analysed using the FMRIB Software Library (FSL) (15). Data were brain extracted, motion corrected, tag-control subtracted, followed by spatial smoothing (FWHM 5mm). A high-pass filter (cutoff at 1/240s) was applied (16,17).

Each subject's dataset was registered first to the subject's high resolution structural using FLIRT linear registration. Then the subject's high resolution structural was registered to the MNI152 standard space using FNIRT non-linear registration. At the group level, a mixed effects analysis incorporating both within and across subjects variance was used to obtain group mean activation maps for the main effect of each stimulus condition on changes in CBF across the whole brain. Cluster-based thresholding was used to find clusters of CBF changes showing effects with a significance level of $p<0.05$, using a z-score cut-off of 2.3 to generate clusters.

III. GLM models

(1) Block Design

In both analyses, individual subject's absolute perfusion time series were used as first level inputs. Each voxel was fit to a model of the 2-min block design to yield a resultant parameter estimate (PE) image that was proportional to localised blood flow related to each stimulus condition. To determine the percent

signal change in CBF relative to the stimulus ON condition, a model of ON > OFF was included into the first level model.

(2) Modelling habituation

As with the block design, individual subject's absolute perfusion time series were used as first level inputs. To model across-block habituation, each stimulus block was individually modelled with a separate regressor such that it was possible to observe the contrast of the first stimulus block > the final stimulus block. The resultant PE image was therefore proportional to localised blood flow related to habituation of perfusion signal across repeated stimulus blocks.

(3) Correlation with individual pain perception

To investigate the relationship between subjective pain report and absolute CBF changes, each subject's perfusion data was fit to a regressor reflective of that subject's pain intensity ratings over the course of the experiment. The resultant PE image was therefore proportional to localised blood flow related to the subjective report of pain intensity.

IV. Region of interest (ROI) investigation of CBF time courses

To further examine the dynamic time courses of CBF changes from key active regions during the experiment, we extracted the absolute CBF time courses from relevant ROIs for each stimulus condition. ROIs were defined by anatomically specific functional-masks generated from the main effect contrast map of stimulus ON>OFF (Mixed Effects; $z>2.3$, $p<0.05$). Each significantly active region defined a ROI for extraction of time course data. Absolute CBF was only

extracted from a volume that contained voxels that showed increased activity within a sphere of 8 mm radius around the voxel with peak activity. This spherical volume was anatomically corrected using the Harvard-Oxford Atlas of cortical structures in FSL. Additionally, these masks were partial volume corrected so that absolute CBF was extracted only from voxels pertaining to grey matter tissue. Individual subject's time courses for each ROI were averaged to obtain group mean absolute CBF time courses for each stimulus condition. Regions observed included: Bilateral insular cortex (anterior and posterior divisions), amygdala, putamen, anterior cingulate cortex, SII, and the contralateral SI.

Psychophsyiological interaction (PPI) analysis

To interrogate whether there is a correlation in activity between different brain areas during the across-block habituation in which regions recruited during pain appear to be less active by the last stimulus block of the paradigm, we carried out the following PPI analysis.

In PPI analysis I, we defined the seed region to be the left posterior insula: a region known to play a role in sensory-discriminative aspects of pain processing. In PPI analysis II, we defined the seed region to the right dorsal medial prefrontal cortex (DMPFC): a higher order frontal region known to play a role in self-reflective processing and monitoring of the self (45,46,47,48).

For both analyses, the following regressors were used: i) a regressor that modelled the shape in activation between pain and control blocks (psychological regressor); ii) a regressor constituent of the extracted time course from the seed region of interest (physiological regressor); iii) a regressor modelling the

interaction between the physiological and psychological regressors; iv) a regressor of no interest modelling the main effect of the pain versus rest condition.

Each voxel was fit to model the interaction between the physiological (EV1) and psychological (EV2) regressors to yield a resultant PE image that reflects the correlation in activity between the seed region and any other region when CBF changes are greater during the first versus the final stimulus blocks.

5.3 Results

5.3.1. Psychophysics

Figure 1a shows the mean pain intensity rating for the mechanical stimulus condition used in this study. The mean pain intensity rating for the paradigm was 4.31 (s.e. = 0.128). The mean unpleasantness rating was 4.29 (s.e. = 0.058). There was a significant increase in pain intensity (Student t-test, $p<0.001$) and unpleasantness (Student t-test, $p<0.001$) for the stimulus condition used compared to rest. There was no significant change in pain intensity rating over the course of repeated pain blocks.

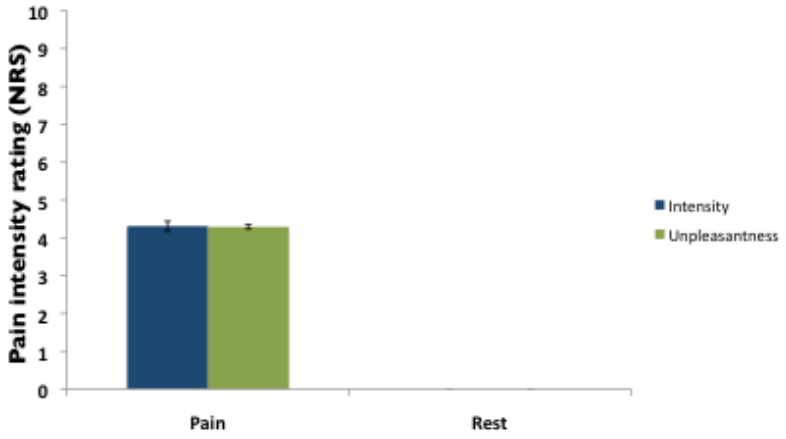

Figure 1a: Psychophysical data. Verbally reported pain intensity (blue) and unpleasantness (green) ratings averaged over consecutive two-minute blocks of mechanical pain. Error bars represent standard error of the mean (SEM).

5.3.2. Perfusion imaging data

i) Relative CBF changes

Significant changes in CBF during the stimulus ON condition versus OFF are shown in Figure 2 (**a**: pain; **b**: combined visual/motor). Coloured regions represent voxels with suprathreshold t-statistics generated from the group-level FEAT analysis. For the motor/visual stimulus, significant increases in CBF occurred in both the motor and visual cortices. For the pain stimulus, significant increases in CBF occurred in many regions shown previously to be involved in processing acute (18,19) and phasic (ASL: 20,21,22; PET: 23,24,25,26,27,28,29,30) pain. These include: contralateral SI, thalamus, cingulate cortex (anterior division), superior frontal gyrus; and bilateral SII, insula (posterior and anterior divisions), putamen, and amygdala. All coordinates are given in MNI space.

a)

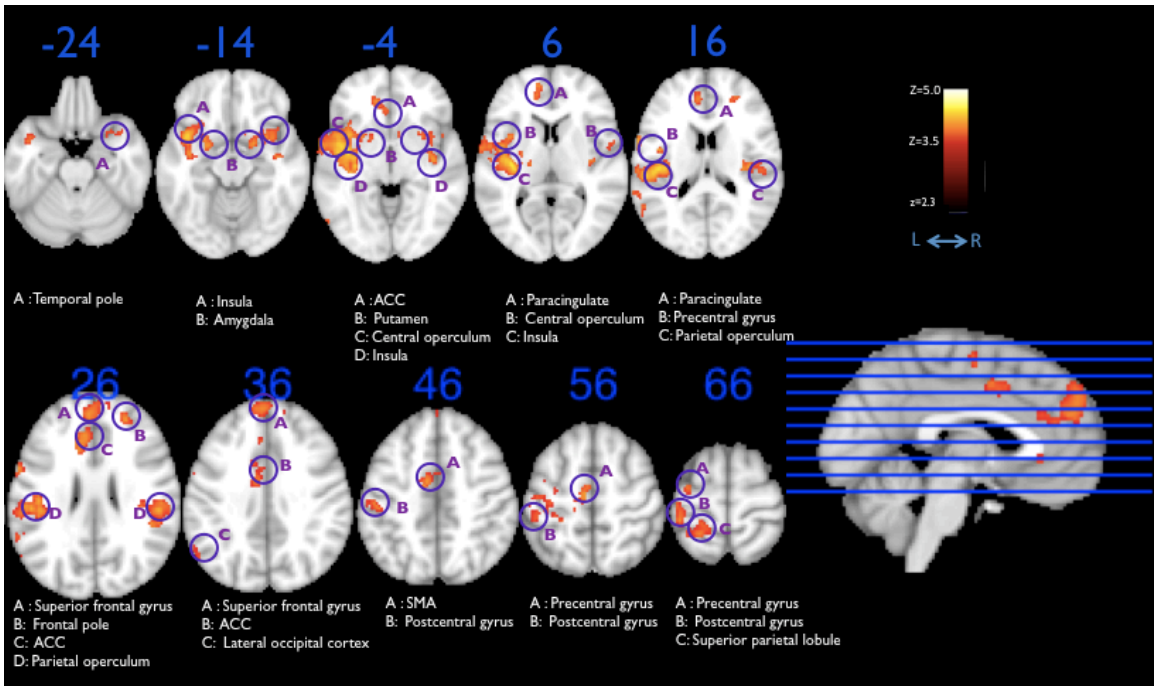

Figure 2: a) Brain perfusion data from the mechanical-induced pain acquired with the multi-TI whole brain pCASL sequence. Averaged zstat maps (n=12) of perfusion activation superimposed on the MNI152 standard template brain (Mixed Effects, cluster corrected; z:2.3-5.0, p<0.05). Perfusion maps represent the contrast of pain stimulus ON > pain stimulus OFF. The sagittal slice shows the column of activation across the whole brain. Axial slices (one slice every 10mm in ascending order) correspond to the plane indicated in the sagittal slice.

b)

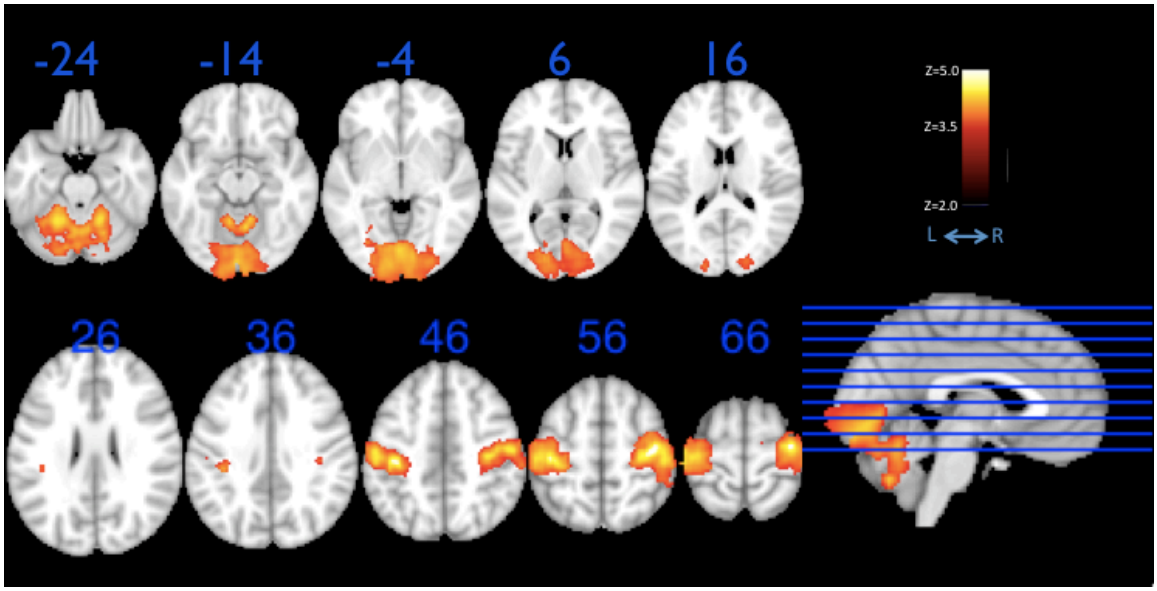

Figure 2: b) Brain perfusion data from the combined visual/motor stimulus paradigm acquired with the multi-TI whole brain pCASL sequence. Averaged zstat maps (n=10) of perfusion activation superimposed on the MNI152 standard template brain (Mixed Effects, cluster corrected; z:2.3-5.0, p<0.05). Perfusion maps represent the contrast of motor/visual stimulus ON > stimulus OFF. The sagittal slice shows the column of activation across the whole brain. Axial slices (one slice every 10mm in ascending order) correspond to the plane indicated in the sagittal slice.

% CBF changes

In Table I, the mean values and the related percent signal changes for the different stimulus blocks are shown. We observed a significant increase in percent CBF during the stimulus ON versus OFF blocks, regardless of stimulus modality (*Student t-test, p<0.05). Visual/motor stimulus yields substantially larger percent signal change in CBF compared to pain. There was evidence for habituation across repeated stimulus blocks as there was a significant difference in the percent CBF change during stimulus block 1 versus block 4 (the final block).

a)

REGION	Off1	On1	Block 1 (% change)	Off2	On2	Block 2 (% change)	Off3	ON3	Block 3 (% change)	Off4	On4	Block 4 (% change)
L_ant_ins	72.32	81.9	13.33	75.18	82.64	9.9	75.25	77.33	2.76	76	74.44	-2.05
R_ant_ins	68.64	75.12	9.44	73.52	77.11	4.88	69.45	72.63	4.58	69.18	67.72	-2.11
L_post_ins	77.72	69.56	11.73	69.93	78.42	12.14	71.65	73.84	3.06	71.34	70.19	-1.61
R_post_ins	66.78	73.36	9.85	69.16	75.08	8.56	67.37	71.87	6.68	69.94	66.21	-5.33
L_ACC	73.75	77.45	5.02	73.98	77.49	4.74	73.89	74.03	0.12	70.62	70.02	-0.85
R_ACC	77.58	80.89	4.27	77.17	82.12	6.41	77.57	77.95	0.49	74.54	74.22	-0.43
L_SII	89.79	94.02	4.71	82.84	90.98	9.83	85.8	86.54	0.85	80.51	85	5.58
R_SII	79.4	83.75	5.48	72.73	82.28	13.13	73.37	74.25	1.2	74.25	74.95	0.94
R_thalamus	73.73	81.58	10.65	77.98	75.21	-3.55	73.26	68.54	-6.44	75.24	75.34	0.13
L_amygdala	75.09	80.09	6.67	75.67	81.49	7.69	79.28	78.99	0.36	76.87	75.0579	-2.35
R_amygdala	72.98	78.2695	7.25	75.56	77.64	2.75	75.88	78.057	2.86	73.76	70.57	-4.32

b)

REGION	Off1	On1	Block 1 (% change)	Off2	On2	Block 2 (% change)	Off3	ON3	Block 3 (% change)	Off4	On4	Block 4 (% change)
V1	77.92	100.99	29.61	74.92	93.02	24.16	73.75	93.15	26.31	79.16	88.76	12.13
L_M1	66.25	87.76	32.47	63.11	87.68	38.93	64.6	82.58	27.83	67.62	78.87	16.64
R_M1	65.26	86.28	32.21	62.6	84.92	35.65	66.21	87.2	31.7	66.74	80.66	20.86

Table 1: Mean absolute CBF signal values for each stimulus block (a: pain paradigm; b: motor/visual paradigm). Absolute CBF values were extracted from key ROIs defined by the main effect of stimulus ON > OFF analysis. Percent CBF values (highlighted) represent the relative change in perfusion during the stimulus compared to the OFF condition. Absolute CBF values are in units of ml blood/ 100g tissue/ 60 sec.

Dynamic CBF time courses

Results from the contrast of pain > control show widespread activation across multiple sub-cortical and cortical regions. To observe how each active region's stimulus response differs over time, time courses for key ROIs were extracted from the following regions: bilateral insula (anterior and posterior divisions),

rostral anterior cingluate cortex, SII, and the thalamus. Group mean changes in absolute CBF over the 2-minute stimulus blocks were plotted over time (Figure 3). Error bars represent standard error of the mean.

a)

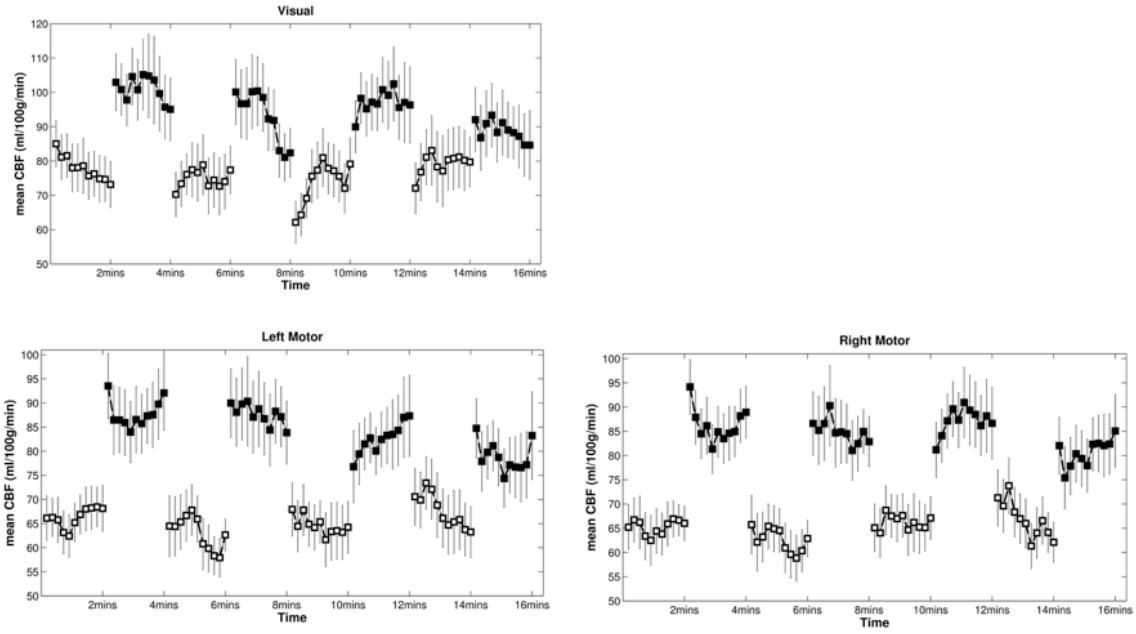

Figure 3a. Dynamic CBF time courses from the combined visual/motor task. Group mean time courses key ROIs defined by the contrast of stimulus ON > OFF. Non-coloured data define absolute CBF during the OFF blocks (no stimulus present) versus the coloured data points showing absolute CBF values during the presence of the stimulus. Unless otherwise specified, time courses on the left correspond to the left (contralateral) anatomical region.

b)

Anterior Insular Cortex:

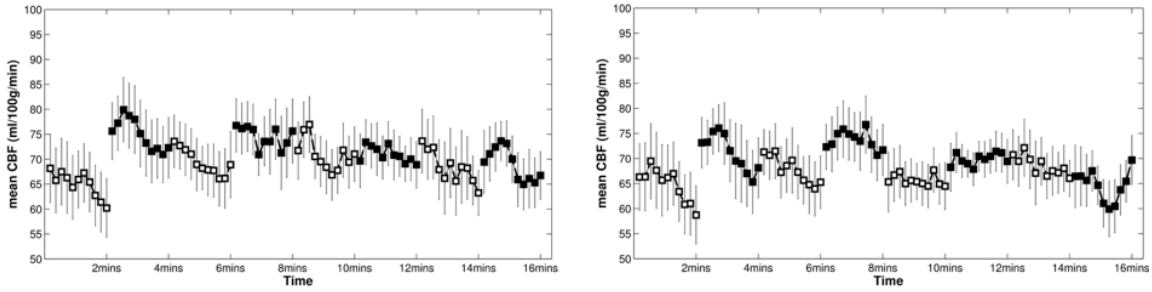

c)

Posterior Insular Cortex:

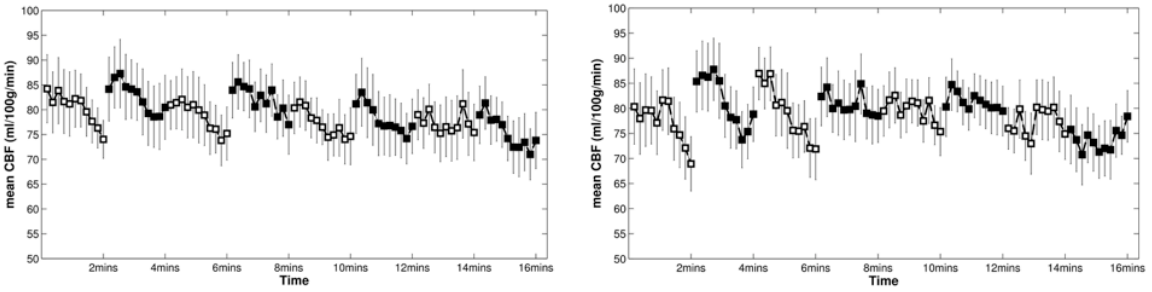

Figure 3b-c. Dynamic CBF time courses during pain. Group mean time courses extracted from key anatomical ROIs defined by the contrast of stimulus ON > OFF. Non-coloured data define absolute CBF during the OFF blocks (no stimulus present) versus the coloured data points showing absolute CBF values during the presence of the stimulus. Unless otherwise specified, time courses on the left correspond to the left (contralateral) anatomical region. The following ROIs are shown above: b) anterior insula; c) posterior insula. Error bars represent the standard error of the mean (SEM).

d)

Rostral Anterior Cingulate Cortex:

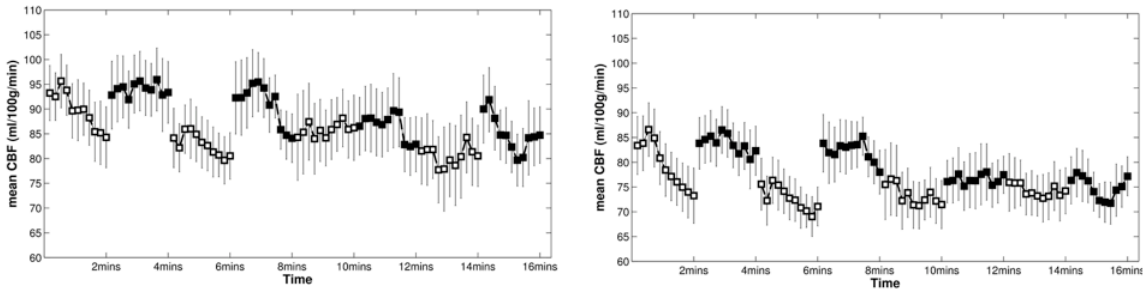

e)

Secondary Somatosensory Cortex:

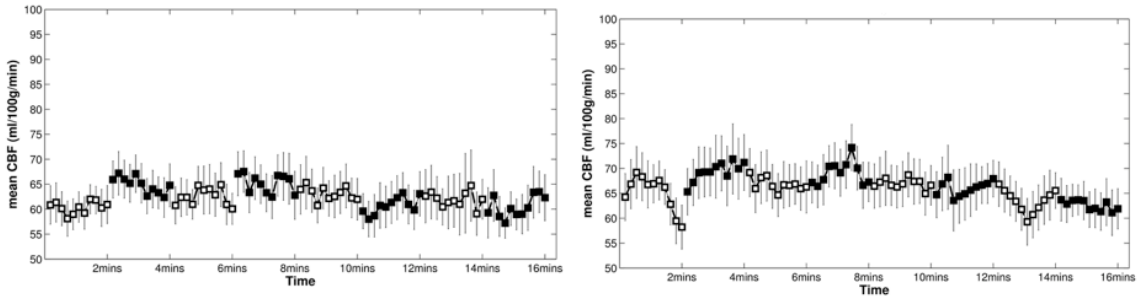

Figure 3d-e. Dynamic CBF time courses (a: combined visual/motor; b-j: pain). Group mean time courses extracted from key anatomical ROIs defined by the contrast of stimulus ON > OFF. Non-coloured data define absolute CBF during the OFF blocks (no stimulus present) versus the coloured data points showing absolute CBF values during the presence of the stimulus. Unless otherwise specified, time courses on the left correspond to the left (contralateral) anatomical region. The following ROIs are shown above: d) rostral anterior cingulate; e) secondary somatosensory cortex (SII). Error bars represent the standard error of the mean (SEM).

f)

Thalamus:

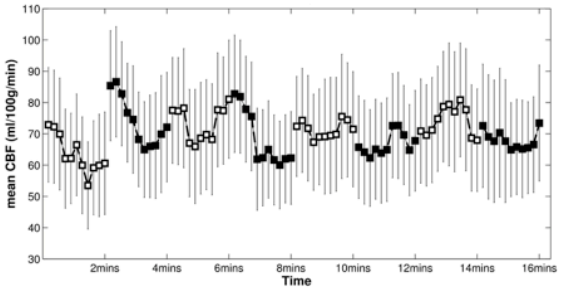

g)

Amygdala:

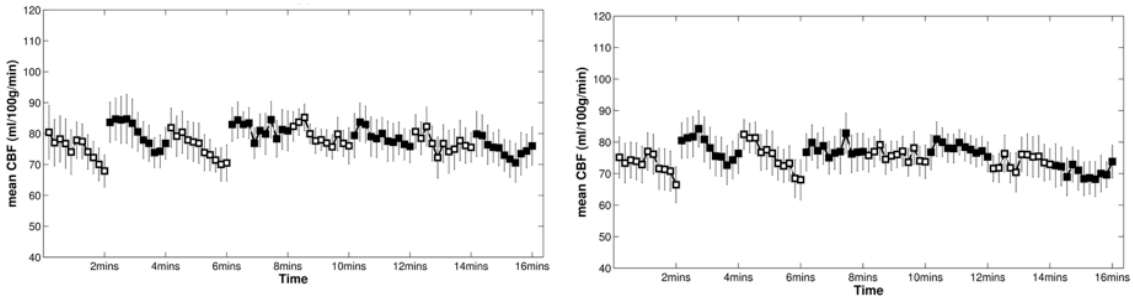

Figure 3f-g. Dynamic CBF time courses (a: combined visual/motor; b-j: pain). Group mean time courses extracted from key anatomical ROIs defined by the contrast of stimulus ON > OFF. Non-coloured data define absolute CBF during the OFF blocks (no stimulus present) versus the coloured data points showing absolute CBF values during the presence of the stimulus. Unless otherwise specified, time courses on the left correspond to the left (contralateral) anatomical region. The following ROIs are shown above: f) thalamus; g) amygdala. Error bars represent the standard error of the mean (SEM).

iii) Correlation with pain intensity ratings

Regions that showed significant correlation between CBF and pain intensity rating during the ON condition are shown in Figure 4. Coloured regions represent voxels with suprathreshold t-statistics generated from the group-level FEAT analysis in which pain intensity was a regressor of interest. Regions that show a significant correlation between pain-related increases in CBF and subjective reports of pain intensity include: contralateral dorsal medial prefrontal cortex (DMPFC), SI, SII, rostral ACC; and bilateral supramarginal gyrus and insula (anterior and posterior divisions).

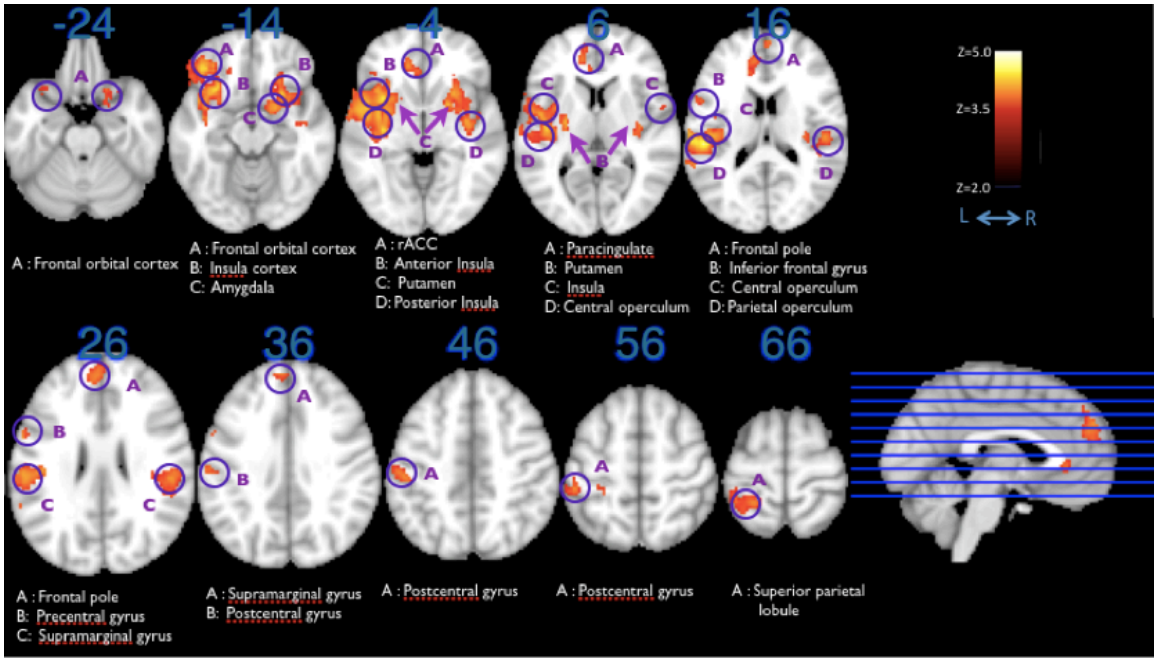

Figure 4: Correlation of CBF changes with pain intensity ratings. Statistical maps represent group mean absolute perfusion changes during pain that correlate with pain intensity reports over the course of the paradigm. Averaged zstat maps (n=12) of perfusion correlated with pain intensity ratings are superimposed on the MNI152 standard template brain (Mixed Effects, cluster corrected; z:2.3-5.0, $p<0.05$). The sagittal slice shows the column of activation across the whole brain. Axial slices (one slice every 10mm in ascending order) correspond to the plane indicated in the sagittal slice.

ii) Effects of habituation

Figure 5 displays the effect of habituation over the course of the tonic stimulus blocks. In Figure 5a, the across-block habituation is shown for the pain stimulus. Significant habituation was visible across various regions when comparing the first to the last stimulus block. These include: contralateral posterior insula, paracingulate, central operculum, bilateral parietal operculum and superior frontal gyrus. In Figure 5b, the across-block habituation is shown for the combined visual/motor stimulus. Significant habituation is observed within both the visual and motor cortex over the course of the stimulus paradigm.

a)

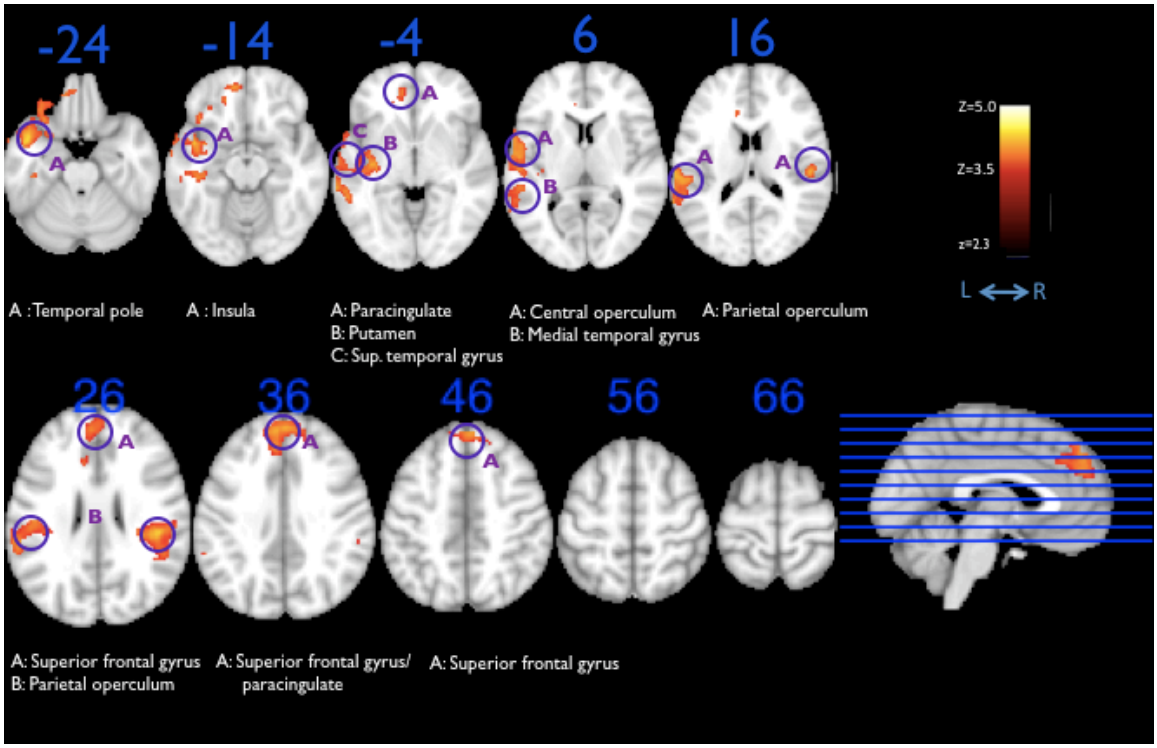

Figure 5: Habituation effects during pain. Statistical maps represent group mean absolute perfusion changes during pain that correlate with a model for across-block habituation during the pain paradigm. Averaged zstat maps (n=12) of perfusion correlated with habituation effects are superimposed on the MNI152 standard template brain (Mixed Effects, cluster corrected; z:2.3-5.0, p<0.05). The sagittal slice shows the

column of activation across the whole brain. Axial slices (one slice every 10mm in ascending order) correspond to the plane indicated in the sagittal slice.

b)

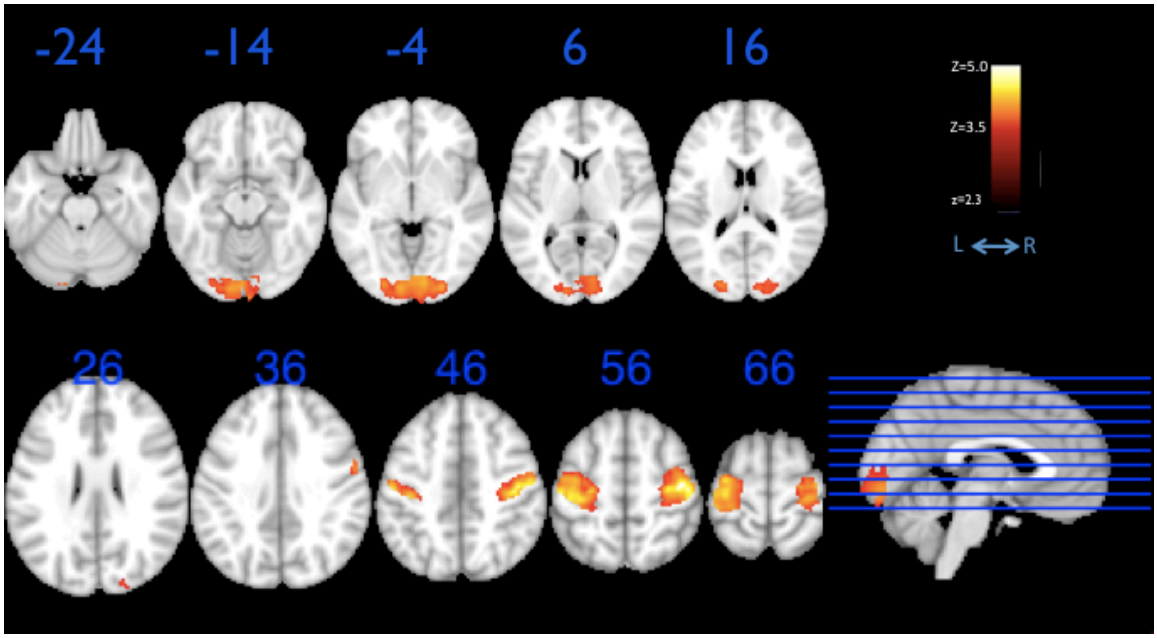

Figure 5: Habituation effects during the combined visual/motor task. Statistical maps represent group mean absolute perfusion changes during visual/motor paradigm that correlate with a model for the across-block habituation within the visual/motor cortices. Averaged zstat maps (n=12) of perfusion correlated with habituation effects are superimposed on the MNI152 standard template brain (Mixed Effects, cluster corrected; z:2.3-5.0, $p<0.05$). The sagittal slice shows the column of activation across the whole brain. Axial slices (one slice every 10mm in ascending order) correspond to the plane indicated in the sagittal slice.

Psychophysiological interaction analysis

To interrogate how pain-relevant regions are functionally interacting over the course of the pain paradigm, we carried out a PPI analysis (31). PPI analyses reveal changes in functional connectivity between brain areas related to changes in a psychological variable. In the current setting, the psychological variable was the type of shift in pain responsiveness experienced (habituation vs. sensitisation) across the stimulus blocks. When investigating across-block habituation (PPI analysis I), regions such as the thalamus, insula, posterior cingulate, and precuneus significantly correlate with activity in the posterior insula (Figure 6a). In contrast, when investigating across-block sensitisaiton (PPI analysis II), regions such as the ACC, medial and superior frontal gyrus, DLPFC, and SI correlate with that observed in the dorsal medial prefrontal cortex (figure 6b). To note, no regions showed a significant correlation with the posterior insula when modelling the effect of across-block sensitisation. Likewise, no regions showed a significant correlation with the dorsal medial prefrontal cortex when modelling the effect of across-block habituation.

i) Seed region: Posterior insular cortex

a)

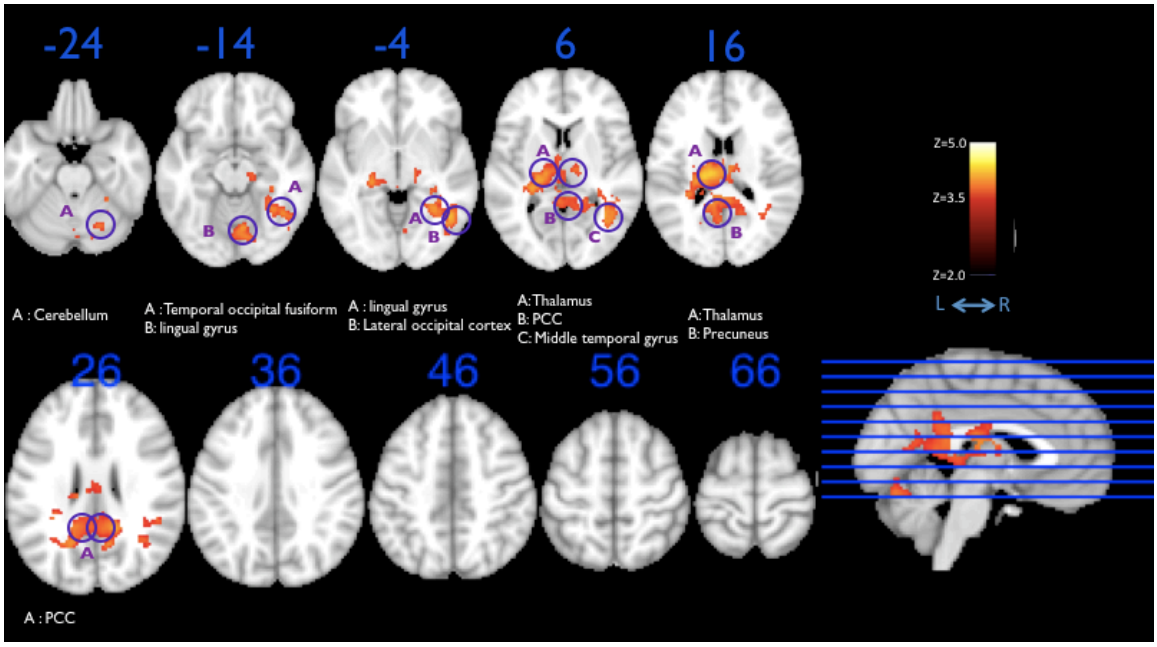

Figure 6: Psychophysiological interaction I. Statistical maps represent group mean absolute perfusion changes that correlate with perfusion changes within key seed regions of interest (a: posterior insular cortex) when modelling the across-block habituation in activation. Averaged zstat maps (n=12) of perfusion correlated with habituation effects are superimposed on the MNI152 standard template brain (Mixed Effects, cluster corrected; z:2.3-5.0, $p<0.05$). The sagittal slice shows the column of activation across the whole brain. Axial slices (one slice every 10mm in ascending order) correspond to the plane indicated in the sagittal slice.

ii) Seed region: Dorsal medial prefrontal cortex

b)

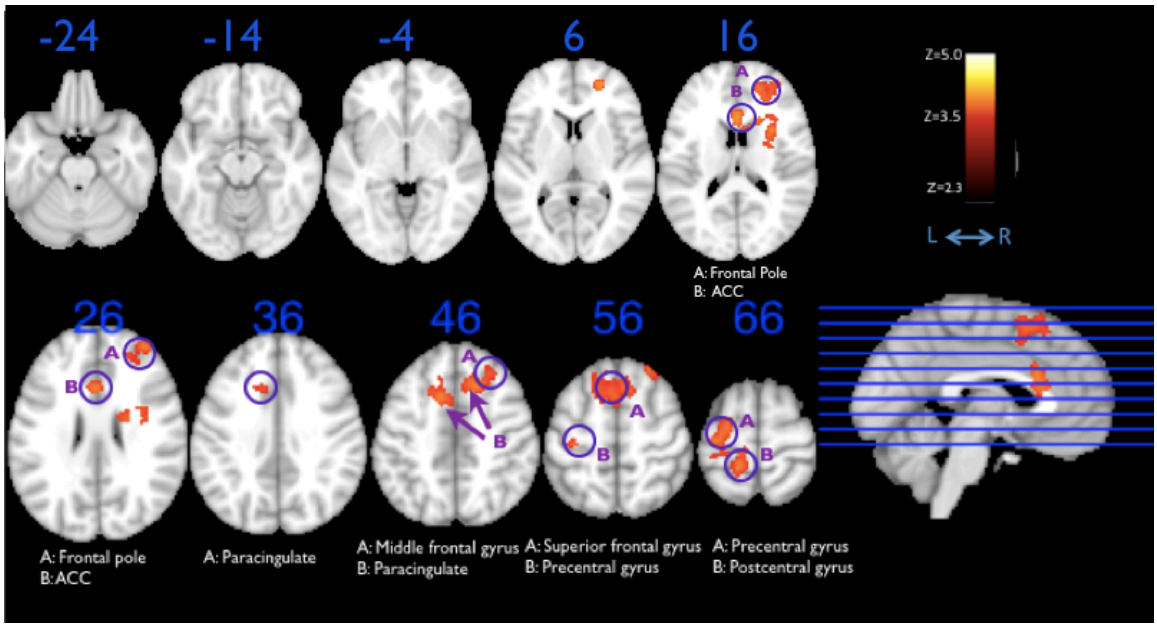

Figure 6: Psychophysiological interaction II. Statistical maps represent group mean absolute perfusion changes that correlate with perfusion changes within key seed regions of interest (b: dorsal medial prefrontal cortex (DMPFC)) when modelling the across-block sensitisation in activation. Averaged zstat maps (n=12) of perfusion correlated with habituation effects are superimposed on the MNI152 standard template brain (Mixed Effects, cluster corrected; z:2.3-5.0, $p<0.05$). The sagittal slice shows the column of activation across the whole brain. Axial slices (one slice every 10mm in ascending order) correspond to the plane indicated in the sagittal slice.

5.4 Discussion

The aims of this investigation were to: i) demonstrate the acquisition of both relative and absolute CBF changes across a whole brain related to different sensory stimuli by employing a novel multi-TI pCASL approach; ii) observe and compare the dynamic CBF time courses across different regions recruited for each sensory task.

Our data confirm that it is possible to obtain robust and reliable functional and absolute perfusion data from across a whole brain using a multi-TI pCASL sequence.

Key findings

1) Using this technique, we show many regions previously known to be active with acute pain stimuli, are also active during tonic pain stimuli. 2) Percent CBF changes reveal relatively small overall changes compared to visual/motor stimulus paradigms. 3) Investigation of the dynamic stimulus responses do not show constant, non-fluctuating responses even though the subjects report the presence of a constant, ongoing pain experience. Instead, time courses extracted from key pain regions reveal fluctuating, non-uniform responses over time that appear to change with repeat stimuli. 4) Employing regressors that model gradual changes in stimulus responses over time (e.g. habituation vs recruitment) suggest a dynamic interplay between cortical regions over the course of the overall experience.

Active ROIs

The data from both experiments shows robust activation in expected anatomical locations for each task. For example, the combined visual/motor task elicits

strong activation in both the motor and visual cortices. In contrast, the pain data shows the activation of regions previously characterised from acute BOLD FMRI studies well known to play key roles in pain processing. Regions such as SI, SII, ACC, anterior and posterior insula, thalamus are all well documented to underlie various aspects of the pain experience (18,19). However, this is one of only a few studies that have successfully shown these regions are continually active during an ongoing pain state (20,21,22). To add, our data also confirm that regions such as the contralateral SI, SII, rACC; and bilateral insula (anterior and posterior divisions), putamen and the supramarginal gyrus show significant correlation with pain intensity rating during the ongoing pain condition (19, 23,28,32,33,34,35).

Extent of activation

There is considerable variation in the extent and duration of CBF changes across different cortical regions as reported by previous ASL studies. While this could be due, in part, to different ASL methodologies employed, we still do not yet know to what extent a given region should be active over the course of a pain experience. From previous investigations of visual and motor paradigms, perfusion changes observed with ASL are approximately in the range of 35-50% for visual activation (36,37,38) versus 50-70% for motor activation (39,40). In contrast, of the few pain ASL studies in print, CBF changes for pain are in the range of 5-10% (20,21). In contrast, a more recent investigation of post-operative dental pain presented CBF changes in the range of 1-5% with pain (22). In general, our observations of both pain- and motor/visual-related perfusion changes align with our prediction that pain would elicit a small overall change in CBF compared to the non-painful task.

Because the overall experience of pain is constituent of various cognitive, emotional, and sensory aspects coded by a number of cortical regions, it is possible that only a small sub-population of a given ROI is necessary to code an aspect of the overall pain experience. It is not necessarily the case that the entire region is utilised to communicate an aspect of the overall experience but rather that a small subsection of neurones are. Here then, percent changes in CBF during pain could reflect the capacity for a number of regions to efficiently devote processing power to various functions without engaging the whole structure.

One could imagine where, in the context of a pain pathology, a region's multi-processing capacity is gradually usurped by the constancy of pain processing thereby undermining its capacity to execute other essential cortical functions. For example, regions may show significantly increased CBF demand thereby reflecting an increased recruitment of that structure specific to that particular pain pathology. This might be partially observable in future ASL imaging studies of chronic pain conditions in which key pain-relevant regions show altered CBF dynamics compared to healthy controls.

Dynamic CBF changes

Investigation of the CBF time courses reflects non-uniform, fluctuating changes over time across each ROI. To add, ROIs appear to have unique stimulus-responses over time; the overall magnitude of which appears to habituate with repeat stimuli. No one region observed appears to match another region's time course. This is contrary to our prediction that it would be possible to see a

constant, well-maintained increase in CBF that mirrored the pain experienced by subjects.

At present, we do not yet know if these complex perfusion dynamics reflect interesting neuronal signalling events (e.g. changes in signalling properties, altered connectivity, oscillation in dynamic flow of information within and between regions) or are specific to changes in neurovascular coupling over time with continued activation. It is possible that the data reflects both meaningful neuronal events related to the experience of the tonic pain and key neurovascular coupling events related to maintaining constant activation for long periods of time.

As discussed previously, ROIs are very likely to be efficiently capable of tasking aspects of processing pain to a subsection of neurones within the region. Additionally, it is likely that, with continued activation, that population of neurones within the region is also able to adapt its functional dynamics such that fewer overall neurones are needed to code that aspect of the experience if the experience continues unchangingly for the duration of the stimulus block. Only if there is a change in the stimulus would a larger population of neurones be recruited. This has been shown extensively in FMRI investigations of the visual (41), motor (42) and somatosensory (43) cortices. This would be expected to be reflected in the CBF demand for a region: while relatively large to begin with, as the active population adapts, less overall energy-demand would be reflected by a reduced CBF demand. At present, it is not well known how pain-relevant regions remain active over time and, relatedly, how continuous activation relates to changes in metabolism and consequently arterial demand and therefore, fluctuations in perfusion signal.

While it was not possible to fully explore the relationship between complex CBF dynamics and changes in neurovascular coupling within the current study, it was possible to begin to interrogate how these changes may reflect interesting cognitive events underlying changes in the experience of the tonic pain state. One way that we attempted to capture this shift in activation was to model the across-stimulus block shifts in activation (i.e. habituation) likely occurring when comparing the first to the final stimulus blocks. Here, various regions show significant habituation across the overall paradigm. To understand how some of the regions are functionally interacting during these across-block effects, we carried out a PPI analysis. Here, results from the PPI analysis I show that during the across-block habituation regions well known to code sensory-discriminative aspects of the pain (e.g. thalamus, PCC) show significant functional connectivity with the posterior insular cortex (44). In contrast, a separate PPI analysis (PPI analysis II) looking at regions showing a gradual recruitment in activation (i.e. regions that become increasingly more active in the last stimulus block compared to the first) show interesting coupling relationships. For example, regions such as the superior frontal gyrus, DLPFC, ACC, caudate, medial and superior frontal gyrus show significant functional connectivity with the seed region DMPFC; a region previously reported to be integral for social cognition, assessing one's external environment and the social cues (emotions, beliefs, judgements) of others (45, 46,47). These results are not entirely unsurprising given that the nature of the experience is likely to change over the course of the experimental session- some regions may be more essential to code an early phase of the experience whilst others are necessary at later stages. For example, the first

stimulus block is the most novel; therefore aspects such as the stimulus intensity, duration, unpleasantness are all new. During this phase, one will devote most of their attention towards exploring these aspects of the external stimuli. However, with repeated stimulation, this sensory information becomes redundant; therefore the need to explore it (i.e. devote attentional processing power to the external stimuli) is reduced. Instead, the bulk of processing is likely to shift one's attention inwards (i.e. conscious attention to one's internal state during the presence of the ongoing stimulus). This is nicely reflected in the across-block habituation data in which more sensory-descriminative regions (i.e. thalamus, insula) gradually reduce their activation whereas regions like the DMPFC in cunjunction with the ACC, medial and superior frontal gyrus gradually become more active.

5.5 Conclusion

In acute pain paradigms, factors related to complex perceptual shifts with time similar to what is presented in the current study are more or less accounted for by the nature of the very short stimulus. The shape of the pain experience mirrors that of the stimulus itself: a quick burst of activation that has a rapid on- and offset. Arguably, this type of stimulus engages the more evolutionarily well-conserved components of pain processing: that we are able to orient, detect and respond to the noxious input quickly with the primary goal of escaping the pain. In a tonic setting, much of the cortical processing of this early stimulus detection/ processing is overtaken by something more complex. For example, when the stimulus is ongoing and there is no possibility to escape it, one is primed to

endure the noxious insult. This invariably will engage a different set of cognitive processes. Additionally, as the tonic stimuli are repeated, these cognitive mechanisms are likely to change. For example, with repeated stimulation, the subject is already primed and aware of the stimulus onset, duration and intensity. As such, the threat-fear valence (i.e. the overall unpleasnantness) of the experience is gradually reduced. Which is to say that subjects gradually acclimate to and therefore psychologically adapt to the pain paradigm. It is possible that these across-block changes in activation reflect this. Currently, there is no way of fully explaining what these shifts in activation patterns mean as we did not utilise ongoing rating scales to try to monitor in real-time various aspects likely to change over the long stimulus blocks.

To add, in a clinical setting, this is exactly what fails to happen. Because the pain state itself is often spontaneous and fluctuating in nature, it is unpredictable and often unabated when present. In this way, the experience itself becomes much more difficult to acclimate to and therefore overcome its unpleasant nature. An obvious next step would be to develop tonic pain paradigms that approximate this kind of experience to more reliably reflect what people experience clinically. Additionally, it might also be useful to study specific types of subjects based not only on the nature of their ongoing pain pathology (i.e. neuropathic, ischemic, inflammatory,etc.) but also based on defining personality traits such as whether a subject has a strong sense of autonomy over their pain (e.g. locus of control); or differently, whether a person expresses no hope of ever being pain-free (e.g. helplessness). These factors may help better articulate how pain patient ‘groups’ have differentially active circuitry specific to their pain experience. Understanding why one group of chronic pain patients is more capable of

successfully ameliorating their pain compared to another group could reliably be done with this type of neuroimaging tool and would provide considerable insight towards development of novel pain therapies.

Overall, the data from this study support the use of a multi-TI pCASL approach to reliably quantify absolute perfusion changes occurring across a whole-brain volume during a tonic pain experience. Results from this experiment show complex stimulus-responses of key pain-relevant regions over time relative to a strong pain stimulus. The underlying cause for this complexity is likely to be related to: i) specific functional interactions between recruited regions; ii) variability in neurovasicular coupling dynamics; and iii) overall habituation to the experimental paradigm design. We are confident that utilisation of this optimised perfusion imaging approach will provide a reliable and robust means of observing CBF changes specific to both experimental and pathological pain states.

5.6 Appendix: Table of activation coordinates

1. Main effect of pain:

Cluster	zstat	MNI	Laterality	ROI
28	4.42	(68 52 43)	L	Central Operculum
28	4.3	(63 54 40)	L	Posterior Insula
28	4.29	(67 62 36)	L	Posterior Insula
28	4.27	(64 58 32)	L	Posterior Insula
28	4.21	(62 54 38)	L	Posterior Insula
28	4.16	(73 49 46)	L	Parietal Operculum
28	4.12	(64 60 33)	L	Posterior Insula
28	4.08	(65 55 40)	L	Posterior Insula
28	3.91	(65 55 37)	L	Posterior Insula
28	3.87	(61 56 33)	L	Putamen
28	3.86	(77 63 36)	L	Superior Temporal Gyrus
28	3.71	(61 56 33)	L	Putamen
28	3.68	(77 63 36)	L	Superior Temporal Gyrus
28	3.62	(76 65 46)	L	Precentral gyrus
28	3.6	(70 50 49)	L	Supramarginal gyrus
28	3.59	(66 61 43)	L	Central Operculum
28	3.58	(55 67 31)	L	Putamen
28	3.56	(67 53 49)	L	Central Operculum
28	3.51	(63 68 34)	L	Anterior Insula
28	3.51	(66 49 48)	L	Parietal Operculum
27	3.47	(49 59 58)	L	Mid-anterior cingulate
27	3.38	(50 79 48)	L	Paracingulate
27	3.37	(48 56 64)	L	SMA
27	3.35	(49 77 48)	L	SMA
27	3.34	(47 59 65)	L	SMA
27	3.33	(51 74 48)	L	ACC
27	3.3	(48 79 48)	L	ACC
27	3.26	(47 87 49)	L	Superior frontal gyrus
27	3.22	(48 85 45)	L	Paracingulate
27	3.18	(52 83 36)	L	White Mater
27	3.14	(52 83 33)	L	White Mater
27	3.13	(46 90 52)	L	Frontal pole
27	3.13	(46 90 52)	L	Superior frontal gyrus
27	3.06	(51 86 40)	L	ACC
27	3.02	(49 60 55)	L	Mid-anterior cingulate
27	3	(50 90 38)	L	Dorsal medial PFC
27	2.95	(45 64 58)	L	Mid-anterior cingulate
27	2.93	(52 87 37)	L	Paracingulate
27	2.8	(51 68 52)	L	White Mater
27	2.74	(45 68 57)	L	ACC
26	3.94	(19 50 48)	R	Parietal Operculum
26	3.78	(21 44 47)	R	Supramarginal gyrus
26	3.58	(16 52 47)	R	Parietal Operculum
26	3.49	(25 57 32)	R	Central Operculum

26	3.47	(25 53 44)	R	Parietal Operculum
26	3.33	(35 64 31)	R	White Mater
26	3.27	(31 67 27)	R	Frontal orbital cortex
26	3.14	(27 67 31)	R	Anterior Insula
26	3.12	(25 56 40)	R	Posterior Insula
26	3.07	(26 51 50)	R	White Mater
26	3.01	(27 57 36)	R	Posterior Insula
26	2.98	(28 52 44)	R	Posterior Insula
26	2.93	(24 69 21)	R	Temporal pole
26	2.8	(30 68 33)	R	Putamen
26	2.76	(31 69 31)	R	Putamen
26	2.73	(19 40 51)	R	Angular gyrus
26	2.43	(28 68 22)	R	Temporal pole
25	3.52	(64 49 67)	L	Postcentral gyrus
25	3.51	(64 44 67)	L	Postcentral gyrus
25	3.51	(67 48 62)	L	Postcentral gyrus
25	3.5	(70 51 60)	L	Postcentral gyrus
25	3.12	(56 40 70)	L	Superior Parietal Lobule
25	2.92	(55 43 68)	L	Postcentral gyrus
25	2.87	(65 55 65)	L	Precentral gyrus
25	2.81	(61 52 62)	L	Precentral gyrus
25	2.78	(57 45 64)	L	Postcentral gyrus
25	2.68	(60 39 68)	L	Superior Parietal Lobule
25	2.66	(60 39 68)	L	Superior Parietal Lobule
24	3.52	(68 67 15)	L	Temporal pole
24	3.4	(72 63 18)	L	Middle temporal gyrus
24	3.37	(67 61 14)	L	Inferior temporal gyrus
24	3.19	(58 68 15)	L	Temporal pole
24	2.98	(59 65 18)	L	Temporal pole
24	2.87	(62 65 18)	L	Temporal pole
24	2.73	(63 64 13)	L	Inferior temporal gyrus
24	2.58	(66 63 18)	L	Inferior temporal gyrus
23	3.32	(32 85 49)	R	Frontal pole
23	3.28	(32 86 51)	R	Frontal pole
23	3.08	(32 84 45)	R	Frontal pole
22	2.93	(76 41 45)	L	Supramarginal gyrus
22	2.81	(74 31 42)	L	Lateral occipital cortex
22	2.69	(76 39 48)	L	Supramarginal gyrus
22	2.67	(74 35 44)	L	Angular gyrus
21	2.97	(60 58 70)	L	Precentral gyrus
21	2.5	(60 57 63)	L	Precentral gyrus
21	2.46	(60 58 65)	L	Precentral gyrus
20	2.54	(74 34 53)	L	Angular gyrus
20	2.52	(72 31 54)	L	Lateral occipital cortex
20	2.42	(76 35 51)	L	Angular gyrus
19	2.88	(19 66 18)	R	Temporal pole
19	2.54	(17 62 17)	R	Inferior temporal gyrus
18	2.8	(73 29 36)	L	Lateral occipital cortex
17	2.95	(54 56 40)	L	Thalamus

16	2.44	(17 64 39)	R	Central Operculum
15	2.48	(37 89 53)	R	Frontal pole
14	2.81	(52 50 66)	L	Precentral gyrus
13	2.43	(70 39 50)	L	Supramarginal gyrus
13	2.34	(73 40 50)	L	Supramarginal gyrus
12	2.49	(43 73 52)	R	ACC
11	2.43	(21 68 34)	R	Temporal pole
10	2.65	(41 68 34)	R	Nucleus Accumbens
9	2.36	(54 69 38)	L	White Mater
8	2.48	(39 68 30)	R	White Mater
7	2.5	(56 65 23)	L	Temporal pole
6	2.33	(64 61 65)	L	Precentral gyrus
5	2.62	(22 56 48)	R	Central Operculum
4	2.43	(73 27 45)	L	Lateral occipital cortex
3	2.53	(62 56 60)	L	Precentral gyrus
2	2.33	(21 57 46)	R	Central Operculum
1	2.42	(71 24 42)	L	Lateral occipital cortex

Table A: Multi-TI Pain vs Baseline. Brain responses to Pain versus the rest conditions (Pain>Rest). Note PFC, prefrontal cortex; ACC, anterior cingulate cortex; PCC, posterior cingulate cortex; SMA, supplementary motor area.

B. Across-block habituation

Cluster	zstat	MNI	Laterality	ROI
3	4.25	(78 49 31)	L	Middle temporal gyrus
3	4.2	(67 67 23)	L	Temporal pole
3	3.98	(74 46 31)	L	Middle temporal gyrus
3	3.89	(79 54 31)	L	Middle temporal gyrus
3	3.7	(64 60 32)	L	Posterior Insula
3	3.69	(67 65 28)	L	Temporal pole
3	3.68	(77 45 33)	L	Middle temporal gyrus
3	3.67	(66 69 20)	L	Temporal pole
3	3.65	(78 40 39)	L	Middle temporal gyrus
3	3.55	(74 44 47)	L	Parietal operculum
3	3.54	(76 49 46)	L	Supramarginal gyrus
3	3.53	(69 52 32)	L	Superior temporal gyrus
3	3.51	(68 51 50)	L	Supramarginal gyrus
3	3.47	(74 45 49)	L	Parietal operculum
3	3.45	(61 75 25)	L	Frontal orbital cortex
3	3.38	(63 55 34)	L	Posterior Insula

3	3.31	(58 68 26)	L	Frontal orbital cortex
3	3.27	(70 49 42)	L	Parietal operculum
2	3.75	(44 86 57)	R	Superior frontal gyrus
2	3.62	(48 86 51)	L	Superior frontal gyrus
2	3.58	(44 88 54)	R	Superior frontal gyrus
2	3.51	(53 87 26)	L	Frontal pole
2	3.2	(48 81 54)	L	Paracingulate
2	3.08	(50 88 30)	L	Dorsal medial PFC
2	2.91	(51 76 47)	L	ACC
2	2.9	(54 83 29)	L	Frontal pole
2	2.83	(50 87 34)	L	Paracingulate
2	2.81	(50 87 36)	L	Paracingulate
2	2.76	(50 75 49)	L	ACC
2	2.75	(54 83 26)	L	Frontal pole
2	2.69	(50 82 36)	L	ACC
2	2.68	(50 80 43)	L	ACC
2	2.64	(54 81 35)	L	White Mater
2	2.62	(51 78 44)	L	ACC
2	2.52	(37 82 60)	R	Frontal pole
2	2.48	(50 84 60)	L	Frontal pole
1	3.95	(22 49 49)	R	Parietal operculum
1	3.56	(23 46 51)	R	Parietal operculum
1	3.49	(20 41 51)	R	Angular gyrus
1	3.48	(19 51 45)	R	Parietal operculum
1	3.41	(28 48 50)	R	White Mater
1	2.92	(24 39 50)	R	White Mater

Table B: Multi_TI Across block habituation. Brain regions that show significant habituation of activation across stimulus blocks. Note: PFC, prefrontal cortex; ACC, anterior cingulate cortex; PCC, posterior cingulate cortex; SMA, supplementary motor area.

5.6 References

1. Aguirre, GK et al. (2002). Experimental design and the relative sensitivity of BOLD and perfusion fMRI. Neuoimage 15(3): 488-500

2. Wang, J. et al. (2003) Arterial spin labelling perfusion fMRI with ver low task frequency. Magn Reson Med 49(5):796-802

3. Garcia, DM et al. (2005) Pseudo-continuous flow driven adiabatic inversion for arterial spin labelling. In: Proceedings of ISMRM 2005, Miami FL. p.37

4. Wu, WC. et al. (2007) A theoretical and experimental investigation of the tagging efficiency of pseudocontinuous arterial spin labelling. Magn Reson Med 58:1020-1027

5. Chen, Y., Wang, D.J.J., Detre, J.A. (2011). Test-Retest Reliability of Arterial Spin Labeling With Common Labeling Strategies. J Magnetic Resonance Imaging 33:940-9

6. Gevers, S. et al. (2011). Robustness and Reproducibility of Flow Territories Defined by Planning-Free Vessel_Encoded Pseudocontinuous Arterial Spin-Labeling. AJNR AM J Neuroradiol. [Epub ahead of print]

7. Ye FQ, Yang Y, Duyn J, Mattay VS, Frank JA, Weinberger DR, McLaughlin AC. (1999). Quantitation of regional cerebral blood flow increases during motor activation: A multislice, steady-state, arterial spin tagging study. Magn Reson Med. 42(2)404-7

8. Wong, E.C., Buxton R.B., Frank L.R. (1997). Implementation of Quantitative Perfusion Imaging Techniques for Functional Brain Mapping using Pulsed Arterial Spin Labeling. NMR in Biomedicine. 10:237-249.

9. Buxton, R.B., Lawrence R.F., Wong, E.C., Siewart B., Warach S., Edelman, R.R. (1998). A general kinetic model for quantitative perfusion imaging with arterial spin labeling. MRM 40:383-396.

10. Buxton & Frank, 1997. A model for the coupling between cerebral blood flow and oxygen metabolism during neural stimulation. J Cereb Blood Flow Metab. 17(1997):64-72

11. Xie, J. Segerdahl, A,R., Tracey, I., Jezzard P. Simultaneous functional and quantitative ASL: an optimal tool for imaging ongoing pain states. ISMRM Abstract, 2011. Montreal Congress.

12. Dai, W., Garcia, D., de Bazelaire, C., Alsop, D.C. (2008). Continuous flow-driven inversion for arterial spin labelling using pulsed radio frequency and gradient fields. MRM 60(6):1488-97.

13. Xie, J., Gallichan, D., Gunn, R.N., Jezzard, P. (2008). Optimal design of pulsed arterial spin labelling MRI experiments. MRM 59(4):826-34.

14. Chappell, M.A., Groves, A.R., Whitcher, B., Woolrich, M.W. (2009). Variational Bayesian inference for a nonlinear forward model. IEEE TSP. 57:223-236

15. Smith SM, Jenkinson M, Woolrich MW, Beckman CF, Behrens TE, Johansen-Berg H, Bannister PR, De Luca M, Drobnjak I, Flitney DE, Niazy RK, Saunders J, Vickers J, Zhang Y, De Stefano N, Brady JM, Mathews PM. Advances in functional and structural MR image analysis and implementation as FSL. Neuroimage 2004; 23(Supp 1):S208-19.

16. Jenkinson M, Bannister P, Brady M. Smth S. Imporived optimization for the robust and accurate linear registration and motion correction of brain images. Neuroimage 2002; 17(2):825-41.

17. Jenkinson M, Smith S. A global optimisation method for robust affine registration of brain images. Med Image Anal 2001; 5(2):143-56.

18. Apkarian AV, Bushnell MC, Treede RD, Zubieta JK. Human brain mechanisms of pain perception and regulation in health and disease. Eur J Pain 2005; 9(4):463-84.

19. Peyron R, Laurent B, Garcia-Larrea L. Functional imaging of brain responseses to pain. A review and meta-analysis. Neurophysiol Clin 2000; 30(5):263-88.

20. Owen DG, Bureau Y, Thomas AW, Prato FS, St Lawrence KS (2008). Quantification of pain-induced changes in cerebral blood flow by perfusion MRI. Pain 136(1):85-96

21. Owen DG, Clarke CF, Ganapathy S, Prato FS, St Lawrence KS. (2010). Using perfusion MRI to measure dynamic changes in neural activation associated with tonic muscular pain. Pain 148(3):375-86

22. Howard, M.A. , Krause, K., Khawaja, N., Massat, N., Zelaya, F., Schumann, G., Huggins, J.P., Vennart, W., Williams, S.C.R., Renton, T.F. (2011). Beyond patient reported pain: perfusion magnetic resonance

imaging demonstrates reproducible cerebral representation of ongoing post-surgical pain. PLoS One 6(2): 1-10.

23. Talbot, J.D., Marrett, S., Evans, A.C., Meyer, E., Bushnell, M.C., Duncan, G.H. (1991). Multiple representations of pain in human cerebral cortex. Science 251(4999):1355-1358.

24. Jones AK., Brown WD., Friston KJ, Qi LY, Frackowiak RS.(1991) Cortical and subcortical localization of response to pain in man using positron emission tomography. Proc Biol Sci. 244(1309):39-44

25. Apkarian, A.V., Stea, R.A., Manglos, S.H., Szeverenyi, N.M., King, R.B., Thomas, F.D. (1992

26. Casey KL, Minoshima S, Berger KL, Koeppe RA, Morrow TJ, Frey KA. (1994). Positron emission tomographic analysis of cerebral structures activated specifically by repetitive noxious heat simuli. J Neurophysiol. 71(2):802-7Svensson P. et al. 1998

27. Coghill RC, Talbot JD, Evans AC, Meyer E, Gjedde A, Bushnell MC, Duncan GH. (1994). Distributed processing of pain and vibration by the human brain. J Neuroscience. 14(7):4095-108Iadarola MJ et al. 1998

28. Tolle, TR, Kaufmann T, Siessmeier T, Lautenbacher S, Berthele A, Munz F, Zieglgansberger W, Willoch F, Schwaiger M, Conrad B, Bartenstein P. (1999) Region-specific encoding of sensory and affective components of pain in the human brain: a positron emission tomography correlation analysis. Ann Neurol. 45(1):40-7

29. Coghill RC, Talbot JD, Evans AC, Meyer E, Gjedde A, Bushnell MC, Duncan GH. (1994). Distributed processing of pain and vibration by the human brain. J Neuroscience. 14(7):4095-108

30. Derbyshire SW, Jones AK, Gyulai F, Clark S, Townsend D, Firestone LL. (1997). Pain processing during three levels of noxious stimulation produces differential patterns of central activity. Pain 73(3):431-45Tolle TR 1999

31. Friston, K.J., Buechel, C., Fink, G.R., Morris, J. Rolls, E., Dolan, R.J. (1997). Psychophysiological and modulatory interactions in neuroimaging. NeuroImage 6(3):218-229.

32. Buchel, C., Bornhovd, K., Quante, M., Glauche, V., Bromm, B., Weiller, C., (2002). Dissociable neural responses related to pain intensity, stimulus

intensity, and stimulus awareness within the anterior cingulate cortex: a parametric single-trial laser functional magnetic resonance imaging study. J Neuroscience 22(3):970-6.

33. Bornhovd, K., Quante, M., Glauche, V., Bromm, B., Weiller, C., Buchel, C., (2002). Painful stimuli evoke different stimulus-response functions in the amygdala, prefrontal, insula, and somatosensory cortex: a single-trial fMRI study. Brain 125(Pt 6):1326-36.

34. Hsieh, J.C., Belfrage, M., Stone-Elander, S., Hansoon, P., Ingvar, M. (1995). Central representation of chronic ongoing neuropathic pain studied by positron emission tomography. Pain 63(2):225-36.

35. Coghill, R.C., Sang, C.N., Maisog, J.M.A., Iadarola, J. (1999). Pain intensity processing within the human brain: A bilateral, distributed mechanism. J Neurophysiology 82(4):1934-43.

36. Uludag K., Dubowitz DJ, Yoder EJ, Restom K, Liu TT, Buxton RB. (2004). Coupling of cerebral blood flow and oxygen consumption during physiological activation and deactivation measured with fMRI. Neuroimage 23(1):148-55

37. Hoge et al. 1999. Stimulus-dependent BOLD and perfusion dynamics in human V1. Neuroimage 9(1999),pp.573-585

38. Zimine, I., Petersen, E.T., Golay, X. (2006). Dual vessel arterial spin labeling scheme for regional perfusion imaging. MRM 56:1140-1144.

39. Ye FQ, Yang Y, Duyn J, Mattay VS, Frank JA, Weinberger DR, McLaughlin AC. (1999). Quantitation of regional cerebral blood flow increases during motor activation: A multislice, steady-state, arterial spin tagging study. Magn Reson Med. 42(2)404-7

40. Yongbi MN, Fera F, Yang Y, Frank JA, Duyn JH. (2002). Pulsed arterial spin labelling: comparison of multisection baseline and functional MR imaging perfusion signal at 1.5 and 3.0 T: initial results in six subject. Radiology 222(2):569-75

41. Kohn, A. & Movshon, J.A. (2004). Adaptation changes the direction of tuning of macaque MT neurons. Nature Neuroscience 7(7):764-772.

42. Noguchi, Y., Inui, K., Kakigi, R. (2004). Temporal dynamics of neural adaptation effect in the human visual stream. J Neuroscience 24(28): 6283-90.

43. Karni, A., Meyer, G., Jezzard, P., Adams, M.M., Turner, R., Ungerieider, L.G. (1995). Functional MRI evidence for adult motor cortex plasticity during motor skill learning. Nature. 377(6545):155-8.

44. Ostrowsky, K., Magnin, M., Ryvlin, P., Isnard, J., Guenot, M., Mauguiere, F. (2002). Representation of pain and somatic sensation in the human insula: a study of responses to direct electrical cortical stimulation. Cerebral Cortex 12:376-385.

45. Amodio, D.M. & Frith, C.D. (2006). Meeting of minds: the medial prefrontal cortex and social cognition. Nat Rev Neuroscience 7(4):268-77.

46. Mitchell, J.P., Macrae, C.N., Banaji, M.R. (2004). Encoding-specific effects of social cognition on the neural correlates of subsequent memory. J Neuroscience 24(21):4912-7.

47. Oschner K.N., Knierim, K., Ludlow, D.H., Hanelin, J., Ramachandran, T., Glover, G., Mackey, S.C. (2004). Reflecting upon feelings: an fMRI study of neural systems supporting the attribution of emotion of self and other. J Cogn Neuroscience 16(10):1746-72.

48. van der Meer, L., Costafreda, S., Aleman, A., David, A.S. (2010) Self-reflection and the brain: a theoretical review and meta-analysis of neuroimaging studies with implications for schizophrenia. Neuoscience Biobehav Rev. 34(6):935-46.

Chapter 6

Imaging the neural correlates of neuropathic pain and pleasurable relief associated with inherited erythromelalgia in a single subject with quantitative arterial spin labelling

6.1 From molecules to man: exploring the link between genes and pain processing within a neuroimaging context

With the advent of BOLD FMRI, studies of acute pain states came an increased awareness and appreciation for the complexity of pain. Which is to say that BOLD investigations provided essential evidence to suggest that pain is generated not by a single cortical entity but rather is an experience that arises from a multitude of emotional and cognitive variables, and therefore from a constellation of subcortical and cortical regions. In a way, the experience of pain is a subjective interpretation of nociceptive afferent input into the brain where it is filtered through an array of higher cortical processes that include aspects of our memory, personality, emotional state and basal neurophysiology. This is made even more complex in the context of chronic pain where there are likely to be a diverse array of both structural and functional abnormalities present across the central nervous system, further obscuring how an individual interprets nociceptive information.

Arguably, the success of future human pain imaging experiments relies, in part, on the ability for the investigations to encapsulate this complexity. Which is to say, that the investigative approach needs to observe not just how the brain functions during pain (or, its relief) but also how biochemical, neuroanatomical, and/or genetic factors relate to cognitive processing of different pain states. Practically, the way to do this is to employ a composite investigative approach that is capable of looking at the pain conditions from the level of the nociceptor up to the cortex where the experience of pain emerges.

In practice, this is still a relatively new concept, limited by significant technical challenges. However, there are some exciting breakthrough studies offering an

exciting view toward this more integrated 'systems approach' to pain neuroimaging.

One strong investigative direction employing this approach is to observe the relationship between disease severity (i.e. magnititude of pain suffered, disease duration) with cortical structural changes. Voxel-based morphometry (VBM) FMRI studies allow one to investigate volumetric differences in cortical anatomy across subjects. Many pain studies have employed this technique to show that chronic pain induces significant grey matter loss over time in key cortical regions well known to be involved in pain processing. For example, Apkarian et al. (2003) showed that chronic low back pain patients showed significantly less grey matter in pain-relevant regions such as the thalamus and the PFC; whereby patients with neuropathic pain-like symptoms showed greater grey matter loss compared to those that did not have pain. Also, the extent of GM loss correlated with the duration of the symptoms (1). Other studies have shown similar effects in various chronic pain pathologies including: irritable bowel syndrome (IBS), chronic regional pain syndrome (CRPS), fibromyalgia, and chronic headache (2,3,4). A recent study by Gwilym, S.E. *et al.* (2010)showed that reduced thalamic grey matter associated with chronic hip pain patients was reversed 9 months after hip-replacement surgery; lending support to the idea that thalamic volumetric changes are associated with decreased pain and increased function in patients (5).

Another essential experimental direction that needs to be pursued is exploring the link between key genetic markers and pain pathologies. While extensive molecular and animal research has shown that genes influence various aspects of nociceptor neurophysiology; the link between pain and genes is still largely

unknown. A few key studies have shown there to be a heritable genetic link to chronic pain in some cases (6,7). To date, only one study has sought to link brain imaging data with genetic information in the context of pain (8). For example, future work exploring how genetic factors predict the likelihood for a person to develop chronic pain may help direct clinical practice by guiding the decision making process about whether a patient should undergo surgery.

Perhaps more importantly however is the way in which genetic factors may be used to infer specific therapeutic targets for different pain pathologies. As discussed recently by Backonja. M. & Woolf, C. (2010), most presently available pain therapies aim to treat symptoms as opposed to modifying the pain pathology itself or, ideally, curing the disease (9). Additionally, the underlying mechanisms promoting a given chronic pain state are not necessarily likely to be the same across all pain pathologies. It can be argued that for some types of chronic pain, genetic information may be highly useful to guide the selection for potent targets to ameliorate a given pain state within an individual. There is a growing body of research to suggest that it is possible to use individual subject's genetic information to understand pain sensitivity. For example, assessment of individual's genes coding for the sodium channel $Na_v1.7$ has been used to show how inherited mutations here relate to alterations in peripheral nociceptor function and therefore the extent of pain experienced: 'gain-of-function' mutation yields increased pain hypersensitivity, whilst 'loss-of-function' mutations lead to decreased pain sensitivity (10,11).

While genomewide association studies will provide essential evidence linking specific genotypes with various pain pathologies, potentially helping to articulate novel therapeutic targets, it is also essential to relate these genetic targets to

changes in cortical processing. Here, neuroimaging can provide a powerful means to link genes to altered nociceptor function and higher cortical processing of pain. We attempted to do this in a single subject that suffers from the genetically inherited painful channelopathy, Erythromelalgia. Because of the unique phenotype of this genetic pain pathology, it was ideally suited for a pain ASL study.

A key aim of this study was to link the subject's genotype to altered peripheral sensory processing and higher cortical processing using a multivariate experimental approach that included genetic assessment, quantitative sensory testing (QST) and neuroimaging with ASL.

6.2 Imaging erythromelalgia-associated pain

Erythromelalgia is characterised by severe burning pain associated with reddening of the extremities (12,13). Inherited erythromelalgia (IEM) has been shown to be due to gain-of-function mutations in the SCN9A gene encoding the voltage gated sodium channel $Na_v1.7$ (14,15,16) that is selectively expressed in sensory and autonomic neurons (16). Sufferers of this disease often report pain 'attacks' which are triggered by mild warming stimuli (e.g. wearing socks or exercise). Many patients report that cooling of the affected limb can ameliorate pain (13,16) and this correlates with the biophysical finding that the hyperpolarizing shift in activation produced by IEM mutations can be partially normalized by cooling (17).

Consequently, because the people suffering from this condition are in a constant, well-maintained source of pain that is easily modulated with a cooling solution, it offers a unique opportunity for investigation within a perfusion imaging context. This allows us to validate our technique as well as provide potential insight into the neural correlates of this ongoing pain and its relief: specifically, whether the analgesia due to cooling is via peripheral or central mechanisms (i.e. pleasant relief). While the previous experiments show the multi-TI pCASL approach is capable of imaging the brain during experimental tonic pain; the next step is to observe if it is possible of resolving pain associate with a pathological condition.

Specifically, we wanted to employ the multi-TI pCASL sequence used in the previous experiment to image a chronic pain state; and relatedly, to link a molecular lesion causing aberrant peripheral nociceptor function to unique patterns of higher cortical processing related to the erythromelalgia-associated pain state.

The aim of the current investigation was to interrogate a rare inherited neuropathic pain condition using a composite experimental procedure that included molecular genetics, quantitative sensory testing (QST) and ASL FMRI in a single subject. The goal of this molecule-to-man approach is to link the unique neurophysiological properties associated with a point-mutation in the sodium channel NAv1.7 to higher cortical pain processing.

To do this, we identified a patient with severe inherited erythromelalgia secondary to an L858F mutation in the voltage gated sodium channel Na_v 1.7. The patient reported severe ongoing foot pain which was exquisitely sensitive to limb cooling. We confirmed this heat hypersensitivity using QST. Additionally, we employed the multi-TI pCASL approach utilized in the previous chapter to image the subject's baseline erythromelalgia pain versus cooling relief. Robust activations of key pain, pain-affect and reward-related centres were observed. This combined approach allowed us to confirm the presence of a temperature sensitive channelopathy of peripheral neurons and to investigate the neural correlates of tonic neuropathic pain and relief in a single subject.

6.3. Methods

A single Erythromelalgia sufferer (female, right handed, age = 32) participated in this study. The subject gave informed consent and the study was subject to institutional ethical review.

1. *Assessment of genotype: molecular genetic assessment*

Following informed consent all 26 coding exons of the SCN9A gene were sequenced to confirm the presence of the L858F mutation in the voltage gated sodium channel Na_v 1.7. All sequencing was completed by collaborators at the Dept. of Gastroenterology, Radboud University Nijmegen Medical Center, The Netherlands.

2. Quantitative sensory testing (QST) and *experimental pain paradigm*

A full QST protocol was conducted in accordance with the German Research Network on Neuropathic Pain (28). The standardised protocol measures 13 psychophysical parameters through seven tests which may be divided into the following groups: a) thermal testing for detection and painful thresholds for cold, warm and paradoxical heat sensations; b) detection thresholds for touch and vibration; c) mechanical pain sensitivity including stimulus response functions for pinprick sensitivity, summation of pain following repetitive stimulation and dynamic mechanical allodynia.

Results from each parameter, irrespective of units of measurement for each test, can be graphically represented for both the control and test sites as a QST profile. Profiles for each site can be compared with the bank of control data by z-transformation of each parameter by the equation (28) : Z-score = $((X_{\text{single patient}}) - \text{Mean}_{\text{controls}}) / \text{Standard Deviation}_{\text{controls.}}$

The resultant z-transformed profile represents all parameters as standard normal distributions where the mean equals zero. As proposed by Rolke et al (2006), the algebraic sign of the score for each parameter was adjusted to represent the patient's sensitivity. Positive Z-values indicate a gain of function, where the patient is hypersensitive to the test stimulus relative to controls. Conversely, negative Z-values indicate a loss of function where the patient is less sensitive. A 95% confidence interval (CI) of a standard normal distribution is used to define the control population, represented in Figure ** by the grey area. This CI is established by the following rule: 95% CI = $\text{Mean}_{\text{controls}}$ +/- $1.96\text{SD}_{\text{controls}}$.

A graphic representation of the experimental stimulus paradigm employed is displayed in Figure 2. A motorized water perfusion system (IceMan, USA) was used to maintain a constant temperature water solution over the subject's feet. Phases of Erythermalgia baseline pain (BASE) were induced with a warm solution (average temperature = 35.5°F, s.e. = 0.72) that was below the heat pain threshold defined by QST (average temperature = 43°F, s.e.= 0). Phases of pain relief (COOL) were induced with a cooling water solution (average temperature = 13.9°F, s.e. = 0.86).

Brain activity was recorded during three 5-minute blocks of each BASE and COOL stimulus temperatures using quantitative perfusion functional imaging. Pain intensity ratings were monitored verbally using a numerical rating scale (NRS: 0 = no pain; 10= worst pain) at the very beginning and end of each stimulus block. Additionally, after each COOL block, a pleasantness score (NRS: 0= not pleasant; 10 = most pleasant) was taken.

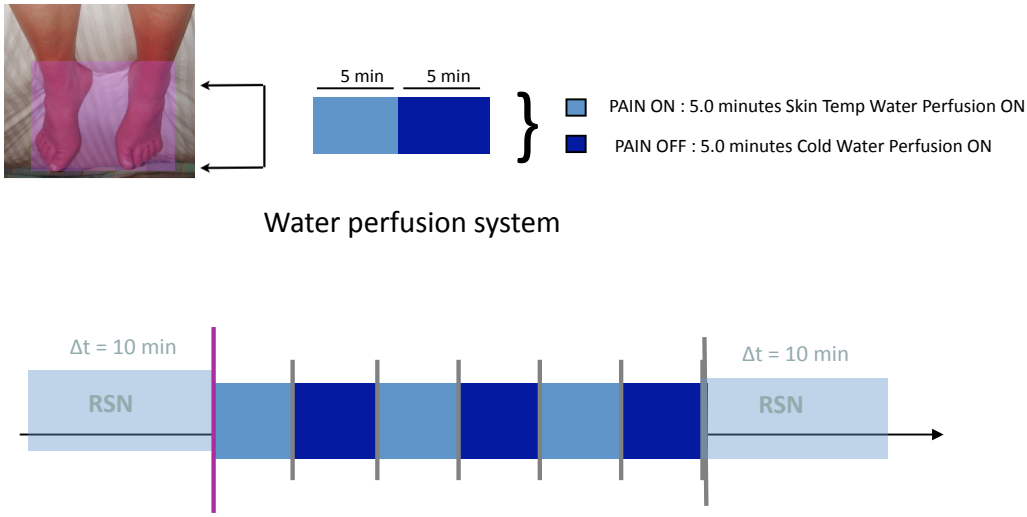

Figure 1: Graphic representation of the erythromelalgia psychophysical paradigm. For clarity, each coloured block represents the temperature of water continuously perfusing over the subject's feet: 'BASE' (mean temperature = 35.5°F, SE=0.72; light gray) versus 'cool' (mean temperature = 13.9, SE = 0.86; dark gray). b) The ASL scan paradigm used. A ten-minute resting-state (RSN) was acquired at the beginning and end of the paradigm. Five-minute blocks of continuous erythromelalgia-associated pain (BASE, light blue) versus pain-relief (cool, dark gray) were repeated three times per scan session. Two separate scan sessions were acquired for this subject. Black bars show when the pain intensity and unpleasantness ratings were taken (verbal report, NRS).

3. *MR parameters*

All subjects were scanned with a pseudo-continuous ASL sequence (29) using gradient-echo EPI readout (TR=3.75s, TE=13ms, 6/8 k-space). Twenty-two axial slices in ascending order (3 x 3 x 4.5 mm voxels, 0.5 mm inter-slice gap) were prescribed for the subject, providing whole brain coverage (including brainstem and cerebellum). The labelling plane was chosen optimally for the

subject based on a time-of-flight scan of the neck, located ~8 cm inferior to the centre of the 26 slices. A 90° pre-saturation pulse was applied before the labelling pulses. The labelling duration was 1.4s and five different post labelling delay (PLD) times were adopted. The five PLD values, [0.64s, 0.792s, 0.896s, 1s, 1.152s], were generated according to Optimal Sampling Schedule theory (30). PLD times were pseudo-randomised per TR. 16 PLD values were applied per each two-minute stimulus block. The volunteer was scanned using a Siemens 3T Verio system fitted with a 32-channel head coil.

4. *Image analysis*

Imaging data were analyzed using the FMRIB Software Library (FSL) (31). All data were pre-processed using standard FSL tools in native space.

At the first level, data were pre-processed using MCFLIRT (motion correction; 32), BET (brain extraction; 33), spatially smoothed (FWHM = 5mm) and high pass filtered (320s). Data were de-noised of non-physiological artefacts through visual inspection of independent components (34). All analysis was carried out in native space. At the first level, the general linear model was adopted for modelling CBF and any contaminating BOLD effects. At the second level, a model of each stimulus condition and relevant contrasts (e.g. BASE > COOL) was fit to the subject's perfusion time series using a fixed effects analysis. At the top level, a fixed effects analysis was used to observe the average CBF changes specific to each contrast (i.e. BASE > COOL : group mean CBF changes showing regions more active during pain versus cooling). Cluster-based

thresholding was used to generate clusters of CBF changes showing effects with a significance level of $p<0.05$, using a z-score cut-off of 2.0.

6.4. Results

6.4.1. Case Report

The patient was assessed at the age of 29 years old. She presented at birth with erythema of the hands and feet and as soon as she was able to talk complained of hot painful feet. Initially she described fluctuations of her symptoms with exacerbations of pain and erythema triggered by warmth, exercise, alcohol and wearing enclosed shoes; her symptoms could be alleviated by cooling. She had previously developed foot ulceration as a consequence of excessive cooling in cold water and at the age of 16 received epidural anaesthesia to control her pain. She currently reports constant foot pain. Her pain has partially responded to topical 5% lidocaine plasters (applied to the feet for 12 hrs a day) and she had also derived some relief from treatment with imipramine 100mg daily. There is no family history of erythromelalgia; her parents and brother are unaffected. On examination she had erythema of the fingers and feet extending up to the mid calf (Figure 2). Neurological examination was normal.

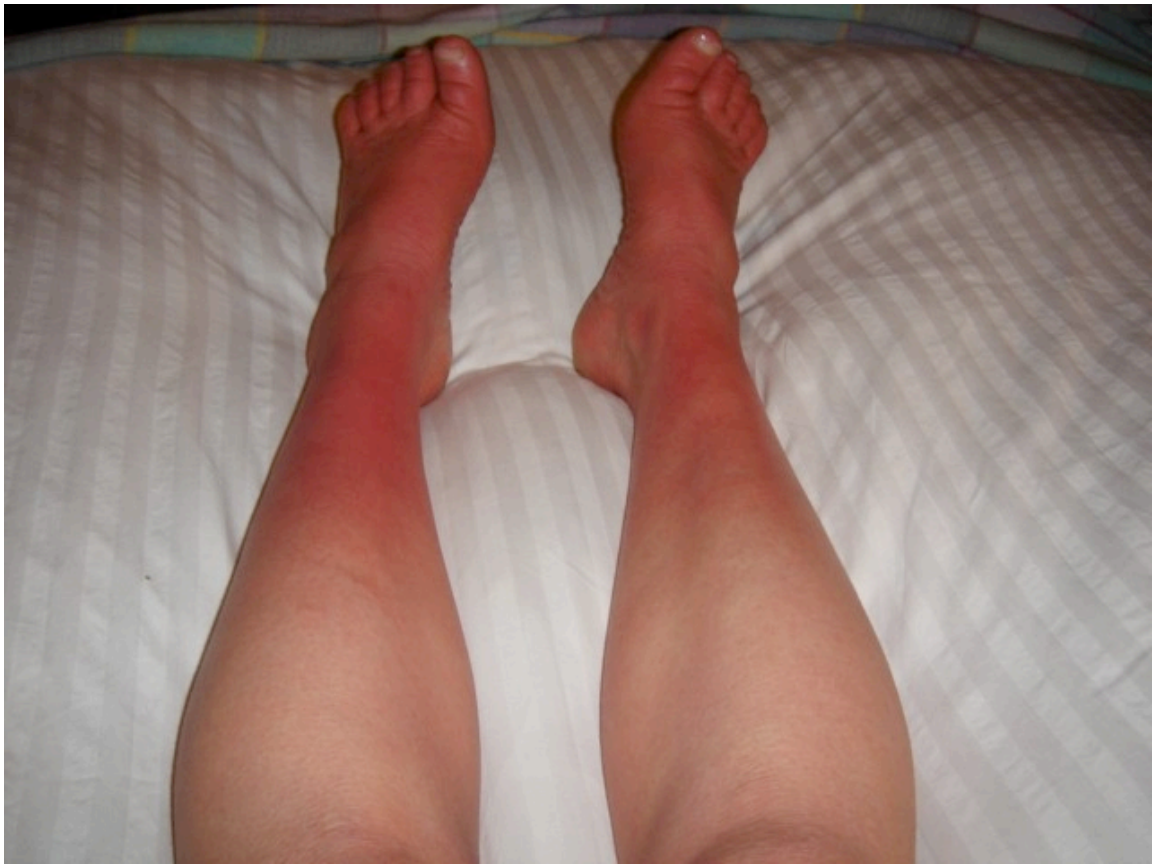

Figure 2: Photograph of the patients legs showing erythema up to the level of the mid calf.

A full QST protocol (28) was conducted in accordance with the German Research Network on Neuropathic Pain (DFNS, Figure 3). This demonstrated hypersensitivity to noxious thermal stimuli applied to the feet (her heat pain threshold was reduced by three standard deviations from the mean of gender and age matched controls). Unexpectedly she had reduced sensitivity to pressure pain and vibration detection in the feet which may relate to trophic changes in the skin following prolonged erythromelalgia.

Figure 3: Quantitative Sensory Test results. Quantitative sensory tests were performed on both hands and feet. These same tests have been repeated in normal healthy controls to comprise an extensive database as generated and held by the German Neuropathic Pain Network (DFNS) (8). This normal data is distributed within the shaded area (mean at 0 ± 2 standard deviations). Data from our subject is reported as Z score profiles for each sensory test as depicted here. Z score is defined as the standard deviation of the recorded result from the mean normal data result. Each data point is discrete however they are connected for graphical illustration as a Z profile. Quantitative Sensory tests included: CDT (cold detection threshold), WDT (warm detection threshold), TSL (thermal sensory limen), CPT (cold pain threshold), HPT (heat pain threshold), PPT (pressure pain threshold), MPT (mechanical pain threshold), MPS (mechanical pain sensitivity), WUR (wind up ratio), MDT (medical detection threshold), VDT (vibration detection threshold). All tests to the control site were within normal limits. Hypersensitivity to heat pain is demonstrated by a lowered heat pain threshold (HPT) in the feet. Hyposensitivity to deep pressure (PPT) and vibration (VDT) is also seen in the feet. These abnormal sensitivities may be attributable to thickening of the skin at the test site. Additionally, the presence of paradoxical heat sensations was tested using thermal sensory limen. 3 paradoxical heat sensations were recorded in the feet (an abnormally high number), whilst there were none in the hands.

6.4.2. Confirmation of the Na_v 1.7 mutation.

DNA sequence analysis revealed a heterozygous missense mutation in SCN9A gene which encodes Na_v ***1.7*** (a C to T substitution at 2572) resulting in the substitution of leucine 858 with phenylalanine (L858F). This mutation has previously been described in a Canadian and Chinese family and is associated with a severe phenotype with an early onset of symptoms (11, 35). DNA sequence analysis of the parents was not performed as neither was clinically affected suggesting a *de novo* mutation. This mutation has previously been shown to cause a hyperpolarizing shift in channel activation (35,39) and an enhanced response to slow depolarizations; cooling can shift the activation midpoint of L858F in a depolarizing direction bringing the threshold of activation of the mutant channel closer to wild type Nav 1.7 (17): this provides a biophysical correlate of the relief of pain by cooling in patients with this mutation.

6.4.3. Psychophysics.

Figure 4a shows the mean pain intensity ratings for the baseline warming and cooling stimuli. The mean pain intensity rating for each condition was (warming = 5.75; S.E. = 0.821; cooling = 0.25, S.E. = 0.41). The mean pain unpleasantness rating during warming was 5.75, S.E. = 0.41. During phases of cooling, the patient always rated the pain intensity and unpleasantness as less than 1 (or, not painful). There was a significant difference in pain intensity (Student t-test, $p<0.001$) and unpleasantness (Student t-test, $p<0.001$) across the conditions. To note: the subject self-reported that her left foot was always in more pain on each scan session. The subject consistently rated every cooling block as very pleasant (8 out of 10).

a)

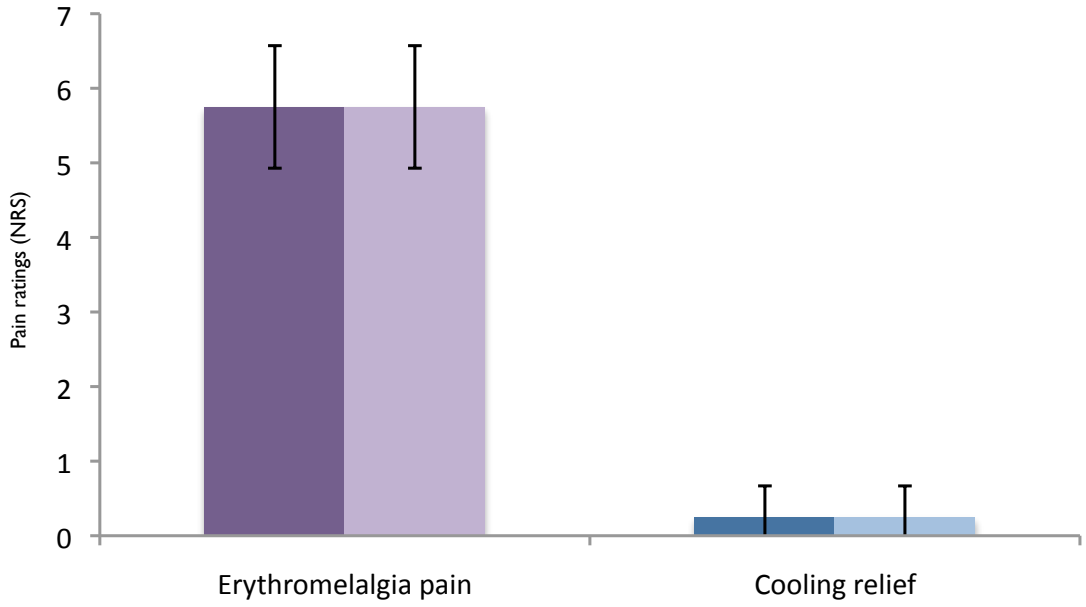

Figure 4: a) Psychophysical data. Verbally reported pain intensity (solid) and unpleasantness (opaque) ratings averaged over the five-minute blocks of Erythromelalgia-associated heat pain (purple) and blocks of pain relief (blue) across both sessions. Error bars represent standard deviation from the mean.

6.4.4. Perfusion imaging data

Significant changes in CBF generated by the contrast of Baseline pain > Cooling relief are shown in Figure 4b. Coloured regions represent voxels with suprathreshold t-statistics generated from the FEAT analysis of variance across sessions. Significant increases in CBF occurred in many regions shown previously to be involved in processing acute (36), phasic (37), and tonic (25,26,27) pain. Active regions include: bilateral thalamus, SI, inferior frontal gyrus, anterior, mid and posterior cingulate, right caudate, right putamen, and the left anterior insula. No significant changes in CBF were observed in the reverse contrast of Cooling relief > Baseline pain. All coordinates are in MNI space.

b)

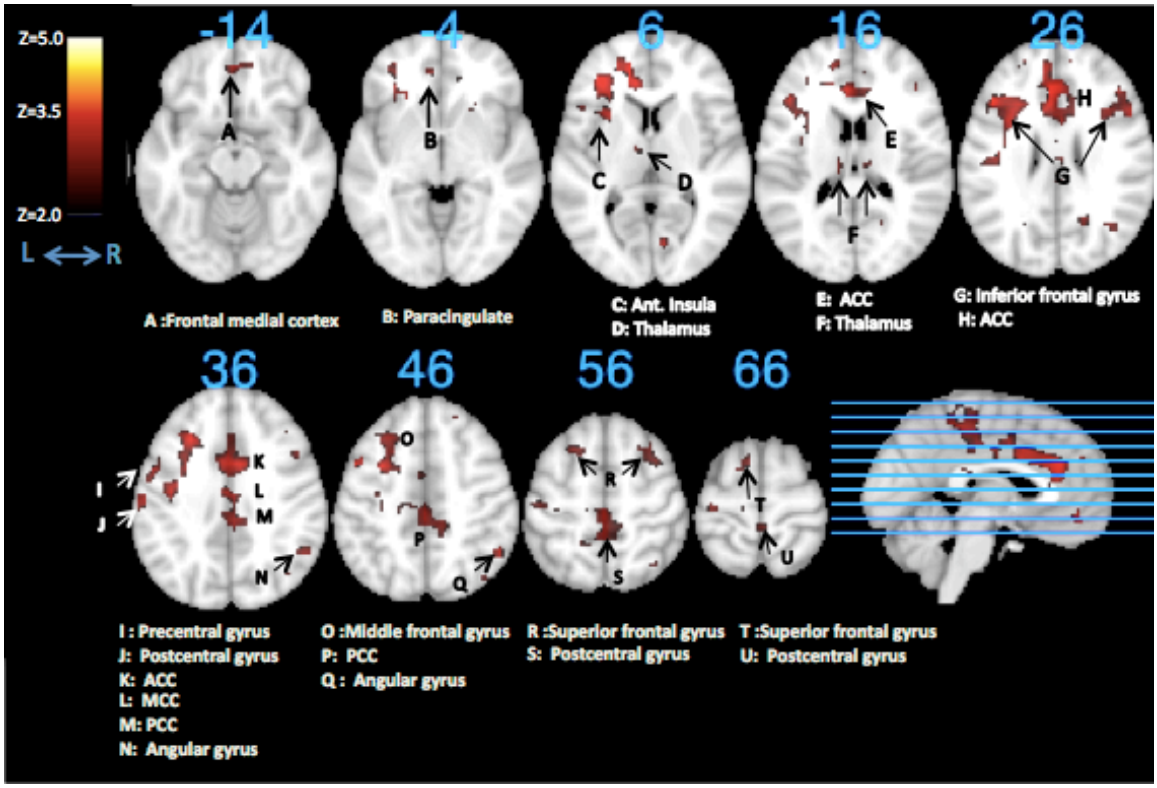

Figure 4b: Brain perfusion data from the Erythromelalgia case study acquired with the multi-TI whole brain pCASL sequence. Averaged zstat maps (n=1) of perfusion activation superimposed on the MNI152 standard template brain (Fixed Effects, cluster corrected; z:2.3-5.0, p<0.05). Perfusion maps represent the contrast of the subject's Erythromelalgia-associated pain versus blocks of cooling pain relief. The sagittal slice shows the column of activation across the whole brain. Axial slices (one slice every 10mm in ascending order) correspond to the plane indicated in the sagittal slice.

6.5 Discussion

In this study we have used a composite diagnostic experimental approach to study a patient presenting with pain and erythema of the extremities. Genetic testing showed that these symptoms were due to the painful channelopathy IEM (due to a L858F Na_v 1.7 mutation). QST demonstrated hypersensitivity to heat and confirmed the temperature dependence of her tonic pain. Finally, a novel perfusion imaging approach was used to investigate the neural correlates of the patient's pain versus phases of cooling relief.

This patient has a severe form of IEM; she was noted to have erythematous feet at birth and although onset of this disorder has previously been described as early as 1-2 years of age (30) we have not seen any previous reports of congenital onset. She has always complained of bilateral foot pain exacerbated by warmth and relieved by cooling. Initially her symptoms were episodic however from her second decade she developed constant foot pain at room temperature that could only be relieved by cooling. IEM occurs as a consequence of gain of function mutations in the voltage gated sodium channel Na_v 1.7 (30,31,4). The patient described here was found to have a substitution of the amino acid phenylalanine for leucine at codon 858 of Na_v 1.7. This is within the S4/5 linker of domain 2 of the channel. This mutation has previously been described and is associated with a severe erythromelalgia phenotype with a young age of onset in a Canadian (15) and a Chinese kindred (39).

NaV 1.7 mutations causing IEM are highly penetrant and give rise to increased DRG cell hyperexcitability (and hence pain) via a number of alterations in

channel function including: A hyperpolarizing shift in channel activation, slowed deactivation and an enhanced response to slow ramp-like stimuli (ramp currents) (40). Particular mutations have distinct effects on channel function and there is a complex relationship between these changes and the clinical severity: the greater the hyperpolarizing shift in activation, the earlier the age of onset (39). However, mutations that also enhance slow inactivation reduce channel availability and lead to a milder phenotype (17). The L858F mutation present in our patient has been reported to cause a large hyperpolarizing shift in voltage dependent activation with no effect on slow inactivation. These biophysical changes therefore correlate with the severe phenotype (39,40). Interestingly cooling has been shown to shift the activation midpoint of L858F in a depolarizing direction bringing the threshold of activation of the mutant channel closer to wild type Nav 1.7 (17). The patient reported here demonstrated noxious heat hypersensitivity on QST of the feet and the level of her tonic pain was strongly modulated by ambient temperature (being rapidly relieved by cooling). We exploited this phenomenon to investigate the imaging correlates of her tonic pain.

The patient showed robust activation of key pain sensory and pain-affect regions during phases of IEM related pain- that ceased during cooling relief. Pain was related to increased perfusion in the bilateral thalamus, SI, inferior frontal gyrus, anterior, mid and posterior cingulate, right putamen, right caudate, and the left anterior insula. There was a lateral dominance of activity in several regions that was contralateral to her greatest foot pain, as would be expected. Our data align with previous tonic pain studies using ASL and PET. For example, regions such

as the insula, thalamus, putamen, cingulate, and SI have all been shown previously to play a role in ongoing pain states. While the present study is unable to interrogate the mechanisms of tonic pain processing, these data provide exciting additional evidence that many regions activated in well-known BOLD FMRI studies of acute pain are also found to be active during a chronic pain state (41,42).

Because of the robust relieving action induced by cooling at the site of the erythromelagia pain, it was possible to image the attenuation of brain regions constituent of a multidimensional pain network. Cooling relief caused a cessation of activation in these regions. No additional regions were observed to be more active during cooling compared to pain. While this could be due to low signal-to-noise related to the single-subject nature of the case, it is clear that the cooling stimulus acting at the site of the erythema is a major component driving pain relief. This would be consistent with the effects of cooling on mutant L858P Nav1.7 function and presumably correlates with reduced ongoing nociceptor activity following cooling. Microneurography has been performed in a cohort of patients with primary erythromelalgia and this demonstrated altered C-fibre function including enhanced activity dependent slowing of afferent units and increased spontaneous activity 436). The effects of cooling on C-fibre function were not investigated in this report.

It is possible that the pleasant relief experienced during cooling reflects a kind of pain-offset reward signal triggered by reduced nociceptor function. While the present study is unable to visualise the neural correlates of this hedonic phase,

our data confirms the temperature-dependence of the L858F Nav1.7 mutation and further, demonstrates the related effects on pain processing in the cortex.

A key goal of this work was to employ a composite investigative approach to study a chronic pain condition. From previous pain neuroimaging studies, it is well known that pain is a complex, subjective experience constituent of sensory, psychological, cognitive and neuropharmacological factors. This is made even more complex in the context of chronic pain where unique combinations of structural and functional abnormalities could possibly be used to define different types of pain disease states (44). The success of future human pain studies relies partly on the capacity to encapsulate this complexity. As a case study, the present work attempted to do this by employing a multivariate investigative approach that interrogated the pain from level of ion channel dysfunction on peripheral nociceptors to higher cortical pain processing in the brain. Interpreting the brain imaging data, although in a single subject, it is clear that the optimised ASL approach used is capable of imaging the effect of chronic pain and relief across a whole brain. Additionally, our data provide evidence that in the case of erythromelalgia, it appears as though cooling relief produces analgesia via attenuation of peripheral inputs rather than via top-down brain mechanisms related to pleasant relief.

We hope that future studies employing a composite, ‘molecule-to-man’ approach as we have done here will help develop a mechanism-based understanding of chronic pain in patients.

6.6 References

1. Apkarian, A.V. et al. (2003) Chronic back pain is associated with decreased prefrontal and thalamic gray matter density. J Neuroscience 24, 10410-10415

2. Davis, K.D., Pope G., Chen J., Kwan C.L., Crawley A.P., Diamant N.E. (2008). Cortical thinning in IBS: implications for homeostatic, attention, and pain processing. Neurology 70(2):153-4.

3. Geha, P.Y., Baliki M.N., Harden R.N., Bauer W.R., Parrish T.B., Apkarian A.V. (2008) The brain in chronic CRPS pain: abnormal gray-white matter interactions in emotional and autonomic regions. Neuron 60(4):570-81.

4. Kuchinad, A., Schweinhardt P., Seminowicz D.A., Wood P.B., Chizh B.A., Bushnell M.C. (2007). Accelerated brain gray matter loss in fibromyalgia patients: premature aging of the brain? J Neuroscience 27(15):4004-7.

5. Gwilym, S.E., Filippini N., Douaud G., Carr A.D., Tracey I. (2010) Thalamic atrophy associated with painful osteoarthritis of the hip is reversible after arthroplasty. Arthritis & Rheumatism 62(10):2930-2940.

6. Katon, W., Egan K., Miller D. (1985) Chronic pain: lifetime psychiatric diagnoses and family history. Am J Psychiatry 142(10):1156-60.

7. Bachiocco, V., Scesi M., Morselli A.M., Carli G. (1993) Individual pain history and familial pain tolerance models: relationship to post-surgical pain. Clin J Pain 9(4):266-71.

8. Zubieta, J.K., Heitzeg M.M., Smith Y.R., Bueller J.A., Xu K., Xu Y., Koeppe R.A., Stohler C.S., Goldman D. (2003). COMT val158met genotype affects mu-opioid neurotransmitter responses to a pain stressor. Science 299(5610): 1240-3.

9. Backonja. M. & Woolf, C. (2010) Future directions in neuropathic pain therapy: closing the translational loop. Oncologist 15 Supp 2:24-9. Review.

10. Fischer TZ & Waxman SG. (2010). Familial pain syndromes from mutations of the NaV1.7 sodium channel. Ann N Y Acad Sci. 1184:196-207

11. Han C, Rush AM, Dib-Hajj SD, Li S, Xu Z, Wang Y, Tyrrell L, Wang X, Yang Y, Waxman SG. (2006). Sporadic onset of erythermalgia: a gain-of-function mutation in Nav1.7/ Ann Neurol 59(3):553-8

12. Mitchell SW. On a rare vaso-motor neurosis of the extremities and on the maladies with which it may be confounded. Am. J Med Sci. 1878; 76: 17-36.

13. van Genderen PJ, Michiels JJ, Drenth JP. Hereditary erythermalgia and acquired erythromelalgia. Am. J. Med. Genet. 1993; 45, 530-532.

14. Yang Y. et al. Mutations in SCN9A, encoding a sodium channel alpha subunit, in patients with primary erythermalgia. J Medical Genetics. 2004; 41, 171-174

15.Drenth JP et al. SCN9A mutations define primary eythermalgia as a neuropathic disorder of voltage gated sodium channels. J Invest Dermatol. 2005; 124(6): 1333-8.

16.Toledo-Aral JJ, Moss BL, He ZJ, Koszowski AG, Whisenand T, Levinson SR, Wolf JJ, Silos-Santiago I, Halegoua S, Mandel G. Identification of PN1, a predominant voltage-dependent sodium channel expressed principally in peripheral neurons. PNAS 1997; 94(4):1527-1532.

17. Han C. et al. Temperature dependence of erythromelalgia mutation L858F in sodium channel Nav1.7. Mol Pain 2007; 19;3:3.

18.Jones AK., Brown WD., Friston KJ, Qi LY, Frackowiak RS.(1991) Cortical and subcortical localization of response to pain in man using positron emission tomography. Proc Biol Sci. 244(1309):39-44

19.Casey KL, Minoshima S, Berger KL, Koeppe RA, Morrow TJ, Frey KA. (1994). Positron emission tomographic analysis of cerebral structures activated specifically by repetitive noxious heat simuli. J Neurophysiol. 71(2): 802-7

20.Coghill RC, Talbot JD, Evans AC, Meyer E, Gjedde A, Bushnell MC, Duncan GH. (1994). Distributed processing of pain and vibration by the human brain. J Neuroscience. 14(7):4095-108

21.Derbyshire SW, Jones AK, Gyulai F, Clark S, Townsend D, Firestone LL. (1997). Pain processing during three levels of noxious stimulation produces differential patterns of central activity. Pain 73(3):431-45

22.Iadarola MJ, Berman KF, Zeffiro TA, Byas-Smith MG, Gracely RH, Max MB, Bennett GJ. (1998). Neural activation during acute capsaicin-evoked pain and allodynia assessed with PET. Brain 121(Pt 5): 931-47

23.Tolle, TR, Kaufmann T, Siessmeier T, Lautenbacher S, Berthele A, Munz F, Zieglgansberger W, Willoch F, Schwaiger M, Conrad B, Bartenstein P. (1999) Region-specific encoding of sensory and affective components of pain in the human brain: a positron emission tomography correlation analysis. Ann Neurol. 45(1):40-7

24.Aquirre GK, Detre JA, Zarahn E, Aslop DC. (2002) Experimental design and the relative sensitivity of BOLD and perfusion fMRI. Neuroimage 15(3): 488-500

25.Owen DG, Bureau Y, Thomas AW, Prato FS, St Lawrence KS (2008). Quantification of pain-induced changes in cerebral blood flow by perfusion MRI. Pain 136(1):85-96

26.Owen DG, Clarke CF, Ganapathy S, Prato FS, St Lawrence KS. (2010). Using perfusion MRI to measure dynamic changes in neural activation associated with tonic muscular pain. Pain 148(3):375-86

27. Howard, M.A. , Krause, K., Khawaja, N., Massat, N., Zelaya, F., Schumann, G., Huggins, J.P., Vennart, W., Williams, S.C.R., Renton, T.F. (2011). Beyond

patient reported pain: perfusion magnetic resonance imaging demonstrates reproducible cerebral representation of ongoing post-surgical pain. PLoS One 6(2): 1-10.

28.Rolke R, Baron R, Maier C, Tolle TR, Treede RD, Beyer A, Binder A, Birbaumer N, Birklein F, Botefur IC, Braune S, FLor H, Huge V, Klug R, Landwehrmeyer GB, Mageri W, Mahofner C, Rolko C, Schaub C, Scherens A, Sprenger T, Valet M, Wasserka B. Quantitative sensory testing in the German Research Network on Neuropathic Pain (DFNS): standardized protocol and reference values. Pain 2006; 123(3):231-43.

29.Dai W., Garcia D., de Bazelaire C., Aslop DC. Continuous flow-driven inversion for arterial spin labelling using pulsed radio frequency and gradient fields. Magn Reson Med. 2008; 60(6):1488-97.

30.Xie, J. Segerdahl, AR., Tracey, I., Jezzard P. Simultaneous functional and quantitative ASL: an optimal tool for imaging ongoing pain states. ISMRM Abstract, 2011. Montreal Congress.

31.Smith SM, Jenkinson M, Woolrich MW, Beckman CF, Behrens TE, Johansen-Berg H, Bannister PR, De Luca M, Drobnjak I, Flitney DE, Niazy RK, Saunders J, Vickers J, Zhang Y, De Stefano N, Brady JM, Mathews PM. Advances in functional and structural MR image analysis and implementation as FSL. Neuroimage 2004; 23(Supp 1):S208-19.

32.Jenkinson M, Bannister P, Brady M. Smth S. Imporived optimization for the robust and accurate linear registration and motion correction of brain images. Neuroimage 2002; 17(2):825-41.

33.Jenkinson M, Smith S. A global optimisation method for robust affine registration of brain images. Med Image Anal 2001; 5(2):143-56.

34.Kelly RE Jr., Alexopoulos GS, Wang Z, Gunning FM, Murphy CF, Morimoto SS, Kanellopoulos D, Jia Z, Lim KO, Hoptman MJ. Visual inspection f independent components: Defining a procedure for artifact removal from FMRI data. J Neuroscience Methods 2010; 189(2):233-45.

35.Han C, Rush AM, Dib-Hajj SD, Li S, Xu Z, Wang Y, Tyrrell L, Wang X, Yang Y, Waxman SG. (2006). Sporadic onset of erythermalgia: a gain-of-function mutation in Nav1.7/ Ann Neurol 59(3):553-8

36.Apkarian AV, Bushnell MC, Treede RD, Zubieta JK. Human brain mechanisms of pain perception and regulation in health and disease. Eur J Pain 2005; 9(4): 463-84.

37.Peyron R, Laurent B, Garcia-Larrea L. Functional imaging of brain responseses to pain. A review and meta-analysis. Neurophysiol Clin 2000; 30(5):263-88.

38.Fischer TZ & Waxman SG. (2010). Familial pain syndromes from mutations of the NaV1.7 sodium channel. Ann N Y Acad Sci. 1184:196-207

39.Han C, Dib-Hajj SD, Lin Z, Eastman EM, Tyrrell L, Cao X, Yang Y, Waxman SG. (2009). Early- and late-onset inherited erythromelalgia: genotype-phenotype correlation. Brain 132(Pt7):1711-22

40.Cheng X, Dib-Hajj SD, Tyrrell L, Te Morsche RH, Drenth JP, Waxman SG. (2011). Deletion mutation of sodium channel NaV1.7 in inherited erythromelalgia: enhanced slow inactivation modulates dorsal root ganglion neuron hyperexcitability. Brain 134(Pt7):1972-86

41.Hsieh, J.C., Belfrage, M., Stone-Elander S., Hansson P., Ingvar M. Central representation of chronic ongoing neuropathic pain studied by positron emission tomography. Pain 1995; 63(2):225-36

42.Iadarola M.J., Max M.B., Berman K.F., Byas-Smith M.G., Coghill R.C., Gracely R.H., Bennett G.J. Unilateral decrease in thalamic activity observed with positron emission tomography in patients with chronic neuropathic pain. Pain 1995; 63(1):55-64

43.Orstavik K, Weidner C, Schmidt R, Schmelz M, Hilliges M, Jorum E, Handwerker H, Torebjork E. (2003). Pathological C-fibres in patients with chronic painful condition. Brain 126(Pt 3):567-78

44.Tracey & Bushnell, (2009). How neuroimaging studies have challenged us to rethink: is chronic pain a disease? J Pain. 10(11):1113-20

Chapter 7

Conclusion

7.1 General conclusion

The primary aim of this thesis was threefold: 1) to develop and validate a safe and reliable method for investigating ongoing experimental pain in healthy human subjects; 2) to optimize a whole-brain ASL FMRI approach the image simultaneously absolute and relative changes in perfusion during ongoing pain; 3) to implement this optimized ASL approach to interrogate the pathological pain condition, erythromelalgia.

In Chapter 2 we show that it is possible to induce robust and reliable ongoing pain states using both thermal and mechanical modalities. Additionally, we show that while the capsaicin-related pain state is capable of inducing the perception of a strong pain in subjects, the model presents a number of caveats for its use in a parametric pain paradigm. We concluded from the capsaicin-specific pain paradigms that the model is well suited to block designs in which the presence of a thermode is used for a maximum stimulus length of 2-minutes. In contrast, the mechanical pain modality shows similarly robust and reliable pain-inducing features with the added bonus of being more flexible in its utility for different pain paradigm designs. Specifically, the psychophysical data observed from the mechanical modality showed a clear ability to induce the perception of a well-maintained ongoing pain in subjects that was able to be parametrically modulated across a range of stimulus intensities without any threat of skin damage.

In Chapter 3, we outline the key features that ASL FMRI investigations need to account for when imaging ongoing pain states and present two key pilot experiments in which we attempt to modify the ASL sequence to accomplish this. In the first pilot experiment, we compared various ASL approaches (CASL & PASL) to BOLD. Results from this study showed that while all of the commonly available ASL sequences suffer from poor SNR, CASL was the optimal method (as measured by spatial SNR, zstat value, and volume of activation) relative to BOLD. As a next step, we employed CASL in a follow-up study that attempted to obtain a whole-brain volume of perfusion contrast; a feature that, to our knowledge at the time, no commonly employed ASL sequence was capable of doing. Results from this study show how an interleaved CASL acquisition paradigm is able to obtain robust perfusion contrast across the whole-brain with the caveat that the method suffers from poor temporal SNR. Simultaneous to finishing this study, we obtained access to a pseudo-continuous ASL (pCASL) FMRI sequence that is capable of obtaining a whole-brain volume of perfusion data without suffering any of the set-backs our interleaved sequence had. Consequently, we concluded from these studies that all subsequent ASL investigations of ongoing pain would employ the pCASL approach.

In Chapter 4 we employed the pCASL FMRI approach to image the neural correlates of ongoing pain in healthy subjects. We attempted to do this in two different FMRI studies. In experiment 1, we employed capsaicin to induce a state of ongoing heat pain in subjects. Here, while the psychophysical data shows the subjects perceived the paradigm to be very painful, the imaging data acquired shows very statistically weak perfusion signal changes. We attribute

this lack of effect to three key factors: i) poorly optimized imaging parameters specific to the pCASL approach used (e.g. small voxel size, non-optimised labeling plane, utilization of parallel imaging); ii) excitation of a pain state that was oscillating in nature and therefore likely to necessitate a more complex analysis approach than the standard GLM we used; iii) poor overall signal-to-noise resultant from a low number of subjects scanned. In experiment 2, we employed the mechanical modality to induce an ongoing pain state that was able to be parametrically modulated with increasing stimulus intensity. Additionally, we optimized our experimental approach given the set-backs suffered in experiment 1. Specifically, while we did not use a parallel imaging approach, we reduced the acquisition blocks to 5-minutes per stimulus intensity and we scanned 18 subjects. Results from this study show robust increases in perfusion in key pain-related regions such as the insula, thalamus, SI, SII and the cingulate. These results align with a small, but emerging body of pain ASL literature showing similar activation of these regions during heat pain (1), isotonic saline injection (2) and post-surgical dental pain (3). Additionally, our data show regions such as the amygdala, posterior insula, thalamus, putamen, SI, SII, anterior cingulate and the frontal orbital cortex show a monotonic increase in CBF with increasing stimulus intensity applied to the periphery. Interestingly, the time course data extracted from key ROIs reveals complex temporal dynamics of CBF changes across each stimulus intensity condition. While the overall trend of each stimulus block is a net increase in CBF with pain, non-linear fluctuations in CBF are evident for each stimulus intensity. Additionally, these temporal patterns appear to be different across each ROI. While there are various potential explanations

for the temporal dynamics observed, we were hesitant as the ASL data reflects relative, not absolute changes in CBF.

In Chapter 5, we wanted to interrogate the complex CBF dynamics observed in the previous pain study by acquiring absolute quantification of CBF changes relative to an ongoing pain state. To do this, we employed an optimized pCASL approach that images multiple inversion times (TIs) for each slice of cortex over the course of the paradigm. By employing this optimized approach, it is possible to model the CBF kinetics across the whole-brain volume to obtain absolute perfusion quantification for each ROI. In this paradigm, subjects were asked to partake in two different sensory experiences: Experiment 1 utilizes a combined visual/motor task; Experiment 2 utilizes the mechanical pain modality used previously. In both experiments, subjects were asked to partake in a simple block design in which the sensory stimulus was applied for a period of 2-minutes versus blocks of rest. The primary aim of this study was to demonstrate the capacity of this imaging approach to observe absolute CBF changes across a whole brain volume for a range of different sensory stimuli; and relatedly, to compare the absolute CBF dynamics across a range of ROIs. This technique also allows for more advanced image analyses to be performed that interrogate functional connections between brain regions across time by use of psychophysiological interaction analysis. Data from these experiments show that the technique resolves robust and reliable absolute perfusion data across a whole brain. Additionally, our data confirm the recruitment of regions such as the contralateral SI, SII, ACC; bilateral insula (anterior and posterior), and the putamen during ongoing mechanical pain. Interestingly, comparison of absolute

CBF changes show that regions recruited during pain show considerably less overall changes in perfusion (e.g. 4-13%) compared to activation in the motor and visual cortices during the non-pain task (e.g. 20-40%). Further, our data confirm the presence of fluctuating, non-uniform CBF dynamics across each of these regions. We are confident that because the multi-TI pCASL approach generates absolute perfusion contrast across the whole brain volume, these effects are not due to signal variability associated with where in the brain the label is applied or at what point a given ROI is maximally perfused with arterial signal: features that previous single-TI ASL approaches suffer from (4,5). However, it is not possible to discern if these complex CBF dynamics are due to functional interactions between regions specific to how the perception of pain unfolds over time or if the effects are related to changes in neurovascular coupling across each ROI with continuous activation.

In Chapter 6 we implemented the multi-TI pCASL approach to image ongoing pain and pleasurable relief associated with the genetically inherited neuropathic pain condition erythromelalgia. The primary aim of this study was to link a subject's genotype to altered peripheral nociception and higher cortical processing of pain using a combined experimental approach that incorporated genetic assessment of the condition, quantitative sensory testing of the phenotype, and neuroimaging of the subject in pain versus phases of relief. Results from this study confirm: i) the presence of a point-mutation in the peripherally expressed sodium channel Nav1.7; ii) the related experience of thermal hypersensitivity during QST examination; and iii) robust activation of pain-related ROIs during erythromelalgia-associated pain but not during cooling

relief. We posit that data from this case study shows the exciting potential of employing the multi-TI pCASL imaging approach to interrogate pathological pain states in clinical populations. While the data confirms the utility of the technique for use in a subject suffering from a unique pain condition; we are confident that this approach can be employed to look at a range of pain pathologies in which the nature of the pain state suffered is robust and well-maintained for a period of time long enough to be imaged.

7.2 Implications for future work

As stated previously, we are confident that the ASL approach developed over the course of this thesis is well-suited to quantify absolute perfusion changes across a whole brain volume. Because the multi-TI pCASL approach makes few assumptions about where the arterial blood is labelled and when each part of the cortex experiences a maximum arterial signal, the technique benefits from being the most robust and reproducible ASL approach (4,5). It is therefore likely that the technique is well-suited to be employed in longitudinal, multi-session or even multi-centre experimental designs.

While the work presented here aligns well with previously published ASL investigations of pain: namely that regions such as the insula, thalamus, SI, SII and the ACC are recruited and remain active over the course of a tonic pain experience (1,2,3); considerable work is needed to understand the complex CBF dynamics observed in Chapter 5. At present, this is the only example of absolute CBF dynamics across a whole-brain dataset during ongoing pain. There are a

number of very exciting future experimental directions to interrogate further these findings.

i) Novel experimental designs

An obvious next step for this work would be to meticulously map-out the stimulus response functions for each pain region of interest for a range of stimulus lengths. Specifically, it is essential to understand how a given region is initially recruited during the onset of a strong pain and then how that region's functional integrity changes over time. It is possible that with increasingly longer stimulus lengths, one would be able to separate out the initial stimulus-orienting phases from later processing associated with enduring an ongoing pain state across each pain-relevant ROI.

Relatedly, a key problem of these tonic pain experiments is the fact the stimulus blocks are very long. Consequently, there is likely to be increasing variability in the cognitive load a given stimulus paradigm engages for stimulus blocks of increasing lengths of time. Future work needs to develop a means of controlling this variability across subjects with experimental designs in which the overall experience unfolds over a long period of time. The present investigations utilize relatively short (i.e. less than 10 minutes per stimulus) block lengths. However, it is conceivable that with longer stimulus blocks, this will become more of an issue. For example, one could imagine employing a randomly generated visual-cue task interspersed throughout the ongoing pain experience. Here, for a brief moment (i.e. 20 seconds) subjects when prompted could follow a visual cue

across a screen. The underlying concept being that subjects will remain attentive and active whilst experiencing pain during the scan. Because the visual task is small and short, it will not only be minimally resolved with ASL but it would be very easily modeled out of the main-effect of pain analysis. For example, the same visual task could be repeated in the control scans such that in the overall analysis only the pain activations are of interest.

At present, we do not utilize a continuous rating system in which the subject is continually asked to rate his/her pain by sliding a lever on a handle whilst being scanned. The primary reason for this was to ensure that the changes in CBF observed were specific to the experience of pain and were not in any way undermined by the cognitive processes associated with rating (e.g. motor planning, memory, metacognition). However, given the added benefit of having continuous behavioral ratings, it might also be advisable to repeat one of the above pain experiments (e.g. Chapter 5) whilst the subjects continuously rate their pain to see if in fact this process undermines any of the pain-relevant activation maps.

ii) Novel analysis approaches

A number of follow-up experiments could be paired with multi-TI pCASL FMRI to interrogate the specific roles of each pain-relevant region. For example, by employing more structured modeling approaches (e.g. PPI or DCM analyses), one would be able to better understand the dynamic interaction between regions in the context of an ongoing pain state (6). Additionally, the bulk of our analysis approach thus far has been guided by a GLM approach. Given our the

complexity of CBF changes observed from the absolute time course data in Chapter 5, it is advisable that more model-free statistical approaches (e.g. ICA) may provide more sensitive means of exploring activation patterns that are not necessarily able to be modeled linearly (7).

iii) Combining ASL with other electrophysiological techniques

In order to better understand how different pain-relevant regions are functionally interacting over the course of the pain experience, it would be possible to pair the multi-TI pCASL approach with another neuroimaging technique such as EEG that benefits from better temporal resolution. For example, a combined ASL-EEG investigation of ongoing pain would allow us to understand how the pain experience unfolds over time across these key ROIs. Simultaneous locking of the neural event to the evoked response might be difficult, but by matching changes in amplitude and power of key EEG rhythms with changes in global perfusion, it would then be possible to better understand how changes in CBF over time across regions may relate to the functional interactions likely occurring between them. Additionally, by employing brian interference techniques such as transcranial magnetic stimulation (TMS) or transcranial direct current stimulation (tDCS) it would be possible to modulate neuronal excitability within a seed region of interest to try to effectively modulate its interaction with other nearby regions of interest and change the overall pain experienced by the subject (8,9).

Another exciting albeit more invasive approach would be to employ perfusion imaging with the intracortical stimulating/recording technique of deep brain stimulation (DBS). Although this kind of work would be restricted to a very sensitive (and small) population of chronic pain sufferers, it is conceivable that

with the appropriate MR-compatible hardware, subjects implanted with electrodes in regions such as the PAG, thalamus, and basal ganglia could record ongoing neural activity whilst simultaneously being scanned to pair the CBF data with real-time neural population recordings during pain versus phases of stimulation-derived relief (10,11).

iv) Translation into animal models

Perhaps most the powerful experimental direction would be to pair this research with translatable animal models of ongoing pain. While there is an extensive body of literature on various pain-relevant rodent models of trauma, chemical and toxin-associated pain; there is a growing body of literature on neuroimaging pain states in rodents. For example, it would be possible to implant electrodes at the level of the spinal cord, the brainstem and/or the cortex such that continuous recordings could be made whilst the animal is experiencing a given pain state. While tremendously labor intensive, this kind of invasive *in vivo* telemetry would provide essential understanding for the temporal dynamics of how afferent nociceptive input enters the cortex; and relatedly how that information recruits activation of key regions of interest. This kind of insight could greatly facilitate the construction of *a priori* hypotheses needed for the PPI and DCM studies discussed previously in humans.

7.3 Summary

In summary, the results of this thesis display that we have successfully: i) developed a safe and reliable approach to investigate tonic pain states in healthy human subjects; ii) optimized a whole brain quantitative ASL approach to image

various ongoing pain states in healthy subjects; iii) implemented the optimized ASL approach to image a pathological pain state specific to erythromelalgia. We are confident that the work presented here will provide a helpful foundation for future perfusion neuroimaging investigations of ongoing pain states both in healthy subjects and various clinical populations, as well as provide a novel functional imaging tool suitable for challenging neuroscience paradigms that require alternative designs beyond phasic stimulation and towards examining tonic states.

7.4 References

1. Owen DG, Bureau Y, Thomas AW, Prato FS, St Lawrence KS (2008). Quantification of pain-induced changes in cerebral blood flow by perfusion MRI. Pain 136(1):85-96

2. Owen DG, Clarke CF, Ganapathy S, Prato FS, St Lawrence KS. (2010). Using perfusion MRI to measure dynamic changes in neural activation associated with tonic muscular pain. Pain 148(3):375-86

3. Howard, M.A. , Krause, K., Khawaja, N., Massat, N., Zelaya, F., Schumann, G., Huggins, J.P., Vennart, W., Williams, S.C.R., Renton, T.F. (2011). Beyond patient reported pain: perfusion magnetic resonance imaging demonstrates reproducible cerebral representation of ongoing post-surgical pain. PLoS One 6(2): 1-10.

4. Chen, Y., Wang, D.J.J., Detre, J.A. (2011). Test-Retest Reliability of Arterial Spin Labeling With Common Labeling Strategies. J Magnetic Resonance Imaging 33:940-9

5. Gevers, S. *et al.* (2011). Robustness and Reproducibility of Flow Territories Defined by Planning-Free Vessel_Encoded Pseudocontinuous Arterial Spin-Labeling. AJNR AM J Neuroradiol. [Epub ahead of print]

6. Liang, M., Mouraux, A., Iannetti, G.D. (2011) Parallel processing of nociceptive and non-nociceptive somatosensory information in the human primary and secondary somatosensory cortices: evidence from dynamic causal modelling of functional magnetic resonance imaging data. J Neuroscience 31(24): 8976-85.

7. Malinen, S., Vartianinen N., Hlushchuk, Y., Koskinen, M., Ramkumar, P., Forss, N., Kalso, E., Hari, R., (2010) Aberrant temporal and spatial brain activity during rest in patients with chronic pain. PNAS USA 107(14):6493-7.

8. Brighina, F., De Tommaso, M., Giglia, F., Scalia, S., Cosentino, G., Puma, A., Panetta, M., Giglia, G., Fierro, B. (2011). Modulation of pain perception by transcranial magnetic stimulation of left prefrontal cortex. J Headache Pain 12(2):185-91.

9. Borckardt, J.J., Reeves, S.T., Beam, W., Jensen, M.P., Gracely, R.H., Katz, S., Smith, A.R., Madan, A., Patterson, D., George, M.S. (2011). A randomized, controlled investigation of motor cortex transcranial magnetic stimulation (TMS) effects on quantitative sensory measures in healhty adults: evaluation of TMS device parameters. Clin J Pain 27(6):488-94.

10. Nguyen, J.P., Nizard, J., Keravel, Y., Lefaucher, J.P. (2011) Invasive brain stimulation for the treatment of neuropathic pain. Nat Rev Neurol. [Ahead of Publication] p1-11.
11. Stadler, J.A. 3rd, Ellens, D.J., Rosenow, J.M. (2011) Deep brain stimulation and motor cortical stimulation for neuropathic pain. Curr Pain Headache Rep. 15(1):8-13.